

University of Mustapha Stambouli

Mascara



جامعة مصطفى إسمطبولي

معسكر

Faculty of Science and Technology

Department of Process Engineering

Laboratory of Water Sciences and Techniques

Doctoral Thesis of 3rd cycle

Specialty: Process Engineering

Option: Chemistry

Title:

Removal of an Organic Dye by Adsorption on Hybrid Material

Presented by: MAHI Omar

26/10/ 2022

The jury members:

| | | |
|-------------|----------------------------|---|
| President: | Pr. BEKOUIDER Ali Mustapha | University Mustapha Stambouli - Mascara |
| Advisor: | Pr. BENYOUCEF Abdelghani | University Mustapha Stambouli - Mascara |
| Co-advisor: | Pr. ZEHAF Abdelhafid | University Mustapha Stambouli - Mascara |
| Examiner : | Pr. BOUSALEM Smain | University Center Ain Temouchent |
| Examiner : | Pr. MOUFFOK Benali | University Djillali Liabes Sidi Bel Abbes |
| Examiner : | MCA. CHOULI Faiza | University Mustapha Stambouli - Mascara |

University year : 2022-2023

Université MUSTAPHA Stambouli
Mascara



جامعة مصطفى إسمطبولي
معسكر

Faculté des Sciences et Technologie

Département de Génie des Procédés

Laboratoire des Science et Techniques de l'eau

THESE de DOCTORAT de 3ème Cycle

Spécialité : Génie des Procédés

Option : Chimie

Intitulée :

Elimination d'un colorant organique par adsorption sur des Matériaux Hybride

Présentée par : MAHI Omar

Le : 26 /10/2022

Devant le jury :

| | | |
|----------------|--------------------------------|--|
| Président : | Pr. Pr. BEKOUIDER Ali Mustapha | Université de Mustapha Stambouli - Mascara |
| Encadreur : | Pr. BENYOUCEF Abdelghani | Université de Mustapha Stambouli - Mascara |
| Co-Encadreur : | Pr. ZEHAF Abdelhafid | Université de Mustapha Stambouli - Mascara |
| Examineur : | Pr. BOUSALEM Smain | Centre Universitaire d'Ain Temouchent |
| Examineur : | Pr. MOUFFOK Benali | Université Djillali Liabes Sidi-Bel-Abbes |
| Examineur : | MCA. CHOULI Faiza | Université de Mustapha Stambouli - Mascara |

Année Universitaire : 2022-2023

ACKNOWLEDGEMENT

I am indebted and grateful to my supervisor Pr. BENYOUCEF Abdelghani, Department of Process Engineering, University Mustapha Stambouli-Mascara, for his invaluable guidance, constant encouragement, kind help and stimulating suggestions during the course of this research work.

I express my sincere gratitude to my supervisor Dr. ZEHRAF Abdelhafid, Department of Process Engineering, University Mustapha Stambouli-Mascara, for their suggestions and help rendered during the research investigation. I am also thankful to all faculty members of the Process Engineering Department for their support.

I wish to record my thanks to the Hydraulic Laboratory members for their valuable help and support during research work.

I express my special thanks to my wife, my family and to all my friends for their love and continued encouragement.

MAHI Omar

Abbreviations

| | |
|------------------------|--|
| A⁰ | Angstrom (10^{-10} m) |
| APS | Ammonium persulfate |
| CNT | Carbon's nanotubes |
| C₀ | Initial concentration |
| C_e | Equilibrium concentration |
| EB | Emeraldine base |
| ES | Emeraldine salt |
| FT-IR | Fourier transform infrared |
| GPA | Giga pascal |
| I | Transmitted intensity of UV-visible light |
| I₀ | Incident intensity of UV-visible light |
| K | Equilibrium constant |
| k₁ | Pseudo-first order rate constant |
| k₂ | Pseudo-second order rate constant |
| K_d | distribution coefficient |
| K_F | Freundlich constant |
| K_L | Langmuir constant |
| k_{int} | Diffusion rate constant |
| OFI | Opuntia ficus indica |
| OFI-A | Opuntia ficus indica activated by NaOH |
| OG | Orange-G dye |
| PANI | Polyaniline |
| PNC | Poly nanocomposite |
| ppm | Parts per million (mg/L) |
| PZC | Point of zero charge |
| q_e | Quantity of adsorbate adsorbed by mass unit of adsorbent at equilibrium |
| Q_{max} | Maximum quantity of adsorbate adsorbed by mass unit of adsorbent |
| R | Universal gas constant ($8.314 \text{ J}\cdot\text{mol}^{-1}\cdot\text{K}^{-1}$) |

| | |
|------------------------------------|-------------------------------------|
| s.cm⁻¹ | Siemens per centimeter |
| SEM | Scanning Electron Microscopy |
| T | Temperature |
| TGA | Thermal gravimetric analysis |
| XRD | X-ray diffraction |
| V | Volume |
| ΔG | Free Gibbs energy Change |
| ΔH | Enthalpy change |
| ΔS | Entropy change |
| λ_{\max} | Maximum absorbance wavelength light |

TABLE OF CONTENTS

| | |
|----------------------------|---|
| GENERAL INTRODUCTION | 1 |
|----------------------------|---|

CHAPTER I: BIBLIOGRAPHIC STUDIES

| | |
|---|----|
| I.1. GENERAL INFORMATION ABOUT POLLUTION | 5 |
| I.1.1. Definition | 5 |
| I.1.2. Sources of water pollution | 5 |
| I.1.2.a. Urban source | 5 |
| I.1.2.b. Industrial source | 5 |
| I.1.2.c. Agricultural source | 5 |
| I.1.2.d. Microbiological source | 6 |
| I.1.2.e. Pollution by dyes | 6 |
| I.1.2.f. Pesticide pollution | 6 |
| I.1.3 GENERAL INFORMATION ABOUT DYES | 7 |
| I.1.3.1. Introduction | 7 |
| I.1.3.2. Definition | 8 |
| I.1.3.3. Nature of dyes | 8 |
| I.1.3.3.1 Natural dyes | 8 |
| I.1.3.3.2 Synthetic dyes | 8 |
| I.1.3.4 Classification of dyes | 9 |
| I.1.3.4.1 Chemical classification | 9 |
| I.1.3.4.1.a. Anthraquinone dyes | 9 |
| I.1.3.4.1.b. Azo dyes | 9 |
| I.1.3.4.1.c. Dyes of diphenylmethane and triphenylmethane | 10 |
| I.1.3.4.1.d. Indigoids dyes | 10 |
| I.1.3.4.1.e. Nitrated and nitrosated dyes | 11 |
| I.1.3.4.2. Dye classification | 12 |
| I.1.3.4.2 a. Acid or anionic dyes | 12 |
| I.1.3.4.2 b. Basic or cationic dyes | 12 |
| I.1.3.4.2.c. Reactive dyes | 13 |

| | |
|---|----|
| I.1.3.5 Hazards of dyes..... | 13 |
| I.1.3.6 Methods of liquid effluent treatment | 13 |
| I.2. HYBRID MATERIALS..... | 15 |
| I.2.1. Introduction | 15 |
| I.2.2. Nanocomposites | 15 |
| I.2.2.1. Nanocomposite constituents | 15 |
| I.2.3. Types of nanocomposites | 16 |
| I.2.3.1. Polymer-based nanocomposites | 17 |
| I.2.3.1.1. Different types of polymer nanocomposites | 18 |
| I.2.3.1.1.a. Polymeric Nanocomposites based on inorganic materials | 19 |
| I.2.3.1.1.b. Polymeric Nanocomposites based on metallic materials | 19 |
| I.2.3.1.1.c. Polymeric carbon-based nanocomposites | 20 |
| I.2.3.1.2. Synthesis of Hybrid Nanocomposites | 21 |
| I.2.4. CONDUCTIVE POLYMERS | 25 |
| I. 2.4.1. Classification of conductive polymers | 26 |
| I. 2.4.2. Electronic structure of conductive polymers | 28 |
| I. 2.4.3. Doping of conductive polymers | 29 |
| I.2.4.4. Load carriers | 31 |
| I.2.5. POLYANILINE (PANI) | 31 |
| I.2.5.1. Doping of polyaniline | 32 |
| I.2.5.2. Synthesis of Polyaniline | 34 |
| I.2.5.3. Polymerization mechanism | 36 |
| I.2.5.4. Factors influencing the electrical conductivity of polyaniline | 38 |
| I.2.5.5. Applications of polyaniline | 39 |
| I.2.6. General Information on Opuntia Ficus Indica | 41 |
| I.2.6.1. Advantages of Opuntia ficus indica | 42 |
| I.3. ADSORPTION | 42 |
| I.3.1 Definition | 42 |
| I.3.1.1. Physical adsorption | 42 |
| I.3.1.2. Chemical adsorption | 43 |
| I.3.2 Adsorption Mechanisms | 44 |
| I.3.3. Physical properties of the adsorbent | 45 |
| I.3.3.1. Adsorbent pores | 45 |

| | |
|---|----|
| I.3.3.2. Adsorbent specific surface area | 46 |
| I.3.4. Solid-liquid interface | 47 |
| I.3.5. Ion exchange | 49 |
| I.3.6. Adsorption Studies | 51 |
| I.3.6.1. Adsorption Isotherm | 51 |
| I.3.6.2. Classification of liquid-solid adsorption isotherms | 51 |
| I.3.6.3. Modelling Techniques | 53 |
| I.3.6.3. a. Langmuir Model | 53 |
| I.3.6.3. b. Freundlich Model | 54 |
| I.3.6.3. c. Langmuir-Freundlich model | 55 |
| I.3.6.4. Thermodynamic parameters related to the adsorption process | 56 |
| I.3.6.5. Adsorption kinetics | 57 |
| I.3.6.5.a. Pseudo-first order model | 58 |
| I.3.6.5.b. Pseudo-second order kinetic model | 58 |
| I.3.6.5.c. Intraparticles diffusion model | 59 |
| I.4. REFERENCES | 60 |

CHAPTER II: MATERIALS AND METHEDS

PREPARATION AND CHARACTERISATION OF ADSORBENTS

| | |
|--|----|
| II.1. INTRODUCTION | 72 |
| II.2. USED PRODUCTS | 72 |
| II.3. PREPARATION OF DIFFRENTS ADSORBENTS | 72 |
| II.3.1. Preparation of the Opuntia Ficus Indica OFI adsorbent | 72 |
| II.3.2. Synthesis of the Polyaniline PANI | 73 |
| II.3.3. Synthesis of the aniline / Opuntia Ficus Indica PANI-OFI nanocomposite | 73 |
| II.4. CHARACTERISATION TECHNIQUES AND APARATUS | 74 |
| II.4.1. X-ray diffraction | 75 |
| II.4.1.1. Generality | 75 |
| II.4.1.2. Interpretation of the XRD diffraction patterns | 77 |
| II.4.2. Fourier Transform Infrared Spectroscopy | 78 |
| II.4.2.1. Principle | 78 |
| II.4.2.3. Interpretation of Fourier Transform Infrared (FTIR) Analysis | 79 |
| II.4.3. Nitrogen Adsorption/Desorption Isotherms (BET) | 80 |

| | |
|---|----|
| II.4.3.1.Principle | 80 |
| II.4.3.2. Interpretation | 82 |
| II.4.4.Thermal gravimetric analysis (TGA) | 83 |
| II.4.4.1. Principle | 83 |
| II.4.4.2. Interpretation | 83 |
| II.4.5. Morphological Study (SEM) | 85 |
| II.4.5.1. Principle | 85 |
| II.4.5.2. Interpretation of SEM images | 85 |
| II.4.6. Point of zero charge (PZC) analysis | 86 |
| II.4.6.1. Operating protocol | 86 |
| II.4.7. Ultraviolet visible (UV-vis) spectroscopy | 87 |
| II.4.7.1. Principle | 87 |
| II.4.7.2 Beer-Lambert's Law | 88 |
| II.4.7.3. Determination of maximum absorbance wavelength (λ_{max}) of Orange G dye..... | 89 |
| II.5. REFERENCES | 90 |

CHAPTER III: ADSORPTION OF OG ONTO OFI-A

| | |
|---|-----|
| III.1 Introduction | 93 |
| III.2 PREPARATION OF SOLUTIONS | 93 |
| III.2.1. Calibration curve for OG | 94 |
| III.3. Effect of different parameters on adsorption of OG onto PANI@OFI-A | 95 |
| III.3.1. Effect of adsorbent dosage | 95 |
| III.3.2. Effect of pH | 95 |
| III.3.3. Effect of Initial OG Concentration and Contact Time | 96 |
| III.4. Adsorption kinetics modeling | 97 |
| III.4.1 Pseudo-first order | 98 |
| III.4.2 Pseudo-first order | 99 |
| III.4.3 Elovich model | 100 |
| III.4.4. Intra-particle diffusion model | 101 |
| III.5. Adsorption isotherms modeling | 104 |
| III.5.1. Freundlich isotherm | 104 |
| III.5.2. Langmuir isotherm | 105 |

| | |
|----------------------------------|-----|
| III.5.3. Temkin isotherm | 106 |
| III.6. Thermodynamic study | 108 |
| III.7. References | 111 |

CHAPTER IV: ADSORPTION OF OG ONTO PANI

| | |
|--|-----|
| IV.1 Introduction | 113 |
| IV.2. Adsorption Study | 113 |
| IV.3. Effect of different parameters on adsorption of OG onto PANI@OFI-A | 114 |
| IV.3.1. Effect of adsorbent dosage | 114 |
| IV.3.2. Effect of pH on the adsorption of OG onto PANI..... | 115 |
| IV.3.3. Effect of Initial OG Concentration and Contact Time | 116 |
| IV.4. Adsorption kinetics modeling | 117 |
| IV.4.1 Pseudo-first order | 117 |
| IV.4.2 Pseudo-second order | 117 |
| IV.4.3 Elovich model | 118 |
| IV.4.4. Intra-particle diffusion model | 119 |
| IV.5. Adsorption isotherms modeling | 121 |
| IV.5.1. Freundlich isotherm | 122 |
| IV.5.2. Langmuir isotherm | 123 |
| IV.5.3. Temkin isotherm | 123 |
| IV.6. Thermodynamic study | 125 |
| IV.7. References | 128 |

CHAPTER V: ADSORPTION OF OG ONTO PANI@OFI-A

| | |
|---|-----|
| V.1 Introduction | 130 |
| V.2. Adsorption Study..... | 130 |
| V.3. Effect of different parameters on adsorption of OG onto PANI@OFI-A | 131 |
| V.3.1. Effect of adsorbent dosage | 131 |
| V.3.2. Effect of pH | 131 |

| | |
|--|-----|
| V.3.3. Effect of Initial OG Concentration and Contact Time | 133 |
| V.4. Adsorption kinetics modeling | 133 |
| V.4.1 Pseudo-first order kinetics model..... | 133 |
| V.4.2 Pseudo-second order kinetics model | 134 |
| V.4.3 Elovich model kinetics model..... | 135 |
| V.4.4. Intra-particles diffusion model | 136 |
| V.5. Adsorption isotherms | 138 |
| V.5.1. Freundlich model | 138 |
| V.5.2. Langmuir model | 139 |
| V.5.3. Temkin isotherm | 139 |
| V.6. Thermodynamic study | 141 |
| V.7. References | 143 |
| General Conclusion | 145 |

INDEX OF FIGURES

CHAPTER I

| | |
|---|----|
| Figure I.1. Anthraquinonic skeleton..... | 09 |
| Figure I.2. Azo skeleton..... | 10 |
| Figure I.3. Indigoid skeleton..... | 11 |
| Figure I.4. Nitrosate skeleton..... | 11 |
| Figure I.5. Congo Rouge skeleton..... | 12 |
| Figure I.6. Capri blue skeleton..... | 12 |
| Figure I.7. Classification of polymer- and non-polymer-based nanocomposites..... | 16 |
| Figure I.8. Uniform dispersion between the filler and matrix in nanocomposites..... | 18 |
| Figure I.9. Methods for synthesizing polymer/metal nanocomposites..... | 21 |
| Figure I.10. Synthesis of PANI nanocomposite by in situ polymerization..... | 24 |
| Figure I.11. Some examples of conducting polymers..... | 25 |
| Figure I. 12. Electrical conductivity of intrinsic conductive polymers..... | 28 |
| Figure I. 13. Theoretical diagram established according to the theory of energy bands..... | 29 |
| Figure I. 14. Conductivity of various conductive polymers and conventional materials..... | 30 |
| Figure I.15. General structure of polyaniline..... | 31 |
| Figure 1.16. Schematic representation of movement of charge along the polymer backbone..... | 33 |
| Figure 1.17. Doping and dedoping of PANI..... | 34 |
| Figure I.18. First steps in the oxidation of aniline and anilinium cations by APS in acidic HCl..... | 38 |
| Figure I.19. Opuntia ficus-indica fruits and cladodes..... | 41 |
| Figure.I.20. Lennard-Jones type diagrams (non-activated adsorption) potential energy versus distance | 44 |
| Figure I.21. Schema of the mechanism of molecule adsorption using microporous adsorbent..... | 45 |
| Figure I.22. Schematic representation of different types of pores..... | 46 |
| Figure I.23. Schematic representation of external and internal adsorbent surface..... | 47 |
| Figure I.24. Model of double layer structure of the solid-liquid interface with examples of specific and non-specific ion adsorption together with their hydration shell..... | 48 |
| Figure I.25. Schematic representation of Na ⁺ , Ca ²⁺ exchange..... | 49 |

| | |
|---|----|
| Figure I.26. Classification of solution adsorption isotherms according to Giles et al..... | 52 |
|---|----|

CHAPTER II

| | |
|---|----|
| Figure.II.1 Schematic representation of the most important steps to prepare the PANI@OFI-A | 74 |
| Figure.II.2. Bragg Diffraction Planes | 76 |
| Figure.II.3. XRD diffraction patterns of: PANI, OFI-A and PANI@OFI-A | 77 |
| Figure.II.4. FT-IR adsorption spectra of: PANI, OFI-A and PANI@OFI-A | 78 |
| Figure.II.5. Adsorption–desorption isotherms of nitrogen at 77 K of PANI, raw OFI, OFI-A and PANI@OFI-A | 82 |
| Figure. II.6. Thermogravimetric analysis of pure PANI, PANI@OFI-A and OFI-A obtained Under N ₂ flow at a heating rate of 10 °C.min ⁻¹ | 84 |
| Figure. II.7. SEM images of the OFI-A (a) and PANI@OFI-A (b) | 85 |
| Figure.II.8. Representation of PZC for PANI@OFI-A and OFI-A | 87 |
| Figure.II.9. UV-Vis Spectrum of orange G dye | 89 |

CHAPTER III

| | |
|---|-----|
| Figure.III.1 Orange G dye calibration curve at ($\lambda_{max}=477nm$) | 94 |
| Figure III.2 Effect of adsorbent dosage on the adsorption of OG onto OFI-A | 95 |
| Figure III.3 Effect of pH on the adsorption of OG onto OFI-A | 96 |
| Figure III.4 Effect of contact time on adsorption | 97 |
| Figure III.5 The pseudo–first order kinetic model for the adsorption of OG onto OFI-A | 99 |
| Figure III.6 The pseudo–second order kinetic model for the adsorption of OG onto OFI-A | 100 |
| Figure III.7 Elovich model for the adsorption of OG onto OFI-A | 101 |
| Figure III.8 Intra-particle diffusion model for the adsorption of OG onto OFI-A | 102 |
| Figure III.9 Comparison between the measured and modelled time profiles for the adsorption of OG onto OFI-A | 103 |
| Figure III.10 Freundlich isotherm for the adsorption of OG onto OFI-A | 105 |
| Figure III.11 Langmuir isotherm for the adsorption of OG onto OFI-A | 106 |
| Figure III.12 Temkin isotherm for the adsorption of OG onto OFI-A | 107 |
| Figure III.13 Comparison of equilibrium isotherms for the adsorption of OG onto OFI-A | 108 |

| | |
|--|-----|
| Figure III.14 Effect of temperature on the adsorption of OG onto OFI-A | 109 |
| Figure III.15 Plot of $\ln(K_d)$ versus $1/T$ for the adsorption of OG onto OFI-A | 109 |

CHAPTER IV

| | |
|---|-----|
| Figure IV.1 Dissociation of Orange G dye in aqueous solution | 113 |
| Figure IV.2 Effect of adsorbent dosage on the adsorption of OG onto PANI (ES) | 114 |
| Figure IV.3 Effect of pH values on the adsorption of OG onto PANI | 115 |
| Figure IV.4 Effect of contact time and initial concentration on adsorption of OG onto PANI | 116 |
| Figure IV.5 The pseudo-first order kinetic model for the adsorption of OG onto PANI | 117 |
| Figure IV.6 The pseudo-second order kinetic model for the adsorption of OG onto PANI | 118 |
| Figure IV.7 Elovich model for the adsorption of OG onto PANI | 118 |
| Figure IV.8. Intra-particle diffusion model for the adsorption of OG onto PANI | 119 |
| Figure IV.9 Comparison between the measured and modelled time profiles for the adsorption of OG onto PANI | 121 |
| Figure IV.10 Adsorption isotherm of OG adsorption onto PANI | 122 |
| Figure III.11 Freundlich isotherm for the adsorption of OG onto PANI | 122 |
| Figure III.12 Langmuir isotherm for the adsorption of OG onto PANI | 123 |
| Figure VI.13 Temkin isotherm for the adsorption of OG onto PANI | 124 |
| Figure IV.14 Comparison of equilibrium isotherms for the adsorption of OG onto PANI | 125 |
| Figure III.15 Effect of temperature on the adsorption of OG onto PANI | 126 |
| Figure IV.16 Plot of $\ln(K_d)$ versus $1/T$ for the adsorption of OG onto PANI | 126 |

CHAPTER V

| | |
|---|-----|
| Figure V.1 Effect of adsorbent dosage on the adsorption of OG onto PANI@OFI-A | 131 |
| Figure V.2 Effect of pH values on the adsorption of OG onto PANI@OFI-A | 132 |
| Figure V.3 Effect of contact time on adsorption of OG onto PANI@OFI-A adsorption | 133 |
| Figure V.4 The pseudo-first order kinetic model for the adsorption of OG onto PANI@OFI-A ... | 134 |
| Figure V.5 The pseudo-second order kinetic model for the adsorption of OG onto PANI@OFI-A | 135 |
| Figure V.6 Elovich model for the adsorption of OG onto PANI@OFI-A | 136 |
| Figure V.7 Intra-particle diffusion model for the adsorption of OG onto PANI@OFI-A | 136 |

| | |
|--|-----|
| Figure V.8 Comparison between the measured and modelled time profiles for the adsorption of OG onto PANI@OFI-A | 137 |
| Figure V.9 Freundlich isotherm for the adsorption of OG onto PANI@OFI-A | 138 |
| Figure V.10 Langmuir isotherm for the adsorption of OG onto PANI@OFI-A | 139 |
| Figure V.11 Temkin isotherm for the adsorption of OG onto PANI@OFI-A | 140 |
| Figure V.12 Comparison of equilibrium isotherms for the adsorption of OG onto PANI@OFI-A | 141 |
| Figure V.13 Plot of $\ln(K_d)$ versus $1/T$ for the adsorption of OG onto PANI@OFI-A | 142 |

INDEX OF TABLES

CHAPTER I

| | |
|---|----|
| Table I. Different types of nanoparticles used in polymer nanocomposites | 18 |
| Table I. 2. The main families of conductive polymers | 27 |
| Table I.3. Gap of the main families of conjugated polymers | 29 |
| Table I.4. Main applications of polyaniline and associated specific properties | 40 |
| Table I.5. IUPAC classification of pore sizes | 46 |
| Table I.6. Some examples of monocomponent isotherms models | 56 |

CHAPTER II

| | |
|---|----|
| Table II.1 Textural characterization of: PANI, raw OFI, OFI-A and PANI@OFI-A | 83 |
| Table II.2 The results of initial pH and final pH for the OFI-A | 86 |
| Table II.3. The results of initial pH and final pH for the PANI@OFI-A | 86 |
| Table II.4. Maximum wavelength and absorption coefficient of different organic compounds | 88 |

CHAPTER III

| | |
|---|-----|
| Table III.1. physicochemical properties and molecular structure of OG | 93 |
| Table III.2 Kinetic parameters for adsorption of OG onto OFI-A..... | 103 |
| Table III.3 different isotherms parameters and correlation coefficient of OG onto OFI-A and at 25 °C and pH = 2 | 107 |
| Table III.4 Thermodynamic parameters for the adsorption of OG onto OFI-A | 110 |

CHAPTER IV

| | |
|--|-----|
| Table IV.1 Kinetic parameters for the adsorption of OG onto PANI | 120 |
| Table IV.2 different isotherms parameters and correlation coefficients of OG adsorption onto PANI (at 25 °C and pH = 2) | 124 |
| Table IV.3 Thermodynamic parameters for the adsorption of OG onto PANI | 127 |

CHAPTER V

| | |
|--|-----|
| Table V.1. Kinetic parameters for the adsorption of OG onto PANI@OFI-A | 137 |
| Table .V.2 different isotherms parameters and correlation coefficient of OG onto PANI@OFI-A (at 25 °C and pH = 2) | 140 |
| Table V.3 Thermodynamic parameters for the adsorption of OG onto PANI@OFI-A | 142 |

Objective:

The objective of this thesis is to develop a new hybrid material from low cost, largely and easily available material and investigate its application as an adsorbent for the elimination of dye from aqueous solution.

GENERAL

INTRODUCTION

GENERAL INTRODUCTION

Dyes are utilized as coloring products in several industries including textile, ink, leather, ceramics, cosmetics, paper, plastic, printing, food and pharmaceuticals [1]. These industries use large quantity of water and discharge their effluents in different aquatic sources. These effluents contain many harmful chemicals that pose serious problems to human beings and aquatic lives [2]. The biodegradation of dyes poses serious water pollution. According to an estimation, approximately 4.0×10^4 to 5.0×10^4 tons of dyes and colors enter the aquatic resources annually. Improper and incomplete treatment of the industrial effluents represent the main reason of water pollution. Approximately 10-15% of color effluents discharged by dye production industries present a major concern as these effluents not only degrade the aesthetic value of the water bodies but also disturb the penetration of light into the water, thereby leading to disturbances in the aquatic lives [3]. The decolorization of dyes are difficult due to their complex structure as most of the dyes contain aromatic rings.

The elimination of dyes from wastewater is of concern to researchers. Some of the dyes present a high toxicity and these lead to fatal diseases like severe headache, nausea, allergic reaction in eyes and some water borne diseases. In dyeing industry a number of dyes are utilized include vat dyes, naphthol dyes, sulphur dyes, indigo dyes ...etc.

A conventional treatment of dye effluents is not very effective due to dyes biodegradability. Dyes are usually treated by physical or chemical processes. Divers techniques are available in the literature for color elimination: photocatalysis, biological oxidation, chemical oxidation, degradation aerobic, nanofiltration separation, ozonation, physical adsorption, flocculation-coagulation, fluid extraction, and solid phase extraction. Which are generally used in the industrial effluents treatment. Among these techniques, adsorption has advantages because of inexpensive, simple design, more proficient and the simplicity of the application process [5].

Activated carbons are well known as adsorbent with high specific surface but their high cost limits its large scale application in developing countries. Therefore, there is a large need for low cost and easily available adsorbents for dyeing industrial wastewater treatment. Several types of biomasses have been investigated for the treatment of dye effluents. Many adsorbents such as lignocellulosic materials, industrial wastes, natural clay and polymers have been used as alternatives to activated carbon [6].

Conductive polymers as polyaniline (PANI) are more important in wide regions. Because of the reasonably good conductivity, redox active, excellent environmental stability, ease of synthesis, highly electroactivity, excellent biocompatibility and low cost [7]. In removal process, PANI is predominately utilized as adsorbent support for poisonous pollutants [8]. By contrary, PANI does not melt or even does not dissolve in most of the common organic solvents. Hence, the developing PANI-based composite is an important way for its wide applications. Besides, now PANI is applied as a hybrid material with other composite to test its potency [9]. Among these nanomaterials we find: PANI@SiO₂, PANI@Al₂O₃, PANI@TiO₂, PANI@ZnO, PANI@SiC, PANI@V₂O₅, PANI@MoS₂, Fe₃O₄@Polyaniline/Itaconic Acid and PANI@Graphene Oxide [10].

In past few years, many investigators have tried to develop a carbon modified -surface for removal of varied pollutants using less expensive precursors, which were primarily industrial and agricultural by-products, such as plant leaves, tree leaves, tea leaves, camphor leaves, Date palm leaves, bamboo leaves, rosemary leaves, olive leaves and Opuntia Ficus Indica (OFI) cladodes. Moreover, OFI cladodes are not consumable. Although a large percentage of the consumables biomaterial is discarded. Moreover, the use of this organic product could be a promising alternative due to its relative plenty, efficacy, low cost and ecofriendly nature [11]. Lately, several investigations evaluated the potential of OFI powder for pollutants removal from aqueous solutions [12]. Choudhary et al. estimated the efficacy in heavy metals (Cu⁺² and Ni⁺²) and malachite green dye elimination from aqueous solutions; Furthermore, their research on oil sands process-affected water. Cid et al. used OFI fruit wastes as adsorbent for textile dyes [13].

The literature survey showed only few reports on the synthesis of hybrid composite using PANI with OFI materials. In this follow-up investigation, we report simple and low-cost synthesis of a novel PANI@OFI-A adsorbent, which involves the application of NaOH-activated OFI-A, followed by in situ polymerization method of aniline. For this purpose, a PANI@OFI-A material was synthesis and used for the removal of Orange G dye from aqueous medium. FT-IR, XRD, SEM, TGA and Brunauer-Emmett-Teller (BET) were used to analyze both the morphology and structure of the composite adsorbent. Adsorption isotherms, kinetic equilibrium, pH effect and thermodynamic tests were investigated to characterize the new developed adsorbent (PANI@OFI-A). Farther more the application of OFI-A and PANI adsorbents for the removal of Orange G has been also investigated in this study.

Our work presented in this manuscript is divided into five chapters:

The first chapter presents a bibliographical study on the different and main sources of pollution, their origins, the effects of pollutants on the environment and detail on some pollutants such as dyes and pesticides. This chapter also includes general information on hybrid materials, conductive polymers as well as materials used for the synthesis of our hybrid adsorbent. Finally, this chapter gives general information about adsorption.

The second chapter is devoted to highlight the description of the basic materials as well as the presentation of the different experimental protocols and characterization methods used.

The experimental part is divided into three chapters, which are the third, fourth and fifth chapters:

The third chapter studies the removal of orange G dye using *Opuntia ficus indica* activated by NaOH (OFI-A) as adsorbent, the fourth chapter examines the elimination of OG dye by adsorption onto polyaniline and the fifth chapter studies the adsorption of OG onto hybrid material, which is synthesized by polymerization of aniline on the OFI-A.

REFERENCES

- [1] Hinderso, H., Ismadji, S., Wicaksana, F., Mudjijati, and Indraswati, N. Adsorption of Benzene and Toluene from Aqueous Solution onto Granular Activated Carbon. *Journal of Chemical Engineering Data*, 46: 788-791. (2001).
- [2] Q.H. Fan, D.D. Shao, J. Hu, W.S. Wu, X.K. Wang. Comparison of Ni²⁺ sorption to bare and ACT-graftattapulgites: effect of pH, temperature and foreign ions, *Sur. Sci.* 602 778 – 785. (2008).
- [3] X.K. Wang, C.L. Chen, W. P. Hu, A. P. Ding, D. Xu, X. Zhou. Sorption of 243Am(III) to multiwall carbon nanotubes, *Environ. Sci. Technol.* 39 2856–2860. (2005).
- [4] PINTA, M., I. Coll. Méthodes de référence pour la détermination des éléments minéraux dans les végétaux, *Les laboratoires membres du Comité Inter-Instituts*, t, 24, no 8-9, 497-504 p Séville. (1968).
- [5] Kjeldahl, J. Méthode de dosage de l'azote dans les substances organiques, *Résumé du compte-rendu des travaux du Laboratoire de Carlsberg, Copenhague*, en commission chez H. Hagerup, Imprimerie de Thiele. (1983)
- [6] ANNE, P. Dosage rapide du carbone organique des sols. *Ann. agron.*, 15^o année, no 2, pp. 161-172.
- [7] WALKLEY, A., BLACK, A. An examination of the Degtjareff method for determining soil organic matter, and a proposed modification of the chromic acid titration method, *Soil Sci.*, 37, pp. 29-38. (1934).
- [8] Carpenter, J.H. The accuracy of the Winkler method for dissolved oxygen analysis. *Limnol Oceanogr.* 10, 135-140. (1965).
- [9] Carritt, D.E., J.H, Carpenter. Comparison and evaluation of currently employed modifications of the Winkler method for determining dissolved oxygen in sea water; a NASCO Report. *J. Mar. Res.* 24, 286-318. (1966).
- [10] Tranchant, J. *Manuel pratique de chromatographie en phase gazeuse*, 3^{ème} édition, Masson (Ed.) Paris. (1982).
- [11] S. Preethi, A. Sivasamy. Removal of safranin basic dye from aqueous solutions by adsorption onto corncob activated carbon, *Ind. Eng. Chem. Res.* 45 7627–7632. (2006).
- [12] V. Zoes, H. Dinel, T. Pare, A. Jaouich. Growth substrates made from duck excreta enriched wood shavings and source separated municipal solid waste compost and separates: physical and chemical characteristics, *Bioresour. Technol.* 78 21–30. (2001).
- [13] Michele Clements. Granular activated carbon management at a water treatment plant. *Magister Ingenieriae, Faculty of engineering, Rand Afrikaans University. F.* (2002).

CHAPTER I

BIBLIOGRAPHIC STUDIES

I.1 GENERAL INFORMATION ABOUT POLLUTION:**I.1.1 Definition:**

Pollution is an unfavorable modification of the natural environment that appears in its entirety or in part, through direct or indirect effects altering the criteria for the distribution of flows energy, radiation levels, physico-chemical makeup of the natural environment and the abundance of living species. For example, water pollution is an alteration of its quality and its nature, which makes its use dangerous and disrupts the aquatic ecosystem. It can concern both surface water and groundwater [1].

I.1.2 Sources of water pollution

Water in nature and a fortiori that which is used for industrial uses and domestic products is never pure, due to the impurities it can contain in the three states: solid, liquid or gaseous and which can be characterized by the size they take in aqueous media.

a. Urban source

The origin of urban wastewater is mainly domestic where populations generate three quarters of wastewater. These effluents are a mixture of water containing excreta human such as toilet and cleaning water (gray water). Waste water urban areas may also contain industrial wastewater, but normally, these must have undergone a pre-treatment to achieve comparable characteristics to those of domestic wastewater to allow joint treatment [2].

b. Industrial source

It constitutes the liquid waste obtained during the extraction and processing of raw materials into industrial products. Wastewater mainly comes from the water consumed in many wet manufacturing operations, such as example: precipitation, washing, cleaning of devices, workshops, filtrations, distillations ...etc [3]. Industrial effluents can generate organic pollution from food industries, paper mills, textile factories, or minerals from metallurgical industries [4].

c. Agricultural source

Pollution of agricultural origin comes mainly from fertilizers and pesticides spread in the soil over very large areas near watercourses [5]. This type of pollution has intensified since agriculture entered a fairly advanced stage of industrialization. The concentration of farms leads to a surplus of animal waste, which ends up enriching rivers and groundwater in nitrogen derivatives, thus encouraging a

source of bacteriological pollution. The massive use of chemical fertilizers (nitrates and phosphates) also alter the quality of the groundwater to which they are drawn [6].

d. Microbiological source

The microbiological quality of the water can also be the cause of problems, whether they are acute or chronic. Accidents can occur during poor disinfection of pipes, giving water of poor microbiological quality, which can be a risk of several pathologies, especially digestive [7].

e. Pollution by dyes

Dyes occupy an important place in synthetic organic compounds. They are used in large quantities in industries: textile, ink, plastic, paper, cosmetics, tannery, and are therefore common industrial pollutants. Their releases into aquatic systems cause damage to the environment due to their toxicity, which imposes their treatment. But the complexity of these pollutants is that their color affects enormously the effectiveness of conventionally applied treatments.

The textile industry is a large consumer of water for the dyeing phases of fabrics. The rinsing waters are loaded with dyes. These dye effluents are highly stable and recalcitrant to biodegradation [8]. A number of dyes are recognized dangerous for public health such as Nylosan Red and Supranol Yellow. The removal of color is a critical issue for the environment. These dyes are difficult to degrade because of their complex structures and xenobiotic properties. The presence of dyes in water, even at low concentrations, is very noticeable and undesirable. It reduces the penetration of light, which gives derogatory effects on photosynthesis [9].

f. Pesticide pollution

There is no doubt about the value of the use of pesticides in agricultural areas and sanitary. With six billion and a few hundred million inhabitants currently in the world, the recourse to a truly "clean" agriculture for to feed everyone would be a utopia. The use of pesticides is therefore a necessary evil we cannot rid it. The capital stake would therefore be to use them with an environmental impact reduced to a minimum [10].

The use of pesticides around the world has seen a marked evolution, without we might as well take into account, as appropriate, their impacts on health and the environment. Some of these products are characterized by their very wide toxicity spectra, their bioaccumulation and their persistence in different natural media and chains food [11].

Indeed, several studies have shown the existence of pesticides in their initial form or in the form of residues in different environmental compartments (surface water, groundwater, soil ...etc.) as well as in agricultural products. It goes hand in hand that the contamination of the environment by pesticides exposes everyone to variables levels of these products that can have negative impacts on the health and well-being of populations [12]. Since the 1940s, the first pesticides have appeared on the market, with very positive results in terms of increasing agricultural yields allowing the effective control of microorganisms harmful to crops. Twenty years later, the first accusations of harm to health and the environment were heard. About that, the United Nations report published in 2004 by the United Nations for food (FAO), the United Nations Development Program (UNDP) and by the World Health Organization (WHO) reports that the number of poisonings by pesticides are estimated at 1 to 5 million cases each year. In addition, there are approximately 220,000 deaths from pesticides per year worldwide [13]. If developing countries only use 25% of the pesticides produced in the world, 99% of poisonings due to these phytosanitary products have been produced in these countries and particularly in rural areas, most often due to improper handling of products (dosage, storage).

I.2 GENERAL INFORMATION ABOUT DYES

I.2.1 Introduction

The water available to humans, and also to the rest of the ecosystem, is less of 1% of the total volume of freshwater on earth. The quality of the part available and potentially usable by humans (0.1%) has continued to degrade and sometimes irreversibly [14]. The generating capacity is exceeded because of our toxic liquid, solid or gaseous discharges more and more important. So clean water is becoming scarce in many parts of the world such as North Africa, India, the Gulf countries. The textile industry is recognized polluting since its discharges are made up of recalcitrant organic molecules that cannot be treated by traditional methods of depollution. Synthetic dyes including 15% consist of nitrogenous dyes are one of the main sources of pollution in water. Despite the considerable efforts in wastewater treatment, unfortunately it is estimated that still today only 60% of polluted water is routed to a station purification, the rest being discharged into the natural environment. One of the most alarming phenomena is the increasing accumulation of recalcitrant substances which are difficult to biodegrade in waters. The situation is worsened by the lack or insufficiency of an adequate water treatment system capable of reducing the concentration of toxic substances that represent chronic chemical hazards. It can be said that poorly treated wastewater leads to inevitably degradation

of the quality of the water sources and consequently of the drinking water which, moreover, is lacking in many countries [15].

I.2.2 Definition

A dye is a colored chemical substance capable of transmitting its coloring to other bodies. It is an unsaturated and aromatic organic compound. The first materials dyes were of plant origin (madder, indigo, gaude) or even animal (carmine drawn from cochineal). Today, almost all coloring materials are synthetic derived from hydrocarbon derivatives contained in coal tar [16].

I.2.3 Nature of dyes

Dyes, chemical dyes compounds, natural or synthetic, in general organic, which have the property of permanently coloring the support to which they are applied under certain conditions. Modern industrial terminology defines a colorant as a product containing the pure organic dye with different additives and cutting agents, which facilitate its use. There are two types of dyes:

I.2.3.1 Natural dyes

There are few natural dyes, while there are thousands of synthetic dyes. Natural dyes are extracted from plants, trees, lichens or insects and molluscs. Yellow dyes are the most numerous. We meet two categories of natural dyes: mordant dyes and vat dyes, only the former are poorly soluble in water

I.2.3.2 Synthetic dyes

The raw materials of synthetic dyes are compounds such as benzene, from the distillation of hard coal. It is for this reason that synthetic dyes are commonly referred to as coal tar dyes. From these raw materials, the intermediates are produced by a series of chemical processes, which in general, correspond to the replacement of one or more hydrogen atoms of the starting product, by particular elements or radicals.

I.2.4 Classification of dyes

The main classifications most commonly encountered in industry are based on chemical structures of synthetic dyes and application methods to different substrates (textiles, paper, leather, plastics, etc.).

I.2.4.1 Chemical classification

The classification of dyes according to their chemical structures is based on the nature of the group chromophore.

a. Anthraquinone dyes

From a commercial point of view, the most important after azo dyes. Their general formula derived from anthracene (Figure I.1) shows that the chromophore is a quinone nucleus on which hydroxyl or amino groups can attach [17].

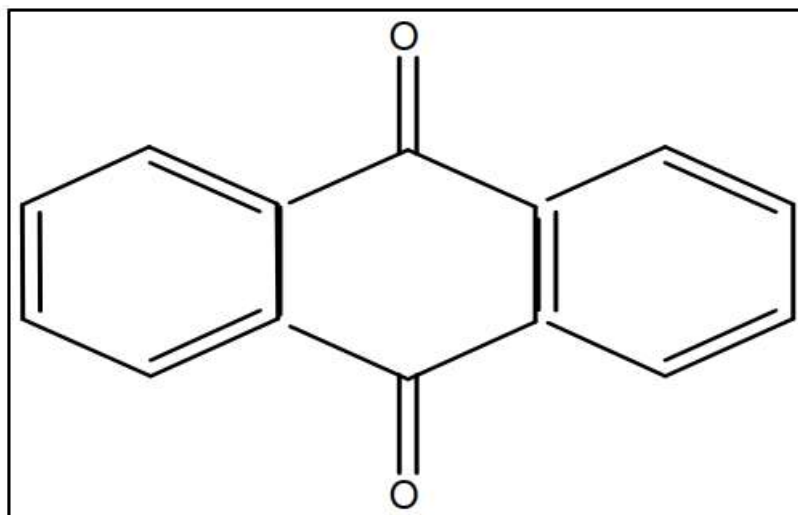


Figure I.1 : Anthraquinone structure

b. Azo dyes

Nitrogenous dyes are the most commonly used dyes in the textile industry, they are organic compounds containing a nitrogen group (Figure I.2) which is shown to be stable as textile dyes [18]. Nitrogenous dyes are resistant to light, acids, bases and oxygen, which make their use in the textile industry very widespread [19].

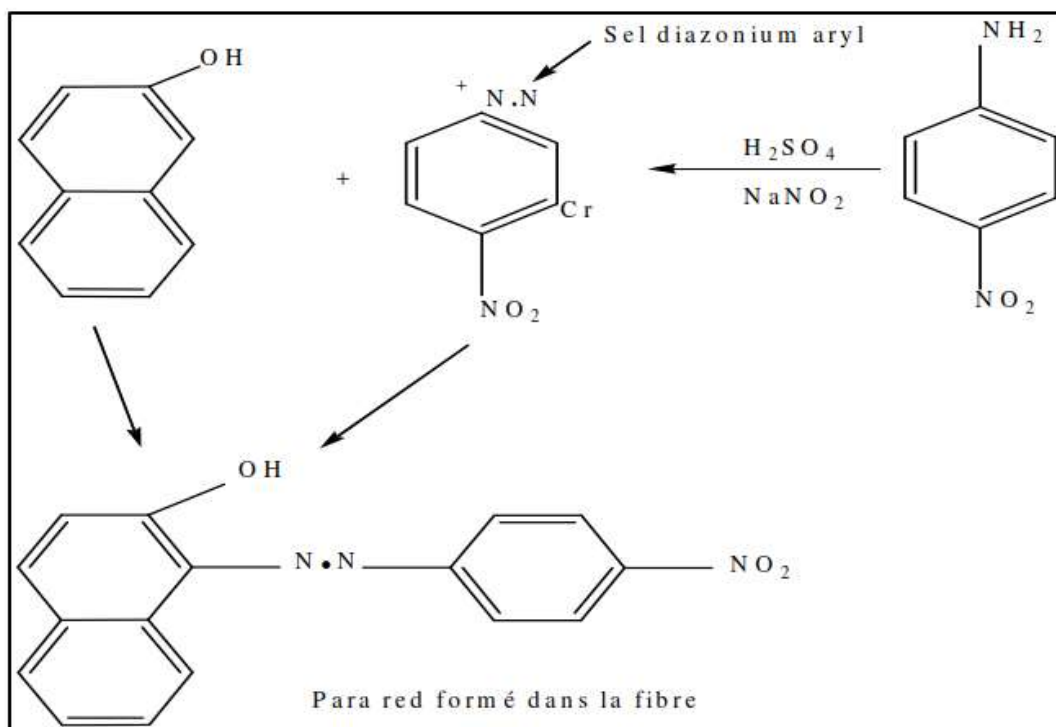


Figure I.2. Azo structure

C. Dyes of diphenylmethane and triphenylmethane

These dyes represent a much smaller category than that of azo and anthraquinone compounds. The main application is the coloring of paper for which the character of the result obtained is not a major handicap [20].

d. Indigoids dyes

Take their name from the indigo from which they derive. Thus, the selenium, sulfur and oxygenated indigo blue cause significant hypsochromic effects with colors which can range from orange to turquoise (Figure I.3) [21].

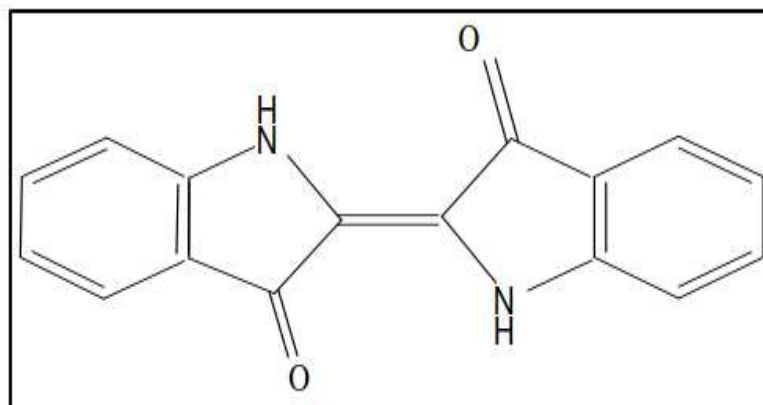


Figure I.3. Indigoid structure

e. Nitrated and nitrosated dyes

Form a very limited in number and relatively old class of dyes. They are currently still used because of their very moderate price linked to the simplicity of their structure molecular (Figure I.4), characterized by the presence of a nitro group (-NO₂) in the ortho position of an electron donor group (hydroxyl or amino groups) [22].

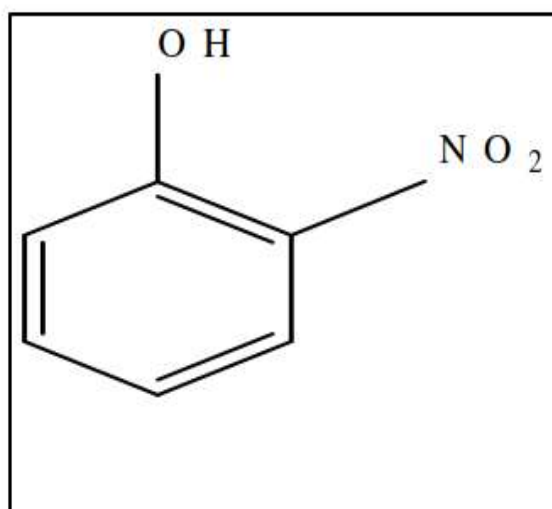


Figure I.4. Nitrosate structure

I.2.4.2 Dye classification

a. Acid or anionic dyes

Soluble in water due to their sulphonate or carboxylate groups (Figure I.5), they are so called because they allow to dye animal fibers (wool and silk) and some modified acrylic fibers (nylon, polyamide) in a slightly acid bath. The dye affinity-fiber is the result of ionic bonds between the sulfonic acid part of the dye and the groups amino of textile fibers [23].

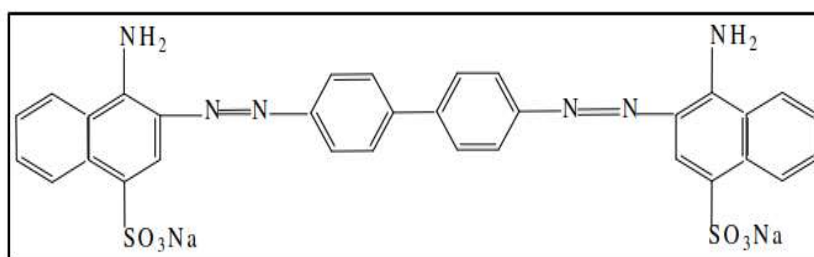


Figure I.5. Congo Rouge structure

b. Basic or cationic dyes

Are salts of organic amines, which gives them good solubility in water. They belong to very different chemical classes such as azodi and triphenylmethane (Figure I.6). These dyes received the name of cationic dyes, but have different structures [24].

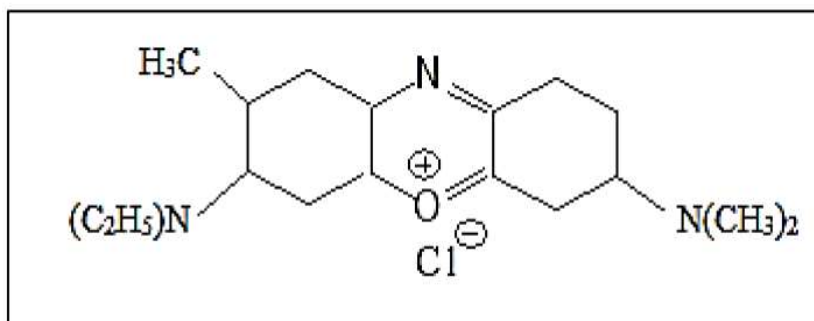


Figure I.6. Capri blue structure

c. Reactive dyes

Reactive dyes are the newest class of dyes. They owe them name to their method of attachment to the fiber. Their molecule contains a group chromophore and a reactive chemical function of triazine or vinylsulfone type ensuring the formation of a covalent bond with the fibers, they enter more and more frequently in the dyeing of cotton and possibly in that of wool and polyamides [25, 26].

I.2.5 Hazards of dyes:

Eutrophication: Under the action of microorganisms, dyes release nitrates and phosphates in the natural environment. These mineral ions introduced in too large a quantity can become toxic to fish life and affect the production of drinking water. Their consumption by aquatic plants accelerates their anarchic proliferation and leads to oxygen depletion by inhibiting photosynthesis in the most deep streams and stagnant water.

Under-oxygenation: When large loads of organic matter are added to the environment via occasional discharges, the natural regulatory processes can no longer compensate for bacterial oxygen consumption. Estimates that the degradation of 7 to 8 mg of organic matter by microorganisms is sufficient to consume the oxygen contained in liter of water [27].

Colour, turbidity, odour: The accumulation of organic matter in watercourses leads to the appearance of bad tastes, bacterial proliferation, pestilential odors and abnormal colours. Willmott et al [28] evaluated that a coloration could be perceived by the human eye from 5×10^{-6} g/L. Apart from the unsightly appearance, coloring agents have the ability to interfere with the transmission of light in water, thus blocking the photosynthesis of aquatic plants.

I.2.6: Methods of liquid effluent treatment

The treatment of textile waste, taking into account their heterogeneity of composition, will always lead to the design of a treatment chain ensuring the elimination of the various pollutants in successive stages. The first step is to eliminate the insoluble pollution by through pre-treatment (screening, grit removal, oil removal, etc.) and / or physical treatments or physicochemical ensuring a solid-liquid separation. Most depollution technics commonly involved in the second stage in the textile industries according to Barclay et al. as well as Buckley et al. [29, 30]. They are divided into three types:

a. Physical

- Precipitation methods (coagulation, flocculation and sedimentation),
- Adsorption,
- Reverse osmosis and filtration,
- Incineration

b. Chemical

- Oxidation (oxygen, ozone, oxidants such as NaOCl and H₂O₂),
- Reduction (Na₂S₂O₄),
- Compleximetric method,
- Ion exchange resin.

c. Biological

- Aerobic treatment,
- Anaerobic treatment.

I.2. HYBRID MATERIALS

I.2.1. Introduction

The nanoparticle includes the particles having size between 1 and 100 nm. These particles have different properties at their atomic level due to their size. This change in properties of nanoparticles is beneficial in many fields [31]. Nanotechnology is one of the most interesting fields for researchers since the last century. Numbers of developments have been made since then in the field of nanotechnology. Nanoparticles can be classified as metal nanoparticles, non-metal ceramic nanoparticles, semiconductor nanoparticles, and a well-known type is carbon nanoparticles [32]. Nanoparticles have those chemical and physical properties which makes them very different from that of the corresponding bulk materials due to their small size and large surface to volume ratio. They attract much attention because of their potential applications in many fields including optics, electronics, magnetism, ceramics, and catalysis [33].

I.2.2. Nanocomposites

Nanocomposites are those composites in which one phase has nanoscale morphology like nanoparticles, nanotubes, or lamellar nanostructure. They have multiphases, so are multiphase materials, at least one of the phases should have dimensions in the range of 10–100 nm. To overcome the limitation of different engineering materials now-a-days, nanocomposites are emerged to provide beneficial alternatives. Nanocomposites can be classified on the basis of their dispersed matrix and dispersed phase materials [34]. With the help of this rapidly expanding field, now-a-days, it has been possible to generate many exciting new materials with novel properties via innovative synthetic approaches. The properties of the so-called found not only depended on the properties of their originals, but also crucially on their interfacial and morphological characteristics. Of course, we cannot ignore the fact that sometimes it also happened that the newly generated property in the material is unknown to the parent constitute materials [35, 36]. Hence, the idea behind nanocomposite is to use building blocks with dimensions in nanometer range to design and create new materials with unprecedented flexibility and improvement in their physical properties.

I.2.2.1. Nanocomposite constituents

Composites are by definition materials made up of at least two phases: one continuous phase called matrix.

matrix which ensures the cohesion and the transfer of the constraints towards, the other phase called the reinforcement so because its presence allows in general to increase their mechanical properties (rigidity, resistance to breakage, hardness, ...) and to improve physical properties, such as behavior to fire and abrasion, temperature resistance (conservation of mechanical characteristics at high temperature) or electrical properties.

In addition to the high properties, they provide the characteristics sought in are low density, compatibility with matrices and ease of processing. [37].

I.2.3. Types of nanocomposites

Nanocomposite materials can be classified in the following way based on the presence or absence of polymeric material in the composite.

The nanocomposites in which the compositions do not contain any polymers or polymer-derived materials are called non-polymer-based nanocomposites (Figure I.7). Non-polymer-based nanocomposites are also known as inorganic nanocomposites. They can be further classified into metal-based nanocomposites, ceramic-based nanocomposites, and ceramic-ceramic-based nanocomposites [38].

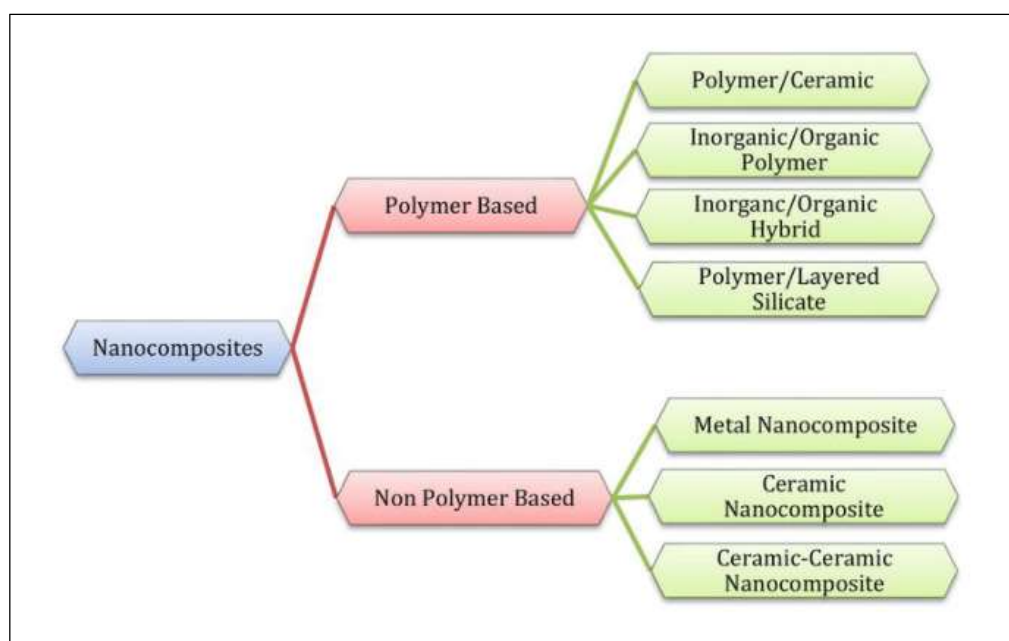


Figure I.7. Classification of polymer- and non-polymer-based nanocomposites.

I.2.3.1. Polymer-based nanocomposites

The polymer or co-polymer, which contains nanoparticles or nanofillers dispersed in the polymer matrix is termed as poly nanocomposites. One dimension (1D) must be lying in the range of 1–50 nm and these possess several shapes like as platelets, fibers, spheroids, etc. Poly nanocomposites are in the category of multiphase systems such as, MPS namely composites, blends, and foams, which can absorb about 95% of the production of plastics. So these systems need controlled mixing, the achieved dispersion should be stable, dispersed phase should be oriented, and the compounding strategies which are involved for all MPS, which includes poly nanocomposites (PNC) is almost the same [39].

Polymer nanocomposites are proposed as a class of materials with unique properties but, the most challenging property of PNCs is the complex interfacial areas in between the polymer matrices because of this small scale large specific area is created that highlights the importance of polymer-nanoparticle interactions. So to achieve properties, such as, mechanical, thermal, optical, and electric, we need to analyze the intercalation process among the nanoparticles and polymer bases [40].

Polymer nanocomposites are known to be a class of reinforced polymer with a very low, i.e., less than about 5% of nanometric clay particles. These substances gained huge attention simultaneously from both the academic institution as well as from industrial sectors commonly in the area of nanocomposites. This is actually due to their drastically enhanced or improved thermal, mechanical as well as the barrier properties as compared to the micro- and also the conventional composites. These materials can be differentiated notably by improved fire resistance and thermal stability, improved barrier properties, and increased recyclability [41].

However, despite of having so many advantages, it is still very much difficult to prepare a uniform dispersion between the filler and the matrix, as shown in Figure.I.8. Hence, unlikely, it reflects the lower mechanical as well as thermal properties in the produced nanocomposites.

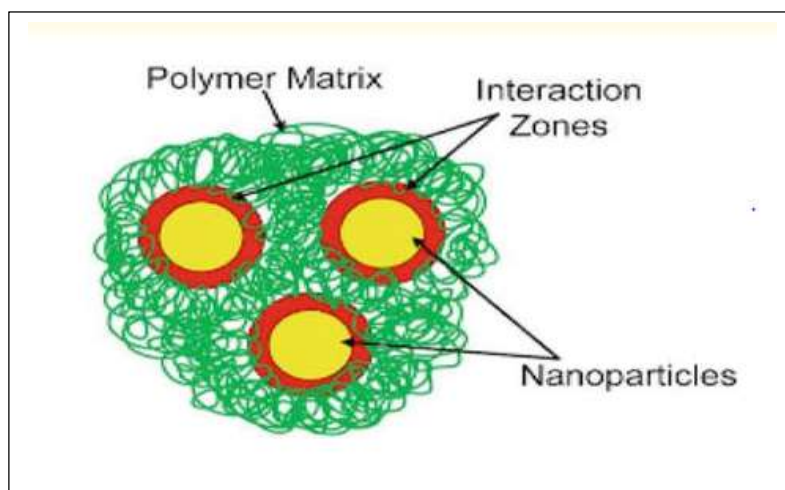


Figure I.8. Uniform dispersion between the filler and matrix in nanocomposites.

I.2.3.1.1. Different types of polymer nanocomposites

Many nanocomposites are made from a polymer in which nanoparticles have been dispersed. Indeed, the incorporation of nanofillers within polymer materials makes it possible to modify their mechanical [42], thermal [43, 44], electrical [45] or magnetic [46] properties and thus widen their domain of application Table I.1 lists the nanocomposites according to their nature and the form of the nanofillers used as reinforcements in the polymers.

Table I.1 different types of nanoparticles used in polymer nanocomposites

| Nature of nanocharge | Form | Examples |
|-----------------------|--------------------------------|---|
| Inorganic | Spheres Fibers Platelets | Preformed silica [47]. Metal oxides, carbonate [48]. Calcium [49]. Sepiolite [50], Potassium titanate [51], Lamellar silicates[52]. |
| Metallic | Spheres | Magnetite [53], Gold particles [54]. |
| Carbon-based compound | Spheres Fibers Platelets | Carbon black [55]. Nanotubes [56], Cellulose [57], Graphene [58] Graphite [59] |

I.2.3.1.1.a. Polymeric Nanocomposites based on inorganic materials.

Polymer composites made up of inorganic nanoparticles and organic polymers represent a new class of materials that have more performance properties compared to their microparticle counterparts [60]. Inorganic particles provide mechanical and thermal stability and new functionalities, which depend on the chemical nature, structure, size and crystallinity of inorganic nanoparticles (silica, oxides of transition metals, nanocells, metal phosphates, metal chalcogenides and nanometallic). Inorganic particles provide better mechanical, thermal, magnetic, electronic and optical properties [61]. Various processes are used for the preparation of inorganic nanocomposites based on polymers. The most important are:

- I. Molten intercalation.
- II. Direct mixing of polymers and particles.
- III. Chemical synthesis.
- IV. In situ polymerization.
- V. Sol-gel process.

I.2.3.1.1.b. Polymeric Nanocomposites based on metallic materials

Metal/polymer nanocomposite materials combine properties of several components.

Nowadays, they are regarded as promising systems for advanced functional applications [62].

Therefore, the incorporation of nanoparticles metal in the polymer has paved the way for a generation of materials having electrical, optical or mechanical unique that make them attractive for applications in areas such as optics, [63] the photoimaging and modeling [64], sensor design [65], catalysis [66] and antimicrobial coatings [67]. The search for new methods preparing metallic nanocomposite materials has been greatly stimulated due to their attractive properties and promising applications. One of the main interests of metallic nanoparticles is their unique physical properties which can be adapted by chemical control of their shape and size [68]. Among these, nanoscale gold and silver play a primary role because these nanoparticles exhibit a very intense absorption band in the visible region due to their surface plasmon resonance. Metal / polymer nanocomposites can be prepared by two approaches:

I. The first involves a dispersion of metallic nanoparticles in a polymerizable formulation, or in a polymer matrix. In this case, the reduction of the metal ions and the polymerization occur successively, hence the aggregation of the nanoparticles, which makes this synthesis procedure often problematic.

II. In the second approach, the nanoparticles are generated in situ during polymerization to avoid agglomeration. The polymerization reaction and the synthesis of nanoparticles which take place simultaneously have been the subject of in-depth studies.

Another technique consists of polymerizing the matrix around a metallic nanocore using chemically compatible ligands [69] or polymeric structures [70].

I.2.3.1.1.c. Polymeric carbon-based nanocomposites

Carbon nanofillers such as nanotubes and graphene exhibit excellent properties due to their high mechanical strength and high aspect ratio. Graphene and its polymer nanocomposite derivatives have demonstrated immense potential applications in electronics, aerospace, automotive, defense industries and green energy thanks to their exceptional reinforcement in composites. To take full advantage of its properties, the integration of individual graphene into polymer matrices is essential. Compared to carbon nanotubes, graphene has a higher surface area to volume ratio, which makes it potentially more favorable for improving mechanical, electrical, thermal, gas permeability and microwave absorption properties [71]. The nanotubes of carbon (CNT) are considered unique elements promoting the development of various polymer composites because of their unique properties such as high electrical conductivity ($\sim 10^6 \text{ s.m}^{-1}$), the improved resistance to traction (50 GPA) and low density. These characteristics make them useful in a wide range of industrial applications [72].

There are three main mechanisms of interaction of the polymer matrix with carbon:

- a. Micro-mechanical interconnection.
- b. Chemical bond between the nanotubes and the matrix.
- c. Poor van der Waals adhesion between filler and matrix.

I.2.3.1.2. Synthesis of Hybrid Nanocomposites

To endow polymer nanocomposites with new properties, synthetic methods that have an effect on the control of particle size distribution, dispersion and interfacial interactions are essential. Synthesis techniques for nanocomposites are different from those for conventional composites. The development of nanocomposites polymers is difficult because of the physicochemical differences between systems. Each polymer system may require a set of processing conditions and different synthetic techniques, which in general give non-equivalent results; considerable research has been done to develop suitable synthetic techniques for making good polymer nanocomposites [73].

The methods for producing polymer nanocomposites are all based on a first step of dispersing the nanoparticles in a liquid, however they differ by the type of organic phase [74] and by the subsequent treatment to be carried out: heat treatment, elimination of any solvent. .

The nanopowders are mainly metals, semiconductors, or metal oxides. This section mainly studies how to form nanocomposites with metal oxides and polymers. Generally, there are three preparation methods for synthesizing polymer / metal oxide nanocomposites (Figure 1.9). The first is the direct (solution mixing). The second is a sol-gel process, which begins with the association of molecular precursors at room temperature, then the formation of a metal oxide by hydrolysis and condensation. The third is the in-situ polymerization of monomers in the presence of metal oxide nanoparticles. [75]

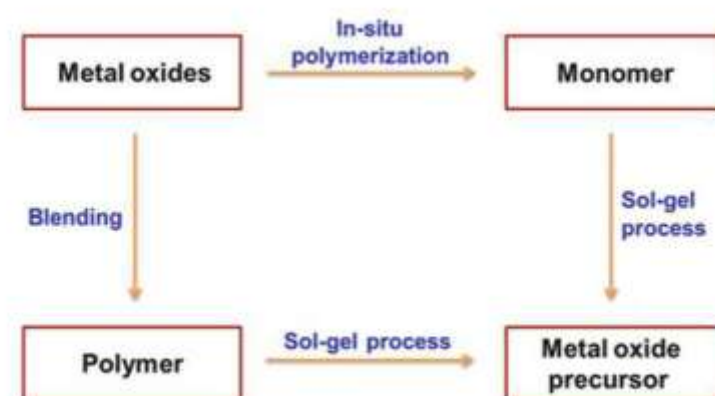


Figure I.9. Methods for synthesizing polymer/metal nanocomposites

1. Direct mixing

Direct mixing is the simplest method of preparing polymer / metal oxide nanocomposites. This ex-situ method is popular because it does not limit the nature of the nanoparticles and host polymers used. Depending on the conditions, the mixture can normally be divided into molten mixture and solution mixture. The main difficulty in the direct mixing process is always the efficient dispersion of the nanoparticles in the polymer matrix because the latter tend to agglomerate.

a. Molten mixtures

One of the conventional techniques for preparing polymer composites is to disperse particles in a polymer, generally a thermoplastic, in the molten state. The dispersion of the particles is improved if they are functionalized by organic molecules whose chemical nature is compatible with that of the polymer. Currently, this process is used for a wide range of materials such as metal oxides and carbon nanotubes.

Molten blending is the fastest method to introduce new nanocomposites to the market since it can take full advantage of well-constructed polymer processing equipment, including extruders or injectors.

Although the processing conditions of the polymers are optimized to obtain a good uniform dispersion of the metal oxide nanoparticles in the polymer matrix, the surface characterization indicates the clustering of the nanoparticles. Agglomeration has been attributed to particle interactions mediated by steric forces in the polymer matrix. On the other hand, mixing polymers and nanoparticles of metal oxides to produce nanoparticles that are homogeneous and well dispersed in the polymer poses significant challenges.

Despite the aforementioned advantages of melt blending, polymer degradation could be a significant problem that should not be overlooked. Since a certain elevated temperature is normally required during melt mixing, the polymer matrix and the compatibilizer can degrade the organic surfactant, which can lead to a significant decrease in the mechanical properties of the final products.

b. Mixing of solutions

This method consists in dispersing nanoparticles in a polymer solution using a suitable solvent, then in evaporating this solvent to form nanocomposite films or sheets.

The advantages of solution mixing include the thorough mixing of the inorganic filler with the polymer in a solvent, which facilitates the disintegration and dispersion of nanoparticles from the filler.

This method consists of three steps: dispersion of the nanoparticles in an appropriate solvent, mixing with the polymer (at room temperature or high temperature), and recovery of the nanocomposite by precipitation or casting of a film.

In this process, the dispersion of the nanoparticles can be obtained by magnetic stirring, mixing by shearing, reflux or, most often, by ultra-sonication.

Solution mixing can overcome some of the limitations of melt mixing if the polymer and nanoparticles are both dissolved or dispersed in solution. On the other hand, for industrial applications, melt processing is the preferred choice due to its low cost and simplicity for large scale production for commercial applications.

II. Sol-Gel treatment

Several approaches have been developed to improve the compatibility between organic and inorganic components. Among the many methods under development, the sol-gel route has been widely applied due to its ability to control miscibility between organic and inorganic components at the molecular level. The term sol-gel is associated with two reaction steps: sol and gel. A sol is a colloidal suspension of solid particles in the liquid phase and a gel is the interconnected network formed between the phases.

The nanocomposites organo -inorganiques are normally prepared by the sol-gel method in the solvent containing precursors and organic polymers. The most direct route is to hydrolyze and condense the precursors in the presence of a polymer in a solvent system.

Materials prepared by sol-gel treatment have uniformity, high purity, and low sintering temperatures compared to those prepared by conventional solid state reactions. Sol-gel materials are

classified by the mode of formation and the types of bonds between the components: organic, organometallic and inorganic.

The most important problem associated with the sol-gel process is that the gelation process leads to a considerable decrease in internal stress, which can lead to contraction of fragile materials due to the evaporation of solvents, small molecules and water. In addition, the precursors are expensive and sometimes toxic, preventing further improvement and application.

III. In-situ polymerization

The nanometric particles are dispersed in the solution of the monomers and the resulting mixture is polymerized by simple polymerization methods. The advantage of this method is the possibility of grafting the polymer onto the surface of the particles. The key to in situ polymerization is proper dispersion of the particles in the monomer. This often requires modification of the particle surface, because although dispersing is easier in a liquid than in a viscous molten bath, the settling process is also faster. [76]

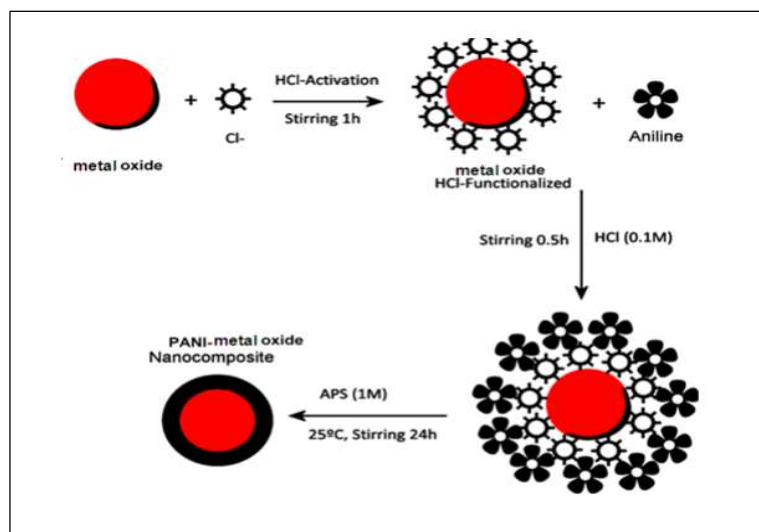


Figure I.10. Synthesis of PANI nanocomposite by in situ polymerization

1.2.4. Conductive polymers

The discovery of conducting polymers dates back in the 1970s when a student of a Japanese professor Shirakawa, made a mistake by putting too much catalyst in the polymerization of acetylene. This resulted in the formation of a silvery film instead of a black powder. When MacDiarmid heard about this, he invited Shirakawa to his laboratory at the University of Pennsylvania. They tried to modify the polyacetylene by oxidation with iodine vapor, which changed the optical properties of the material. They asked Heeger to have a look at the conductivity and he found that the conductivity has increased ten million times [77]. The discovery by these professors was considered a major breakthrough in science; this earned them a noble prize in Chemistry in 2000. Since then the field has grown immensely, and given rise to many new and exciting applications. The conducting polymers have conjugated double bonds in their backbone. There are many different types of conducting polymers. Figure.I.11 below shows the most common conducting polymers [78].

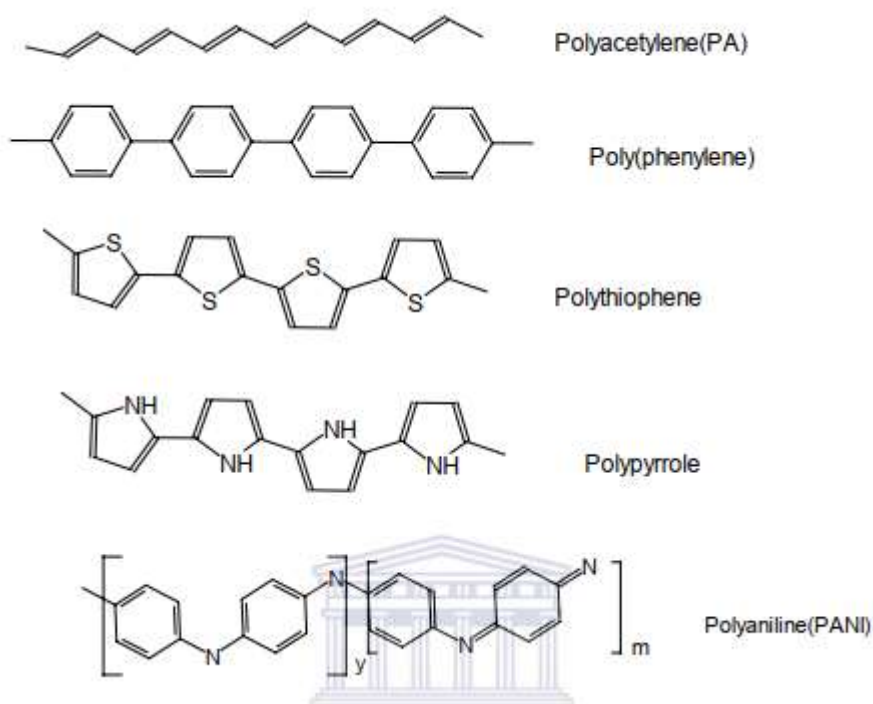



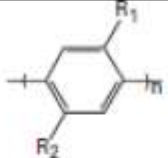
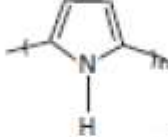
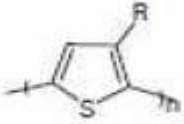
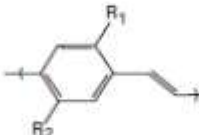
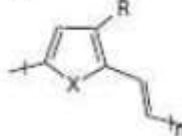
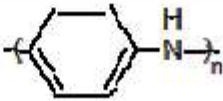
Figure I.11. Some examples of conducting polymers

I. 2.4.1. Classification of conductive polymers

Conductive polymers belong to the family of π -conjugated polymers. These polymers are characterized by an alternating structure of single bonds (σ type) and double bonds (π -type) in their carbon chains, allowing the delocalization of π electrons along the macromolecule. Conductive polymers can be classified according to the structure of their carbon chain into different families [79].

- Polyene polymers whose carbon chain is linear, such as polyacetylene (PA).
- Heterocyclic aromatic polymers whose chain contains aromatic heterocycles such as polyparaphenylene (PPP) and its derivatives, polypyrrole (PPy), polythiophene (PT) and its derivatives or polyethylene dioxythiophene (PEDOT).
- Mixed polymers whose chains alternate heterocycles and double bonds, such as polyphenylene vinylene and its derivatives (PPV) and polyheteroarylene vinylene and its derivatives (PTV).
- Aromatic polymers with heteroatoms whose chain is formed of aromatic rings containing heteroatoms such as polyparaphenylene sulfide (PPS) and Polyaniline (PANI) (Table I. 2).

Table I. 2. The main families of conductive polymers

| Family | Example of polymer |
|--|--|
| The polymers polyene | Polyacetylene  |
| The polymers aromatic heterocyclic | <p>polyparaphenylene </p> <p>Polypyrrole </p> <p>Polythiophene </p> |
| The polymers mixed | <p>Polyphenylene vinylene </p> <p>Polyheteroarylene vinylene </p> |
| The polymers aromatic with heteroatoms | Polyaniline  |

The conductivity of a material generally depends on the density of charge carriers and their mobility. In the case of metals, the charge carriers are electrons, while in conductive polymers, electrons as well as holes are able to move freely generating a current.

Conductivity also varies with temperature; it decreases with increasing temperature for metals [80], while it increases for conductive polymers [81]. The conductivity of the latter can be controlled by doping (Figure I. 12). It can evolve from an insulating state $\sigma < 10^{-10} \text{ S.cm}^{-1}$, to that of a semiconductor $\sigma \sim 10^{-5} \text{ S.cm}^{-1}$, to that of a conductor $> 10^5 \text{ S.cm}^{-1}$ [82].

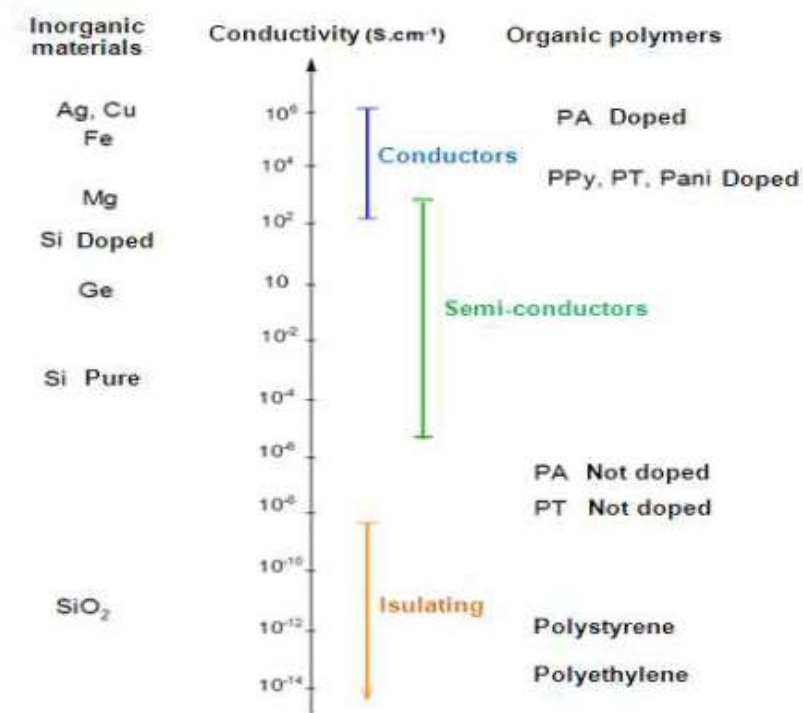


Figure I. 12. Electrical conductivity of intrinsic conductive polymers

I. 2.4.2. Electronic structure of conductive polymers

In the case of conductive polymers, electronic conduction and the transport of charges cause the creation of free charge carriers along the polymer chain. Their electronic structure depends on band theory, originally designed to interpret conduction in semiconductors.

In a semiconductor, the energy bands correspond to the energy levels that are allowed, or prohibited, for the electrons of the elements or compounds that make up the material. The last band filled is called the BV valence band or HOMO (High Occupied Molecular Orbitals) and the next higher band is the BC or LUMO (Lowest Unoccupied Molecular Orbitals) conduction band. The energy band between these two levels corresponds to the forbidden band or the Fermi energy or more simply "gap".

The energy difference E_g between these two levels ($E_g = E_{BC} - E_{BV}$), of the order of an electronvolt (eV), constitutes the width of the gap which determines the intrinsic electrical properties

of the material [83]. The position of the energy bands for a metal, a semiconductor and an insulator, is shown schematically in figure I. 13.

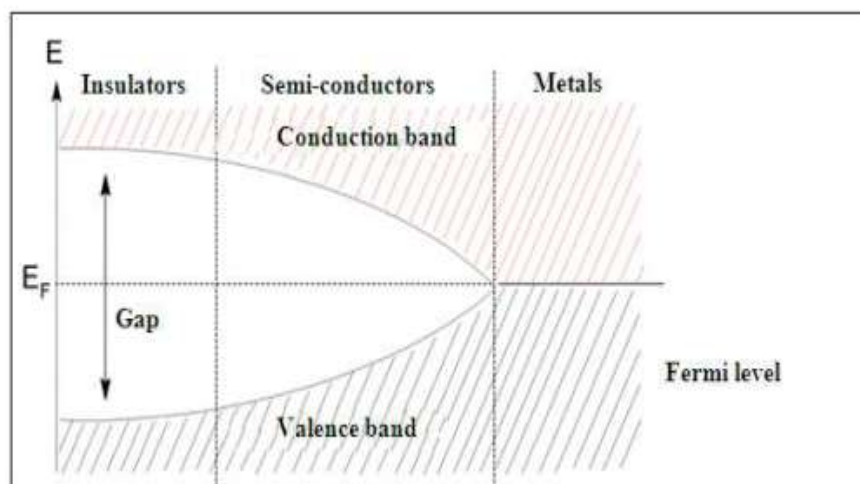


Figure I. 13. Theoretical diagram established according to the theory of energy bands

The undoped π -conjugated polymers are semiconductors or even insulators in the neutral state. Their electronic conductivity σ is of the order of $10^2 - 10^{-8} \text{ S.cm}^{-1}$. Table I. 3 groups together the gaps of the most studied conjugated polymers.

Table I.3. Gap of the main families of conjugated polymers [84]

| Conjugated polymer | Gap (eV) | Conjugated polymer | Gap (eV) |
|--------------------|-----------|--------------------|----------|
| PPP | 2.7 | Trans-PA | 1.4 -1.5 |
| PPV | 2.5 -2.7 | Pani-EB | 1.4 |
| PPY | 3.2 | Pani-PNGP | 1.8 -2.0 |
| PT | 2.0 - 2.1 | Pani-LEB | 3.8 |

I. 2.4.3. Doping of conductive polymers

Conductive polymers in the neutral or reduced state are insulators. Through a process called doping, they are transformed into conductive materials by the introduction of mobile charge carriers. The term doping is adopted from solid-state physics by analogy to the doping of inorganic semiconductors. However, the doping of conductive polymers is totally different from that of inorganic semiconductors.

In fact, the doping of polymers is a chemical reaction to increase the conductivity of the polymer to reach values close to that of metals (Figure I. 16).

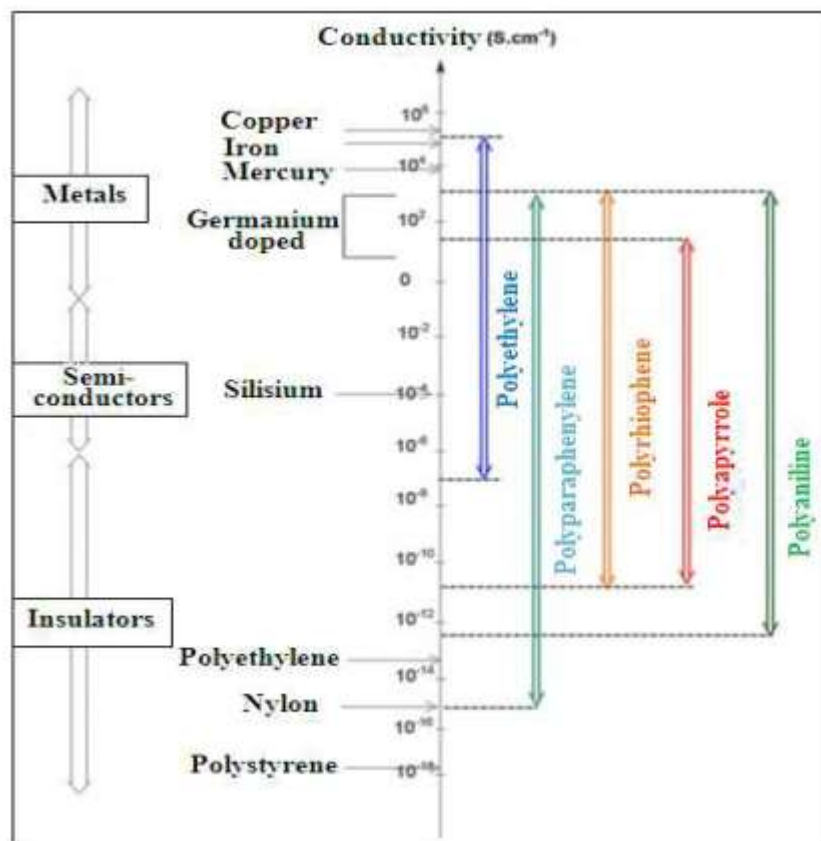


Figure I. 14. Conductivity of various conductive polymers and conventional materials

Generally, this doping is carried out by an oxidation-reduction reaction which consists in introducing donor species: n-type doping (reduction of the polymer) or acceptors of electrons: p-type doping (polymer oxidation). These species are called dopants or counter ions, which ensure the electroneutrality of the material. Electric charges are then created on the polymer chains. The increase in the doping rate makes it possible to witness an insulator-conductor transition [85].

1.2.4.4. Load carriers

Electronic conduction in the case of conductive polymers and the transport of charges in general first require the possibility of creating free charge carriers. Indeed, during the injection of a charge into a polymeric backbone, a charge defect is created, accompanied by a local modification of the geometry of the chain. As seen previously, energy states are then created in the gap due to the shift of the valence band and the conduction band [86].

Conjugated polymers are classified into two categories according to the symmetry of their ground state. The degenerate ground state where several different forms of the same polymer have the same energy (case of polyacetylene). The non-degenerate ground state where the permutation leads to a different energy structure, possibly several forms associated with local energy minima, but only one form is associated with the general minimum (case of polythiophene).

The introduction of charges by doping these polymers leads to the formation of charge carriers on the macromolecular chain. These charges formed are called solitons for polymers in the degenerate ground state and polaron or bipolaron for polymers in the non-degenerate ground state [87].

1.2.5. POLYANILINE (PANI)

Owing to its high conductivity, environmental stability and low cost of production, polyaniline (PANI) has been the subject of much investigation compared to other conducting polymers. PANI can be synthesized electrochemically or chemically by using an appropriate oxidant in an acidic medium. There are three forms of PANI, fully oxidized pernigraniline, half-oxidized emeraldine base (EB), and fully reduced leucoemeraldine base (LB) [88, 89]. Emeraldine is the most stable form of PANI and it is the most conductive form when it is doped (emeraldine salt).

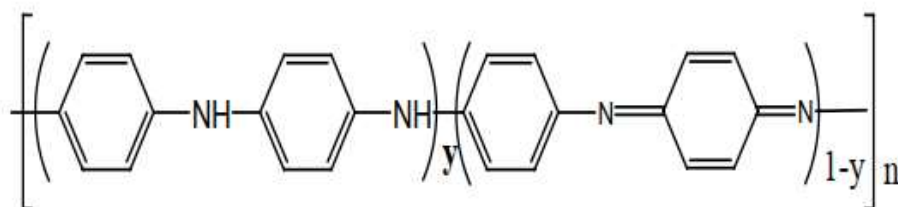


Figure I.15. General structure of polyaniline.

PANI has many potential applications, in nanowires, electronics, electrochromic devices, batteries [90-91], etc., but all these applications are limited by the difficulty to process PANI. PANI itself is difficult to process; it does not dissolve in common solvent and it decomposes before melting. Many studies have been done in an effort to make PANI processable such as addition of side chain to the monomer aniline or doping with bulky dopants to make PANI soluble [92]. The problem with these bulky dopants was the solvent toxicity and difficult preparation [93].

Another way to overcome the problem of processability is to prepare its nanocomposites or nanotubes/rods. Polyaniline has been used in many cases for synthesis of nanocomposites and nanotubes/rods by using clay, transitional metals oxides such as titanium oxide (TiO_2), vanadium oxide (V_2O_5), tin oxide [94-95] etc. These nanocomposites can be prepared chemically or electrochemically. The potential of polyaniline transitional metals nanocomposites have introduced these materials into applications such as electronic devices, non-linear optical systems and photo electrochemical systems [84]. It is believed that the combination of n-type semiconductor of transitional metals and p-type of PANI is responsible for the improvement in the polyaniline photo current values due to the occurrence of excitons dissociation at the interface.

1.2.5.1. Doping of polyaniline

For a polymer to be electrically conductive it must behave like a metal, that is, it must have free electrons that are mobile. The basic requirement is that the material must have conjugated double bonds, in addition, the electrons must be disturbed- by removing electrons (oxidation) or by inserting one (reduction). This process is called doping.

Doping is reversible with little or no degradation of the polymer backbone. During this process the polymer, which is an insulator or semiconductor, is converted to metallic polymer, which is conductive. The conductivity can be increased up to 100 fold by this process of doping. Whether the polymer is doped chemically or electrochemically, the doping can be divided into two: p-doping (oxidation) and n-doping (reduction)

p- type of doping is the partial oxidation of the polymer π backbone [96]. This was discovered by treating the polyacetylene with iodine (the oxidizing agent). In the p-type doping the electron is removed from the polymer backbone as described above. n-type doping is the partial reduction of the polymer π backbone. It was also discovered when polyacetylene was treated with reducing agent (liquid sodium). Like in the oxidation, the electron is inserted in the π backbone and the polymer

becomes negatively charged. The negative ion will move along the polymer backbone with the help of solitons.

Doping is reversible with little or no degradation of the polymer backbone.

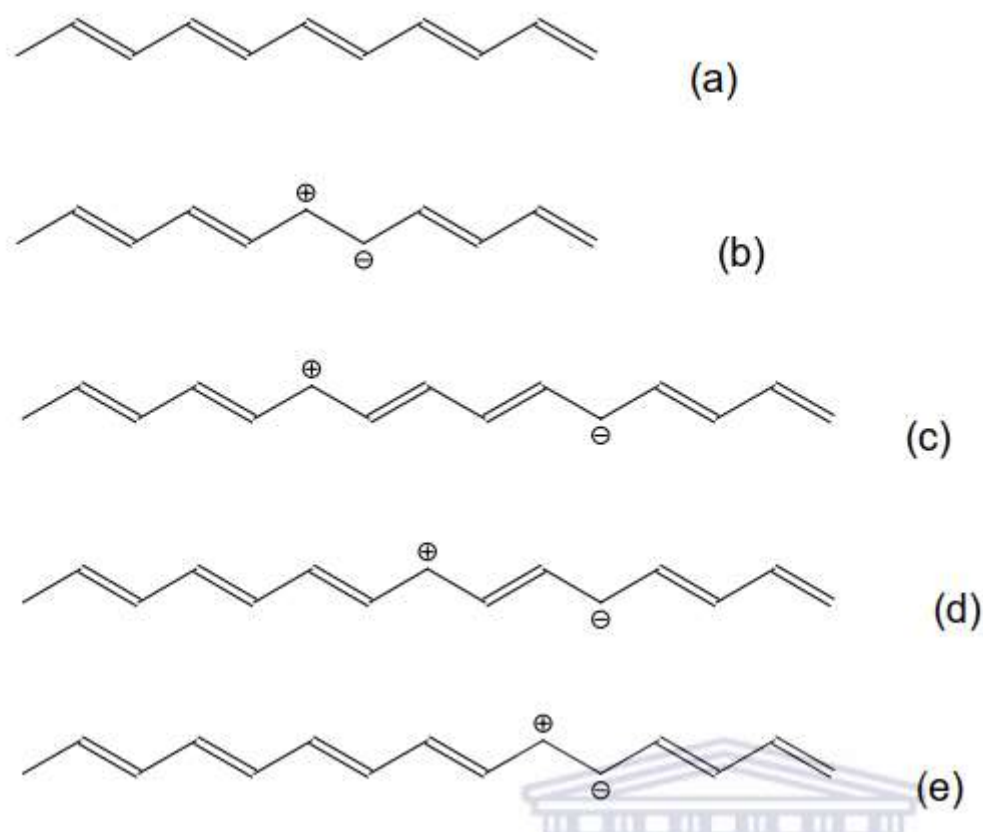


Figure. 1.16. Schematic representation of movement of charge along the polymer backbone.

When the polymer is oxidized, the oxidizing agent attracts an electron from the polymer chain [97]. The polymer will now become positively charged, this is termed radical cation or polaron. The lone electron of the polymer double bond, from which an electron was removed, can move easily. As a consequence the double bond successively moves along the molecule. When the polymer chain is strongly oxidized the polarons condense pair-wise into so-called solitons. These solitons are responsible for charge transport along the polymer backbone.

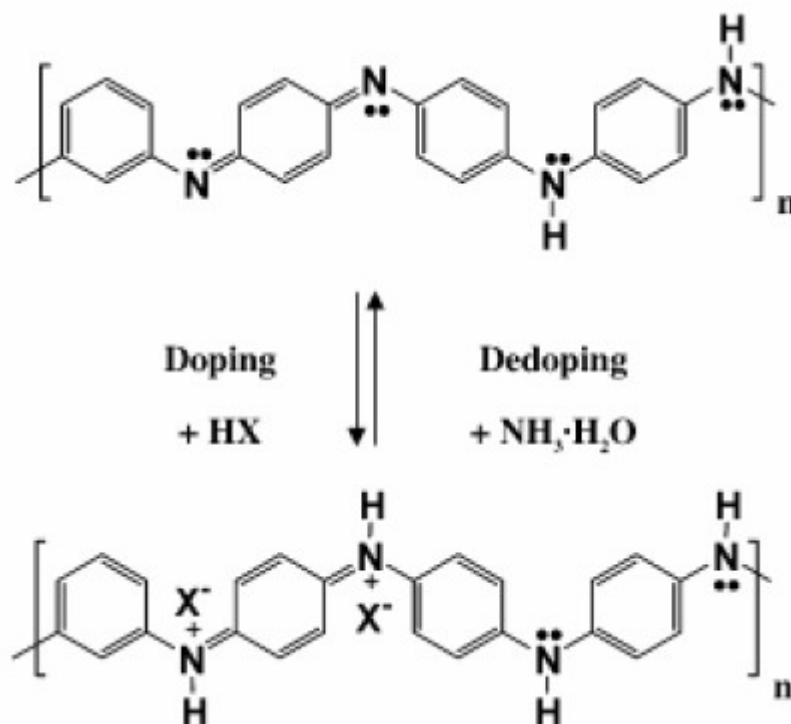


Figure 1.17. Doping and dedoping of PANI

I.2.5.2. Synthesis of Polyaniline

Various synthetic methods have been developed for the production of Polyaniline. There are physical methods such as electrospinning [98], lithography [99], spincoating [91] and pulsed plasma irradiation [92], but also chemical methods using a template or "template", with hard templates called "hard template" [93] or with flexible templates called "soft template" [94-96], or also without the use of a template (template-free method); for example polymerization without stirring [97], mechanochemical synthesis [98] and electrochemical synthesis (cyclic voltammetry [99], potentiostatic [100] and galvanostatic [101] mode).

As part of our work, we have chosen to synthesize Polyaniline by the oxidative chemical polymerization of aniline (C₆H₅)NH₂ by an oxidizing agent. This synthetic route was developed by MacDiarmid et al in 1985 [102]. It has the advantage of being simple and often used to synthesize PANI.

Several studies have shown that various experimental parameters influence the properties of the polymer obtained. These parameters can be classified in a hierarchical order according to their importance: the nature of the oxidant, the oxidant / monomer molar ratio, the polymerization time and the nature of the dopant:

- The nature of the oxidant

The standard synthesis procedure is carried out with ammonium persulfate $(\text{NH}_4)_2\text{S}_2\text{O}_8$ (APS) as an oxidant. However, the choice of the oxidizing must satisfy two criteria: its ability to oxidize aniline ($E_{\text{oxidant}} > E_{\text{aniline}}$) and its stability in the reaction medium. MacDiarmid et al [103] synthesized PANI in an acidic aqueous medium (HCl) in the presence of aniline by adding a solution of $(\text{NH}_4)_2\text{S}_2\text{O}_8$ ($E^\circ (\text{SO}_4^{2-}/\text{SO}_5^{2-}) = 1760 \text{ mV/ECS}$). Many oxidizing agents were then used such as KIO_3 , KMnO_4 , FeCl_3 , K_2CrO_4 , KBrO_3 , etc. The only condition is to avoid any chemical degradation (iodination, chlorination, decomposition following crosslinking reactions chemicals...) caused by the oxidant during its reaction with the monomer, such as the example of hydrogen peroxide H_2O_2 ($E^\circ (\text{H}_2\text{O}_2/\text{H}_2\text{O}) = 1530 \text{ mV/ECS}$) [104].

- The oxidant / monomer molar ratio

Another parameter of the synthesis which influences the properties of the polymer obtained is the oxidant / aniline ratio. Pron et al [105] suggested using a normalized ratio which is defined by

$$K_N = 2.5 \frac{n_{\text{aniline}}}{n_{\text{oxydant}} n_e}$$

n_{aniline} = mole's number of aniline

n_{oxydant} = number of moles of oxidant oxidizing

n_e = number of electrons needed to reduce an oxidant molecule

For a polymerization reaction where PANI is obtained in its emeraldine form, each monomer must remove on average 2.5 electrons. In the case of ammonium peroxodisulphate, the K_N ratio is equal to 1.25 due to the electronic nature of the couple $(\text{S}_2\text{O}_8)^{2-}/(\text{SO}_4^{2-})$.

- The time of polymerization

The time of the synthesis reaction plays an important role in the formation of polyaniline. Studies by Cao et al [106]. and Gospodnova et al [107]. demonstrated the existence of two competitive mechanisms during the preparation of the polymer:

polymerization and degradation of the molecular chain at quinone diimines sites. The latter was found to increase with increasing synthesis time (greater than 4 hours for the standard procedure).

- The nature of the dopant

The standard procedure uses hydrochloric acid (HCl) as a dopant [108, 110]. The conductive powder PANI (HCl), once compacted in the form of a pellet reveals an electrical conductivity of the order of 1 to 20 S.cm⁻¹. Many dopants were then used by various researchers :

- Mineral acids: sulfuric acid (H₂SO₄) [111], hydrofluoric acid (HF) [112], perchloric acid (HClO₄) [113].

- Organic acids: formic acid, acetic acid, acrylic acid [114].

- Sulfonic acids: camphor sulfonic acid (CSA) [115-117], methanesulfonic acid (MeSA) [118], p-toluenesulfonic acid (PTSA) [119], dodecyl benzenesulfonic acid (DBSA) [120]

- Les acides phtaliques [121]

1.2.5.3. Polymerization mechanism

Even if many teams have been interested in the polymerization mechanism of aniline [122-124], these mechanisms remain to this poorly known day. The acidity of the reaction medium increases during the polymerization of the aniline because protons are produced during the reaction. Even when the reaction is carried out under alkaline or weakly acidic conditions, i.e. under conditions where the aniline is essentially unprotonated (pH > pK_a of aniline = 4.6), the proportion of anilinium cation can increase sharply during the reaction. Aniline oxidizes more easily than the anilinium cation. Thus, the oxidation of anilinium sulfate occurs slowly in the first moments. The oxidation of aniline is rapid and generates a significant exotherm in the first moments when the polymerization starts in a

weakly acidic, neutral or alkaline medium, then, when the pH reaches the value of 3.5, the reaction slows down considerably because the aniline is then essentially protonated. The reaction remains slow in the pH range 2.5-3.5. In this pH range, chain growth occurs by oxidation of $C_6H_5NH^{+3}/C_6H_5NH_2$ by non-protonated oligoaniline pernigraniline chains. At around pH 2-2.5, the reaction accelerates due to the protonation of pernigraniline. This is because the oxidizing power of protonated pernigraniline is much stronger than that of non-protonated pernigraniline. Stejskal's team recently proposed a mechanism for the oxidation of anilinium sulfate and aniline by ammonium persulfate (APS) in aqueous solution [125, 127]

(Figure I.18) . Polymerization of anilinium sulfate and aniline leads to para-linked trimers and tetramers by N-C bonds. The nitrenium cation of aniline is the main electrophile formed

during the priming step. It should be emphasized that the dimer formed is predominantly 4-aminodiphenylamine (4-ADPA). In an acidic medium, the electrophilic substitution of the anilinium cation with the nitrenium cation should preferably take place in the meta position and lead to 3-aminodiphenylamine. Thus, despite the low proportion of aniline in an acidic medium, the markedly higher reactivity of aniline compared to the anilinium cation leads to the predominant 4-ADPA dimer. 4-ADPA is rapidly oxidized by peroxydisulfate to give N-phenyl-1,4-benzoquinonediimine (PBQI). Another reaction path for the oxidation of aniline results in the formation of substituted phenazines such as pseudomauvein, by ortho N-C coupling. The formation of these substituted phenazines is limited in an acidic medium ($pH < 2.5$). The self-assembly of these phenazine units leads to the formation of particular morphologies for the polyaniline such as nanofibers, nanotubes, or nanospheres.

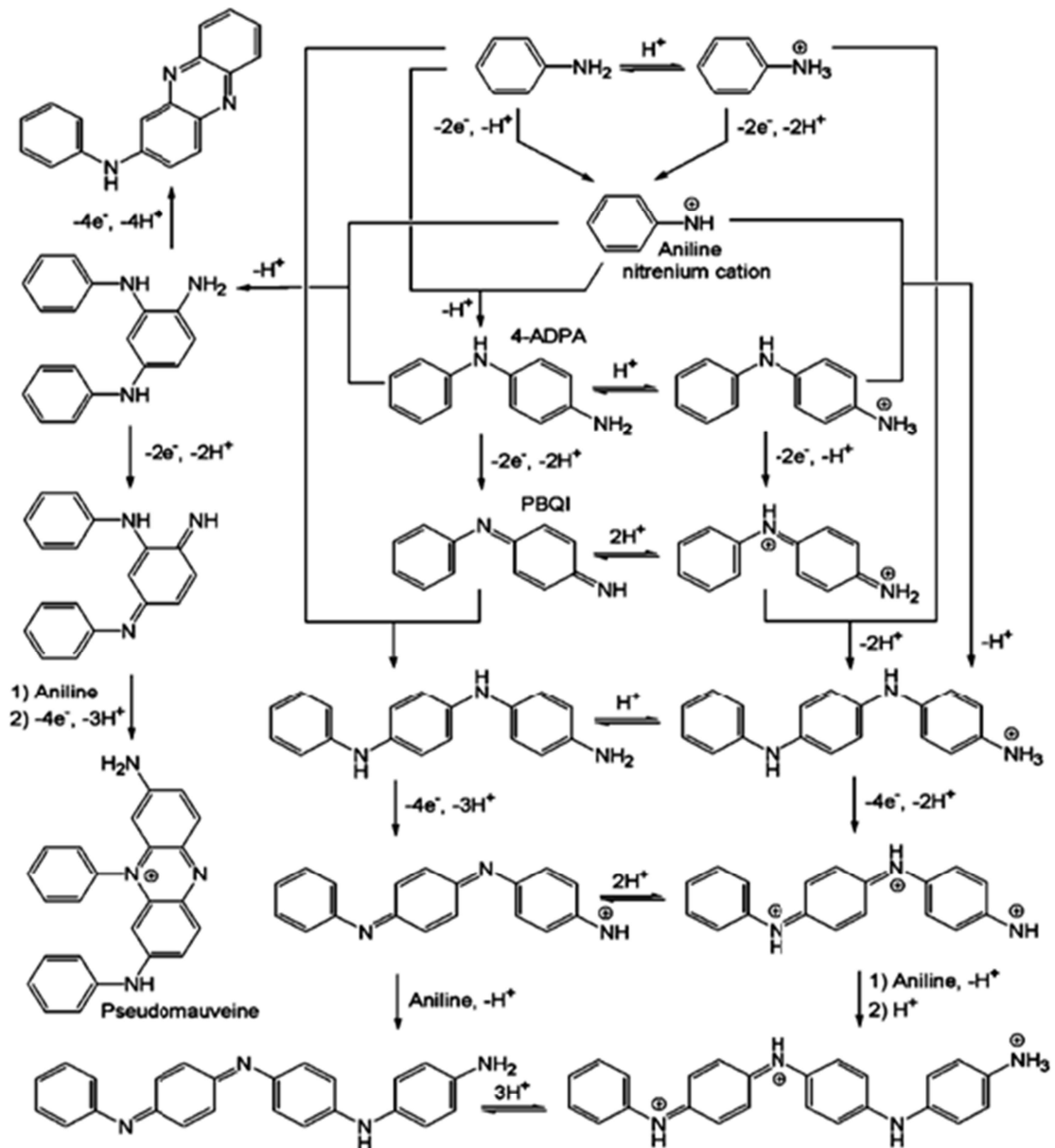


Figure I.18. First steps in the oxidation of aniline and anilinium cations by APS in acidic HCl

[128]

1.2.5.4. Factors influencing the electrical conductivity of polyaniline

The overall conductivity (σ) of PANI is the sum of the intra-molecular (intra), inter-molecular (inter) and inter-domain (domain) conductivities (Equation 1.1).

$$\sigma = \sigma_{\text{intra}} + \sigma_{\text{inter}} + \sigma_{\text{domain}} \quad (\text{Equation 1.1})$$

Intra-molecular charge transfer depends on the well-defined band structure specific to the polymer. Any defect in the structure can lead to a decrease in intramolecular (intra) conductivity. Inter-domain (domain) conductivity is associated with clusters of organized polymer chains trapped in an insulating matrix, the movement of charge carriers from one crystalline region to another crystalline region or between a crystalline region and an amorphous region. The four main factors that influence the conductivity of PANI are:

- (1) molecular mass, (2) rate of crystallinity and inter-chain distance, (3) level of oxidation and molecular arrangement, (4) the doping rate and the type of dopant [129-131].

Thus, a chain distortion observed at high molar masses leads to a decrease in electrical conductivity [132-134]. It is generally accepted that the intra-molecular mobility of charged species along the chain, and to some extent the inter-molecular jump of charge carriers, increases with increasing rate of crystallinity. This leads to an increase in conductivity. Moreover, a decrease in the inter-chain distance increases the possibility of inter-chain jump of the charge carriers and therefore leads to an increase in conductivity [135-137]. A 50% doping rate of the emeraldine base form leads to maximum conductivity because it leads to an ideal polaron structure. On the other hand, the formation of bipolaron at higher doping rates (> 50%) causes a decrease in conductivity [138-140].

1.2.5.5. Applications of polyaniline

Polyaniline is particularly interesting because of its possibilities of chemical or electrochemical polymerization from inexpensive reagents, easy doping and processing combined with high electronic conductivity and finally good stability to water. environment and during operation. Its use, alone or in mixtures [141-143] makes it possible to achieve a wide range of conductivity ranging from 10^{-12} to 10^3 S.cm⁻¹. Also, the existence of three degrees of oxidation and an easy to control doping allows to consider the use of PANI in multiple applications. Polyaniline has properties analogous to inorganic semiconductors and can therefore potentially replace them in conventional electronic and optoelectronic devices, such as photovoltaic cells, field effect transistors (FET), organic light-emitting diodes (OLED), capacitors, etc. PANI has also entered the formulation of paints, inks and conductive adhesives for various applications as conductive coating, anticorrosion treatment, or as electromagnetic or antistatic shielding.

The main applications of polyaniline are summarized in Table.I.4.

Table I.4. Main applications of polyaniline and associated specific properties

| Specific properties | Applications | Ref |
|---|--|--------------|
| Electrical conductor | Paints, inks, conductive adhesives | [145-146] |
| | Antistatic textile | [147] |
| | Electrostatic discharge materials | [148-150] |
| Viscosity increases under electric field | Electro-rheological (ER) material | [151-153] |
| Conductivity electric or change of color after exposure to liquids or vapors acid , basic or neutra | Gas sensor: NH ₃ , CO ₂ , NO ₂ , CO, Cl ₂ , O ₃ | [154-157] |
| | Toxic gas sensor, compounds volatile organic | [158], [160] |
| | Chemical sensor, humidity, petroleum | [159]-[161] |
| | PH sensor, mercury, biosensor | [162-164] |
| | Vitamin C detector, bacteria | [165], [167] |
| Change of color in depending on the medium pH | "Acid-Base" indicator | [166] |
| Change of morphology of the process of protonationdeprotonation and oxidationreduction | Gas separation membranes | [167], [169] |
| | Solution separation membranes neutral | [168], [170] |
| Change in oxidation state loading and unloading at both of the ion diffusion. | Ion exchange material | [171], [173] |
| Values of capacity very high | Capacitor | [172], [174] |
| | Energy storage devices | [175], [177] |
| Absorptivity and reflectivity of radiation electromagnetic | Shielding against the interference electromagnetic | [176-178] |
| Modulation possible of the conductivity | Digital memory device conductivity | [179] |
| Variations of constraint under pulsed current. | Artificial muscle | [180], [182] |
| Capacity at accumulate and transform energy (understood of the frequencies optical) and by therefore, to memorize (to erase) of information | Electrode for rechargeable batteries | [181-183] |
| | Microbial fuel cell anode (MFC) | [184] |
| | Electrochromic screen and smart window | [185-187] |
| Possibility of edit his electro-donor properties or electro-acceptor in function oxidation state | p-n heterojunctions | [188], [190] |
| | Solar cell | [189], [91] |
| | Diode | [190-192] |
| Program of color under electrical stress | Polymer light emitting diode | [193], [194] |

I.2.6. General Information on *Opuntia Ficus Indica*

Cactus (*Opuntia ficus-indica*) commonly known as prickly pear belongs to the family Cactaceae. *Opuntia ficus indica* produces sweet, nutritionally rich edible fruits, its tender cladodes are used as fresh green vegetable and salad (Figure I.19).

Family Cactaceae is reported to contain about 130 genera and nearly 1500 all well adapted to arid lands and to a diversity of climates and are naturalized in several areas all over the world, including the Mediterranean basin, Middle East, South Africa, Australia and India. In South Africa, Mediterranean areas and South American this species is also cultivated for its edible fruit (prickly pear), although in some countries different parts of the plant are utilized in the food and cosmetic industry. *Opuntia ficus-indica*, fruits and stems, have been traditionally used in folk medicine in several countries for several medicinal purposes. However, many researchers have focused his investigations for studying genus *Opuntia* in order to discover the properties of plant that could form the basis of their use in the prevention and cure of chronic diseases. Therefore, clinical pharmacologic interest in the efficacy and safety of the phytochemicals present in genus *Opuntia* has grown during recent years due to the realization that many people self-medicate using this plant [184].



Figure I.19. *Opuntia ficus-indica* fruits and cladodes.

I.2.6.1. Advantages of *Opuntia ficus indica*:

Scientifically, biomass is defined as the total mass of all organisms, plant and animal or otherwise in a given area. It can be any naturally occurring materials that are in our surroundings. Technically it constitutes organic and inorganic materials from the animal and plants sources however the majority of folks are using this term for plant-based materials, which are in debate, these unused plant or plant-based materials are specifically known as *Opuntia ficus indica*. Today it is well known that biomass is a rich source of energy and other daily useful products. Biomass is emerged as a potential alternative this is attributed to their green nature, low cost, easy and large availability. Environmental activities, natural resource conservation, and strict laws are passed by developing steps. Countries obligate researchers to develop materials having renewable characteristics [185]. *Opuntia ficus indica* emerged as a suitable candidate as it is derived from renewable resources and it is environmentally –friend furthermore other features like amazingly low weight and high strength make it further attractive for future use.

This study aimed to use *Opuntia ficus indica* for the preparation of a new hybrid material, which will be investigated as adsorbent for the elimination of Orange-G dye from aqueous solution.

I.3. ADSORPTION

I.3.1. Definition

Adsorption is a process in which a substance (adsorbate), in gas or liquid phase, accumulates on a solid surface. It is based on the capability of porous materials with large surfaces to selectively retain compounds on the surface of the solid (adsorbent). There are two types of adsorption; physical and chemical adsorptions [186].

I.3.1.1. Physical adsorption

A physisorption involves the formation of weak physical interactions, where no exchange of electrons is observed. Moreover, only relatively weak long-range van der Waals forces can be formed between the surface and the adsorbate, as well as among adsorbates. Because the adsorbate - surface interactions are weak, this type of adsorption can be easily reversed by heating. Physisorption usually has a low heat of adsorption ranging from 20 to 40 kJ.mol⁻¹, hence this type of adsorption is stable

only to temperatures below 150°C. Because of the weak Van der Waals forces between the adsorbate and adsorbent, lateral interactions are very important for adsorbed molecules[187].

I.3.1.2. Chemical adsorption:

A chemisorption involves the formation of new chemical bonds between the adsorbate and the surface site. In chemical sorption an exchange of electrons takes place between the adsorbed molecule and the surface site. This sorption mechanism is characterized by higher energies of interactions, equivalent to strong chemical bonds ($\geq 100 \text{ kJ.mol}^{-1}$) and therefore can be more stable at high temperatures. Electrostatic sorption involves the formation of Coulomb attractions between adsorbed ions and charged functional groups. The term “electrostatic sorption” is used specifically to ion exchange. The term "adsorption" is used to describe the uptake of the components (gaseous, liquid or solids) on external or internal surfaces of the solids. According to the second law of thermodynamics, adsorption of substances on solids takes place to reduce the surface tension, so free surface energy of the solids. The energy of formation of a chemical bond on the surface on a solid can be depicted by means of Lennard-Jones potential energy curve [188]. Therefore, Lennard Jones potential can be used to explain the energetic phenomenon occurring during an adsorption or desorption process. Figure.I.20 represents the energy of the molecule as a function of the distance (z) from the mass center of the molecule to the surface. The well is the result of the balance of two forces: van der Waals attraction and repulsion present between the clouds of electrons in the atoms, from the surface and those of the adsorbed molecule. When a molecule reaches the well, it is trapped or another term “adsorbed” by this potential energy until the molecule has sufficient energy to be desorbed. Thus, the lower the energy of the molecule, the easier it is for the molecule to fall in the well and stick in the chemisorption well. As shown, there are two types of wells presented on the curve, chemisorption and physisorption wells. The physisorption well is located further than the chemisorption one (when the distance is large), because the bonds formed are short-ranged and stronger in the case of chemisorption.

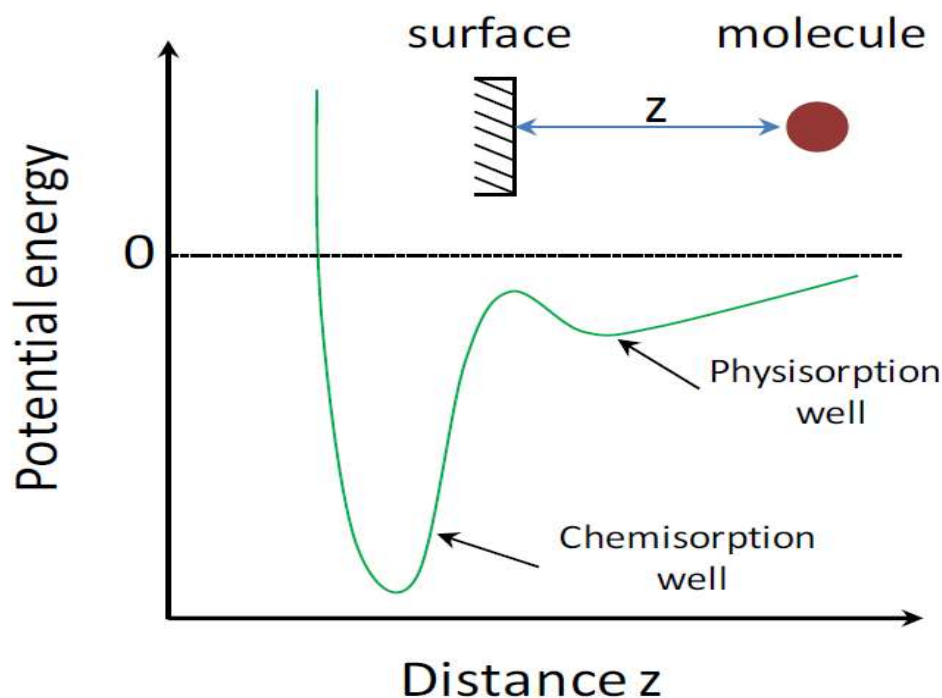


Figure I.20. Lennard - Jones type diagrams (non-activated adsorption)

potential energy versus distance.

From the thermodynamic point of view, any systems will try to reduce its energy to reach the lowest values of Gibbs energy G . Adsorption is the process that occurs in the isolated system with a constant temperature. Therefore, for such system Gibbs free energy describes by the following relation: $\Delta G = \Delta H - T\Delta S$ where, ΔH and ΔS are respectively, the changes in enthalpy and entropy during the process.

A spontaneous process is always accompanied by a decrease in the Gibbs energy, leading to $\Delta G < 0$, this implies the increase in the disorder of the system or entropy changes during the process $\Delta S > 0$ [189].

I.3.2 Adsorption Mechanisms

The adsorption process of the adsorbate molecules from the bulk liquid phase into the adsorbent surface is presumed to involve the following stages (Fig.I.21):

1. Mass transfer of the adsorbate molecules across the external boundary layer towards the solid particle.
2. Adsorbate molecules transport from the particle surface into the active sites by diffusion within the pore-filled liquid and migrate along the solid surface of the pore.

3. Solute molecules adsorption on the active sites on the interior surfaces of the pores.
4. Once the molecule adsorbed, it may migrate on the pore surface through surface diffusion.

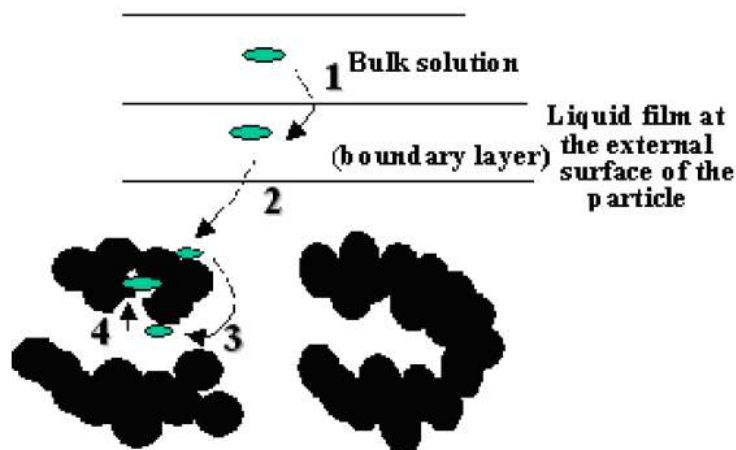


Fig.I.21. Schema of the mechanism of molecule adsorption using microporous adsorbent.
[190]

I.3.3. Physical properties of the adsorbent

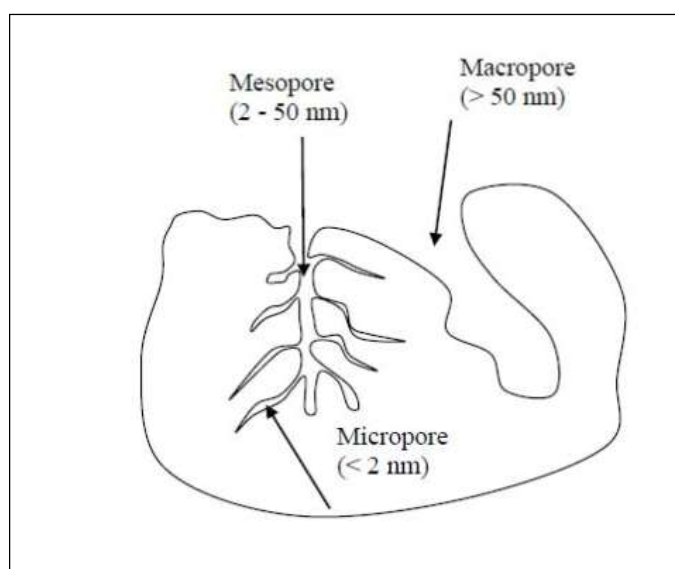
The most important property of adsorbent, which determines its usage, is the pore structure and the specific surface area.

I.3.3.1. Adsorbent pores

The total number of pores, their shape and size determine the adsorption capacity and even the dynamic adsorption rate of the adsorbent. The range of pore sizes which is defined according to the International Union of Pure and Applied Chemistry (IUPAC) is summarized in Table I.4 [191]. A schematic representation of the porous structure of adsorbent is shown in (Figure.I.22).

Table I.5. IUPAC classification of pore sizes

| Pores | Pore width (W; nm) |
|-----------------|--------------------|
| Ultramicropores | $W < 0.7$ nm |
| Supermicropores | $0.7 < W < 2$ nm |
| Micropores | < 0.2 nm |
| Mesopores | 2 – 50 |
| Macropores | $W > 50$ |

**Figure.I.22.** Schematic representation of different types of pores.

I.3.3.2. Adsorbent specific surface area

The specific surface area is another important property that determines adsorbent usage and its capacity. The total surface area of activated carbon, ranging from 500 to 2000 $\text{m}^2.\text{g}^{-1}$, quantifies adsorption sites for molecules to attach [192]. The micropores usually provide the largest proportion of the internal surface of the activated carbon and contribute to most of the total pore volume.

Mesopores, macropores and the nonporous surface of sample represent the external surface (Fig.I-23). Despite most of the adsorption takes place in the micropores, the meso- and macropores play also an important role in any adsorption process because they serve as passage for the adsorbate to reach micropores. Moreover, the multilayer adsorption only takes place in meso- and macropores.

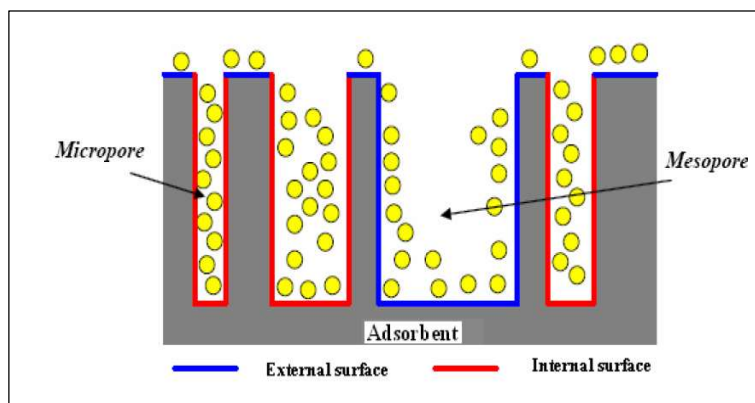


Fig.I-23. Schematic representation of external and internal adsorbent surface.

I.3.4. Solid-liquid interface

The solid-liquid interface is the common boundary surface formed by two different phases of matter (e.g., solid and liquid), where many important chemical, physical and biological processes occur. The solid – liquid interface formed during the sorption process will be discussed in this section. Adsorption at the solid-liquid interface is of a very complex nature compared to solid-gaseous interface. As adsorption takes place at an interface covered by the solvent molecules, which can potentially be strongly adsorbed must be displaced from the surface to make way for the adsorbent.

The distributions or accumulation of ions in the vicinity of the solid surface can be described using different model based on the double layer structure. One of the oldest model of such electrolyte-solid system was developed by Helmholtz in 1874 [193]. This model states that two layers of opposite charge form at the surface/electrolyte interface and are separated by an atomic distance. The Helmholtz model was modified by Gouy and Chapman, where the latter introduced the creation of a diffuse layer. Later Stern combined the two previous models. Thus, in Stern's model it is possible to recognize two regions of ion distribution - the inner region (compact or Stern layer) and the diffuse layer. Stern layer consists of inner (IHP) and outer (OHP) Helmholtz planes. The graphical representation of hydration shell in double layer is represented in (Figure I.23).

All ions in solution bear around them a shell from the solvent molecules and interact strongly with the solvent as well as with the solid. The ionic compound can be adsorbed on the surface of the

solid in well-defined adsorbate geometry and this type of chemisorption is called specific adsorption. The ion exists with a hydration shell in the solution but if it is specifically adsorbed, it must discard this shell, at least partially, when it attaches to the surface. This will happen only if the formation of the bond between the ion and the surface can overcome that part of energy of solvation between the solvent and the ion that is lost owing to specific adsorption. Specifically adsorbed ions do not lose all their interactions with the solvent but there are no solvent molecules between ions and the solid surface. If the solvent-ion interactions are stronger than ion-surface interactions, ions preserve their hydration shell. In this case, adsorption is non-specific. Specifically adsorbed ions are principally bound by chemical interactions (covalent or coordinate bond), but non-specifically adsorbed ions are principally bound by electrostatic attraction.

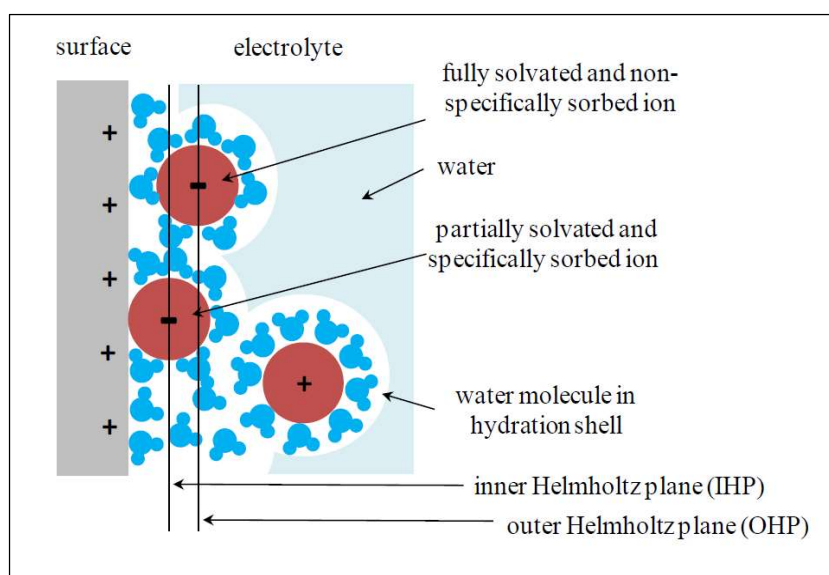


Figure I.24. Model of double layer structure of the solid-liquid interface with examples of specific and non-specific ion adsorption [194], together with their hydration shell.

Specifically adsorbed ions form Inner Helmholtz plane, while the outer Helmholtz plane is formed by non-specifically adsorbed ions.

Different sorption mechanisms can be found at the solid-liquid interface: co-precipitation or dissolution (when solid is partially dissolute in suspension with an ion liberation, that can precipitate on the surface with species presented in solution); surface complexation (sorption of reactive solute occurs on the specific sites of adsorbent); surface precipitation (at variance with latter, this sorption mechanism is independent from the number of sorption sites) and ion exchange that will be described in the following part.

I.3.5- Ion exchange

The notion of ion exchangers comes from the property of insoluble solid materials to contain exchangeable ions (named, counter-ions). These charged ions can be replaced or exchanged in stoichiometric amount with other anions in contact with the surrounding solution. For example, Na^+ neutralizes negative charges of clay platelets (of cationic clays). If the clays particles are placed in CaCl_2 electrolyte solution, the Ca^{2+} ions present in the solution displace Na^+ from clay interlayer to take up its place [195] based on an exchange mechanism as demonstrated in (Figure I.25). The ability to exchange ions is due to the properties of the structure of the materials.

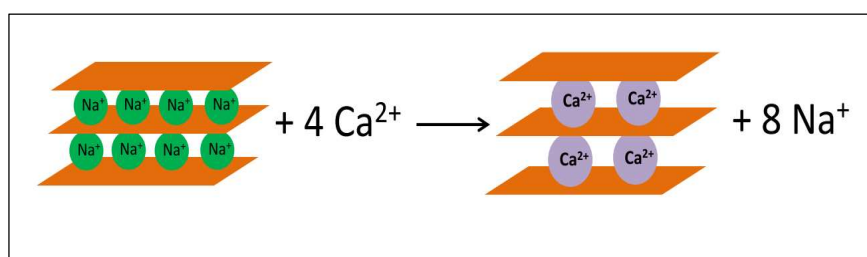


Figure I.25. Schematic representation of Na^+ - Ca^{2+} exchange.

If a solid contains exchangeable anions, it is called anion exchanger. In contrast, if the sorbent contains cations, this is a cation exchanger. The name amphoteric ion exchanger is used when exchanger contains both anions and cations. Ion exchange is similar to the adsorption process, as both process described the uptake of substances by a solid in solution. However, there is a specific difference between these two processes. Ion exchange is only a stoichiometric process in contrast to adsorption, which can be also nonstoichiometric. It means that in the ion exchange process for every charged specie removed from solution another charge compensator of the equal charge is released from the solid. However, the aim is to neutralize the structure's charge of exchanger that is why if one di-charged ion is released from the structure it will be replaced by another di-charged or two mono-charged ions. Both ions, exchanged and removed must have the same, positive or negative charge [196]. Secondly, in ion exchange only ions are sorbed, whereas in adsorption processes, electrically neutral species can also be removed [197]. However, it is difficult to differentiate them

practically, because sometimes common sorbent material can be adsorbent and exchanger at the same time (ex: activated alumina, with its exchangeable hydroxide ions [198]).

A water-swollen ion exchange material surrounded by an aqueous solution can be used as an example to demonstrate what is a complex ion exchange system [199]. The exchanger is composed of a dimensional framework with either positive or negative electric charges, compensated by the counter-ions, as mentioned above. Counter-ions are free to move within the framework and can diffuse in the pores. In contact with the electrolyte solution, the exchanger takes up the solvent with additional mobile ions. This term includes the counter-ions, different from those in the structure and co-ions with charge of the same sign as the framework charge. Hence, counter-ion can leave the framework, simultaneously with the incorporation of another counter-ion in the framework to compensate the charge of the system. The ion exchange process has been established as diffusion controlled, with the rate determining mechanism being the inter-diffusion of the two counter-ions [200]. The counter-ion content of the ion exchanger is a specific property of the material, named – ion-exchange capacity. It depends on the framework charge and it is independent from the nature and the charge of the counter-ions. For cationic exchangers, the constant is named cation-exchange capacity (CEC) and for anionic anion-exchange capacity (AEC).

Ionic exchanger is sometimes able to preferentially select some ions. This preference can be caused by different factors:

- The nature of the interactions between the solid and the counter-ions
- The size and the valence of the counter-ions
- Other interactions than electrostatic (London forces between the counter-ion and the matrix, as well as interactions of the solvent molecules with one another)
- The steric exclusion of large ions from the framework. This ability to choose between the counter-ions is called the selectivity of exchanger.

Many different natural and synthetic solids possessed exchange properties. But the main ones are: natural and synthetic inorganic ion exchangers (MOFs), ion exchange resins and ion exchange coals [201].

I.3.6. Adsorption Studies

I.3.6.1. Adsorption Isotherm

Adsorption isotherm expresses the quantity of material adsorbed per unit mass of adsorbent as a function of the equilibrium concentration of the adsorbate. The necessary data are derived from experiments where a specified mass of adsorbent is equilibrated with a known volume at a specific concentration of a chemical and the resultant equilibrium concentration is measured in solution by the mass balance equation:

$$q_e = \frac{(C_0 - C_e) * V}{m}$$

Where C_0 is initial liquid-phase concentration of solute, m is the mass of adsorbent and V is the isotherm solution volume.

At a given temperature, the relationship between the equilibrium concentration of adsorbate in the solution and the amount of adsorbate on adsorbent is called the adsorption isotherm [202].

I.3.6.2. Classification of liquid-solid adsorption isotherms

For the adsorption onto liquid-solid interface, according to the nature of the initial portion of the curve and its slope, Giles et al. proposed a classification of adsorption isotherms. This classification divides the various types of isotherms onto four main groups: **S**, **L** (Langmuir type), **H** (high affinity) and **C** (constant partition), see Figure I.26. The isotherm of **L** type is the most classical and widespread form among the sorption curves. For **L** type, species adsorption is favored in the beginning of the process, when all adsorption sites are vacant. It is usually indicative of molecules adsorbed flat on the surface. **S** curve arises due to the vertical orientation of the adsorbed molecules at the surface during the adsorption process. The **S** curve isotherm occurs as a result of the interactions among the adsorbed molecules. **H** type curve is characterized by a sharply vertical part of the initial slope, indicating highly strong interactions between the adsorbate and the adsorbent. All the molecules in the solute are adsorbed onto the solid. **H** curves arise in special cases where the adsorbate has a high affinity with the substrate.

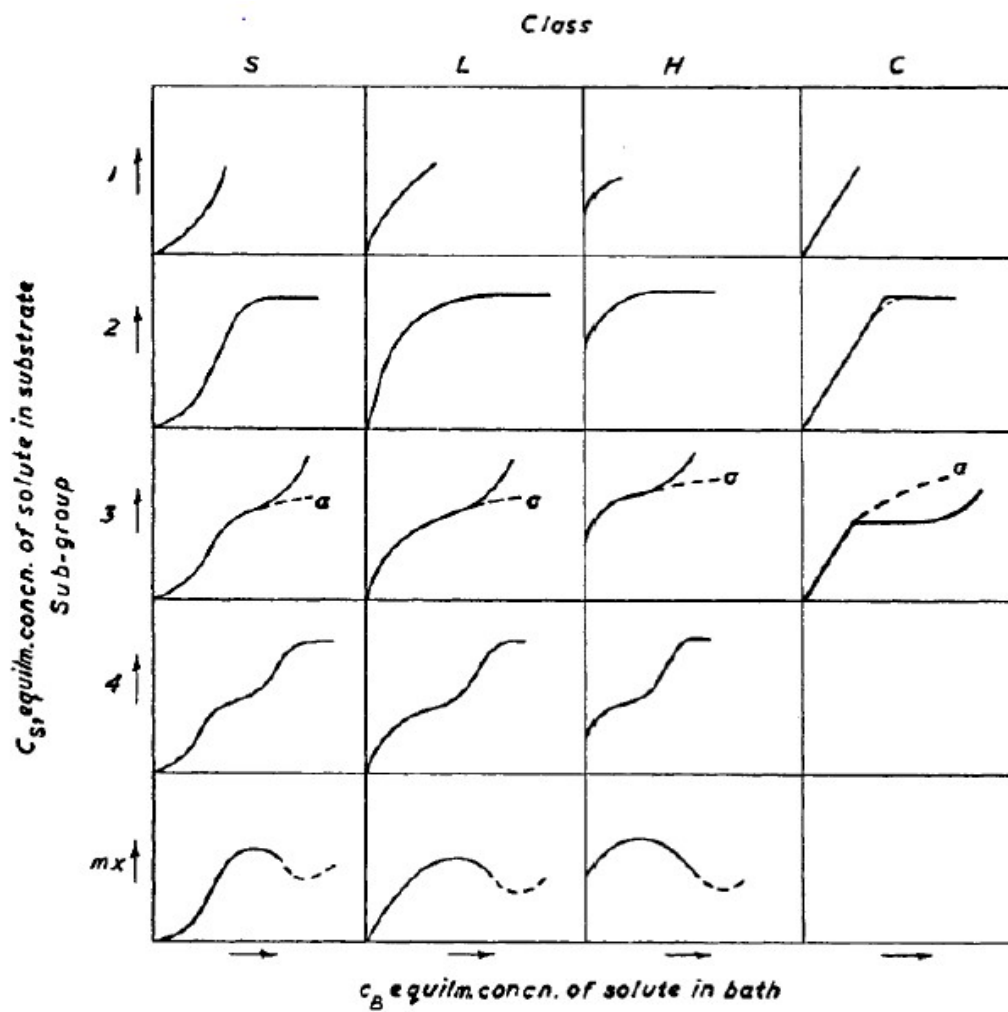


Figure I.26. Classification of solution adsorption isotherms according to Giles et al. [204].

The last group of the isotherm curves is the *C* type and this can only be found in special cases. In the latter, the solutes penetrate into the solid more readily than the solvent [203].

I.3.6.2. Modelling Techniques

A number of models have been developed to represent the actual sorption/desorption processes of organic pollutants with various solid phases [206]. Some models have a theoretical basis; however, they may have only limited experimental utility because the assumptions involved in the development of the relationship apply only to a limited number of adsorption processes. Other models are more empirical in their derivation, but tend to be more generally applicable. In the latter case, the theoretical basis is uncertain. Langmuir and Freundlich equations are the most commonly used for modelling adsorption isotherms.

1.3.6.3.a. Langmuir Model

The Langmuir adsorption model describes the equilibrium between aqueous and solid phase systems as a reversible chemical equilibrium between species. There are three main assumptions in Langmuir adsorption equation: (a) the adsorption energy is the same at all sites, (b) adsorption is on localized sites with no interaction between adsorbed molecules, and (c) the maximum adsorption possible is a complete monolayer. The adsorbent surface (solid phase) is made up of fixed individual sites where molecules of adsorbate (organic pollutant) may be chemically bound. This can be expressed mathematically by denoting an unoccupied surface site as $(-S)$ and the adsorbate in solution as species (A) , with concentration (C) , and considering the reaction between the two to form occupied sites $(-SA)$:



For the Langmuir adsorption isotherm, it is assumed that this reaction (Eq. I.1) has a fixed free energy of adsorption not dependent on the extent of adsorption and not affected by interaction among sites. In addition, each site is assumed to be capable of binding at most one molecule of adsorbate. If q_{max} is the maximum number of moles of a pollutant adsorbed per mass adsorbent when the surface sites are saturated with an adsorbate (full monolayer), and q_e is the number of moles of adsorbate per mass adsorbent at equilibrium, then according to the law of mass action Eq. (I.2) follows: [207]

$$k = \frac{[-SA]}{[-S][A]} = \left[\frac{q_e}{(q_{max} - q_e) \cdot C_e} \right] \quad (I.2)$$

Where:

k is equilibrium constant, and C_e is the equilibrium concentration in solution. The rearrangement of Eq. (I-3) leads to the well known Langmuir equation

$$q_e = q_{max} * \frac{k \cdot c_e}{(1 + k \cdot c_e)} \quad (I.3)$$

For determination the constants in the Langmuir model, two versions of linearization can be used. Version 1 is represented by plotting C_e versus C_e/q_e , according to Eq. (I-4) used at high concentration. Version 2 is represented by plotting $1/C_e$ versus $1/q_e$, according to Eq. (I-5) used at low concentration.

$$\frac{C_e}{q_e} = \frac{C_e}{q_{max}} + \frac{1}{k q_{max}} \quad (I.4)$$

$$\frac{1}{q_e} = \frac{1}{q_{max}} + \frac{1}{q_{max} k C_e} \quad (I.5)$$

I.3.6.3. b. Freundlich Model

The Langmuir model involves an assumption that the energy of adsorption is the same for all surface sites and not dependent on degree of coverage. Since in reality the energy of adsorption may vary because real surfaces are heterogeneous, the Freundlich adsorption model (Freundlich, 1926) attempts to account for this:

$$q_e = k_f \cdot C_e^{\frac{1}{n}} \quad (I.7)$$

Where C_e is the equilibrium concentration in solution, k_f is an equilibrium constant indicative of sorption strength and (n) is the degree of non-linearity (most often $n < 1$).

A linear form of Eq. (I-7) can be used as shown in Eq. (I.8):

$$\text{Ln}(q_e) = \text{Ln}(k_f) + \frac{1}{n} \cdot \text{Ln}(C_e) \quad (I.8)$$

If $\text{Ln}(q)$ is plotted as a function of $\text{Ln}(C_e)$, a straight line should be obtained with an intercept on the ordinate of $\text{Ln}(k_f)$ and slope n . [208]

I.3.6.3. c. Langmuir-Freundlich model

This model has three parameters in the following form :

$$q_e = \frac{k_{lf} \cdot b \cdot C_e^{1/n}}{1 + k_{lf} \cdot C_e^{1/n}} \quad (I.9)$$

Also known by the Sips equation [209]. It was used for the adsorption of benzene and toluene from aqueous solutions on granulated activated carbons [210].

In addition to these three major models there is a wide range of available theoretical models and empirical fitting functions used to evaluate the monocomponent isotherms, table I.6 represent some examples of these models.

Table I.6. Some examples of monocomponent isotherms models [210]

| Model | Equation | Description |
|------------------------------|---|---|
| Langmuir-Freundlich | $q = q_{max} \cdot \frac{(K.C)^{\gamma}}{[1+(K.C)^{\gamma}]}$ | Empirical model (monolayer adsorption on heterogeneous surface) |
| Jovanovic | $q = q_{max} \cdot (1 - e^{-kC})$ | Monolayer adsorption on homogenous surface with the possibility of mechanical contacts between adsorbed and adsorbed molecules |
| Jovanovic-Freundlich | $q = q_{max} \cdot (1 - e^{-(kC)^{\gamma}})$ | Semi-empirical model adsorption on heterogeneous surface, derived from Jovanovic's model |
| Brunauer-Emmett-Teller (BET) | $q = \frac{q_{max} \cdot K_1 \cdot C}{(1 - K_2 \cdot C) \cdot (1 + (K_1 - K_2) \cdot C)}$ | Described the multi-layer adsorption (the adsorption of molecules to the surface of particles forms a new surface layer to which additional molecules can adsorb) |
| Toth | $q = q_{max} \cdot \frac{K \cdot C}{[1 + (K \cdot C)^{\gamma}]^{1/\gamma}}$ | Empirical model adsorption on heterogeneous surface |

I.3.6.4. Thermodynamic parameters related to the adsorption process

Adsorption isotherms are generally used for the characterization of adsorbents, but this characterization is incomplete without having information on the quantity of energy involved. Adsorption is an exothermic process which therefore occurs with a release of heat, which leads to heating of the solid and a reduction in quantities adsorbed. Temperature variations are often important in processes industrial adsorption and can be one of the main factors in the degradation of performance. [211]

- **Distribution coefficient**

The distribution coefficient is a special case of the Langmuir relation and is defined for low concentrations of adsorbed species. The distribution coefficient K_d is defined as the ratio of the quantities fixed per gram of solid to the quantity of solute remaining in solution by volume of solution. The distribution coefficient characterizes the affinity of the solute for the adsorbent, can be translated by the below expression. [212, 213]

$$K_d = \frac{q_e}{C_e} \quad (I.10)$$

The Gibbs-Helmholtz thermodynamic relationship: $\Delta G = \Delta H - T\Delta S$ associated with the relation obtained by Van't Hoff integration:

$$\Delta G = -RT \cdot \ln(K_d) \quad (I.11)$$

We can determine enthalpy and entropy from the equation:

$$\ln K_d = \frac{\Delta S}{R} - \frac{\Delta H}{RT} \quad (I.12)$$

The plot of the line $\ln K_d$ as a function of $1/T$ makes it possible to calculate the values of the thermodynamic parameters ΔH and ΔS from the ordinate and the slope. For the adsorption to be effective, the free energy must be negative. [214]

I.3.6.5. Adsorption kinetics

The rate at which thermodynamic equilibrium is attained in a system that is not in equilibrium is generally described by kinetics. The adsorption process continues until the equilibrium is reached. The reverse process occurs during desorption which also continues until the equilibrium is attained. [215]. Adsorption, either physical or chemical, includes the mass transfer of the adsorptive from the solution to the surface of the adsorbent. The adsorption takes place in four basic steps in the presence of a porous adsorbent [216]

1. Bulk solution transport: The adsorptive is first transported to the hydrodynamic boundary layer surrounding the adsorbent. This transport occurs either by diffusion or turbulent mixing.
2. External film diffusion – The adsorptive is then transported through the hydrodynamic boundary layer to the surface of the adsorbent by the assistance of molecular diffusion. The thickness of the boundary layer affects the rate of transport and depends on the velocity of the bulk solution.
3. Internal (pore) transport – The adsorptive is next transported through the pores of adsorbent to the adsorption sites via intraparticle diffusion i.e. either molecular diffusion through the

solution in the pores (pore diffusion) or by the diffusion along the adsorbent surface (surface diffusion) after adsorption has taken place.

4. Adsorption: The final step is the adsorption in which the adsorptive adheres to the adsorbent surface on the available sites. This step is very rapid and therefore one of the previous diffusion steps will control the rate of mass transfer.

Desorption, occurs in the reverse manner; it begins with desorption and ends with transport from the concentration boundary layer around the adsorbent into the solution.

I.3.6.5.a. Pseudo-first order model

The pseudo-first order kinetic model, was developed by Lagergren (1898) and it is widely applied to describe the rates of adsorption processes.

$$\frac{dq_t}{dt} = k_1(q_t - q_e) \quad (I.11)$$

Where q_e and q_t are the amounts adsorbed (mg/g) at equilibrium and at time t , k_1 is the pseudo-first order rate constant. Equation (I.11) can be linearized to the form of Equation (I.12) and the rate constant k_1 can be calculated from the plot of $\log(q_e/(q_e - q_t))$ versus time.

$$\log(q_e - q_t) = \log(q_e) - \frac{k_1}{2.303} t \quad (I.12)$$

The first-order equation does not always fit well with the whole range of contact time and usually it is applicable only over the initial stage of the adsorption processes [217].

I.3.6.5.b. Pseudo-second order kinetic model

The pseudo-second order kinetic model based on sorption equilibrium capacity, Eq.(I.13), is also widely used since it is a good representation of the experimental data. The model can be used to predict the behavior over the whole range of adsorption. [218].

$$\frac{dq_t}{dt} = k_2(q_e - q_t)^2 \quad (I.13)$$

where k_2 is the rate constant for the pseudo-second order adsorption [g/(mg.min)].

An integrated and rearranged form of the pseudo-second order model is presented in Eq.(I.14). If the model is applicable, the plot of t/q versus t should give a linear relationship and values of q_e and k_2 can be then calculated from the slope and intercept [219].

$$\frac{t}{q_t} = \frac{1}{k_2 q_e^2} + \frac{1}{q_e} t \quad (I.14)$$

where $k_2 q_e^2$ equals to the initial adsorption rate h (mg of adsorbate/(g of adsorbent·min)).

I.3.6.5.c. Intra-particle diffusion model

The intra-particle diffusion rate is determined using the following equation:

$$q_t = k_{int} t^{1/2} \quad (I.15)$$

With, k_{int} : Diffusion rate constant (mg/g.min^{1/2}) The plot of q_t as a function of time $t^{1/2}$ will give a line of slope equal to k_{int} and intercept equal to C . C is a constant depending on the adsorption capacity according to intra-particle diffusion model. [220].

I.4. REFERENCES

- [1] B.K. Hordern, M. Ziółtek, J. Nawrocki, Catalytic ozonation and methods of enhancing molecular ozone reactions in water treatment. *Appl. Catal. B* 46, 639–669 (2003)
- [2] Z. Yang, T.A. Asoh, H. Uyama, Removal of cationic or anionic dyes from water using ion exchange cellulose monoliths as adsorbents. *Bull. Chem. Soc. Jpn.* 92, 1453–1461 (2019)
- [3] Tahir, H., Sultan, M. and Q. Jahenzeb, 2009. Remediation of azo dyes by using house hold use black tea as an adsorbent. *American Journal of Biotechnology*, 8: 3584-3589.
- [4] Chandra, T. C., Mirna, M.M., Sandaryanto, Y. and S. Ismadji, 2007. Adsorption of basic dyes on to activated a carbon prepared from durian shell: Studies of adsorption equilibrium and kinetics, *Chemical Engineering Journal*, 127:121-129.
- [5] Rocher, V., Siaugue, J.M., Cabuil, V. And A. Bee, 2008. Removal of organic dyes by magnetic alginate bead, *Water Res.*,42: 1290–1298.
- [6] Karim, M.M., Dasa, A. K. And S.H. Lee, 2006. Treatment of colored effluent of the textile industry in Bangladesh using zinc chloride treated indigenous activated carbons. *Analytica Chimica Acta*, 576: 37–42.
- [7] Y. Tang, X. Yin, M. Mu, Y. Jiang, X. Li, H. Zhang, T. Ouyang, Anatase TiO₂@MIL-101(Cr) nanocomposite for photocatalytic degradation of bisphenol A. *Colloids Surf. A* 596, 124745 (2020)
- [8] M. Ballesteros Martín, J. Sánchez Pérez, J. García Sánchez, L. Montes de Oca, J. Casas López, I. Oller, S. Malato Rodríguez, Degradation of alachlor and pyrimethanil by combined photo-Fenton and biological oxidation. *J. Hazard. Mater.* 155, 342–349 (2008)
- [9] H. Laksaci, A. Khelifi, B. Belhamdi, M. Trari, The use of prepared activated carbon as adsorbent for the removal of Orange-G from aqueous solution. *Microchem. J.* 145, 908–913 (2019)
- [10] H. Murthy, H. Manonmani, Aerobic degradation of technical hexachlorocyclohexane by a defined microbial consortium. *J. Hazard. Mater.* 149, 18–25 (2007)
- [11] A. Ahmad, L. Tan, S. Shukor, Dimethoate and atrazine retention from aqueous solution by nanofiltration membranes. *J. Hazard. Mater.* 151, 71–77 (2008)
- [12] M. Maldonado, S. Malato, L. Pérez-Estrada, W. Gernjak, I. Oller, X. Doménech, J. Peral, Partial degradation of five pesticides and an industrial pollutant by ozonation in a pilot-plant scale reactor. *J. Hazard. Mater.* 138, 363–369 (2006)
- [13] A. Belalia, A. Zehhaf, A. Benyoucef, Preparation of hybrid material based of PANI with SiO₂ and its adsorption of phenol from aqueous solution. *Polym. Sci. Ser. B* 60, 816–824 (2018)
- [14] M. Mekhloufi, A. Zehhaf, A. Benyoucef, C. Quijada, E. Morallon, Removal of 8-quinolinecarboxylic acid herbicide from aqueous solution by adsorption on activated-montmorillonites. *Environ. Monit. Assess.* 185, 10365–10375 (2013)
- [15] Y. Su, M. Ji, J. Li, C. Chang, S. Dong, Y. Deng, Y. Yang, L. Gu, Subcritical fluid extraction treatment on egg yolk: product characterization. *J. Food Eng.* 274, 109805 (2020)
- [16] E.T. Özer, B. Osman, B. Parlak, An experimental design approach for the solid phase extraction of some organophosphorus pesticides from water samples with polymeric microbeads. *Micro-chem. J.* 154, 104537 (2020)

- [17] A.M. Donia, A.A. Atia, W.A. Al-amrani, A.M. El-nahas, Effect of structural properties of acid dyes on their adsorption behavior from aqueous solutions by amine modified silica. *J. Hazard. Mater.* 161, 1544–1550 (2009)
- [18] N. Ouasfi, S. Bouzekri, M. Zbair, H. Ait Ahsaine, S. Bakkas, M. Bensitel, L. Khamliche, C. Doukkali, E. Jadida, Carbonaceous material prepared by ultrasonic assisted pyrolysis from algae (*Bifurcaria bifurcata*): response surface modeling of aspirin removal. *Surf. Interfaces* 14, 61–71 (2019)
- [19] A. Elouahli, M. Zbair, Z. Anfar, H.A. Ahsaine, H. Khallok, R. Chourak, Z. Hatim, Apatitic tricalcium phosphate powder: high
- [20] E. Ghiasi, A. Malekzadeh, Removal of various textile dyes using LaMn(Fe)O_3 and $\text{LaFeMn}_{0.5}\text{O}_3$ nanoperovskites; RSM optimization, isotherms and kinetics studies. *J. Inorg. Organometal. Polym. Mater.* 30, 2789–2804 (2020)
- [21] M. Abdelsalam, S.A. Kosa, A.A. Al-Beladi, Application of nano-clay for the adsorptive removal of Orange G dye from aqueous solution. *J. Mol. Liq.* 241, 469–477 (2017)
- [22] A. Hsini, A. Esseki, N. Aarab, M. Laabd, A.A. Addi, R. Lakhmiri, A. Albourine, Elaboration of novel polyaniline@almond shell bio-composite for effective removal of hexavalent chromium ions and Orange G dye from aqueous solutions. *Environ. Sci. Pollut. Res.* 27, 15245–15258 (2020)
- [23] Nigarn, P., Banat, L.M., Singh, D. And R. Marchant, 1996. Microbial process for decolourisation of textile effluents containing azo, diazo and reactive dyes, *Process Biochem.* 31: 435–42.
- [24] McKay, G., Prasad, G.R. and P.R. Mowli, 1986. Equilibrium studies for the adsorption of dyestuff from aqueous solutions by low cost materials, *Water Air Soil Pollut.*, 29: 273–83.
- [25] Batzias, F.A. and D.K. Sidiras, 2004. Dye adsorption by calcium chloride treated beech sawdust in batch and fixed-bed systems, *J. Hazard. Mater.*, 18: 167–174.
- [26] Garg, V.K., Amita, M., Kumar, R. And R. Gupta, 2004. Basic dye (methylene blue) removal from simulated wastewater by adsorption using Indian rosewood sawdust: a timber industry waste, *Dyes Pigments*, 63, 243–250.
- [27] Malik, P.K., 2004. Dye removal from wastewater using activated carbon developed from sawdust: adsorption equilibrium and kinetics, *J. Hazard. Mater. B*, 113: 81–88.
- [28] Mahmut, I., Zacara, O. and A.S. Engilb, 2005. Adsorption of metal complex dyes from aqueous solutions by pine sawdust, *Bioresour. Technol.*, 96: 791–795.
- [29] Annadurai, G., Juang, R-S. And D.J. Lee, 2002. Use of cellulosebased wastes for adsorption of dyes from aqueous solutions, *J. Hazard. Mater.* , 92: 263–274.
- [30] T. Sen, S. Mishra, N.G. Shimpi, Synthesis and sensing applications of polyaniline nanocomposites: a review. *RSC Adv.* 6, 42196–42222 (2016)
- [31] K. Akag, Interdisciplinary chemistry based on integration of liquid crystals and conjugated polymers: development and progress. *Bull. Chem. Soc. Jpn.* 92, 1509–1655 (2019)
- [32] S. Benykhlef, A. Bekhoukh, R. Berenguer, A. Benyoucef, E. Morallon, PANI-derived polymer/ Al_2O_3 nanocomposites: synthesis, characterization and electrochemical studies. *Colloid Polym. Sci.* 294, 1877–1885 (2016)
- [33] F. Chouli, I. Radja, E. Morallon, A. Benyoucef, A novel conducting nanocomposite obtained by p-anisidine and aniline with titanium(IV) oxide nanoparticles: synthesis, characterization, and electrochemical properties. *Polym. Compos.* 38, 254–260 (2017)

- [34] S. Daikh, F.Z. Zeggai, A. Bellil, A. Benyoucef, Chemical polymerization, characterization and electrochemical studies of PANI/ZnO doped with hydrochloric acid and/or zinc chloride: differences between the synthesized nanocomposites. *J. Phys. Chem. Solids* 121, 78–84 (2018)
- [35] F.Z. Kouidri, R. Berenguer, A. Benyoucef, E. Morallon, Tailoring the properties of polyanilines/SiC nanocomposites by engineering monomer and chain substituents. *J. Mol. Struct.* 1188, 121–128 (2019)
- [36] D. Ouis, F.Z. Zeggai, A. Belmokhtar, A. Benyoucef, B. Meddah, K. Bachari, Role of p-benzoquinone on chemically synthesized nanocomposites by polyaniline with V₂O₅ nanoparticle. *J. Inorg. Organometal. Polym. Mater.* (2020). <https://doi.org/10.1007/s10904-020-01508-7>
- [37] E.S. Lyle, C. McAllister, D.C. Dahn, R. Bissessur, Exfoliated MoS₂-polyaniline nanocomposites: synthesis and characterization. *J. Inorg. Organomet. Polym. Mater.* 30, 206–213 (2020)
- [38] E. Parthiban, N. Kalaivasan, S. Sudarsan, Dual responsive (pH and magnetic) nanocomposites based on Fe₃O₄@polyaniline/itaconic acid: synthesis, characterization and removal of toxic hexavalent chromium from tannery wastewater. *J. Inorg. Organomet. Polym. Mater.* 30, 4677–4690 (2020)
- [39] M.K.M. Nodeh, S. Soltani, S. Shahabuddin, H.R. Nodeh, H. Sereshti, Equilibrium, kinetic and thermodynamic study of magnetic polyaniline/graphene oxide based nanocomposites for ciprofloxacin removal from water. *J. Inorg. Organomet. Polym. Mater.* 28, 1226–1234 (2018)
- [40] K.K. Beltrame, A.L. Cazetta, P.S.C. de Souza, L. Spessato, T.L. Silva, V.C. Almeida, Adsorption of caffeine on mesoporous activated carbon fibers prepared from pineapple plant leaves. *Ecotoxicol. Environ. Saf.* 147, 64–71 (2018)
- [41] G. Yang, S. Song, J. Li, Z. Tang, J. Ye, J. Yang, Preparation and CO₂ adsorption properties of porous carbon by hydrothermal carbonization of tree leaves. *J. Mater. Sci. Technol.* 35, 875–884 (2019)
- [42] S. Wong, H.H. Tumari, N. Ngadi, N.B. Mohamed, O. Hassan, R. Mat, N.A.S. Amin, Adsorption of anionic dyes on spent tea leaves modified with polyethyleneimine (PEI-STL). *J. Clean. Prod.* 206, 394–406 (2019)
- [43] Y. Hu, Y. Zhu, Y. Zhang, T. Lin, G. Zeng, S. Zhang, Y. Wang, W. He, M. Zhang, H. Long, An efficient adsorbent: simultaneous activated and magnetic ZnO doped biochar derived from camphor leaves for ciprofloxacin adsorption. *Bioresour. Technol.* 288, 121511 (2019)
- [44] A. Ghazali, M. Shirani, A. Semnani, V.Z. Shahabadi, M. Nekoeinia, Optimization of crystal violet adsorption onto Date palm leaves as a potent biosorbent from aqueous solutions using response surface methodology and ant colony. *J. Environ. Chem. Eng.* 6, 3942–3950 (2018)
- [45] M. Muthu, D. Ramachandran, N. Hasan, M. Jeevanandam, J. Gopal, S. Chun, Unprecedented nitrate adsorption efficiency of carbon-silicon nano composites prepared from bamboo leaves. *Mater. Chem. Phys.* 189, 12–21 (2017)
- [46] O. Bensebia, K. Allia, Analysis of adsorption–desorption moisture isotherms of rosemary leaves. *J. Appl. Res. Med. Aromat. Plants* 3, 79–86 (2016)
- [47] S. Knani, F. Aouaini, N. Bahloul, M. Khalfaoui, M.A. Hachicha, A. BenLamine, N. Kechaou, Modeling of adsorption isotherms of water vapor on Tunisian olive leaves using statistical mechanical formulation. *Phys. A* 400, 57–70 (2014)
- [48] M. Choudhary, R. Kumar, S. Neogi, Activated biochar derived from *Opuntia ficus-indica* for the efficient adsorption of malachite green dye, Cu²⁺ and Ni²⁺ from water. *J. Hazard. Mater.* 392, 22441 (2020)

- [49] M. Choudhary, M.B. Ray, S. Neogi, Evaluation of the potential application of cactus (*Opuntia ficus-indica*) as a bio-coagulant for pre-treatment of oil sands process-affected water. *Sep. Purif. Technol.* 209, 714–724 (2019)
- [50] A.A.P. Cid, I.V. Ugalde, A.M.H. González, J.G. Serrano, Textile dyes removal from aqueous solution using *Opuntia ficus-indica* fruit waste as adsorbent and its characterization. *J. Environ. Manag.* 130, 90–97 (2013)
- [51] Min Zhi Rong, Ming Qiu Zhang, Guang Shi, Qiu Long Ji, Bernd Wetzels, Klaus Friedrich Graft *Tribology International* 36 697– 707 (2003).
- [52] In-Yup Jeon and Jong-Beom Baek, 3, 3654-3674 doi: 10. 3390/ma3063654 (2010).
- [53] Armelao L, Barreca D, Bottaro G, Gasparotto A, Gross S, Maragno C, Tondello E *Coord. Chem. Rev.*, 250, 1294-1314 (2006).
- [54] Jin R.C, Cao Y. W, Mirkin C. A, Kelley K. L, Schatz G. C, Zheng J. G, *Science* 294, 1901-1903 (2001).
- [55] Tizazu G, Adawi A. M, Leggett G. J, Lidzey D. G, *Langmuir* 25 (18), 10746–10753 (2009).
- [56] Shenhar R, Rotello V. M, *Acc. Chem. Res.* 36, 549-561(2003).
- [57] Vriezema D.M, Comellas-Aragones M, Elemans J.A.A.W, Cornelissen J.J.L.M, Rowan A.E. and Nolte R.J.M, *Self-Assembled Nanoreactors. Chem. Rev.* 105,1445-1490 (2005).
- [58] Humberto Palza, *International Journal of Molecular Sciences, Int. J. Mol. Sci*, 16, 2099- 2116 (2015).
- [59] El-Sayed M. A, *Acc. Chem. Res.*, 34, 257-264 (2001).
- [60] Mandal T.K, Fleming M. S, Walt. D.R, *Nano Lett.*, 2, 3-7 (2002).
- [61] Corbierre M. K, Cameron N. S, Sutton M, Mochrie S. G. J, Lurio L. B, Ruhm A, Lennox R. B, *J. Am.Chem. Soc*, 123, 10411-10412 (2001).
- [62] Dilini Galpaya, Mingchao Wang, Meinan Liu, Nunzio Motta, Eric Waclawik, Cheng Yan. *Graphene*, 1 30-49 (2012).
- [63] T. Filleter, A.M. Beese, M.R. Roenbeck, X. Wei, H.D. Espinosa, *Nanotub. Superfib. Mater.* 61–85 (2014)
- [64] Park C. I, Park, O. O, Kim, H. J, *Polymer* 42, 7465 (2001).
- [65] H. Althues, J. Henle, and S. Kaskel. *Chemical Society Reviews*, 36(9):1454–1465, (2007).
- [66] Okpala (2014) , the benefits and applications of nanocomposites , *international journal*
- [67] G. Malandrino, S. T. Finocchiaro, R. T. Nigro, *Chem. Mater*, 16, 5559 (2004).
- [68] N. Chopra, V.G. Gavalas, L.G. Bachas, B.J. Hinds, L.G. Bachas, *Anal. Lett.* 40 2067 (2007).
- [69] K. Kerman, M. Saito, S. Yamamura, Y. Takamura, E. Tamiya, *Trends Anal. Chem.* 27 585 (2008).
- [70] D.C. Chow, M.S. Johannes, W.K. Lee, R.L. Clark, S. Zauscher, A. Chilkoti, *Materials Today*, 8 30 (2005).
- [71] M. A. Gondal, M. A. Dastageer and A. Khalil. *Synthesis of nano-WO₃ and its catalytic activity for enhanced antimicrobial process for water purification using laser induced photocatalysis. Catalysis communication*, 11 (3) : 214-219, 2009. 17

- [72] J. R. Darwent. Photo-oxydation of water sensitized by WO₃ powder. *Journal of chemical society*, 78 (2) : 359-367, 1982. 17
- [73] C. G. Granqvist. Electrochromic tungsten oxide films : Review of progress 1993-1998. *Solar Energy Materials and Solar Cells*, 60 (3) : 201-262, 2000. 17
- [74] G. Aka. Chimie du solide partie b : défauts ponctuels dans les solides, modèle du cristal réel. École Nationale Supérieure de Chimie de Paris : Paris, 12-24, 2006. 18 C Lambert-Mauriat and V. Oison. Density-functional study of oxygen vacancies in monoclinic tungsten oxide. *J. Phys. : Condesn. Matter*, 18 : 7361–7371, 2006. vii, 18, 20
- [75] B. O. Loopstra, P. Boldrini. Neutron diffraction investigation of WO₃. *Acta. Crystallagr. B*, 21, 1996. 20, 68, 69
- [76] I. P. Swainson, K. R. Locherer and E. K. H. Sajle. Transition to a new tetragonal phase of WO₃ : crystal structure and distorsion parameters. *Journal Phys. : Cond. Mat.*, 11 (21) : 4143–4156, 1999. 20
- [77] S. Yamazoe, Y. Hitomi, T. Shishido, T. Tanaka. XAFS study of tungsten L-1- and L-3-edges : Structural analysis of WO₃ species loaded on TiO₂ as a catalyst for photooxidation of NH₃. *Journal of Physical Chemistry C*, 112 (17) : 6869–6879, 2008. 20
- [78] G. Poirier, F. C. Cassanjes, Y. Messaddeq, S. J. L. Ribeiro, A. Michalowicz, M. Poulain. Local order around tungsten atoms in tungstate fluorophosphate glasses by X-ray absorption spectroscopy. *Journal of NonCrystalline Solids*, 351 (46-48) : 3644-3648, 2005. 20
- [79] N. J Simon, Cryogenic properties of inorganic insulating materials for ITER Magnets, A Review, 1994.
- [80] Schweizer M. Docteur nopal le médecin du bon dieu. APB Edition, Paris, 1997, 81pp.
- [81] Briha O. Potentialité thérapeutiques d'Opuntia ficus-indica au Maroc et Tunisie. Thèse de doctorat en pharamacie. Université Mohamed V Rabat. Maroc. 2012, 171 pp.
- [82] Lamghari El Kossori R, Villaume C, El Boustani E, Sauvaire Y, Méjean L. Composition of pulp, skin and seeds of prickly pear fruit (Opuntia ficus-indica sp.). *Plant. Foods. Hum.Nutr.*, 1998, 52 : 263-270.
- [83] Nouveaux aliments pour les ruminants à base de fruits de cactus, ministère de l'agriculture et de la pêche maritime, royaume du Maroc, N°176 Mai, 2009
- [84] C.K. Chiang, C.R. Fincher, Y.W. Park, A.J. Heeger, H. Shirakawa, E.J. Louis, S.C.Gau , A.G. MacDiarmid, *Phys. Rev. Lett.* 39 (1977) p 1098
- [85] M. Leclerc, R. Prud'homme, *Macromolecules* 20 (1987) p 2153
- [86] D.M. Ivory, G.G. Miller, J.M. Sowa, L.W. Shacklette, R.R. Chance, R.H. Baughman, *J. Chem. Phys.*,71(1979) p 1506
- [87] M. Rehahn, A.D. Schluter, G. Wegner, *Makromol. Chem.* 191 (1990) p 1991
- [88] C.L. Gettinger, A.J. Heeger, J.M. Drake, D.J. Pine, *J. Chem. Phys.* 101 (1994) p 1673 J. Roncali, *Chem. Rev.* 92 (1992) p 711
- [89] A.F. Diaz, K.K. Kanazawa, G.P.J. Gardini, *Chem. Soc., Chem. Commun.* (1979) p 635
- [90] D.K. Moon, A.B., Padias, H.K. Hall, T. Huntoon, P.D. Clavert, *Macromolecules* 28 (1995) p 6205

-
- [91] A.G. MacDiarmid, J.E. Chiang, M. Halpern, W.S. Huang, S.L. Mu, N.L. Somarisi, W. Wu, S.I. Yaniger, *Molec. Cryst. Liq. Cryst.* 121 (1985) p 173
- [92] C. Yong, P. Smith, A.J. Heeger, *Synth. Met.* 57 (1993) p 3514
- [93] X.G. Li, M. R, Huang, Y. Yang, *J. Polym.* 32 (2000) p 348
- [94] B. Zhao, K.G. Neoh, E.T. Kang, *Chem. Mater.* 12 (2000) p 1800
- [95] G.G. Wallace, P.R. Teasdale, G.M. Spinks, L.A.P. Kane-Maguire, *Conductive electroactive polymers-intelligent materials systems*, 2nd Edition, CRC Press (2003) p 237
- [96] R.S. Kohlman, and A.J., Epstein, *Handbook of Conducting Polymers*. Marcel Dekker, inc. 2nd Edition, New York, (1998)
- [97] C.C. Bidwell, *Phys. Rev.* 58 (1940) p 561
- [98] C.L. Choy, *Polymer* 18 (1977) p 984
- [99] A.J. Attias, *Polymères conjugués et polymères conducteurs électroniques*, *Techniques de l'ingénieur*, traité d'électronique, E1 862-1 (2002) p 1
- [100] O. Solomeshch, Y.J. Yu, V. Medvedev, A. Razin, *B. Synth. Met.* 157 (2007) p 841
- [101] G. Grem, G. Leditzky, B. Ulrich, *Synth. Met.* 51 (1992) p383
- [102] J. Obrzut, F. E. Karasz, *J. Chem. Phys.* 87 (1987) p 2349
- [103] P. Reiss, A. pron, *Encyclopedia of Nanoscience and nanotechnology*, H. S. Nalwa ,American Scientific Publishers, Stevenson Ranch, Californy, 6 (2004) p 587
- [104] A.J. Heeger, *Handbook of conducting polymers*, M. Dekker, New York, 2 (1986) p 279
- [105] J. L. Bredas, *Conjugated polymers and related materials: the interconnection of chemical and electronic structure*, B. Randy (1993) p 187
- [106] A.J. Heeger, *Synth. Met.* 125 (2002) p 23
- [107] J L. Bredas, G. B. Street, *Acc. Chem. Res.* 18 (1985) p 309
- [108] F.F. Runge, *Annalen der Physik und Chemie* 107 (1834) p 65
- [109] J. Fritzsche, *Journal fur praktische Chemie*,20 (1840) p 453
- [110] H. Letheby, *J. Chem. Soc.* 15 (1862) p 161
- [111] E. Noelting, *Scientific and Industrial History of Aniline Black*, WM. J. Matheson & Co (1889)
- [112] J.J. Coquillon, *Compt. Rend.* 81 (1985) p 408
- [113] A.G. Green, A.E. Woodhead, *J. Chem. Soc. Trans.* 97 (1910) p 2388
- [114] O.W. Brown, W.C. Friche, *J. Phys. Chem.* 51 (1947) p 1394
- [115] H. Shirakawa, E.J. Louis, A.G. MacDiarmid, C.K. Chiang, A. J. Heeger , *J. Chem. Soc. Chem. Commun.* 16 (1977) p 578
- [116] A.G. MacDiarmid, J.C. Chiang, M. Halpern, W.S Huang., S.L. Mu, N.L.D. Somasiri, W. Wu, S.I. Yaniger, *Molecular Crystals and Liquid Crystals*, 121 (1985) p 173
-

- [117] J.P. Travers, J. Chroboczek, F. Devreux, F. Genoud, M. Nechtschein, A. Syed, E.M. Genies, C. Tsintavis, *Mol. Cryst. Liq. Cryst.* 121 (1985) p 195
- [118] A.G. MacDiarmid, *Conjugated Polymers and Related Materials, The polyanilines : a novel class of conducting polymers*, W. R. Salaneck, I. Lundström et B. Ranby, Oxford University Press, part 2 (1993) p 73
- [119] M. Dioromedof, F.H. Cristofini, R. DeSurville, M. Jozefowicz, L.T. Yu, R. Buvet, *J.Chem. Phys* 68 (1971) p 1005
- [120] A. G. MacDiarmid, J. C. Chiang, M. Halppern, W. S. Huang, S. L. Mu, N. L. Somasiri, *Mol. Cryst. Liq. Cryst. Sci. Technol. A* 121 (1985) p 173
- [121] M. Ginder, A.F. Richter, A.G. MacDiarmid, A.J. Epstein, *Bull. Am. Phys. Soc.* 31 (1986) p 582
- [122] A.G. Macdiarmid, A.J. Epstein, *Lower-dimensional system and Molecular Electronic*, Plenum Press, New-York, (A991) p 303
- [123] A.G. Macdiarmid, *Conjugated polymers and Related Materials : the interconnection of chemical and electronic structure*, Eds, W.R. Salaneck, I. Lundstrom, R. Ranby, Oxford University Press, Oxford, Part 2, p (1993) 73
- [124] A. Pron, P. Rannou, *Prog. Polym. Sci.* 27 (2002) p 135
- [125] M. Dioromedof, F. Hautier-Cristofini, R. de Surville, M. Jozefowicz, L.T. Yu, R. Buvet. *J. Chim. Phys.* 68 (1971) p 1005
- [126] F. Genoud, C. Menardo, M. Nechtschein, J.P. Tavers, P. Hany, *springer series in solid- state*, Eds. H. Kuzmany, M Mehning, S. Roth, Springer-verlag, Heidelberg 76 (1987) p 244
- [127] E.T. Kang, K.G. Neoh, K.L. Tan. B.T.G Tan, *Synth. Met.* 46 (192) p 227
- [128] A.G. MacDiarmid, W.E. Jones Jr., I.D. Norris, J. Gao, A.T. Johnson Jr., N.J. Pinto, J. Hone, B. Han, F.K. Ko, H. Okuzaki, M. L laguno *Synth. Met.* 119 (2001) p 27
- [129] C.D. Liu, S.Y. Wu, J.L.Han, K.H. Hsieh, *J. Appl. Poly. Sci.* 115 (2010) p 2271
- [130] D. Chaudhuri, S. Datar, R. Viswanatha, D.D. Sarma, H. Amenitsch *Appl. Phys. Letter.* 87 (2005) p 093117
- [131] S.R. Mohanty, N.K. Neog, R.S. Rawat, P. Lee, B.B. Nayak, B.S. Acharya, *Phys. Letter.A* 373 (2009) p 1962
- [132] S.P. Surwade, N. Manohar, S.K. Manohar, *Macromolecules* 42 (2009) p 1792
- [133] S.M. Yang, K.H. Chen, Y.F. Yang, *Synth. Met.* 152 (2005) p 65
- [134] X. Zhang, W.J. Goux, S.K. Manohar, *J. Am.Chem. Soc.* 126 (2004) p 4502
- [135] L.J. Pan, L. Pu, Y. Shi, S.Y. Song, Z. Xu, R. Zhang, Y.D. Zheng *Adv. Mater.* 19 (2007) p 461
- [136] W. Li, H.L. Wang, *J. Am.Chem. Soc.* 126 (2004) p 2278
- [137] S. Xing, C. Zhao, S. Jing, Z. Wang, *Polymer* 47 (2006) p 2305
- [138] P. Nickels, W.U. Dittmer, S. Beyer, J.P. Kotthaus, F.C. Simmel, *Nanotechnology* 15 (2004) p 1524
- [139] T. Jeevananda, J.H. Lee, Siddaramaiah, *Mater. Letter.* 62 (2008) p 3995

- [140] X. Jing, Y. Wang, D. Wu, L. She, Y. Guo, *J. Polym. Sci. A: Polym. Chem.* 44 (2006) p 1014
- [141] X. Lu, H. Mao, D. Chao, W. Zhang, Y. Wei, *Macro.Chem. Phys.* 207 (2006) p 2142
- [142] W. Huang, B.D. Humphrey, A.G. MacDiarmid, *J. Am.Chem. Soc., Faraday Transactions 1: Physical Chemistry in Condensed Phases* 82 (1986) p 2385
- [143] A.G. MacDiarmid, J.C. Chiang, A.F. Richter, A.J. Epstein, *Synth. Met.* 18 (1987) p 285
- [144] A.G. MacDiarmid, J.C. Chiang, A.F. Richter, N.L.D. Somarisi, *Conducting Polymers :Special applications*, Ed. L. Alcacer, Reidel, Dordrecht, (1984) p 105
- [145] A.Pron, F. Genoud, C. Mnerdo, M. Nechtschein, *Synth. Met.* 24 (1988) p 193
- [146] A. Pron, P. Rannou, *Prog. Polym. Sci.* 27 (2002) p 135
- [147] Y. Cao, A. Andreatta, A. J. Heeger, P. Smith, *Polymer* 30 (1989) p 2305
- [148] N. Gopodinova and L. Terlemzyan. *Prog. Polym. Sci.* 23 (1998) p 1443
- [149] J. Stejskal, I. Spurina, *Pure Appl. Chem.* 77 (2005) p 815
- [150] J. Stejskal, R. G. Gilbert, *Pure Appl. Chem.* 74 (2002) p 857
- [151] A. Andreatta, Y. Cao, J. C. Chiang, A. J Heeger, P. Smith, *Synth. Met.* 26 (1988) p 383
- [152] M. Lapkowski, *Synth. Met.* 35 (1990) p 169
- [153] J. Yano, T. Ohnishi, A. Kitani, *Synth. Met.* 101 (1999) p 752
- [154] M.V. Kulkarni, A.K. Viswanath, U.P. Mulik, *Mater. Chem. Phys.* 89 (2005) p 1
- [155] Y.Z. Wang, J. Joo, C.H. Hsu, A.J. Epstein, *Synth. Met.* 68 (1995) p 207
- [156] E.R. Holland, S.J. Pomfret, P.N. Adams, L. Abell, A.P. Monkman, *Synth. Met.* 84 (1997) p 777
- [157] Y.F. Nicolau, P.M. Beadle, E. Banka, *Synth. Met.* 84 (1997) p 585
- [158] S.K. Jeong, J.S. Suh, E.J. Oh, Y.W. Park, C.Y. Kim, A.G. MacDiarmid, *Synth. Met.* 69 (1995) p 171
- [159] V.I. Krinichnyi, S.V. Tokarev, H.K. Roth, M. Schrödner, B. Wessling, *Synth. Met.* 156 (2006) p 1368
- [160] Y. Cao, A. J. Heeger, *Synth. Met.* 52 (1992) p 193
- [161] I. Kulszewicz-Bajer, M. Zagórska, J. Niziol, A. Pron, W. Luzny, *Synth. Met.* 114 (2000) p 125
- [162] G. G. Wallace, G. M. Spinks, and L. A. P. Kane-Maguire, *Conductive Electroactive Polymers: Intelligent Materials Systems*, CRC Press. 2002.
- [163] D. Nicolas-Debarnot and F. Poncin-Epaillard, —Polyaniline as a new sensitive layer for gas sensors,|| *Anal. Chim. Acta*, vol. 475, no. 1–2, pp. 1–15, Jan. 2003.
- [164] G. Zotti, S. Cattarin, and N. Comisso, —Cyclic potential sweep electropolymerization of aniline: The role of anions in the polymerization mechanism,|| *J. Electroanal. Chem. Interfacial Electrochem.*, vol. 239, no. 1–2, pp. 387–396, Jan. 1988.
- [165] M. Takakubo, —Molecular orbital study of the initial reaction paths in the electrochemical polymerization of aniline,|| *Synth. Met.*, vol. 33, no. 1, pp. 19–26, Nov. 1989.

- [166] F. Lux, —Properties of electronically conductive polyaniline: a comparison between well-known literature data and some recent experimental findings, *Polym. J.*, vol. 35, no. 14, pp. 2915–2936, Jul. 1994.
- [167] Y. Wei, X. Tang, Y. Sun, and W. W. Focke, —A study of the mechanism of aniline polymerization, *J. Polym. Sci. Part Polym. Chem.*, vol. 27, no. 7, pp. 2385–2396, Jun. 1989.
- [168] N. Gospodinova, L. Terlemezyan, P. Mokreva, and K. Kossev, —On the mechanism of oxidative polymerization of aniline, *Polym. J.*, vol. 34, no. 11, pp. 2434–2437, 1993.
- [169] N. Gospodinova, P. Mokreva, and L. Terlemezyan, —Chemical oxidative polymerization of aniline in aqueous medium without added acids, *Polym. J.*, vol. 34, no. 11, pp. 2438–2439, 1993.
- [170] G. Ćirić-Marjanović, E. N. Konyushenko, M. Trchová, and J. Stejskal, —Chemical oxidative polymerization of anilinium sulfate versus aniline: Theory and experiment, *Synth. Met.*, vol. 158, no. 5, pp. 200–211, Mar. 2008.
- [171] G. Ćirić-Marjanović, M. Trchová, and J. Stejskal, —Theoretical study of the oxidative polymerization of aniline with peroxydisulfate: Tetramer formation, *Int. J. Quantum Chem.*, vol. 108, no. 2, pp. 318–333, 2008.
- [172] J. Stejskal, I. Sapurina, and M. Trchová, —Polyaniline nanostructures and the role of aniline oligomers in their formation, *Prog. Polym. Sci.*, Jul. 2010
- [173] J. K i, L. Starovoytova, M. Trchová, E. N. Konyushenko, and J. Stejskal, —NMR Investigation of Aniline Oligomers Produced in the Early Stages of Oxidative Polymerization of Aniline, *J. Phys. Chem. B*, vol. 113, no. 19, pp. 6666–6673, May 2009
- [174] S. Bhadra, S. Chattopadhyay, N. K. Singha, and D. Khastgir, —Improvement of conductivity of electrochemically synthesized polyaniline, *J. Appl. Polym. Sci.*, vol. 108, no. 1, pp. 57–64, 2008.
- [175] S. Bhadra, N. K. Singha, and D. Khastgir, —Polyaniline by new miniemulsion polymerization and the effect of reducing agent on conductivity, *Synth. Met.*, vol. 156, no. 16–17, pp. 1148–1154, Aug. 2006.
- [176] S. Bhadra, N. K. Singha, S. Chattopadhyay, and D. Khastgir, —Effect of different reaction parameters on the conductivity and dielectric properties of polyaniline synthesized electrochemically and modeling of conductivity against reaction parameters through regression analysis, *J. Polym. Sci. Part B Polym. Phys.*, vol. 45, no. 15, pp. 2046–2059, 2007.
- [177] S. Bhadra, N. K. Singha, and D. Khastgir, —Dual functionality of PTSA as electrolyte and dopant in the electrochemical synthesis of polyaniline, and its effect on electrical properties, *Polym. Int.*, vol. 56, no. 7, pp. 919–927, 2007.
- [178] S. Bhadra and D. Khastgir, —Degradation and stability of polyaniline on exposure to electron beam irradiation (structure–property relationship), *Polym. Degrad. Stab.*, vol. 92, no. 10, pp. 1824–1832, Oct. 2007.
- [179] A. G. MacDiarmid, —Polyaniline and polypyrrole: Where are we headed?, *Synth. Met.*, vol. 84, no. 1–3, pp. 27–34, Jan. 1997.
- [180] S. Bhadra, N. K. Singha, and D. Khastgir, —Electrochemical synthesis of polyaniline and its comparison with chemically synthesized polyaniline, *J. Appl. Polym. Sci.*, vol. 104, no. 3, pp. 1900–1904, 2007.
- [181] G. Vettorazzi, B. Radaelli-Benbenuti, *International Regulatory Aspects for Pesticides Chemicals. Vol II: Toxicological data profiles.* CRC Press Inc. Boca Raton, Florida. (1982).

- [182] S. Kobayashi, H. Uyama, and S. Kimura, —Enzymatic Polymerization,|| Chem. Rev., vol. 101, no. 12, pp. 3793–3818, Dec. 2001.
- [183] R. Cruz-Silva, C. Ruiz-Flores, L. Arizmendi, J. Romero-García, E. Arias-Marin, I. Moggio, F. F. Castillon, and M. H. Farias, —Enzymatic synthesis of colloidal polyaniline particles,|| Polymer, vol. 47, no. 5, pp. 1563–1568, Feb. 2006.
- [184] Griffith MP (2004) The origins of an important cactus crop, *Opuntia ficus-indica* (Cactaceae): new molecular evidence. *Am J Bot* 91: 1915-1921.
- [185] Saenz C (2000) Processing technologies: an alternative for cactus pear (*Opuntia* spp.) fruits and cladodes. *Journal of Arid Environments* 46: 209-225.
- [186] S. Bhadra, N. K. Singha, and D. Khastgir, —Polyaniline by new miniemulsion polymerization and the effect of reducing agent on conductivity,|| Synth. Met., vol. 156, no. 16–17, pp. 1148–1154, Aug. 2006.
- [187] E. R. Holland, S. J. Pomfret, P. N. Adams, L. Abell, and A. P. Monkman, —Doping dependent transport properties of polyaniline-CSA films,|| Synth. Met., vol. 84, no. 1–3, pp. 777–778, Jan. 1997.
- [188] P. Kiattibutr, L. Tarachiwin, L. Ruangchuay, A. Sirivat, and J. Schwank, —Electrical conductivity responses of polyaniline films to SO₂-N₂ mixtures: effect of dopant type and doping level,|| React. Funct. Polym., vol. 53, no. 1, pp. 29–37, Oct. 2002.
- [189] S. Roth and W. Graupner, —Conductive polymers: Evaluation of industrial applications,|| Synth. Met., vol. 57, no. 1, pp. 3623–3631, Apr. 1993.
- [190] B. Wessling, —Dispersion as the link between basic research and commercial applications of conductive polymers (polyaniline),|| Synth. Met., vol. 93, no. 2, pp. 143–154, Mar. 1998.
- [191] M. S. Cho, S. Y. Park, J. Y. Hwang, and H. J. Choi, —Synthesis and electrical properties of polymer composites with polyaniline nanoparticles,|| Mater. Sci. Eng. C, vol. 24, no. 1–2, pp. 15–18, Jan. 2004
- [192] T. Hino, S. Taniguchi, and N. Kuramoto, —Syntheses of conductive adhesives based on epoxy resin and polyanilines by using N-tert-butyl-5-methylisoxazolium perchlorate as a thermally latent curing reagent,|| J. Polym. Sci. Part Polym. Chem., vol. 44, no. 2, pp. 718–726, 2006.
- [193] M. Hosoda, T. Hino, and N. Kuramoto, —Facile preparation of conductive paint made with polyaniline/dodecylbenzenesulfonic acid dispersion and poly(methyl methacrylate),|| Polym. Int., vol. 56, no. 11, pp. 1448–1455, 2007.
- [194] R. A. de Barros, C. R. Martins, and W. M. de Azevedo, —Writing with conducting polymer,|| Synth. Met., vol. 155, no. 1, pp. 35–38, Oct. 2005.
- [195] Y. Yoshioka and G. E. Jabbour, —Desktop inkjet printer as a tool to print conducting polymers,|| Synth. Met., vol. 156, no. 11–13, pp. 779–783, Jun. 2006.
- [196] D. Bowman and B. R. Mattes, —Conductive Fibre Prepared From Ultra-High Molecular Weight Polyaniline for Smart Fabric and Interactive Textile Applications,|| Synth. Met., vol. 154, no. 1–3, pp. 29–32, Sep. 2005.
- [197] A. Ohtani, M. Abe, M. Ezo, T. Doi, T. Miyata, and A. Miyake, —Synthesis and properties of high-molecular-weight soluble polyaniline and its application to the 4MB-capacity barium ferrite floppy disk's antistatic coating,|| Synth. Met., vol. 57, no. 1, pp. 3696–3701, Apr. 1993.
- [198] K. F. Schoch Jr., W. A. Byers, and L. J. Buckley, —Deposition and characterization of conducting polymer thin films on insulating substrates,|| Synth. Met., vol. 72, no. 1, pp. 13–23, Apr. 1995.

- [199] V. G. Kulkarni, J. C. Campbell, and W. R. Mathew, —Transparent conductive coatings, *Synth. Met.*, vol. 57, no. 1, pp. 3780–3785, Apr. 1993.
- [200] M. S. Cho, Y. H. Cho, H. J. Choi, and M. S. Jhon, —Synthesis and Electrorheological Characteristics of Polyaniline-Coated Poly(methyl methacrylate) Microsphere: Size Effect, *Langmuir*, vol. 19, no. 14, pp. 5875–5881, Jul. 2003.
- [201] I. S. Lee, M. S. Cho, and H. J. Choi, —Preparation of polyaniline coated poly(methyl methacrylate) microsphere by graft polymerization and its electrorheology, *Polymer*, vol. 46, no. 4, pp. 1317–1321, Feb. 2005.
- [202] I. S. Lee, J. Y. Lee, J. H. Sung, and H. J. Choi, —Synthesis and electrorheological characteristics of polyaniline-titanium dioxide hybrid suspension, *Synth. Met.*, vol. 152, no. 1–3, pp. 173–176, Sep. 2005.
- [203] M. S. Cho, H. J. Choi, and W.-S. Ahn, —Enhanced Electrorheology of Conducting Polyaniline Confined in MCM-41 Channels, *Langmuir*, vol. 20, no. 1, pp. 202–207, Jan. 2004.
- [204] H. J. Choi, T. W. Kim, M. S. Cho, S. G. Kim, and M. S. Jhon, —Electrorheological characterization of polyaniline dispersions, *Eur. Polym. J.*, vol. 33, no. 5, pp. 699–703, May 1997.
- [205] H. Bai, Q. Chen, C. Li, C. Lu, and G. Shi, —Electrosynthesis of polypyrrole/sulfonated polyaniline composite films and their applications for ammonia gas sensing, *Polymer*, vol. 48, no. 14, pp. 4015–4020, Jun. 2007.
- [206] M. Irimia-Vladu and J. W. Fergus, —Suitability of emeraldine base polyaniline-PVA composite film for carbon dioxide sensing, *Synth. Met.*, vol. 156, no. 21–24, pp. 1401–1407, Dec. 2006.
- [207] X. B. Yan, Z. J. Han, Y. Yang, and B. K. Tay, —NO₂ gas sensing with polyaniline nanofibers synthesized by a facile aqueous/organic interfacial polymerization, *Sens. Actuators B Chem.*, vol. 123, no. 1, pp. 107–113, Apr. 2007.
- [208] V. Dixit, S. C. K. Misra, and B. S. Sharma, —Carbon monoxide sensitivity of vacuum deposited polyaniline semiconducting thin films, *Sens. Actuators B Chem.*, vol. 104, no. 1, pp. 90–93, Jan. 2005.
- [209] S. Jain, A. B. Samui, M. Patri, V. R. Hande, and S. V. Bhoraskar, —FEP/polyaniline based multilayered chlorine sensor, *Sens. Actuators B Chem.*, vol. 106, no. 2, pp. 609–613, May 2005.
- [210] M. Ando, C. Swart, E. Pringsheim, V. M. Mirsky, and O. S. Wolfbeis, —Optical ozone-sensing properties of poly(2-chloroaniline), poly(N-methylaniline) and polyaniline films, *Sens. Actuators B Chem.*, vol. 108, no. 1–2, pp. 528–534, Jul. 2005.
- [211] J.-S. Kim, S.-O. Sohn, and J.-S. Huh, —Fabrication and sensing behavior of PVF₂ coated-polyaniline sensor for volatile organic compounds, *Sens. Actuators B Chem.*, vol. 108, no. 1–2, pp. 409–413, Jul. 2005.
- [212] S. H. Hosseini and A. A. Entezami, —Preparation and characterization of polyaniline blends with polyvinyl acetate, polystyrene and polyvinyl chloride for toxic gas sensors, *Polym. Adv. Technol.*, vol. 12, no. 8, pp. 482–493, 2001.
- [213] S. S. Joshi, C. D. Lokhande, and S.-H. Han, —A room temperature liquefied petroleum gas sensor based on all-electrodeposited n-CdSe/p-polyaniline junction, *Sens. Actuators B Chem.*, vol. 123, no. 1, pp. 240–245, Apr. 2007.
- [214] R. Nohria, R. K. Khillan, Y. Su, R. Dikshit, Y. Lvov, and K. Varahramyan, —Humidity sensor based on ultrathin polyaniline film deposited using layer-by-layer nano-assembly, *Sens. Actuators B Chem.*, vol. 114, no. 1, pp. 218–222, Mar. 2006.

-
- [215] C. Muthukumar, S. D. Kesarkar, and D. N. Srivastava, —Conductometric mercury [II] sensor based on polyaniline–cryptand-222 hybrid, *J. Electroanal. Chem.*, vol. 602, no. 2, pp. 172–180, Apr. 2007.
- [216] A. Talaie, J. Y. Lee, Y. K. Lee, J. Jang, J. A. Romagnoli, T. Taguchi, and E. Maeder, —Dynamic sensing using intelligent composite: an investigation to development of new pH sensors and electrochromic devices, *Thin Solid Films*, vol. 363, no. 1–2, pp. 163–166, Mar. 2000.
- [217] K. Arora, G. Sumana, V. Saxena, R. K. Gupta, S. K. Gupta, J. V. Yakhmi, M. K. Pandey, S. Chand, and B. D. Malhotra, —Improved performance of polyaniline-uricase biosensor, *Anal. Chim. Acta*, vol. 594, no. 1, pp. 17–23, Jun. 2007.
- [218] J. Ren, F. He, L. Zhang, C. Su, and Z. Liu, —A new B-PAn-P system for the detection of bacteria population, *Sens. Actuators B Chem.*, vol. 125, no. 2, pp. 510–516, Aug. 2007.
- [219] Y. Andreu, S. de Marcos, J. R. Castillo, and J. Galbán, —Sensor film for Vitamin C determination based on absorption properties of polyaniline, *Talanta*, vol. 65, no. 4, pp. 1045–1051, Feb. 2005.
- [220] A. A. Syed and M. K. Dinesan, —Polyaniline: Reaction stoichiometry and use as an ion-exchange polymer and acid/base indicator, *Synth. Met.*, vol. 36, no. 2, pp. 209–215, Jun. 1990.

CHAPTER II

MATERIALS AND METHODS

II. PREPARATION AND CHARACTERISATION OF ADSORBENTS

II.1. INTRODUCTION

This chapter presents firstly general description of used products and the procedures followed in the preparation of OFI-A (Opuntia ficus indica activated by (NaOH)), the synthesis of the PANI (polyaniline) and the Hybrid material PANI@OFI-A, also the analytical techniques use for the characterization of the different material used for the removal of organic dye (Orange-G). Finally, the selected method for detection of the pollutant in the aqueous solution.

II.2. USED PRODUCTS

All the products that have been used to perform the experiments are.

- Aniline's monomer ($C_6H_5NH_2$) is of analytical grade obtained from Aldrich (99%) (The aniline monomer was vacuum distilled before using)
- Hydrochloric acid (HCl) is analytical grade obtained from Merck (37%, d -1.18) is used as a doping agent.
- A solution of Ammonium Hydroxyde (NH_4OH) is obtained from (Haene Reidel) is used as a dedopiant.
- Ammonium persulfate ($(NH_4)_2S_2O_8$) is obtained from (Haene's Riedel; 98%) is used as an oxidizer.
- Methanol (CH_3OH) and Sodium Hydroxide (NaOH) obtained from the laboratory.
- The distilled water used to prepare solutions is obtained from a Gesellschaft fur labortechnikmbH (D-309 38 Burgwedel).
- The demineralized water used for the purification of the resulting materials is Produced by an ultra Elga Labwater Purelab system.
- OFI (Opuntia ficus indica) Collected from local area (Mascara Province) and we have done the preparation it in the laboratory of the university of Mustapha Stambouli.
- Orange-G dye (OG) Pestanal® ($C_{16}H_{10}N_2Na_2O_7S_2$).
-

II.3. PREPARATION OF DIFFRENTS ADSORBENTS

II.3.1. Preparation of the Opuntia Ficus Indica OFI-A adsorbent

OFI cladodes were collected from local area Mascara, Algeria. The OFIs were washed several times with distilled water to remove lingering impurities, soluble particles and other contaminants.

The washed OFI leaves were cut to small size pieces (approximate 1–3 cm), after removing thorns thoroughly and dried at 105 °C for 24 hours until the total humidity elimination, which was contained within the sample.

The dried OFI was crushed (Raw OFI). Further, after activation of the Raw OFI by 1 M NaOH, then the produced sample was thorough washed with distilled water to remove and soluble impurity till the pH of the filtrate was neutral (pH ~ 7) and the washing water is clean to ensure the removal of any color from the sample, the obtained material was dried at 105 °C. Finally, the produced material was crushed again and sieved in a sieve of 0.125mm. This activated sample were marked as OFI-A. This obtained adsorbent OFI-A was stored in a closed and dried container at room temperature until use.

II.3.2. Synthesis of the Polyaniline PANI

Polyaniline PANI was prepared as follows:

1 ml of aniline mixed with 50 ml HCl (1 M) to prepare a solution of aniline (0.22 M), the solution stirred continuously for 1 hour, the solution kept at (0 to 5 °C). A mass of ammonium persulfate APS ($(\text{NH}_4)_2\text{S}_2\text{O}_8$ (2.45 g) was dissolved in 50 ml of HCl (1 M) to prepare a solution of APS 0.22 M.

The prepared solution of APS (0.22 M) added slowly to the aniline solution with continuous stirring. The Temperature of the reaction mixture should kept at (0 to 5 °C) during the reaction, the mixture turned green after some few minutes, which indicates the formation of polyaniline in its doped state. The reaction mixture kept with continuous stirring for 24 hours. The prepared polymer collected on a filter paper and washed with demineralized water. The obtained PANI emeraldine salt (ES) rinsed in excess of 0.5 M NH_4OH at room temperature for 3h, the polyaniline PANI was rinsed with ethanol and demineralized water to remove entire impurities then dried at 60 °C in a vacuum drying oven. The dried PANI crushed and sieved through a sieve of 0.125 mm size and stored away from humidity [1].

II.3.3. Synthesis of the aniline / *Opuntia Ficus Indica* PANI/OFI-A nanocomposite

The aniline /OFI-A nanocomposite was prepared as follow.

111 mg of dried OFI-A added to 50 ml of HCl (1M), the mixture kept under stirring for 1 hour, 1 ml of aniline was added to the previous mixture, (the aniline concentration in the solution is 0.22 M and OFI-A /aniline weight ratio is 10%), the mixture stirred for 20 min.

The oxidizing solution which is prepared separately by dissolving 2.45g of ammonium persulfate ($(\text{NH}_4)_2\text{S}_2\text{O}_8$) into 50 ml of 1M HCl solution. The 50 ml of oxidizing solution added slowly to the OFI-A /aniline solution (ensuring the 1:1 aniline/oxidant molar ratio), the mixture was kept in an ice bath ($T < 5\text{ }^\circ\text{C}$) with continuous stirring, the reaction turned green after some few minutes, which is the indication of the formation of polyaniline in its doped state. The reaction mixture was stirred for 24 hours.

The obtained product was washed with NH_4OH 0.5M at room temperature for 3h. The hybrid adsorbent was rinsed with ethanol and deionized water to remove entire impurities then dried at $60\text{ }^\circ\text{C}$ in a vacuum drying oven [1-3].

The dried hybrid adsorbent crushed and sieved in a sieve of 0.125 mm size, and stored in a dry place.

A graphical exemplification of the most important steps for preparing the PANI@OFI-A is presented in (Fig.II.1.).

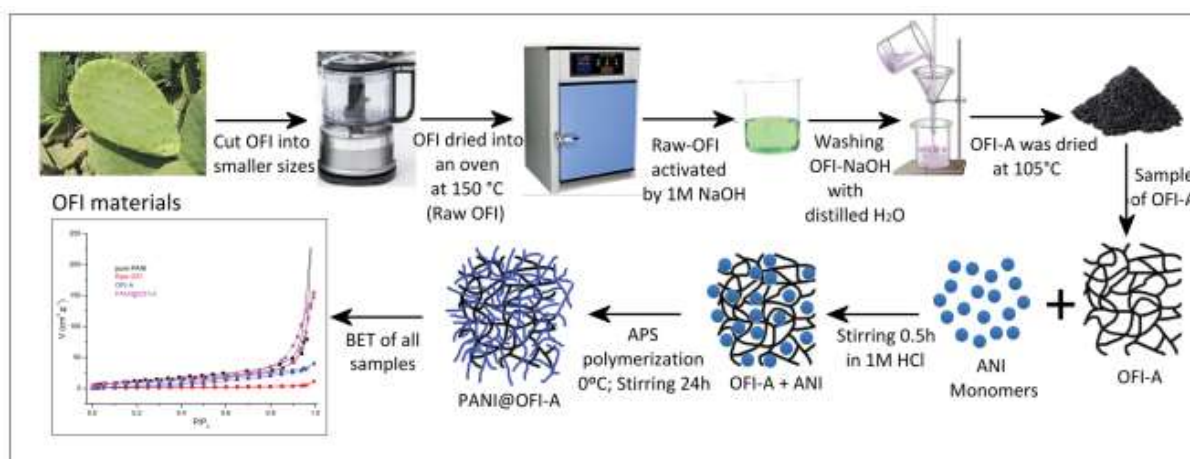


Figure.II.1 Schematic representation of the most important steps to prepare the PANI@OFI-A

II.4. CHARACTERISATION TECHNIQUES AND APARATUS

This section describes the analytical techniques used for the characterization of prepared adsorbents. The different samples were characterized using a number of techniques including: Fourier transform infrared spectroscopy (FTIR), thermogravimetric analysis (TGA), X-ray diffraction (XRD) analysis, scanning electron microscopy (SEM) and Brunauer-Emmet-Teller (BET) surface area analysis.

Also the techniques used for the quantitative analysis of dyes during adsorption studies are described in this section

II.4.1. X-ray diffraction

II.4.1.1. Generality:

X-ray diffraction (XRD) is a powerful nondestructive technique for characterizing crystalline materials. It provides information on structures, phases, preferred crystal orientations (texture), and other structural parameters, such as average grain size, crystallinity, strain, and crystal defects. X-ray diffraction peaks are produced by constructive interference of a monochromatic beam of X-rays scattered at specific angles from each set of lattice planes in a sample. The peak intensities are determined by the distribution of atoms within the lattice. Consequently, the X-ray diffraction pattern is the fingerprint of periodic atomic arrangements in a given material.

X-ray diffraction (XRD) is an analytical technique used to characterize crystalline phases of a wide variety of materials, typically for mineralogical analysis and identification of unknown materials. Powder diffraction data are fundamentally derived by the atomic and molecular arrangements explained by the physics of crystallography.

There are several advantages of XRD techniques in science laboratories:

- Nondestructive, fast, and easy sample preparation.
- High-accuracy for d-spacing calculations.
- Can be done in situ.
- Allows characterizing single crystal, poly, and amorphous materials.
- Standards are available for thousands of material systems[4].

During this thesis work, the device used to characterize the thin films synthesized is a D8 Advance diffractometer (Bruker) with Bragg-Brentano geometry in $\theta/2\theta$ configuration with a copper anticathode ($K \alpha_1 = 1.5406 \text{ \AA}$). radiations, as a general rule the doublet $K\alpha$ ($K\alpha_1$ and $K\alpha_2$) [5]. Like all electromagnetic waves, cause the electron cloud to move relative to the nucleus in atoms. These induced oscillations cause re-emission of electromagnetic waves of the same frequency: this phenomenon is called Rayleigh scattering (figure II.2). The wavelength of X-rays being of the order of magnitude of interatomic distances (a few Angstroms), the interference of the rays scattered by the atoms constituting the crystallized matter will be alternately constructive or destructive. Depending on the direction of space, we will therefore have a significant flow of X photons, or on the contrary very weak; these variations according to the directions form the phenomenon of X-ray diffraction.

The directions in which the interferences are constructive, called "diffraction peaks", can be determined very simply by the following formula, called Bragg's law :

$$n\lambda = 2d\sin\theta \quad (II.1)$$

Where:

- λ is the wavelength of the x-ray,
- d is the spacing of the crystal layers (path difference),
- θ is the incident angle (the angle between incident ray and the scatter plane), and
- n is an integer.

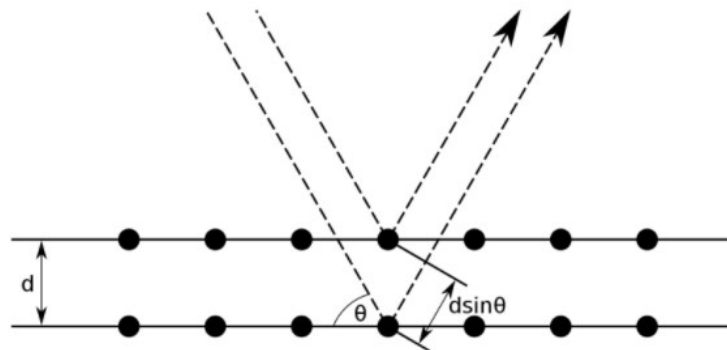


Figure.II.2. Bragg Diffraction Planes

In order to identify the phases constituting the samples studied, the diffractograms obtained are compared with the JCPDS files of the ICDD database. The position of the diffraction peaks is obtained in degrees (2θ) and related to the distance (d_{hkl}) between the planes (h, k, l) of the structure probed by means of Bragg's law. Thus, it is possible to identify the crystal system (s) formed and the lattice parameters of the structure. Scherrer's (approximate) formula makes it possible to determine the size of crystallites:

$$d = \frac{k \cdot \lambda}{\beta \cdot \cos \theta} \quad (II.2)$$

Where λ is the X-ray wavelength in nanometer (nm), β is the peak width of the diffraction peak profile at half-maximum height resulting from small crystallite size in radians and K is a constant related to crystallite shape, normally taken as 0.9. The value of β in 2θ axis of diffraction profile must be in radians. The θ can be in degrees or radians, since the $\cos(\theta)$ corresponds to the same number.

The crystalline properties of samples were characterized by X-ray diffraction (XRD) using $\text{CuK}\alpha$ as a radiation ($\lambda = 1.5405 \text{ \AA}$) using a Bruker CCD-Apex instrument [6].

II.4.1.2. Interpretation of the XRD diffraction patterns

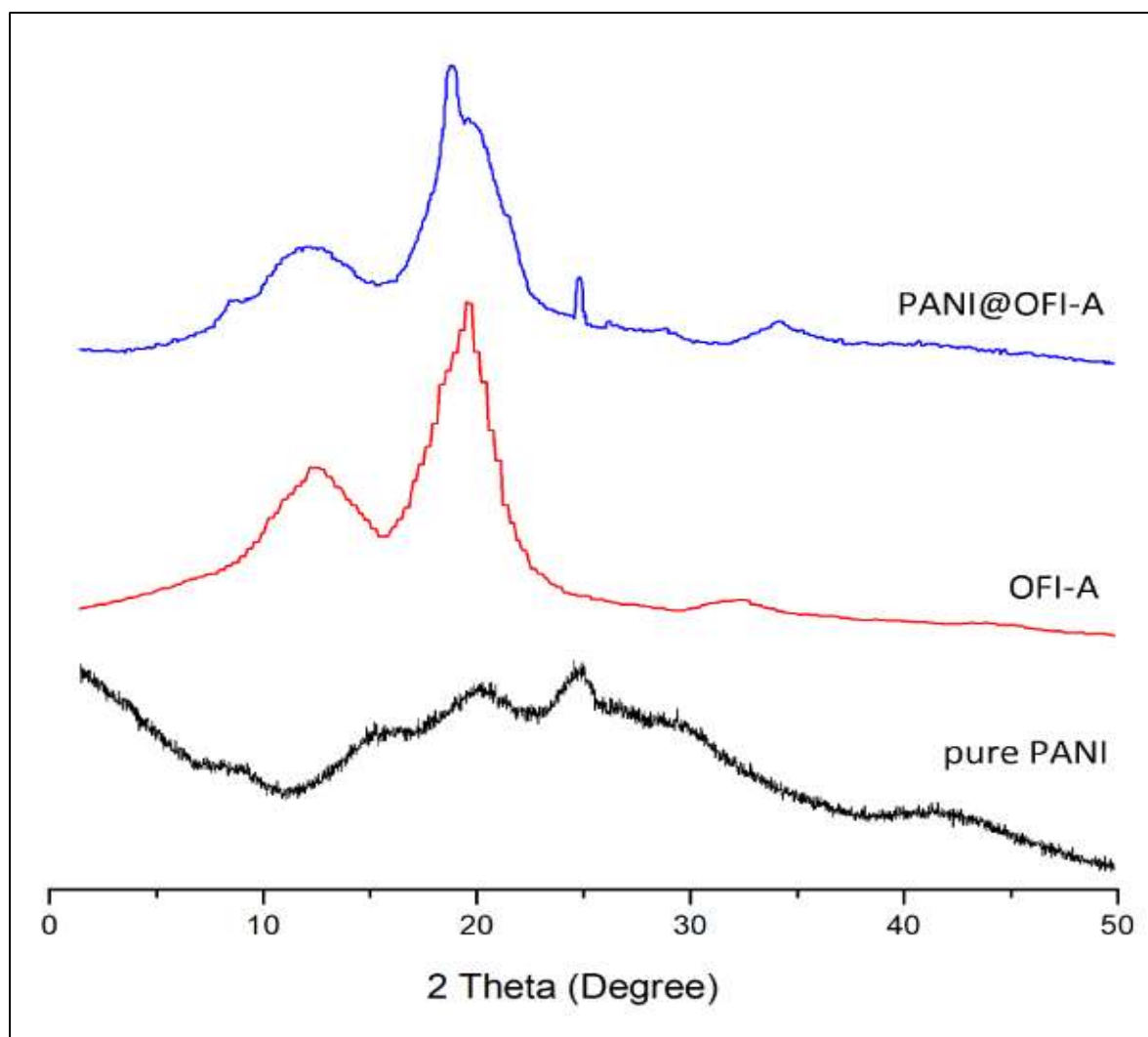


Figure.II.3. XRD diffraction patterns of: PANI, OFI-A and PANI@OFI-A

(Figure II.3) illustrates the results of the XRD test for pure PANI, OFI-A and PANI@OFI-A. The pure PANI XRD pattern shows weak and broad peaks in the angles of $2\theta = 15.69^\circ$, 20.10° and 24.77° , which is due to the amorphous structure and crystallinity of PANI [7]. In addition, the OFI-A showed peaks around $2\theta = 11.21^\circ$ and 19.84° with various intensities.

The peak at $2\theta = 11.21^\circ$ assigned low intensity illustration amorphous zone of the sample and the peak at $2\theta = 19.84^\circ$ represent the high intensity indicating the crystalline region of the sample. Finally, on hybrid material, appeared peaks around $2\theta = 20.04^\circ$ and 24.84° indicated the crystalline structure of a single-phase hexagonal-vortex monocrystal for this adsorbent. According to the data of XRD, it can be deduced that PANI@OFI-A have a high crystallinity compared to other materials, which is due to the good density and uniform distribution of polymer chain as fillers and the formation of crystalline masses.

II.4.2. Fourier Transform Infrared Spectroscopy

II.4.2.1. Principle

Fourier transform infra-red (FTIR) technique is based on the excitation of molecular vibrations by light absorption. It is widely used in the determination of structure and identification of both organic and inorganic compounds. It is mainly used in the identification of functional groups present in a given sample.

In infrared spectroscopy, infrared radiation is passed through a sample. Some of the infrared radiation is absorbed by the sample and some is transmitted. The resulting spectrum represents the molecular absorption and transmission, creating a molecular fingerprint of the sample. Like a fingerprint, no two unique molecular structures produce the same infrared spectrum. This makes FTIR spectroscopy useful for several types of analyses, including: identification of an unknown material, quality control of samples and the determination of amounts of components in a mixture.

The sample analysis process entails the emission of infrared radiation from a black body source. The beam of radiation passes through an aperture which controls the amount of energy presented to the sample and ultimately to the detector. The beam enters the interferometer where 'the spectral encoding' takes place. The resulting interferogram signal then exits the interferometer. The beam enters the sample compartment where it is transmitted through or reflected off the surface of the sample, depending on the type of analysis being carried out. This is where specific frequencies of energy, uniquely characteristic of the sample, are absorbed. The beam finally passes through to the detector for final measurement. The detectors used are specially designed to measure the special interferogram signal [8, 9]. FTIR spectroscopy was used in this study for the analysis of the various adsorbent materials prepared in this work.

II.4.2.3. Interpretation of Fourier Transform Infrared (FTIR) Analysis

FT-IR spectra of PANI, OFI-A and PANI@OFI-A are showed in (Fig.II.4.) OFI-A showed bands related to the hydroxyl vibration were observed at 3331 cm^{-1} and 3223 cm^{-1} [10], which are assigned to the stretching of $-\text{OH}$ groups and the $\text{C}-\text{H}$ stretching peak at 3008 cm^{-1} and 2900 cm^{-1} is attributed to $\text{C}-\text{H}$ stretching and bending vibrations [11]. The weak band at 2207 cm^{-1} due to the nitrile groups ($\text{C}\equiv\text{N}$) and the intense band at 2122 cm^{-1} are due to the $\text{C}\equiv\text{C}$ stretching vibration. Furthermore, the peak observed at 1560 cm^{-1} and 1511 cm^{-1} is due to the $\text{C}=\text{O}$ stretching vibration of the ionic carboxyl group and $\text{N}-\text{H}$ deformation of amines, respectively [12].

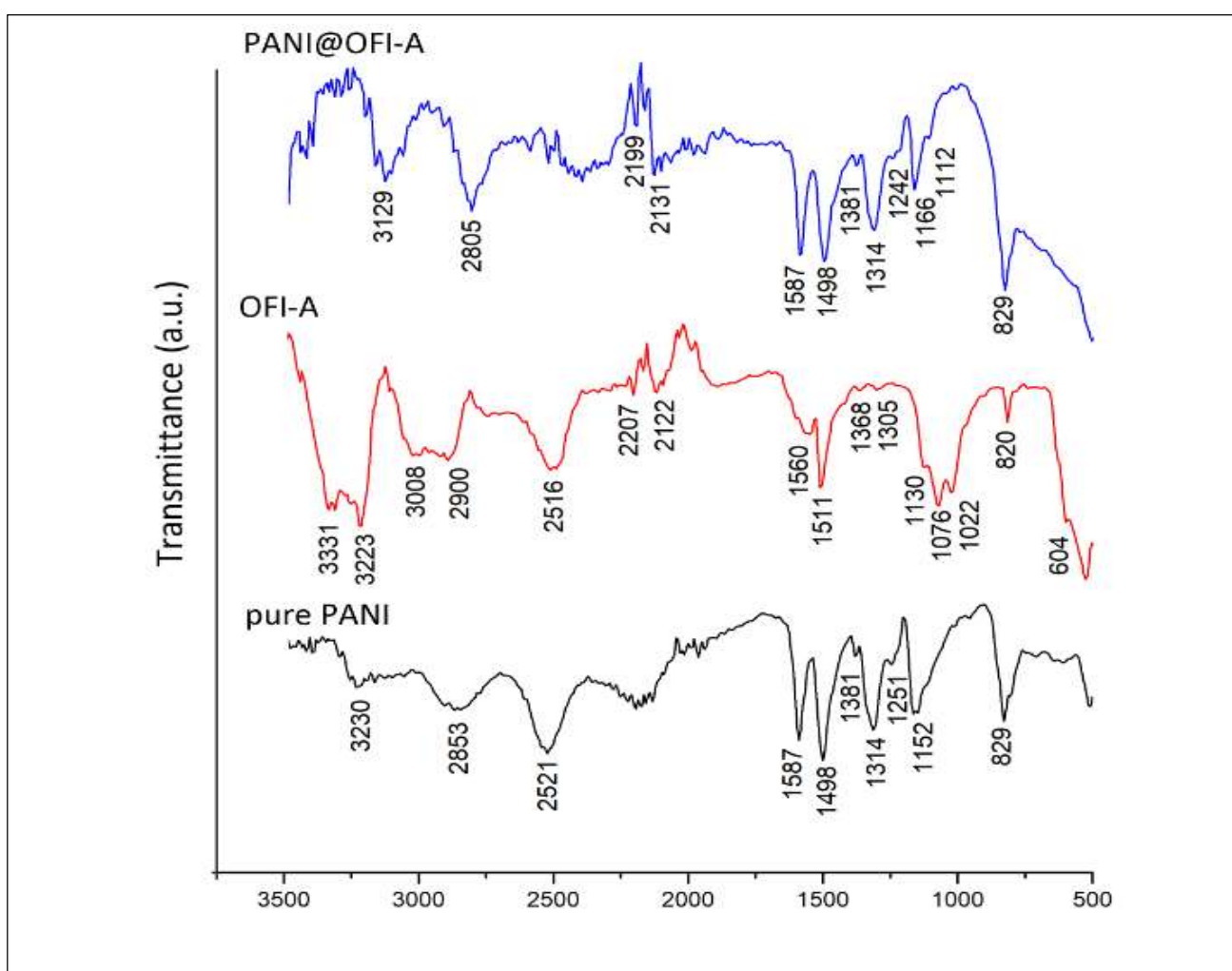


Figure.II.4. FT-IR adsorption spectra of: PANI, OFI-A and PANI@OFI-A

The bands around 1305 cm^{-1} are attributed to stretching of $\text{C}-\text{O}-\text{C}$ in $\alpha\text{-O-4}$ and $\beta\text{-O-4}$ linkages of lignin and peak at 1130 cm^{-1} are due to $\text{C}-\text{O}$ stretching vibrations of $\text{C}-\text{O}-\text{C}$ glycosidic linkages of hemicelluloses [13]. The peak at 1076 cm^{-1} assigned to $\text{C}-\text{O}$ stretching vibration of

primary alcohol and to C–N stretching vibration of amine groups [14], and the band at 1022 cm^{-1} indicate the presence of β -d pyranose form of the glucoyl residue [15]. Besides, the presence of O–C–O bending and CH deformation occurred in the range of $500\text{--}850\text{ cm}^{-1}$ [16]. On the other hand, the changes in functional groups of PANI@OFI-A were confirmed. Furthermore, the presence of PANI into composite was confirmed by the peaks at 1498 cm^{-1} , due the ring stretching vibration of benzenoid rings [17] at 1314 cm^{-1} , and at 1242 cm^{-1} from the C–N stretching of a secondary aromatic amine [18]. Moreover, the bands at 829 cm^{-1} resulted from the =N–H structure formed during the protonation [19]. Some OFI-A bands presented a red shift in the hybrid material probably due to a chemical interaction between OFI-A and PANI chains.

II.4.3. Nitrogen Adsorption/Desorption Isotherms (BET)

II.4.3.1. Principle

This technique was named after S. Brunauer, P. H. Emmet and E. Teller (BET). The three developed the method in 1938 as they were working on ammonia catalysts. It is the first method developed to measure the specific surface area of finely divided and porous solids. The method is applied in the analysis of pharmaceuticals, catalysts, projectile propellants, medical implants, filters, cements and adsorbents. The BET method is based on the adsorption of gas on a surface. Adsorption is a consequence of surface energy change. The energy is minimized in the bulk when every atom or molecule is surrounded by neighbours. The amount of gas adsorbed at a given pressure allows for the determination of surface area.

In a gas sorption experiment, the material is heated and degassed by vacuum force or inert gas purging to remove adsorbed foreign molecules. Controlled doses of an inert gas, such as nitrogen, krypton, or argon, are introduced and the gas is adsorbed, or alternatively, withdrawn and desorbed. The sample material is placed in a vacuum chamber at a constant and very low temperature, usually at the temperature of liquid nitrogen ($-195.6\text{ }^{\circ}\text{C}$), and subjected to a wide range of pressures, to generate adsorption and desorption isotherms. The amounts of gas molecules adsorbed or desorbed are determined by the pressure variations due to the adsorption or desorption of the gas molecules by the material (the adsorbent). Various amounts of gas molecules will be adsorbed or desorbed at different doses of the gas (the adsorbate). Knowing the area occupied by one adsorbate molecule, σ (for example, $\sigma = 16.2\text{ \AA}^2$ for nitrogen), and using an adsorption model, the total surface area of the material can be determined [20].

The concept of the theory is an extension of the Langmuir theory (a theory for monolayer molecular adsorption) to multilayer adsorption. The BET theory assumes that: gas molecules physically adsorb on the surface of a solid in layers infinitely, there is no interaction between each

adsorption layer, and the Langmuir equation can be applied to each of the layers. The resulting BET equation is expressed by:

$$\frac{P}{n(P_0 - P)} = \frac{1}{cn_m} + \frac{(c - 1).P}{cn_m \cdot P_0} \quad (\text{II. 3})$$

Where P, P₀, c, n, n_m are the adsorption pressure, the saturation vapour pressure, a constant, the amount adsorbed (moles per gram of adsorbent) at the relative pressure P/P₀, and the monolayer capacity (moles of molecules needed to make a monolayer coverage on the surface of one gram of adsorbent), respectively. Through the slope and intercept of a plot of P/[n(P₀-P)] against (P/P₀), n_m can be determined. The specific surface area, S, can then be derived using the following equation:

$$S = N_A n_m \sigma \quad (\text{II. 4})$$

N_A is Avogadro's number and σ is the area occupied by the adsorbed species. The specific surface area that can be determined by gas sorption ranges from 0.01 to over 2000 m²/g. Determination of pore volume and pore size distribution of porous materials can be made from the N₂ gas adsorption/desorption isotherm using an assessment model, suitable for the shape and structure of the pores. The range of pore sizes that can be measured using gas sorption is from a few Angstroms up to about half a micron [21].

II.4.3.2. Interpretation

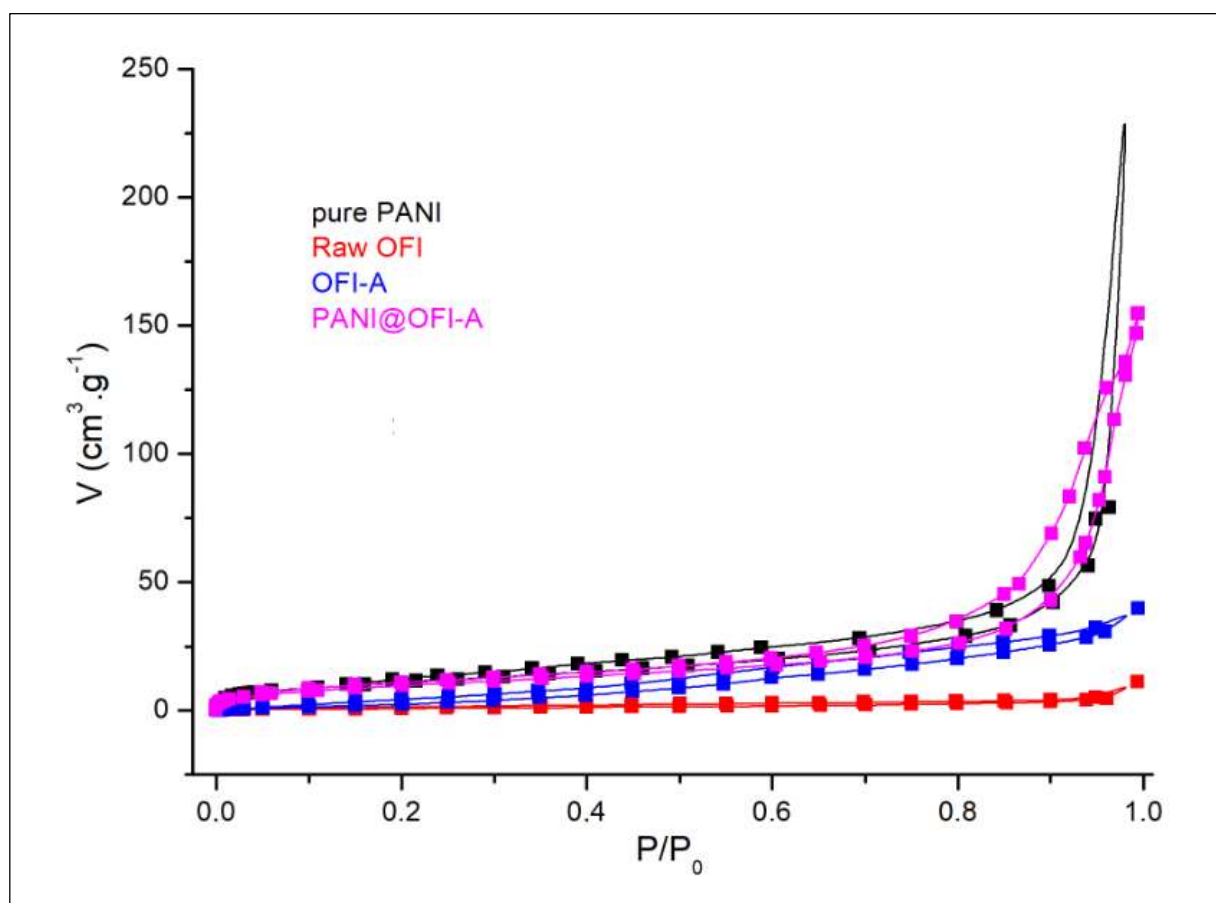


Figure.II.5. Adsorption–desorption isotherms of nitrogen at 77 K of:
PANI, raw OFI, OFI-A and PANI@OFI-A

Surface area is among the most significant physical properties that limit the quality and efficacy of an adsorbent. Variances of surface area and particle porosity seriously impact its performance.

The textural properties of OFI-A and PANI@OFI-A were explored by N_2 adsorption/desorption at 77 K (Figure.II.5). Both isotherms presented H3-type hysteresis loops belonging to type IV according to the International Union of Pure and Applied Chemistry (IUPAC) classification system. Table.II.2 shows that the porous PANI@OFI-A presents a larger surface area compared with OFI-A (37.912 vs 23.954 $m^2 g^{-1}$) due to an increment in the micropore volume (V_{DR} , Table.II.1).

Table.II.1. Textural characterization of: PANI, raw OFI, OFI-A and PANI@OFI-A

| Adsorbent | S_{BET} $\text{m}^2.\text{g}^{-1}$ | $V_{\text{DR}} N_2$ $\text{cm}^3.\text{g}^{-1}$ | V_{meso} $\text{cm}^3.\text{g}^{-1}$ |
|------------|--|--|--|
| PANI | 41.205 | 0.432 | 0.035 |
| Raw OFI | 6.003 | 0.004 | 0.005 |
| OFI-A | 23.954 | 0.009 | 0.012 |
| PANI@OFI-A | 37.912 | 0.031 | 0.038 |

II.4.4. Thermal gravimetric analysis (TGA)

II.4.4.1. Principle

Thermogravimetric analysis (TGA) measures the amount and rate of change in the weight of a material as a function of temperature or time (isothermal conditions) in a controlled atmosphere. Measurements are used to primarily determine the composition of material and to predict their thermal stability. The technique can characterise materials that exhibit weight loss or gain due to decomposition, oxidation or dehydration. The breaking and formation of chemical bonds at elevated temperatures leads to changes in the weight of the sample which is monitored by a very sensitive analytical balance.

In TGA, the weight of a sample is continuously recorded as the temperature is increased. Samples are placed in a crucible that is positioned in a furnace on a quartz beam attached to an automatic recording balance. The horizontal quartz beam is maintained in the null position by the current flowing through the transducer coil of an electromagnetic balance. A pair of photosensitive diodes acts as a position sensor to determine the movement of the beam. Any change in the weight of the sample causes a deflection of the beam, which is sensed by one of the photodiodes. The beam is then restored to the original null position by a feedback current sent from the photodiodes to the coil of the balance. The feedback current is proportional to the change in weight of the sample [22].

II.4.4.2. Interpretation

Thermogravimetric analyses (TGA) give the weight change under heat treatment then the amount of the volatilized species. Samples (about 20 mg) were heated from 60 to 900°C under nitrogen flow at a heating rate of 10 °C/min in a SDT Q600 (TA Instruments) Thermobalance.

The thermograms of pure PANI, OFI-A and PANI@OFI-A are represented in (Figure.II.6) OFI-A formed from cellulose, lignin, hemicellulose etc.

These materials will generally decompose around 460 °C. The thermal decomposition of OFI-A takes place in three steps. The first step between 60 and 220 °C related to degradation of hemicelluloses and pectins with 9.07% weight loss. The second step between 220 and 350 °C, in which degradation of cellulose and some amount of hemicellulose occurs (56.02% weight loss) and the final step between 350 and 800 °C, which is responsible for the decomposition of lignin and some part of cellulose (15.46% weight loss). Similarly, thermogram of the PANI@OFI-A presented maximum thermal stability as compared to OFI-A, which was due to the realization of covalent bonds between PANI chains and the OFI-A. The PANI@OFI-A also displayed three-stage degradations.

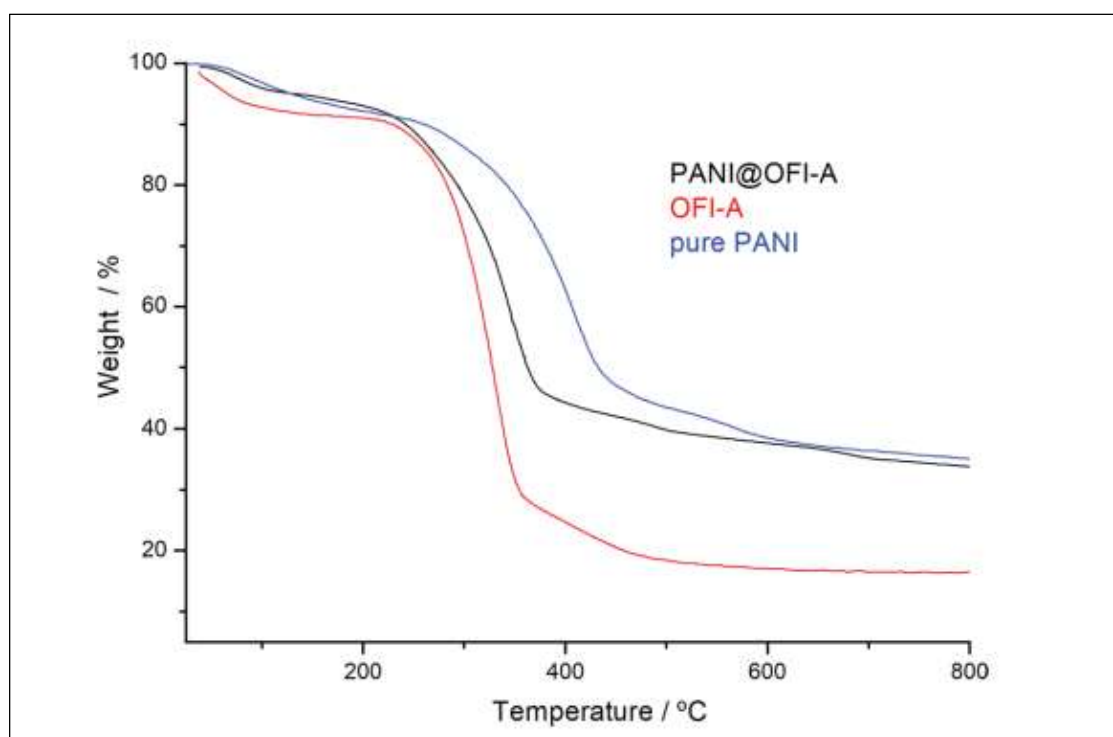


Figure. II.6. Thermogravimetric analysis of pure PANI, PANI@OFI-A and OFI-A obtained under N₂ flow at a heating rate of 10 °C.min⁻¹

The first step of decomposition (60–220 °C) consisted of degradation of the short size free radicals transferred unsaturated chain end of PANI and dehydration which resulted in 6.64% mass loss, the second step of decomposition (220–350 °C) consisted of degradation of, hemolytic scission of the chain due to H–H bonds and random scission [23], which resulted in 37.52% mass loss and the final step (350–800 °C) consists of thermal degradation of PANI chains and decomposition of OFI-A material which resulted in 21.89% mass loss.

II.4.5. Morphological Study (SEM)

II.4.5.1. Principle

The Scanning Electron Microscopy (MEB or SEM) is a technique of electronic microscopy based on the electrons-material interactions, capable of producing images of the sample surface. The principle of the MEB is based on the fact that an electron beam bombards the surface of the sample to be analyzed which re-emits certain particles. These particles are analyzed by various detectors which give a three dimensions image of the surface. Due to the excited state of the atoms present in the material by interaction with the incidental electrons, photons X are emitted (de-excitation process). The emission volume of photons X, (μm^3) depends upon the energy of the incidental electrons, the atomic number of the sample and the level energy initially ionized[24].

II.4.5.2. Interpretation of SEM images

The morphology of prepared materials is studied through SEM microscopic method. The related images of OFI-A and PANI@OFI-A were shown in (Fig.II.7)

In (Fig.II.7a) the OFI-A adsorbent presented a highly porous structure with roughness and wrinkles on the surface. Besides, In the SEM image of PANI@OFI-A, (Fig.II.7b), the existence of nanoporosity indicates that the main structure of OFI-A is retained after the polymerization process of PANI, due to the linkage of the polymeric chains onto the OFI-A, the uniformity of roughness was obtained at the surface of OFI-A.

This layer linkage structure of prepared PANI@OFI-A makes it good candidate to be used as a good adsorbent for the removal of various organic and inorganic pollutants.

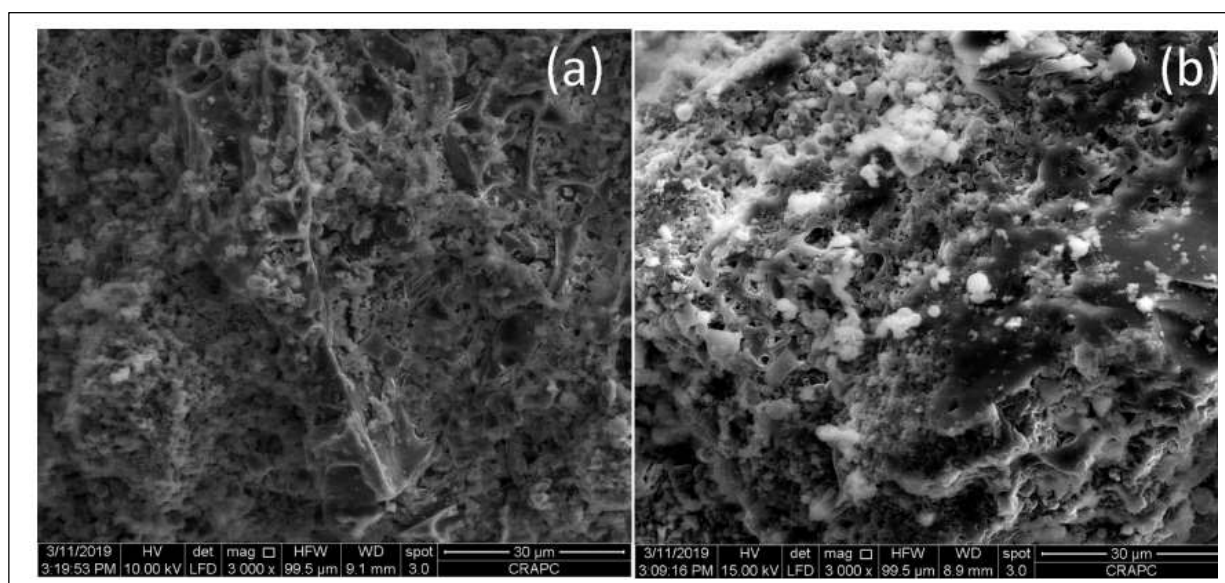


Figure. II.7. SEM images of the OFI-A (a) and PANI@OFI-A (b)

II.4.6. Point of zero charge (PZC) analysis

The point of zero charge (PZC) designates a pH wherein the net total particle charge is zero. PZC is among the most significant parameters helpful in the description of variable-charge surfaces.

II.4.6.1. Operating protocol

The point of zero charge of the adsorbents was determined by the solid addition method (Balistreri and Murray 1981). To a series of 100 mL conical flasks, 45 mL of KNO₃ solution of known strength was transferred. The initial pH (pH_i) values of the solution were roughly adjusted from 2 to 10 by adding either 0.1 N HNO₃ or NaOH. The total volume of the solution in each flask was made exactly to 50 mL by adding the KNO₃ solution of the same strength. The pH_i solutions were then accurately noted and 0.1 g of the adsorbent was added to each flask, which were securely capped. The suspensions were then manually shaken and allowed to equilibrate for 24 h with intermittent manual shaking. The pH values of the supernatant liquid were noted. The difference in the initial and final pH values (pH_f) was plotted against the pH_i. The point of intersection of the resulting curve is taken as PZC (Figure.II.8.). The values are given in Table II.2 and table.II.3

Table.II.2 The results of initial pH and final pH for the OFI-A

| | | | | | | | | | |
|-----------------------------------|------|------|------|------|------|-------|-------|-------|-------|
| pH _i | 2 | 3 | 4 | 5 | 6 | 7 | 8 | 9 | 10 |
| pH _f | 2.67 | 6.23 | 6.61 | 6.68 | 6.58 | 6.6 | 6.65 | 6.74 | 6.78 |
| pH _f - pH _i | 0.67 | 3.23 | 2.6 | 1.68 | 0.58 | -0.40 | -1.35 | -2.26 | -3.22 |

Table. II.3. The results of initial pH_i and final pH_f for the PANI@OFI-A

| | | | | | | | | | |
|-----------------------------------|------|------|------|------|------|-------|-------|-------|-------|
| pH _i | 2 | 3 | 4 | 5 | 6 | 7 | 8 | 9 | 10 |
| pH _f | 2.68 | 6.23 | 6.66 | 6.75 | 6.80 | 6.89 | 6.95 | 7.2 | 7.5 |
| pH _f - pH _i | 0.68 | 3.23 | 2.66 | 1.75 | 0.80 | -0.89 | -1.15 | -2.22 | -3.22 |

Figure.II.8 shows that OFI-A and PANI@OFI-A have a point of zero charge (PZC) at around 6.86 and 6.56 respectively, at pH below the PZC, the surface of the adsorbent is positively charged, while above PZC the adsorbent surface becomes most negatively charged by losing protons. Thus, PANI@OFI-A and OFI-A supposed to possess adsorption capacities higher towards OG above pH=2 probably due to electrostatic attraction, which is observed during study [25].

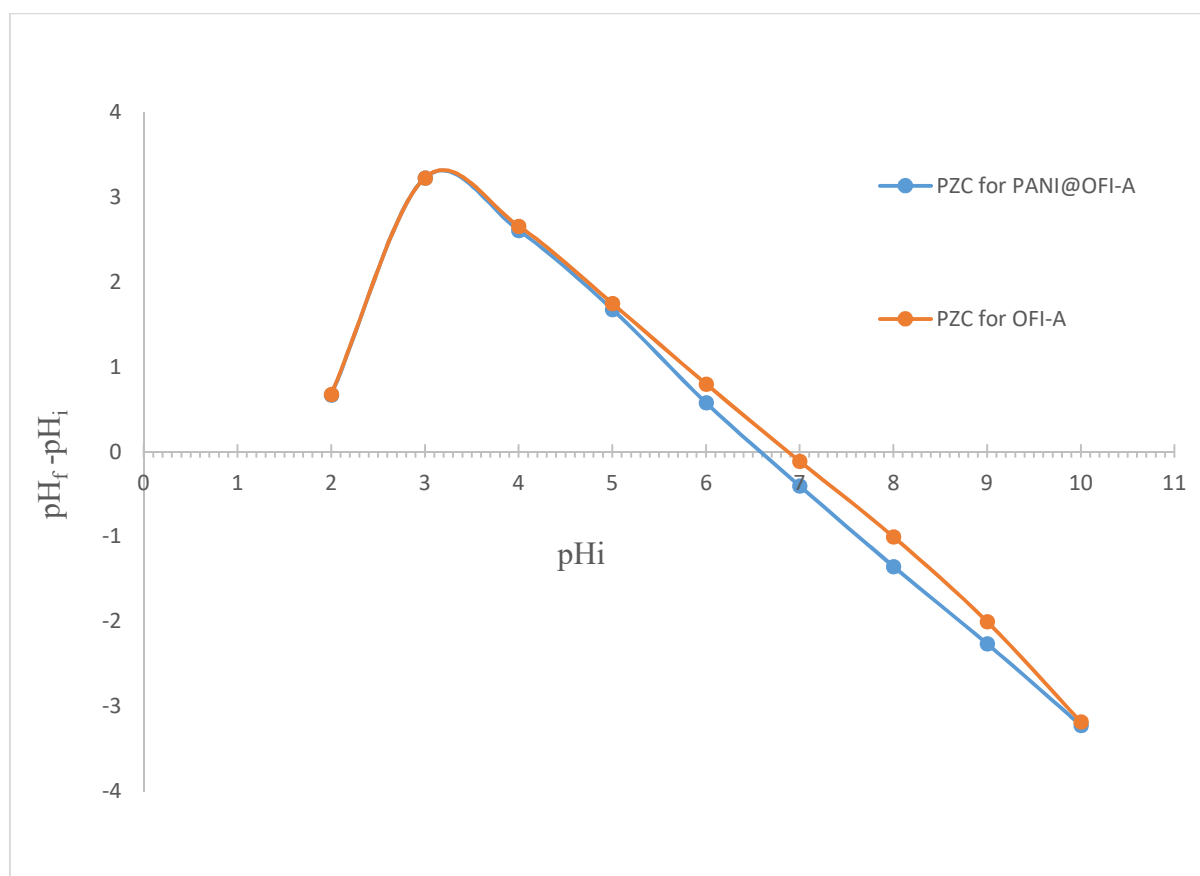


Figure.II.8. Representation of PZC for PANI@OFI-A and OFI-A

II.4.7. Ultraviolet visible (UV-vis) spectroscopy

II.4.7.1. Principle

The different emerging and aromatic compounds present in water are determined by means ultraviolet visible (UV-vis) equipment. Molecular spectroscopy based upon ultraviolet-visible is widely used for the identification and determination of organic species. The wavelength of the ultraviolet-visible is between 200-400 nm for ultraviolet and 400-800 nm for visible, and the absorption radiation of the molecules generally occurs in one or more electronic absorption bands (Table II.4); each of which is made up of numerous closely packed but discrete lines. Each line arises from the transition of an electron from the ground state to one of the many vibrational and rotational energy states associated with each excited electronic energy state [26].

In the absorption of organic compounds, two types of electrons are responsible for the absorption of ultraviolet and visible radiation:

- 1) shared electrons (associated with more than one atom).
- 2) unshared outer electrons (localized in halogens, oxygen, sulphur and nitrogen).

Organic compounds with aromatic ring like benzene, aniline, benzaldehyde (table 3.7), emerging compounds (paracetamol, atrazine, iodixanol, diclofenac,...) contain double bonds which exhibit useful absorption peaks in the ultraviolet spectra region due to the electrons in unsaturated bonds (that are easily excited).

Table.II.4. Maximum wavelength and absorption coefficient of different organic compounds [26]

| Compound | $\pi \rightarrow \pi^*$ (Band E) | | $\pi \rightarrow \pi^*$ (Band B) | | $\pi \rightarrow \pi^*$ (Band K) | | $n \rightarrow \pi^*$ (Band R) | |
|--------------|-------------------------------------|------|-------------------------------------|------|-------------------------------------|-------|-----------------------------------|----|
| | λ max | E | λ max | E | λ max | E | λ max | E |
| Phenol | 211 | 6200 | 270 | 1450 | | | | |
| Aniline | 230 | 8600 | 280 | 1430 | | | | |
| Benzaldehyde | | | 280 | 1400 | 242 | 14000 | 330 | 60 |
| Benzoic Acid | 202 | 8000 | 270 | 800 | 230 | 10000 | | |
| Toluene | 208 | 7900 | 262 | 230 | | | | |

II.4.7.2. Beer-Lambert's Law

Absorbance is the parameter that is used to quantify the UV-vis spectra and the different concentration of the molecules in solutions. The absorbance (A) is defined by:

$$A = -\log_{10}(T) = -\log_{10}\left(\frac{I}{I_0}\right) \quad (\text{II.5})$$

Where:

T is the transmittance, I_0 the incident intensity and I transmitted intensity

The functional relationship between the quantity measured of an absorption method (A) and the quantity sought (the analyte concentration c) is known as Beer-Lambert's Law

$$A = -\log_{10}\left(\frac{I}{I_0}\right) = \epsilon \cdot c \cdot l \quad (\text{II.6})$$

where:

ϵ is the molar absorptivity ($\text{L}\cdot\text{cm}^{-1}\cdot\text{mol}^{-1}$), l is the path length of radiation through the absorbing medium (cm) and c is the concentration ($\text{mol}\cdot\text{L}^{-1}$) [27]

II.4.7.3. Determination of maximum absorbance wavelength (λ_{\max}) of Orange G dye.**• Ultraviolet--visible spectrum.**

A plot of absorbance vs. wavelength obtained by measuring the amount of radiation absorbed by a sample of OG as a function of the wavelength of incident radiation in the ultraviolet to visible range (200 - 800 nm).

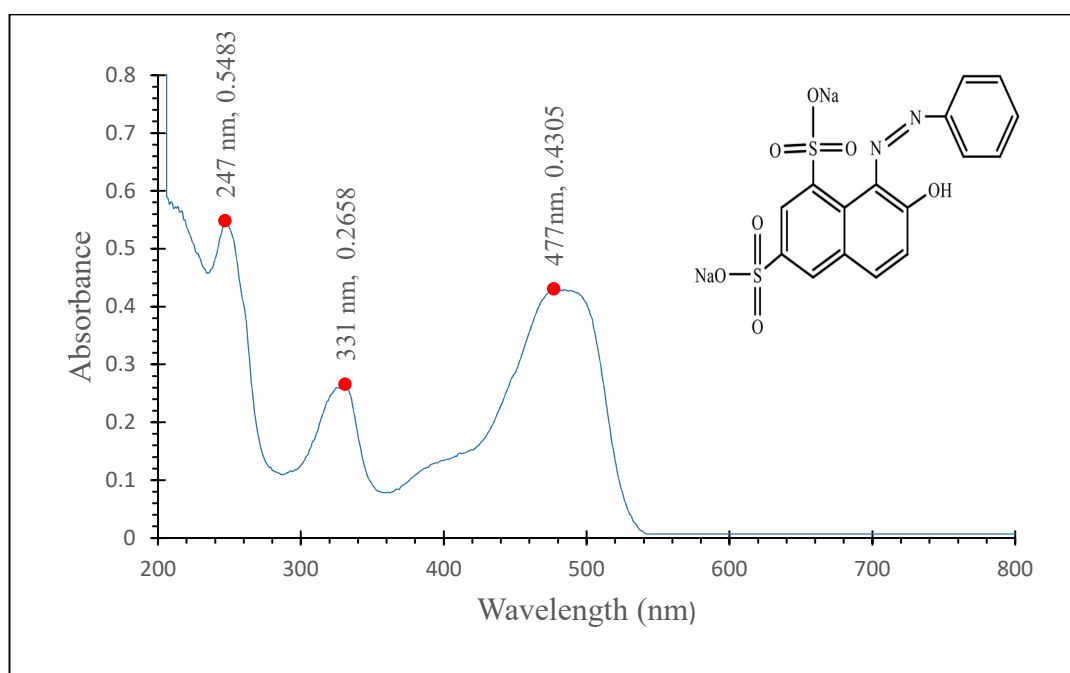


Figure.II.9. UV-Vis Spectrum of orange G dye

The UV-Vis spectrum of Orange G dye showed a major band in the visible region, with maximum absorption at 477 nm (λ_{\max}) due to azo-hydrazone tautomerization of the azo bond ($-N=N-$) [28,29]. Two other bands, at 331 and 247 nm, were associated with naphthalene and benzene rings, respectively [28-30]. The λ_{\max} of the dye (477 nm) was chosen for further investigations.

II.5. REFERENCES

- [1] Yamani K, Berenguer R, Benyoucef A, Morallón E (2019) Preparation of polypyrrole (PPy)-derived polymer/ZrO₂ nanocomposites: effects of nanoparticles interface and polymer structure. *Journal of Thermal Analysis and Calorimetry*. 135:2089-2100.
- [2] Kouidri FZ, Berenguer R, Benyoucef A, Morallon E (2019) Tailoring the properties of polyanilines/SiC nanocomposites by engineering monomer and chain substituents. *Journal of Molecular Structure*. 1188:121-128.
- [3] Bousalem S. Zeggai FZ. Baltach H, Benyoucef A (2020) Physical and electrochemical investigations on hybrid materials synthesized by polyaniline with various amounts of ZnO nanoparticle. *Chemical Physics Letters*. 741:137095.
- [4] A. A. Bunaciu and H. Y. Aboul-enein, "X-Ray Diffraction : Instrumentation and Applications Critical Reviews in Analytical Chemistry X-Ray Diffraction : Instrumentation and Applications," no. May, 2015, doi: 10.1080/10408347.2014.949616.
- [5] Broll, N. Caractérisation de solides cristallisés par diffraction X | Techniques de l'Ingénieur <http://www.techniques-ingenieur.fr/base-documentaire/mesures-analyses-th1/etudes-de-structure-et-caracterisation-42386210/caracterisation-de-solides-cristallises-par-diffraction-x-p1080/> (accessed Aug 11, 2016).
- [6] Graef, M. D.; McHenry, M. E. *Structure of Materials: An Introduction to Crystallography, Diffraction and Symmetry*; Cambridge University Press, 2007.
- [7] D. Ouis, F.Z. Zeggai, A. Belmokhtar, A. Benyoucef, B. Meddah, K. Bachari, Role of p-benzoquinone on chemically synthesized nanocomposites by polyaniline with V₂O₅ nanoparticle. *J. Inorg. Organometal. Polym. Mater.* (2020). <https://doi.org/10.1007/s10904-020-01508-7>
- [8]. Kellner, R.; Mermet, J. M.; Otto, M.; Widmer, H. M. *Analytical Chemistry*, Wiley-VCH, New York, 1998, pp. 541-546, 691-700.
- [9] Pavia, D. L.; Lampman, G. M.; Kriz, G. S. *Introduction to spectroscopy: A guide for for students of organic chemistry*. Thomson Learning, Inc, 2001, 3rd edition, 14-24, 353-358.
- [10] W.A. Khanday, G. Kabir, B.H. Hameed, Catalytic pyrolysis of oil palm mesocarp fibre on a zeolite derived from low-cost oil palm ash. *Energy Convers. Manag.* 127, 265–272 (2016)
- [11] A. Sila, N. Sayari, R. Balti, O.M. Alvarez, N.N. Arroume, N. Moncef, A. Bougatef, Biochemical and antioxidant properties of peptidic fraction of carotenoproteins generated from shrimp by-products by enzymatic hydrolysis. *Food Chem.* 148, 445–452 (2014)

- [12] A. Ebringerova, M.G. Polissiou, Determination of the degree of esterification of pectinates with decyl and benzyl ester groups by diffuse reflectance infrared Fourier transform spectroscopy (DRIFTS) and curve-fitting deconvolution method. *Carbohydr. Polym.* 56, 465–469 (2004)
- [13] M. Choudhary, R. Kumar, S. Neogi, Activated biochar derived from *Opuntia ficus-indica* for the efficient adsorption of mala-chite green dye, Cu^{2+} and Ni^{2+} from water. *J. Hazard. Mater.* 392, 122441 (2020)
- [14] K. Kandasamy, M. Venkatesh, Y.A. SyedKhadar, P. Rajasingh, One-pot green synthesis of CdS quantum dots using *Opuntia ficus-indica* fruit sap. *Mater. Today* 26, 3503–3506 (2020)
- [15] D. Gopi, K. Kanimozhi, L. Kavitha, *Opuntia ficus indica* peel derived pectin mediated hydroxyapatite nanoparticles: synthesis, spectral characterization, biological and antimicrobial activities. *Spectrochim. Acta A* 141, 135–143 (2015)
- [16] C.Y. Gan, N.H.A. Manaf, A.A. Latiff, Physico-chemical properties of alcohol precipitate pectin-like polysaccharides from *Parkia speciosa* pod. *Food Hydrocoll.* 24, 471–478 (2010)
- [17] F.Z. Kouidri, R. Berenguer, A. Benyoucef, E. Morallon, Tailoring the properties of polyanilines/SiC nanocomposites by engineering monomer and chain substituents. *J. Mol. Struct.* 1188, 121–128 (2019)
- [18]. C.Y. Gan, N.H.A. Manaf, A.A. Latiff, Physico-chemical properties of alcohol precipitate pectin-like polysaccharides from *Parkia speciosa* pod. *Food Hydrocoll.* 24, 471–478 (2010)
- [19] D. Ouis, F.Z. Zeggai, A. Belmokhtar, A. Benyoucef, B. Meddah, K. Bachari, Role of p-benzoquinone on chemically synthesized nanocomposites by polyaniline with V₂O₅ nanoparticle. *J. Inorg. Organometal. Polym. Mater.* (2020). <https://doi.org/10.1007/s10904-020-01508-7>
- [20] Mahboub, R.; Mouzdahir, Y. E.; Elmchaouri, A.; Carvalho, A.; Pinto, M.; Pires, J. Characterization of a delaminated clay and pillared clays by adsorption of probe molecules. *Colloids and Surfaces A: Physicochem. Eng. Aspects*, 2006, 280, 81–87.
- [21] Sing. K. S. W.; Haul, R. A. W.; Pierotti, R. A.; Siemieniowska, T. Reporting physisorption data for gas/solid systems with special reference to the determination of surface area and porosity. *Pure & Applied Chemistry*, 1985, 57 (4), 603-619.
- [22] Willard, H. H.; Merrit, L. L. (Jr); Dean, J. A.; Settle, F. A. (Jr). *Instrumental Methods of Analysis*, 1988, 7th edition, pp. 321-338, 767-769, Warsdworth Publishing Company, Belmont, California.
- [23] M. Ferriol, A. Gentilhomme, M. Cochez, N. Oget, J.L. Mieloszynski, Thermal degradation of poly (methyl methacrylate) (PMMA): modelling of DTG and TG curves. *Polym. Degrad. Stab.* 79, 271–281 (2003)
- [24] R.R. Gil, B. Ruiz, M.S. Lozano, E. Fuente, The role of crosslinking treatment on the pore structure and water transmission of biocollagenic materials, *J. Appl. Polym. Sci.* 130 (2013) 1812–1822.

- [25] A. Skoog, M. West, F.J. Holler, *Fundamentals of Analytical Chemistry*, 6 th, Saunders HBJ, Orlando, 1992.
- [26] E. Pretsch, T. Clerc, J. Seibl, W. Simon, *Tables of Spectral Data for Structure Determination of Organic Compounds.*, 4 th, Springer-Verlag, Zurich, 1980.
- [27] Y. Zhou, J. Lu, Y. Zhou, Y. Liu, Recent advances for dyes removal using novel adsorbents: a review. *Environ. Pollut.* 252, 352–365 (2019)
- [28] Zhang, S.-J.; Yu, H.-Q.; Zhao, Y.; *Water Res.* 2005, 39, 839.
- [29] Zhang, R.; He, Q.; Huang, Y.; Wang, X.; *Arch. Biochem. Biophys.* 2016, 596, 1.
- [30] Feng, W.; Nansheng, D.; Helin, H.; *Chemosphere* 2000, 41, 1233.

CHAPTER III

ADSORPTION OF ORANG G ONTO OFI-A

III.1 Introduction

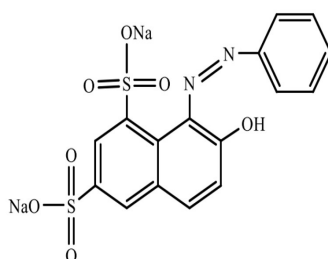
In this chapter we will investigate the adsorption of an organic pollutant which is orange G dye (Table.III.1) onto *Opuntia ficus-indica* treated with NaOH (OFI-A).

OG dye has been found to exert hazardous and inevitable harmful effects on aquatic species and the entire water environment [1]. It has been reported as one of the highly poisonous anionic dye, which shows some chromosomal damage and clastogenic activity [2]. Its toxic, carcinogenic and teratogenic effects to the living organisms has been attributed to the azo group in its chemical structure [3]. Not only OG, but the intermediates formed during its degradation are also toxic too. OG is likewise harmful to plants and animals [4]. Furthermore, for humans, exposure to OG may result in irritation of the gastrointestinal and respiratory tract. It has also shown genotoxic effects on experimental animals such as Swiss albino mice and anaerobic biomass in aqueous solution [5].

Table.III.1. physicochemical properties and molecular structure of OG. [6]

| Property | Orange G (OG) |
|-----------------------------------|--|
| Chemical formula | $C_{16}H_{10}N_2Na_2O_7S_2$ |
| Chemical name | 7-hydroxy-8-(phenylazo)-1,3-naphthalenedisulfonic acid disodium salt |
| Generic name | Acid Orange 10 |
| Abbreviation | AO10 |
| Classification | Azo dye |
| Color | Orange |
| λ_{max} | 475 nm |
| pKa | 11.5 |
| Molecular size (\AA^3) | 13.08 x 7.53 x 4.98 |
| Melting point | 141 $^{\circ}\text{C}$ |
| Water solubility | 50 g/l (20 $^{\circ}\text{C}$) |

Chemical structure



III.2 PREPARATION OF SOLUTIONS

The stock solution was prepared by dissolving 1 g of orange G dye in 1L of demineralized water, the prepared stock solution with a concentration of 1000mg/L used for the preparation of the sub-solutions with different concentration, which used for the OG adsorption onto OFI-A studies. The concentration of each sub-solution that was prepared from the stock solution was verified by analyzing it with the UV-visible at the maximum absorption wavelength of OG ($\lambda_{\max} = 477$ nm).

III.2.1. Calibration curve for OG

The method consists in the preparation of series of sub-solutions with different known concentration 5, 10, 15, 20, 25, 30 ppm and measure the absorbance of each solution and trace the concentration versus absorbance, which should be a line passes through the origin.

The equation of the straight line giving the concentration of OG solution as a function of the absorbance A is: ($C = 25.011 \times A$) which represented in (Figure III.1), with a regression coefficient $R^2 = 0.9997$. This equation used to determine the concentration of a given solution.

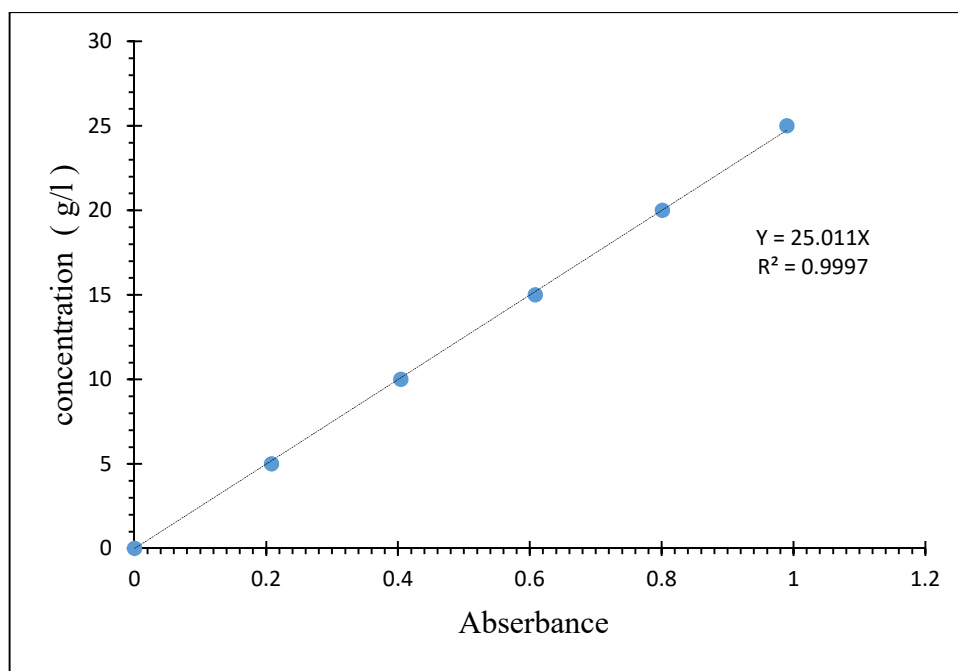


Figure.III.1 Orange G dye calibration curve at ($\lambda_{\max} = 477$ nm)

III.3. Effect of different parameters on the adsorption of OG onto PANI@OFI-A

To study the effect of parameters such as adsorbent dosage, pH and initial concentration batch experiments were carried out for the adsorption of anionic dyes (OG) onto OFI-A in a thermostatic orbital shaker at a constant speed of 125 cycles per minute at 25°C.

III.3.1. Effect of adsorbent dosage

The effect of adsorbent dose on the adsorption of OG was investigated by incubating different quantities of OFI-A in 50 mL of 100 ppm OG solution for 2 h. The experimental result is given in Figure III.2. It is observed that the OG dye removal increases and the OG final concentration decreases as the adsorbent mass increases from 0.1 to 3.2 g/L keeping all other parameters constant. This is due to the availability of more surface functional groups at higher concentration [8]. However, above the adsorbent dose of 1.5g/L were the percentage of dye removed reaches 80 %, the increase of the adsorbent mass above 1.5 g/L has low effect on the dye removal.

$$\text{Dye Removal \%} = \frac{C_0 - C_f}{C_0} * 100\%$$

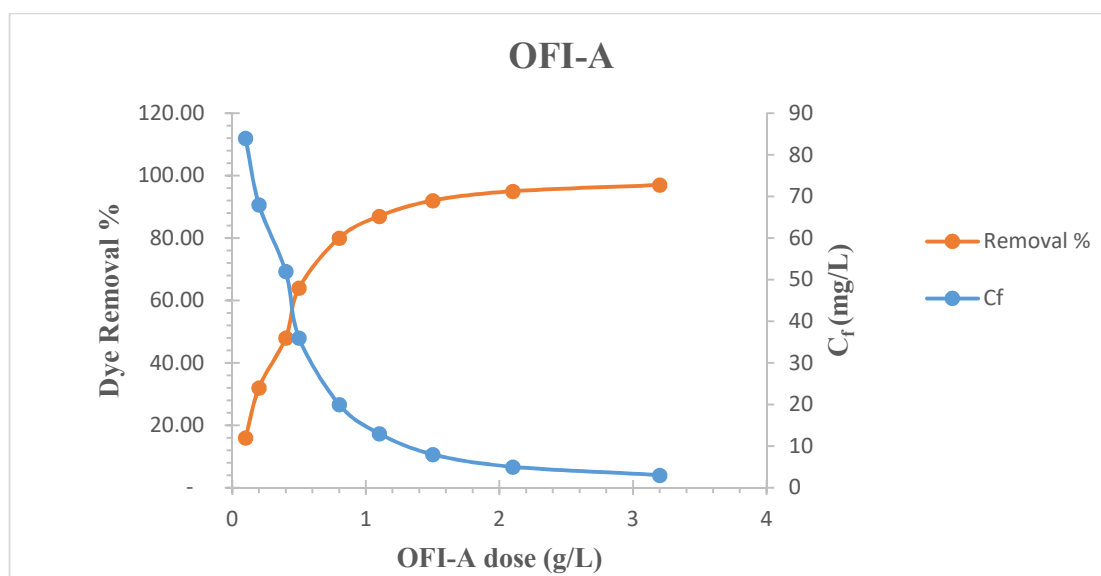


Figure III.2 Effect of adsorbent dosage on the adsorption of OG onto OFI-A

III.3.2. Effect of pH

The pH of the solution is one of the major factors influencing the adsorption capacity of the compounds that can be ionized. In order to study the effect of pH, 400 mg.l⁻¹ of OG solutions were introduced with appropriate amounts of hydrochloric acid (HCl) and sodium hydroxide (NaOH) to

adjust the pH from 1 to 12, the mass of adsorbent used is $m = 0.5$ g of OFI-A, which is incubated in the prepared solutions for 30 min at room temperature. As the pH value increase from (1 to 12) the OG removal percentage decrease, the maximum removal percentage occurred at pH= 2 and was calculated as 8.04 mg.g^{-1} , as can be seen in Figure.III.3 the adsorbed amount of OG started increasing at pH =7 and continue increasing with the decrease of pH and reached the highest adsorbed amounts of OG at pH = 2. In this range of pH the OFI-A surface is positively charged ($\text{pH} < \text{pH}_{\text{PZC}} = 6.56$) [9].

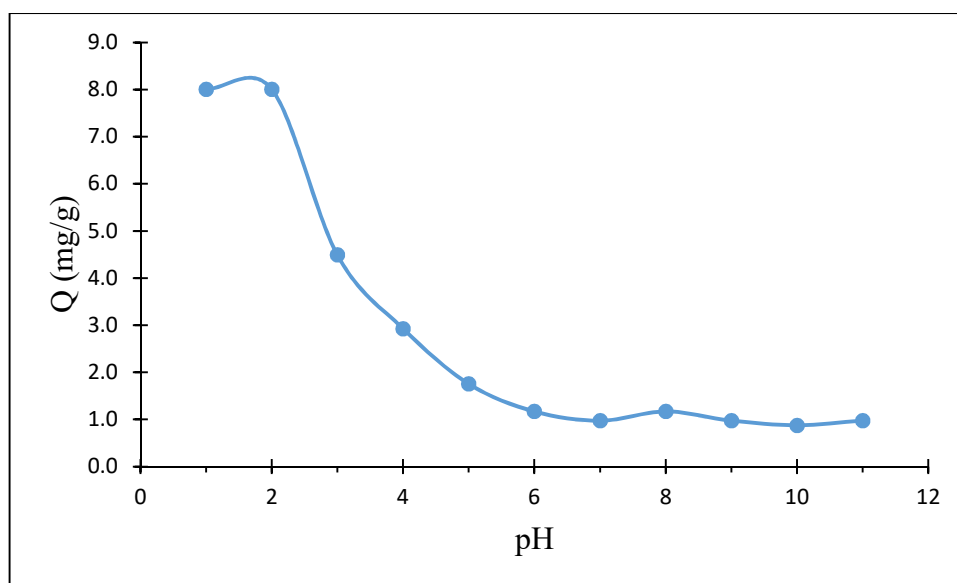


Figure III.3 Effect of pH on the adsorption of OG onto OFI-A

III.3.3. Effect of contact time on adsorption of OG onto OFI-A

The study of contact time effect on the adsorption of OG shows rapid adsorption of dye in the first 10 min and thereafter, the adsorption rate decreased gradually and the equilibrium reached within 30 min, as shown in (Figure III.4).

In the initial stage of adsorption, a large number of vacant sites are available and after lapse of some time, the remaining vacant sites are difficult to be occupied by the dye molecule due to repulsive forces between the solute molecules on the solid surface and the bulk phase. This result in slowing down of adsorption during the later period. Aggregation of dye molecules with the increase in contact time also makes it impossible to diffuse deeper into the adsorbent pore structure. The time beyond which no adsorption takes place is considered as equilibrium time. The equilibrium time for the adsorption of OG onto OFI-A was found as 30 min. The adsorption curves

were single smooth and continuous leading to saturation indicating the possible monolayer coverage on the surface of the adsorbent by the dye molecules [10].

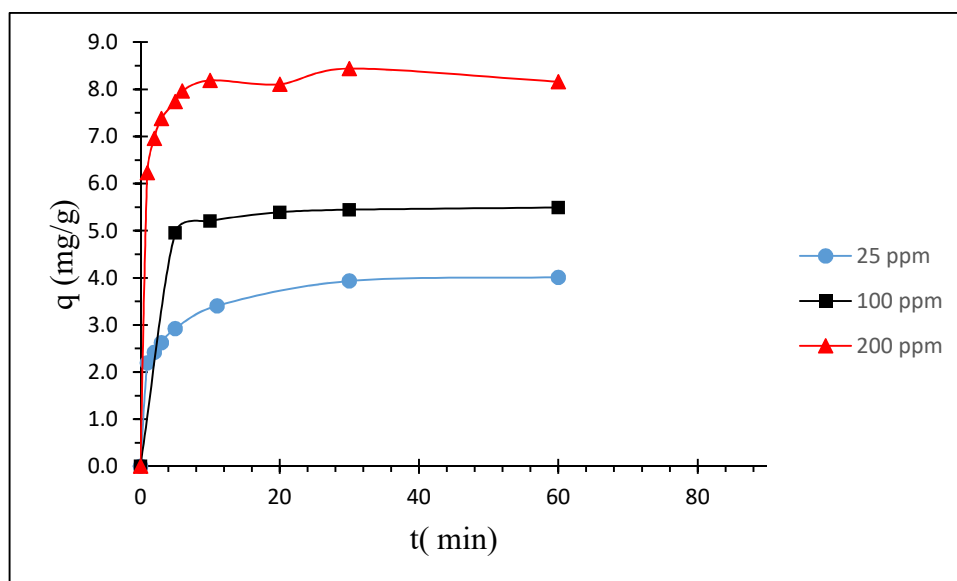


Figure III.4 Effect of contact time on adsorption of OG onto OFI-A

III.4. Adsorption kinetics modeling

Adsorption of dyes, in aqueous systems, onto adsorbents is a time-dependent process. In order to investigate the mechanism of sorption and rate controlling steps, kinetic models have been used to test experimental data. The mechanism of adsorption is generally considered to involve three steps, one or any combination of which can be the rate-controlling mechanism. They are

- 1) The transport of the adsorbate ions from the bulk phase to the exterior surface of the adsorbent.
- 2) The transport into the adsorbent by either pore diffusion or surface diffusion.
- 3) The adsorption on the surface of the adsorbent.

The slowest of these steps determines the overall rate of the adsorption process.

To investigate the adsorption processes of OG on OFI-A, four kinetic models such as pseudo-first order, pseudo-second order, intra-particle diffusion and Elovich were selected to fit the experimental kinetic data.

III.4.1 Pseudo-first order

This model assumes that the rate of change of solute uptake with time is directly proportional to difference in saturation concentration and the amount of solid uptake with time.

It was the earliest equation which describes the adsorption rate based on the adsorption capacity. However, in most of cases the pseudo-first order equation does not fit well for the whole range of adsorption time. The differential form of the equation is given by Lagergren (1898) [11].

$$\frac{dq_t}{dt} = k_1(q_t - q_e) \quad (III.1)$$

where q_e and q_t are the amounts of dye adsorbed (mg/g) on adsorbent at equilibrium time and at various time t (min) respectively and k_1 is the rate constant of pseudo-first order kinetics (min^{-1}). Integrating Equation (III.1) for the boundary conditions $t = 0$ to $t = t$ and $q_{t=0} = 0$ mg/g to q_t gives:

$$\text{Ln}(q_e - q_t) = \text{Ln}(q_e) - k_1 t \quad (III.2)$$

This is the linear form of the pseudo-first order model. In order to obtain the rate constants, the straight line plots of $\log (q_e - q_t)$ against t for different dye concentrations have been analyzed (Figure III.5). The rate constant, k_1 , Equilibrium capacity, q_e and correlation coefficients R^2 for adsorption of OG onto OFI-A adsorbent were calculated from these plots are listed in (Tables III.2).

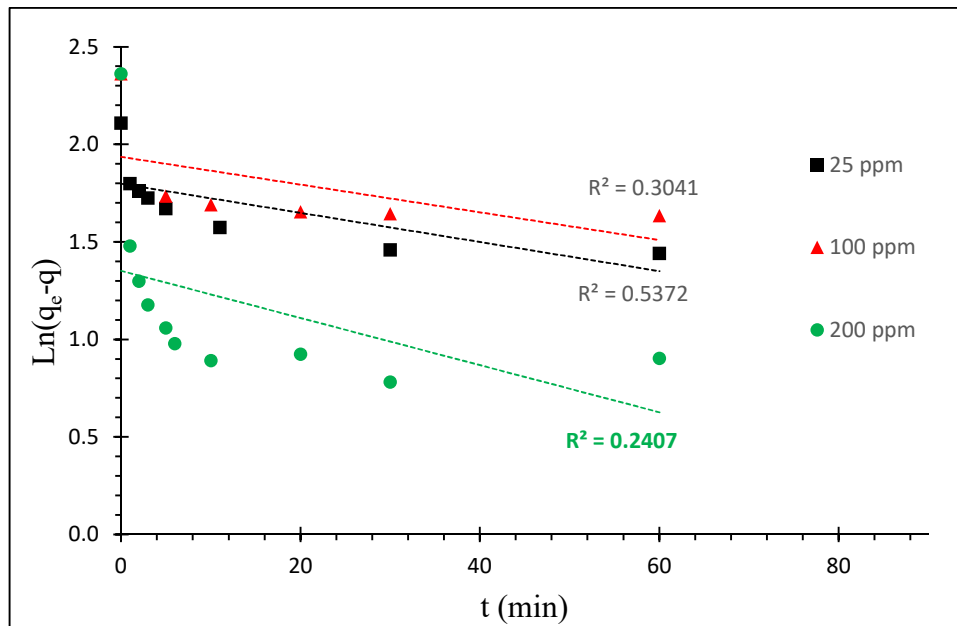


Figure III.5 The pseudo-first order kinetic model for the adsorption of OG onto OFI-A

III.4.2 Pseudo-second order

The pseudo-second order model for the adsorption of divalent metal ions onto peat particles, based on the sorption capacity of adsorbents was described by Ho and McKay (1997).

The various assumptions of Ho pseudo-second order model are.

1. The energy of adsorption for each ion is the same and independent of surface coverage.
2. The sorption occurs only on localized sites and involves no interactions between adsorbed ions
3. The rate of adsorption is almost negligible in comparison with the initial rate of adsorption.

Ho and McKay (1997) gave the sorption kinetics following pseudo-second order model.

The differential equation has the following form [12].

$$\frac{dq_t}{dt} = k_2(q_e - q_t)^2 \quad (III.3)$$

Where k_2 is the rate constant of the pseudo-second order kinetics ($\text{g.mg}^{-1}.\text{min}^{-1}$). The linear form of the pseudo-second order model is given by:

$$\frac{t}{q_t} = \frac{1}{k_2 q_e^2} + \frac{1}{q_e} t \quad (III.4)$$

The straight line plot of t/q_t against t has been used to obtain rate parameters (Figure III.6). The values of k_2 , q_e and correlation coefficients R^2 of dye adsorption at different initial concentrations were calculated from these plots are listed in (Tables III.2).

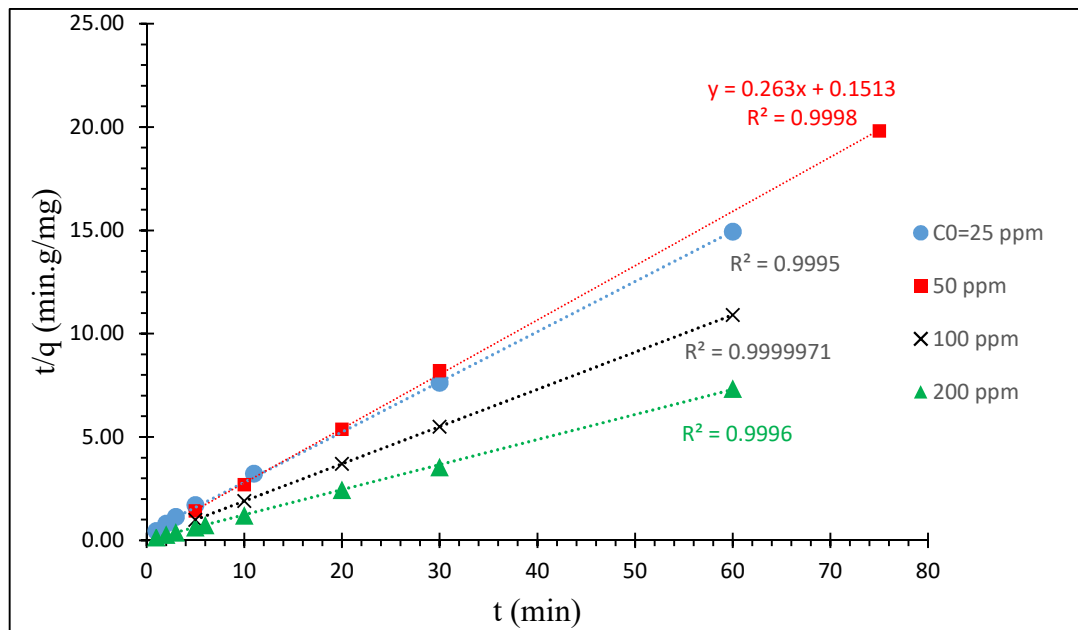


Figure III.6 The pseudo-second order kinetic model for the adsorption of OG onto OFI-A

III.4.3. Elovich model

In reactions involving chemisorption of adsorbate on a solid surface without desorption of products, adsorption rate decreases with time due to an increased surface coverage. One of the most useful models for describing chemisorption is the Elovich equation. The linear form of the Elovich equation is given by.

$$q_t = \frac{1}{\beta} \ln(\alpha\beta) + \frac{1}{\beta} \ln(t) \quad (III.5)$$

The parameters α and β are constants, α is the initial sorption rate of Elovich equation ($\text{g.g}^{-1}.\text{min}^{-1}$), β is adsorption constant (mg.g^{-1}) and q_t is the amount of metal adsorbed/desorbed at time (mg/g), and t is the reaction time (min). A plot of q_t versus $\ln(t)$ (Figure III.7) shows a linear relationship with a slope of $(1/\beta)$ and intercept $(1/\beta) \ln(\alpha\beta)$ [13], Elovich model constants α , β and the correlation coefficient R^2 listed in (Table III.2).

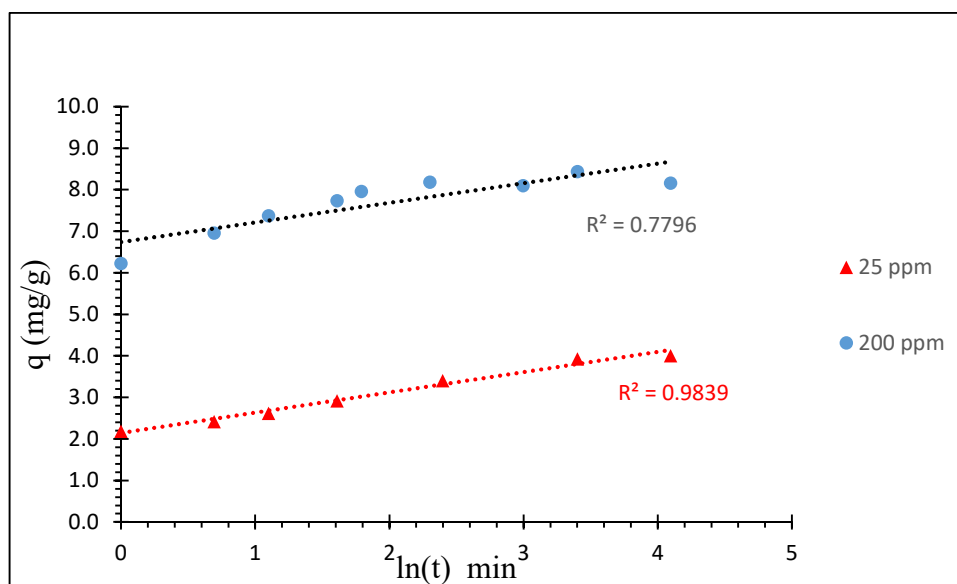


Figure III.7 Elovich model for the adsorption of OG onto OFI-A

III.4.4. Intra-particle model

This model is based on the theory proposed by Weber and Morris (1963). The fractional approach to equilibrium changes according to a function of $(D_t/r^2)^{1/2}$ where 'r' is the radius and 'D' is the diffusivity of solute within the particle. The initial rates of intra-particle diffusion can be obtained by linearization of the curve $q_t = f(t^{1/2})$ is given by [14].

$$q_t = k_{int} t^{1/2} + I \quad (III.6)$$

Where k_{int} is the intra-particle diffusion rate constant ($\text{mg}\cdot\text{g}^{-1}\cdot\text{min}^{-1/2}$) and 'I' is the intercept (mg/g). A plot of q_t versus $t^{1/2}$ should be a straight line (Figure III.8) if intra-particle diffusion was involved in the adsorption process and if these lines pass through the origin then intra-particle diffusion is the rate controlling step. In the present study, it was found that the plot of q_t versus $t^{1/2}$ indicated an initial curved portion followed by linear and plateau. However neither plots passed through the origin. When the plots do not pass through the origin, this is indicative of some degree of boundary layer control [15]. And this further show that the intra-particle diffusion is not the only rate limiting step but also other kinetic models may control the rate of adsorption, all of which may be operating simultaneously [16]. Values of k_{int} and 'I' calculated from the slope and intercept of the plot respectively and given in Tables III.2. The value of 'I' gives an idea about the thickness of the boundary layer i.e., the larger the intercept the greater is the boundary layer effect [17].

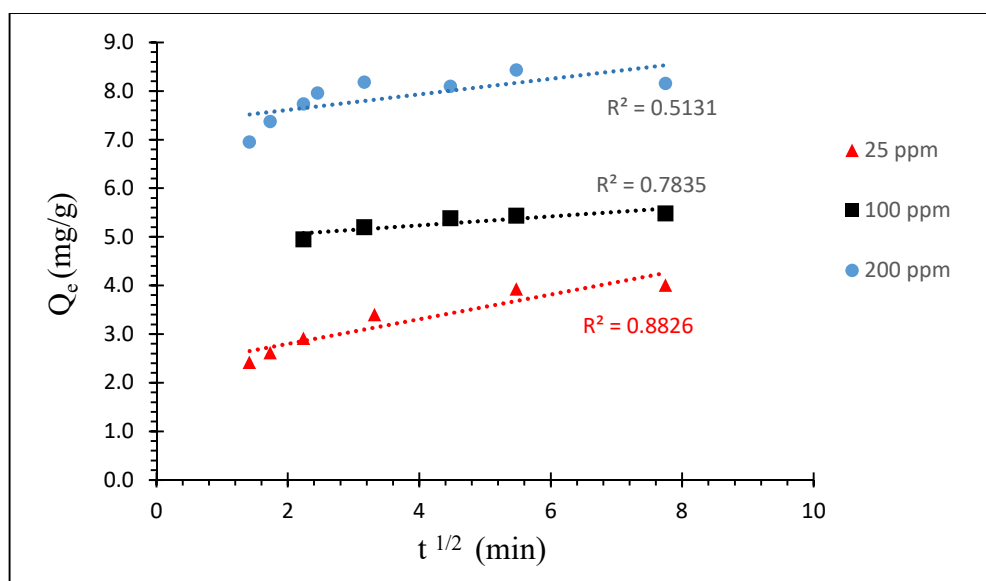


Figure III.8. Intra-particle diffusion model for the adsorption of OG onto OFI-A

Based on the correlation coefficient (R^2) values, the adsorption kinetic for OFI-A can better be described by pseudo-second order. Figure III.9 shows the comparative results using various kinetic models for the adsorption of OG with an initial dye concentration of 200 mg/L. The pseudo-second order kinetics fitted well for the adsorption of OG onto OFI-A compare to other models. The Elovich model Fitted for the first 120 min and thereafter the data deviated from linearity. Thus, the model represents the initial stages adsorption, but it can not be applied to entire adsorption process [18]. Therefore, the pseudo-first order and intra-particles models were inapplicable to this system. The correlation coefficients and the calculated values of ' q_e ' for pseudo-second order kinetic model are in good agreement with the experimental results. From the results obtained, the adsorption systems studied belong to the pseudo-second order kinetic model.

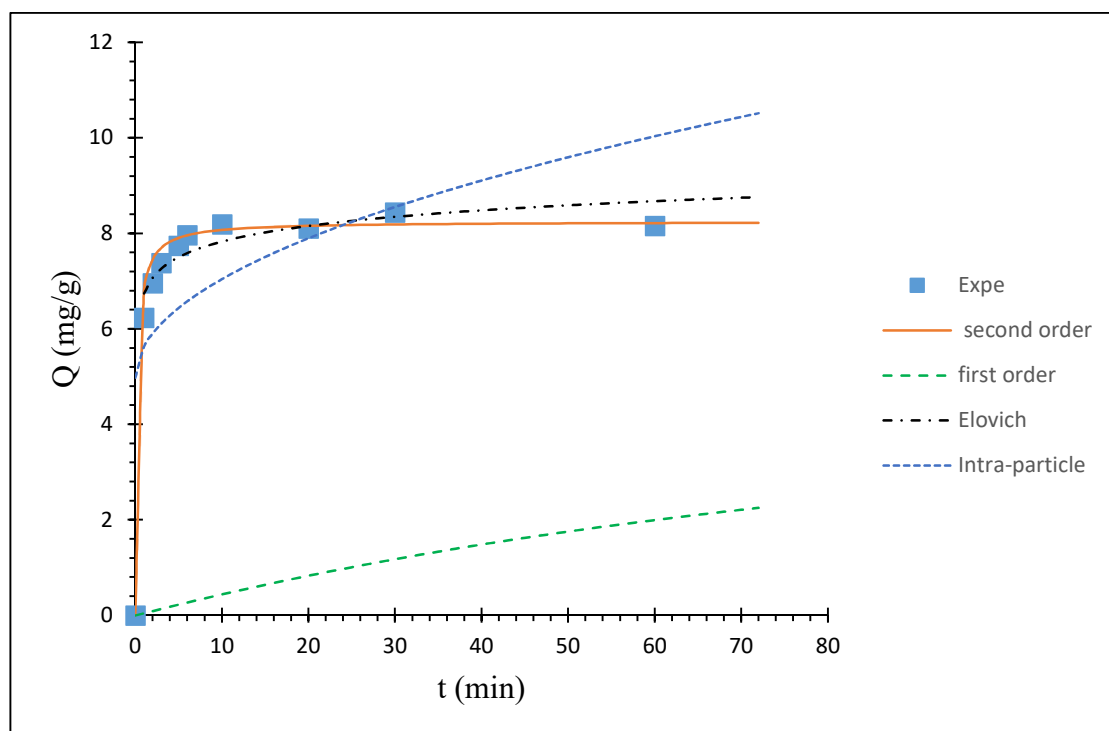


Figure III.9 Comparison between the measured and modelled time profiles for the adsorption of OG onto OFI-A

Table III.2 Kinetic parameters for the adsorption of OG onto OFI-A

| C_0 (ppm) | Q_{Exp} (mg/g) | Pseudo-first order | | | Pseudo-second order | | | Elovich | | | Intra-particle diffusion | | |
|----------------|---------------------|---------------------|--------------------------------|-------|-----------------------|--|-------|--------------------|---------|-------|---|-------|-------|
| | | Q_{cal} (mg/g) | K_1 (min^{-1}) | R^2 | Q_{eqcal} (mg/g) | K_2 ($\text{g}\cdot\text{mg}^{-1}\cdot\text{min}^{-1}$) | R^2 | α | β | R^2 | k_{int} ($\text{g}\cdot\text{mg}^{-1}\cdot\text{min}^{1/2}$) | I | R^2 |
| 25 | 4.01 | 3.29 | 0.0158 | 0.62 | 4.12 | 0.15 | 0.999 | 40.6 | 2.06 | 0.984 | 0.2533 | 2.296 | 0.883 |
| 100 | 5.45 | 6.9 | 0.0071 | 0.055 | 5.55 | 0.295 | 0.999 | $3.57 \text{ E}+8$ | 4.55 | 0.91 | 0.0915 | 4.875 | 0.784 |
| 200 | 8.16 | 3.9 | 0.0121 | 0.24 | 8.2 | 0.564 | 0.996 | $7.6 \text{ E}+05$ | 2.12 | 0.78 | 0.1606 | 7.292 | 0.51 |

III.5. Adsorption isotherms modeling

The adsorption isotherm is an equation relating the amount of solute adsorbed onto the solid and equilibrium concentration of the solute in solution at constant temperature. The different parameters and the underlying thermodynamic assumption of these equilibrium models often provide some insight into the adsorption mechanism, surface properties and affinity of adsorbent. The three commonly used isotherms to explain the equilibrium uptake of solute are Freundlich, Langmuir and Temkin isotherms, which are explained as follows:

III.5.1. Freundlich model

The Freundlich equation (Freundlich 1906) is the earliest known relationship describing the adsorption process. This is basically empirical, but is often used to describe heterogeneous systems. The isotherm assumes that adsorbent surface sites have a spectrum of different binding energies. The Freundlich equation is given by,

$$q_e = k_f \cdot C_e^{\frac{1}{n}} \quad (III. 7)$$

A linear form of Equation (V.) is used to calculate the constants 'K_F' and 'n'.

$$\log(q_e) = \log(k_f) + \frac{1}{n} \cdot \log(C_e) \quad (III. 8)$$

where q_e is the amount of solute adsorbed per unit weight of adsorbent (mg/g), C_e is the equilibrium concentration of the solute in the bulk solution (mg/L), K_F is a Freundlich constant indicative of the relative adsorption capacity of the adsorbent (mg/g) and $1/n$ is adsorption intensity. If the value of $1/n$ lies between 0 to 1, it indicates adsorption process is beneficial. A plot of $\ln(q_e)$ versus $\ln(C_e)$ (Figure.III.10) enables the determination of K_F and 'n' from the intercept and slope of the line respectively (Table III.3).

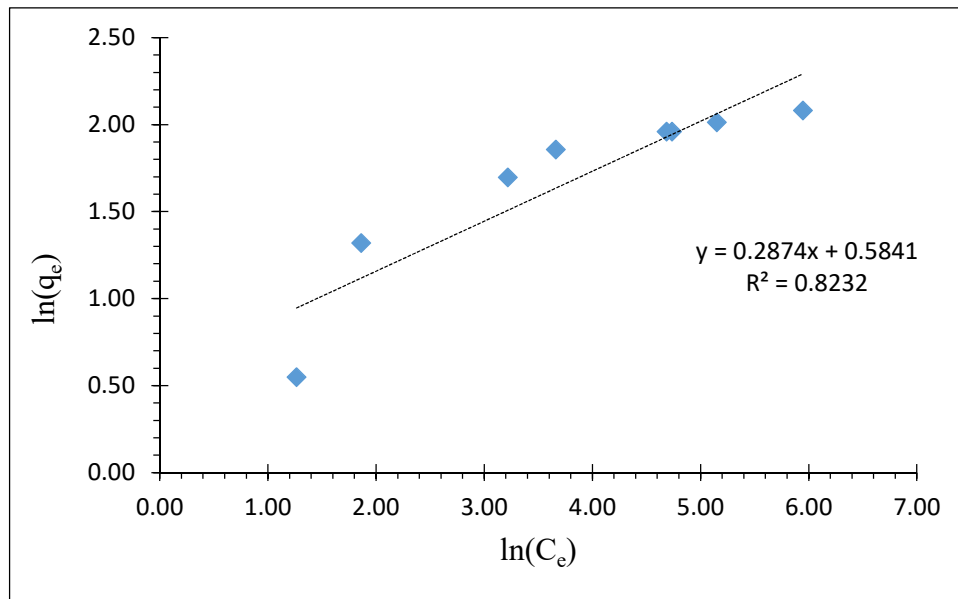


Figure III.10 Freundlich isotherm for the adsorption of OG onto OFI-A

III.5.2 Langmuir isotherm

The Langmuir adsorption isotherm is based on the assumption that adsorption takes place at specific homogeneous sites within the adsorbent and once the solute occupies a site, no further adsorption takes place at that site. Theoretically, the adsorbent has a finite capacity to adsorb the adsorbate. Therefore, a saturation value is reached beyond which no further adsorption takes place. The Langmuir equation is given by (Langmuir 1918).

$$q_e = Q_{max} * \frac{k \cdot c_e}{(1 + k \cdot c_e)} \quad (III.9)$$

A linear form of the above equation is:

$$\frac{C_e}{q_e} = \frac{C_e}{Q_{max}} + \frac{1}{k Q_{max}} \quad (III.10)$$

An essential characteristic of the Langmuir isotherm can be expressed in terms of a dimensionless constant called the equilibrium parameter, R_L defined by.

$$R_L = \frac{1}{1 + K_L \cdot C_0} \quad (III.11)$$

where K_L is the Langmuir constant and C_0 is the highest initial dye concentration (mg/L). The value of R_L indicates the type of isotherm, to be favourable ($0 < R_L < 1$), linear ($R_L = 1$), unfavourable ($R_L > 1$) or irreversible ($R_L = 0$) [19].

The calculated Langmuir constants are reported in (Table III.3)

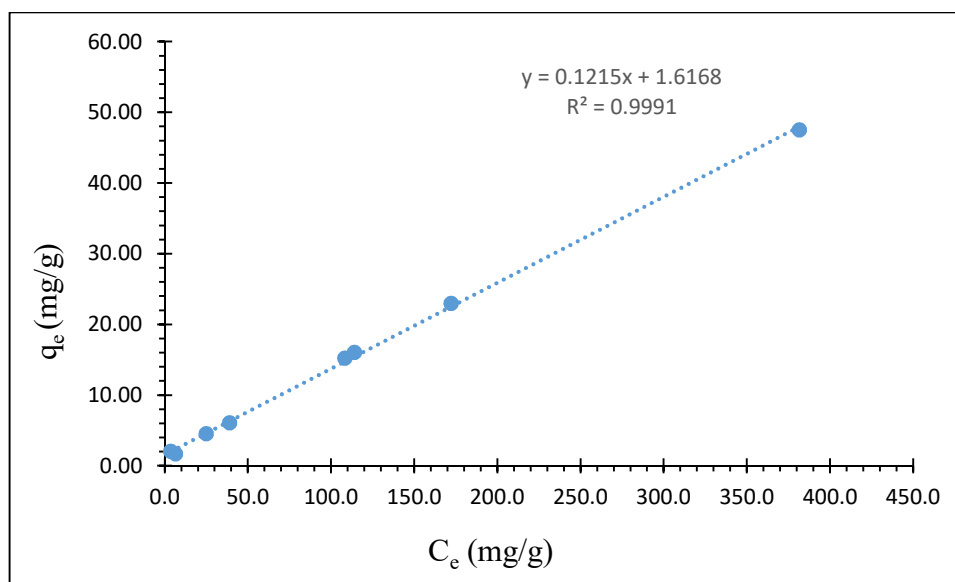


Figure III.11 Langmuir isotherm for the adsorption of OG onto OFI-A

III.5.3 Temkin isotherm

The Temkin isotherm equation assumes that [20].

- the heat of adsorption of all the molecules in the layer decreases linearly with coverage due to adsorbent-adsorbate interactions and
- the adsorption is characterized by uniform distribution of the binding energies

The Temkin isotherm equation is given as.

$$q_e = \frac{R \cdot T}{b} \ln(K_T \cdot C_e) \quad (III. 12)$$

The linear form of the above equation is

$$q_e = B_1 \ln K_T + B_1 \ln C_e \quad (III. 13)$$

where $B_1 = RT/b$, K_T is the equilibrium binding constant (L/mg) corresponding to the maximum binding energy and B_1 is the heat of adsorption. A plot of q_e versus $\ln(C_e)$

(Figure III.12) enables the determination of Temkin isotherm constants B_1 and K_T [21].

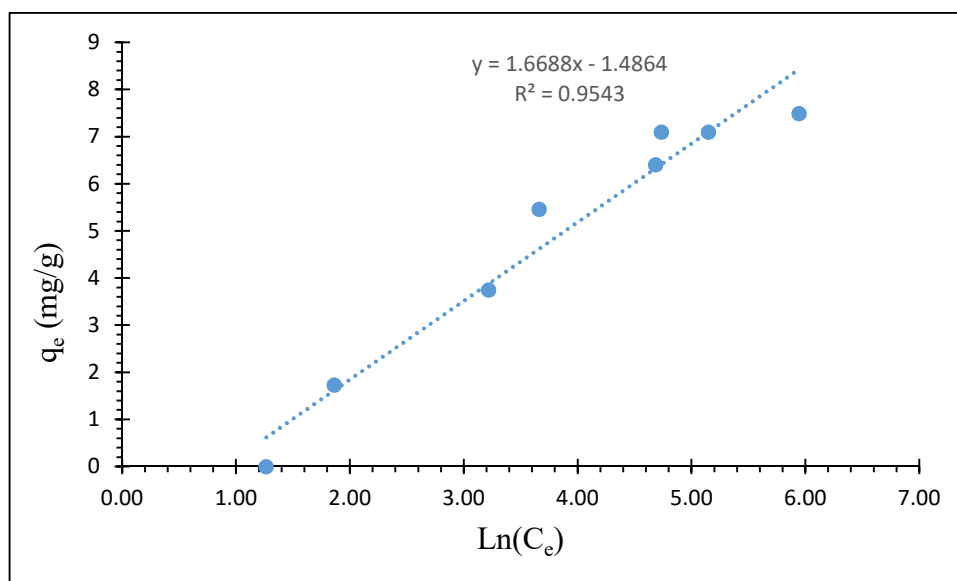


Figure III.12 Temkin isotherm for the adsorption of OG onto OFI-A

Freundlich, Langmuir and Temkin isotherm constants and their correlation coefficients for the OFI-A adsorbent are given in Tables III.2

Based on the correlation coefficient (R^2) value, the adsorption isotherm for OFI-A can better be described by Langmuir equation. Moreover, the dimensionless constant R_L lies within the favorable limit (0 - 1). Figure III.13 shows the comparative fit of Langmuir, Freundlich and Temkin isotherms by plotting experimental values of q_e versus C_e . It is clear that the Langmuir model is the best-fit model for the adsorption of OG onto OFI-A.

Figure III.13 shows that the adsorption of OG onto OFI-A followed the **L2** adsorption type curve, which indicate that adsorption of OG is favored in the beginning of the process, when all adsorption sites are vacant, It is usually indicative of molecules adsorbed flat on the surface.

Table .III.3 different isotherms parameters and correlation coefficient of OG adsorption onto OFI-A (at 25 °C and pH = 2).

| Adsorbent | Langmuir | | | | Freundlich | | | Temkin | | |
|-----------|---------------------|-----------------|-------|--------|------------|------|-------|-----------------|------|-------|
| | Q_{max} (mg/g) | K_L (L/mg) | R_L | R^2 | K_F | n | R^2 | K_T (L/mg) | b | R^2 |
| OFI-A | 8.23 | 0.075 | 0.027 | 0.9991 | 1.79 | 3.48 | 0.823 | 0.41 | 1454 | 0.954 |

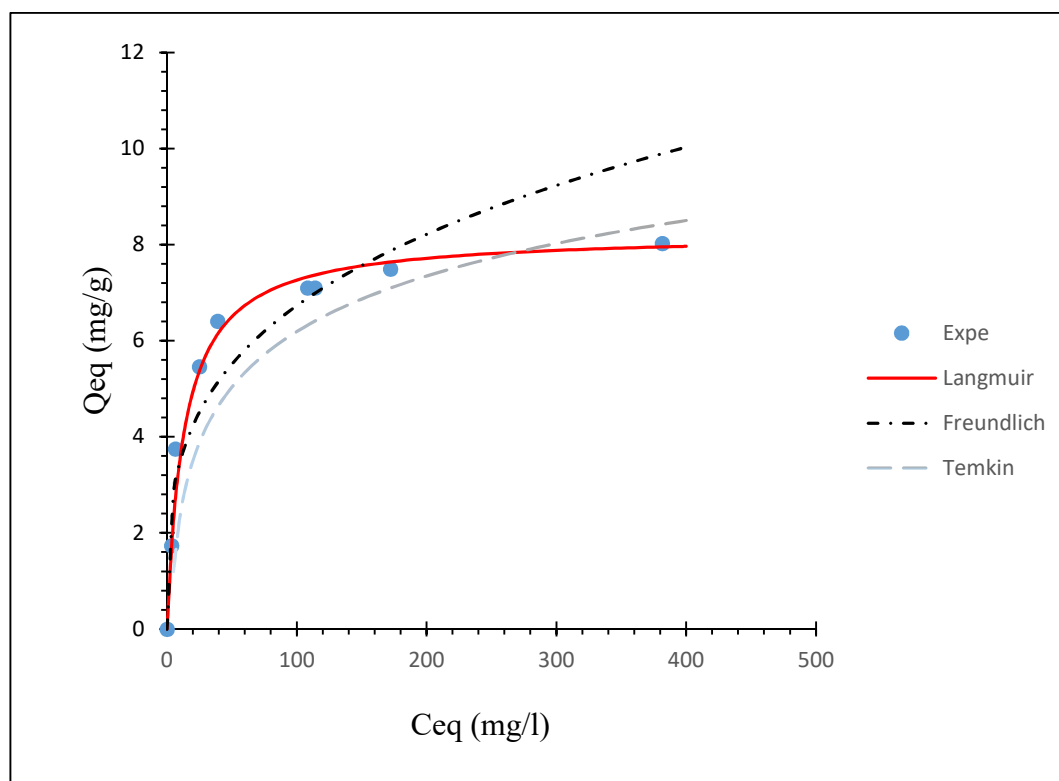


Figure III.13 Comparison of equilibrium isotherms for the adsorption of OG onto OFI-A

III.6 Thermodynamic studies

Increasing the temperature is known to increase the rate of diffusion of the adsorbate molecules into the pores of the adsorbent. It is due to the decrease in viscosity of the solution. In addition changing the temperature will change the equilibrium capacity of the adsorbent for a particular adsorbate. To determine the effect of temperature on the adsorption of OG, experiments were conducted at 288, 298, 308, 318 and 318 K and the results are shown in Figure III.14. The thermodynamic parameters such as free energy change (ΔG°), enthalpy change (ΔH°) and entropy change (ΔS°) can be calculated using equilibrium constants changing with temperature. The values of thermodynamic parameters were calculated using the following relationships:

$$K_d = q_e/c_e \quad (III.14)$$

$$\Delta G^\circ = -R.T . \ln(K_d) \quad (III.15)$$

$$\ln K_d = \frac{\Delta S^\circ}{R} - \frac{\Delta H^\circ}{RT} \quad (III.16)$$

Where R is the gas constant, K_d is the equilibrium constant and T is the solution temperature in Kelvin. The thermodynamic parameters can be calculated from plot of $\ln(K_d)$ versus $1/T$ (Figure III.15).

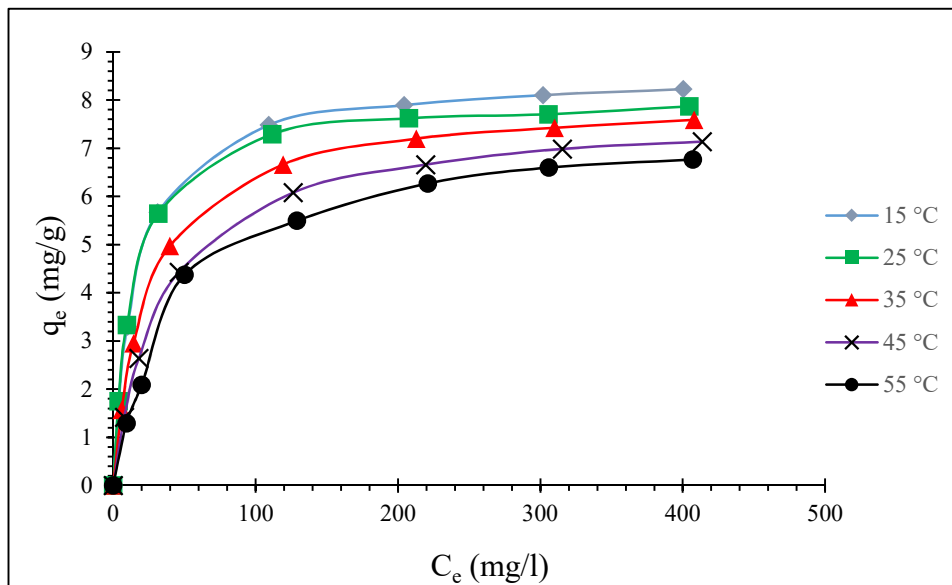


Figure III.14 Effect of temperature on the adsorption of OG onto OFI-A

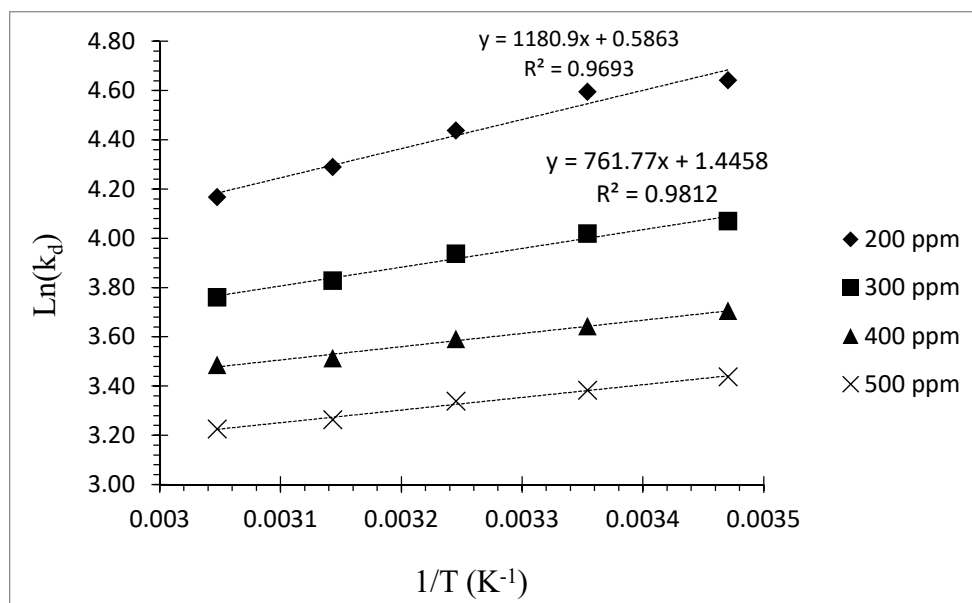


Figure III.15 Plot of $\ln(K_d)$ versus $1/T$ for the adsorption of OG onto OFI-A

Table III.4 Thermodynamic parameters for the adsorption of OG onto OFI-A

| Adsorbent | C ₀ (ppm) | ΔH° (KJ / mol) | ΔS° (KJ / mol.K) | ΔG° (KJ / mol) | | | | | R ² |
|-----------|-------------------------|--------------------------------|----------------------------------|-----------------------------|--------|--------|--------|--------|----------------|
| | | | | 288K | 298 K | 308K | 318K | 328K | |
| OFI-A | 200 | -9.57 | 0.0049 | -10.98 | -11.03 | -11.08 | -11.13 | -11.18 | 0.97 |
| OFI-A | 300 | -6.21 | 0.0117 | -9.59 | -9.71 | -9.82 | -9.94 | -10.06 | 0.98 |
| OFI-A | 400 | -4.10 | 0.0158 | -8.65 | -8.81 | -8.97 | -9.13 | -9.28 | 0.93 |
| OFI-A | 500 | -4.16 | 0.0136 | -8.08 | -8.21 | -8.35 | -8.48 | -8.62 | 0.98 |

The thermodynamic parameters (ΔH , ΔS and ΔG) were estimated in the range of initial dye concentrations 100, 300, 400 and 500 mg/L have been reported in tables III.3. The negative enthalpy values indicate that the OG adsorption reaction onto OFI-A is exothermic and from the obtained enthalpy values, we can assume that the adsorption was physical in nature ($\Delta H < 50$ kJ/mol). The negative values of the Gibbs free energy demonstrate the spontaneity of the process adsorption of the dye by OFI-A, where the adsorption of OG on OFI-A adsorbent is favorable to low temperature [22]. The positive values of ΔS° may be interrelated to the extent of hydration of anionic dye molecules. The reorientation or restructuring of water around dye molecules is very unfavourable in terms of entropy, since the reorientation disturbs the existing water structure and imposes a new and more ordered structure on the surrounding water molecules. Therefore, the positive entropy change may be attributed to the increasing disorder because the number of water molecules surrounding dye molecules decreases and thus the degree of freedom of the water molecules increases [23].

III.7. REFERENCES

- [1] Birjandi N, Younesi H, Bahramifar N. Treatment of wastewater effluents from paper-recycling plants by coagulation process and optimization of treatment conditions with response surface methodology. *Applied Water Science*. 2016;6(4):339-48.
- [2] Wang Z, Huang W, Yang G, Liu Y, Liu S. Preparation of cellulose-base amphoteric flocculant and its application in the treatment of wastewater. *Carbohydrate polymers*. 2019;215:179-88.
- [3] Znad H, Al Ketife AM, Judd S, AlMomani F, Vuthaluru HB. Bioremediation and nutrient removal from wastewater by *Chlorella vulgaris*. *Ecological Engineering*. 2018;110:1-7.
- [4] Yusoff MAM, Imam SS, Shah I, Adnan R. Photocatalytic activity of bismuth oxyiodide nanospheres and nanoplates in the degradation of ciprofloxacin under visible light. *Materials Research Express*. 2019;6(8):0850g5.
- [5] Imam SS, Panneerselvam P. Enhanced rhodamine B dye adsorption by groundnut shell activated carbon coated with Fe₃O₄. *Elixir Applied Chemistry*. 2015;86:34984-9.
- [6] Şentürk İ, Alzein M. Adsorptive removal of basic blue 41 using pistachio shell adsorbent- Performance in batch and column system. *Sustainable Chemistry and Pharmacy*. 2020;16:100254.
- [7] Saini J, Garg V, Gupta R, Kataria N. Removal of Orange G and Rhodamine B dyes from aqueous system using hydrothermally synthesized zinc oxide loaded activated carbon (ZnO-AC). *Journal of environmental chemical engineering*. 2017;5(1):884-92.
- [8] Arslanoglu F.N., Kar F. and Arslan N. (2005), 'Adsorption of dark coloured compounds from peach pulp using powdered activated carbon', *J. Food. Eng.*, Vol.71, pp.156-163.
- [9] Ramakrishna K.R. and Viraraghavan T. (1997), 'Dye removal using low cost adsorbents', *Water Sci. Technol.*, Vol.36, pp.189-196.
- [10] Mall I.D., Srivastava V.C. and Agarwal N.K. (2007), 'Adsorptive removal of Auramine-O: Kinetic and equilibrium study', *J. Hazard. Mater.*, Vol.143, pp.386-395.
- [11] Lagergren S. (1898), 'Zur theoric der sogenannten adsorption geloster stoffe', *Kungliga Svenska Vetenskapsakademiens, Handlingar*, Vol.24, No.4, pp.1-39.
- [12] Ho Y.S. and McKay G. (1998), 'The kinetics of sorption of basic dyes from aqueous solutions by sphagnum moss peat', *Can. J. Chem. Eng.*, Vol.76, pp. 822-826.
- [13] Taylor H.A. and Thon N. (1952), 'Kinetics of chemisorption', *J. Am. Chem. Soc.*, Vol.74, pp.4169-4173.

- [14] Daifullah A.E., El-Reefy S. and Gad H. (1997), 'Adsorption of p-nitrophenol on Inshas incinerator ash and on pyrolysis residue of animal bones', *Adsorpt. Sci. Technol.*, Vol.15, pp.485-496.
- [15] McKay G., Otterburn M.S. and Aja J.A. (1985), 'Fuller's earth and fired clay as adsorbents for dyestuffs', *Water Air Soil Pollut.*, Vol.24, pp.307-322.
- [16] Asfour H.M., Fadali O.A., Nassar M.M. and El-Feundi M.S. (1985), 'Equilibrium studies on adsorption of basic dyes on hard wood', *J. Chem. Technol. Biotechnol.*, Vol.35(A), pp.21-27.
- [17] Kannan N. and Sundaram M.M. (2001), 'Kinetics and mechanism of removal of methylene blue by adsorption on various carbons - a comparative study', *Dyes Pigments*, Vol.51, pp.25-40.
- [18] Poots V.J.P., McKay G. and Healy J.J. (1978), 'Removal of basic dye from effluent using wood as an adsorbent', *J. Water. Pollut. Control Fed.*, Vol.50, pp.926-939.
- [19] Hall K.R., Eagleton L.C., Acrivos A. and Vermeulen T. (1966), 'Pore diffusion and solid diffusion in fixed bed adsorption under constant pattern conditions', *Indian Eng. Chem. Fundam.*, Vol.5, pp.212-218.
- [20] Temkin M.J. and Pyzhev V. (1940), 'Kinetics of ammonia synthesis on promoted iron catalysts', *Acta Physicochim URSS.*, Vol.12, pp.217-222.
- [21] Choy K.K.H., McKay G. and Porter J.F. (1999), 'Sorption acid dyes from effluents using activated carbon', *Resour. Conserv. Recycl.*, Vol.27, pp.57-71.
- [22] Churchley J.H. (1994), 'Removal of dye wastewater colour from sewage effluent. The use of a full scale ozone plant', *Water Sci. Technol.*, Vol.30, No.5, pp.275-284.
- [23] D. Shao, G. Hou, J. Li, T. Wen, X. Ren, X. Wang, PANI/GO as a super adsorbent for the selective adsorption of uranium(VI). *Chem. Eng. J.* 255, 604–612 (2014)

CHAPTER IV

ADSORPTION OF ORANG G ONTO PANI

IV.1 Introduction

In the past two decades, there has been growing interest in the field of conducting polymers in both academia and industry [1]. Polyaniline (PANI) is one of the most extensively used and studied conducting polymers [2-4]. The major practical advantages of polyaniline are its high environmental stability, high electrical conductivity, and easy synthesis [5-7].

The objective of this study is to examine the use of polyaniline (PANI) for the removal of sulfonated dye OG from aqueous solutions and investigate the effect of some parameters such as pH, adsorbent dose, time and temperature on the adsorption of OG by polyaniline and propose a kinetic and an isotherm models.

IV. 2 Adsorption Study:

Emeraldine salt (ES) of PANI was synthesized by the conventional route using a 1:1 molar ratio of aniline to oxidant (APS) in an acidic medium (1 M HCl). After filtration and washing, the product was further doped with hydrochloric acid to achieve the maximum doping. The emeraldine base (EB) was obtained by treatment of the emeraldine salt with ammonium hydroxide. For adsorption experiments, 50 mg of the desired material (EB) was added to 50 mL of OG dye solutions having different concentrations range from 200 to 500 ppm. These solutions were stirred for 24 h. During this process, samples were collected from the reaction beaker at different time intervals and the concentration of the dye was determined by UV-vis absorption spectroscopy at λ_{\max} values of 477 nm using the Beer-Lambert law [8].

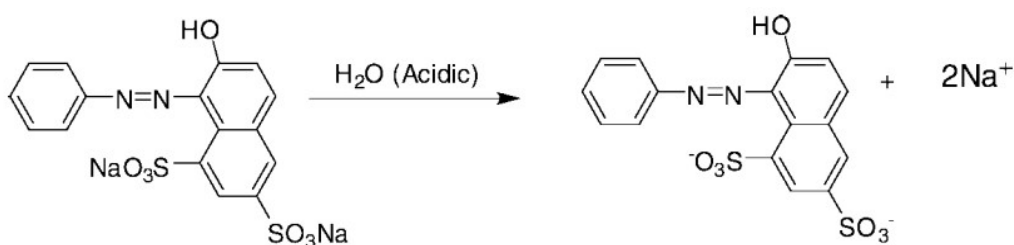


Figure IV.1 Dissociation of Orange G dye in aqueous solution [9].

IV.3. Effect of different parameters on the adsorption of OG onto PANI

To study the effect of parameters such as adsorbent dosage, pH and initial concentration batch experiments were carried out for the adsorption of anionic dyes (OG) onto PANI in a thermostatic orbital shaker at a constant speed of 125 cycles per minute at 25°C [10-11].

IV.3.1. Effect of adsorbent dosage

The effect of adsorbent dose on the adsorption of OG was investigated by incubating different quantities of doped PANI (ES) in 50 mL of OG solution with an initial concentration of 400 ppm at (pH=2) for 24 h. The experiment result are given in Figure IV.2, which shows a proportional relation of the OG dye removal to the doped PANI (ES) dose within the range of 0.1 g/l to 3 g/l this is due to the availability of more surface functional groups at higher concentration [12-13].

The adsorbent dose of 1.6 g/l has the capacity to remove the total dye existed in the aqueous solution and adding of more mass of PANI has negligible effect.

$$\text{Dye Removal \%} = \frac{C_0 - C_f}{C_0} * 100\%$$

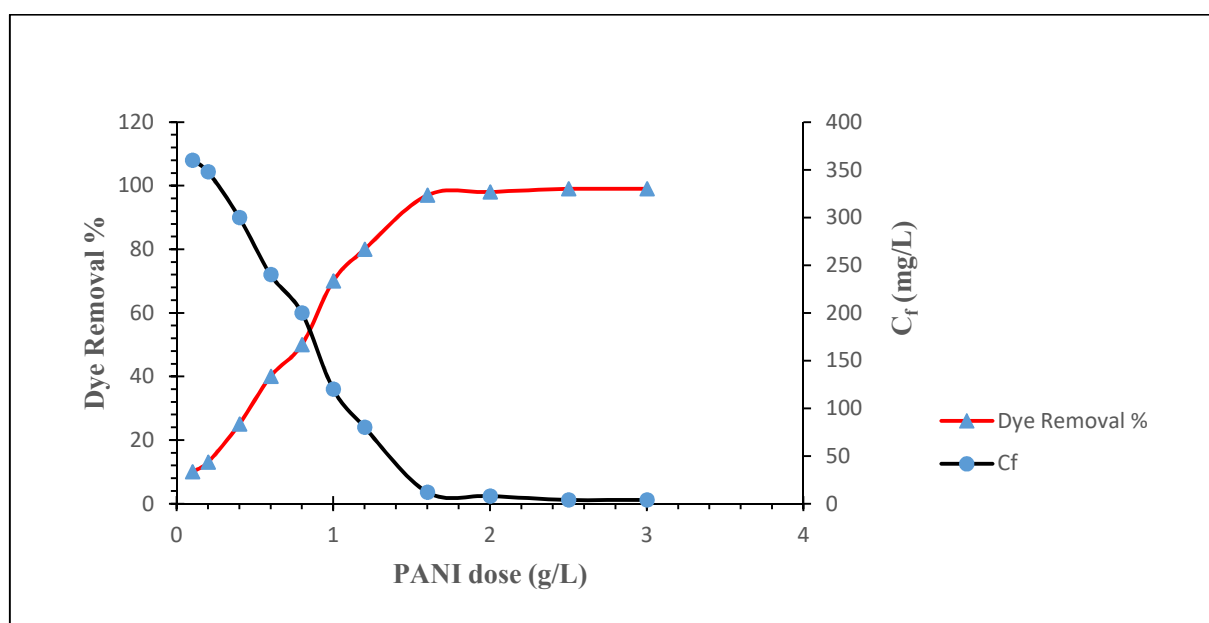


Figure IV.2 Effect of adsorbent dosage on the adsorption of OG onto PANI (ES)

IV.3.2. Effect of pH on the adsorption of OG onto PANI

It is well known that the degree of ionization of a dye molecule depends on the pH of the aqueous medium. Orange G contains two sulfonated groups ($-\text{SO}_3\text{Na}$) and one hydroxyl group ($-\text{OH}$). In acidic aqueous solutions, the functional group of OG ($-\text{SO}_3\text{Na}$) gets ionized, and the dye exists in anionic form as shown in Figure.IV.1. When PANI emeraldine salt (ES) is added to water, the pH of the water becomes acidic ($\text{pH} \approx 3.4$) and does not change during the course of adsorption. The addition of dyes with sulfonated functional groups to this aqueous solution results in the dissociation of the functional group into its anionic form.

The ($-\text{SO}_3^-$) group on the dye could lead to chemical interactions with the positively charged backbone of PANI (ES), and Na^+ ions interact with the chloride ions that are invariably present in doped PANI. This will lead to the adsorption of sulfonated dye on the emeraldine salt of PANI [14].

In basic aqueous solutions (dispersion of emeraldine base in water), no chemical interaction with the PANI backbone would be expected, when the emeraldine base (EB) of polyaniline is used instead of the emeraldine salt (ES) for the above experiments, we found that the base form cannot remove the dye from solution. This indicates that the positively charged backbone and chloride ions that are invariably present in the ES form of PANI are the possible sites for chemical interactions with the sulfonated dye molecules. After the dye was adsorbed on PANI, a base (ammonium hydroxide) was added to the solution. This base dedoped the PANI and resulted in the desorption of the dye [15].

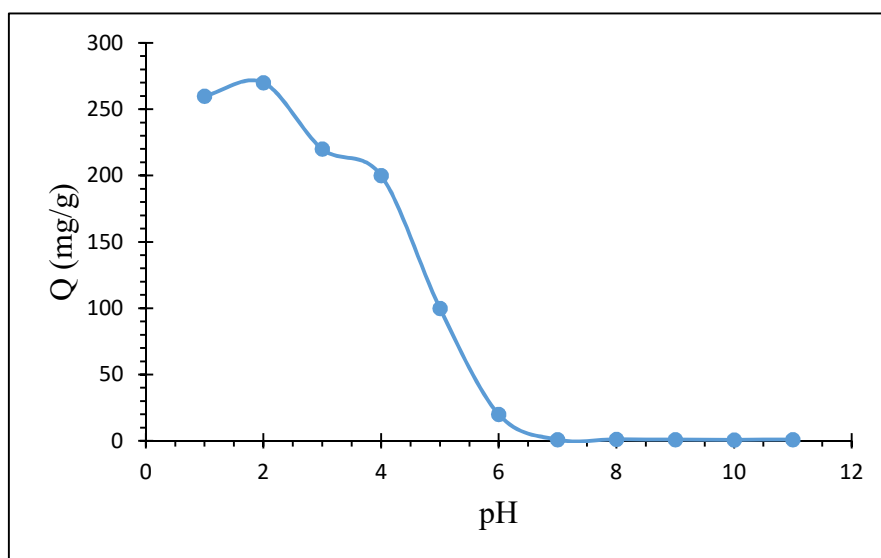


Figure.IV.3. Effect of pH values on the adsorption of OG onto PANI

IV.3.3. Effect of Initial OG Concentration and Contact Time

The effect of contact time on the adsorption of OG was investigated by incubating 0.1 g of doped PANI in different flasks of 250 ml, each flask contains 100 ml of OG solution at (pH = 2) with different OG initial concentration 200, 300, 400 and 500 ppm. The flasks were kept in an isothermal bath shaker at 25 ° C and shaking speed of 125 rpm. 1 ml of solution extracted from each flask after 10, 20, 30, 60, 120, 360 min and 24 hours of adsorption then centrifuged for 5 min using a centrifuge at a speed of 4200 rpm to separate the adsorbent particle from the solution. Then the obtained solution analyzed in UV-vis spectrum to determine its concentration [16].

As shown in figure IV.4 the adsorption reaction reaches the equilibrium within 360 min for the initial concentration of OG $C_0 = 200$ ppm but for the initial concentration $C_0 = 500$ ppm more time is required to reach the equilibrium. Therefore, a duration of 24 h was chosen to be sure that equilibrium is reached.

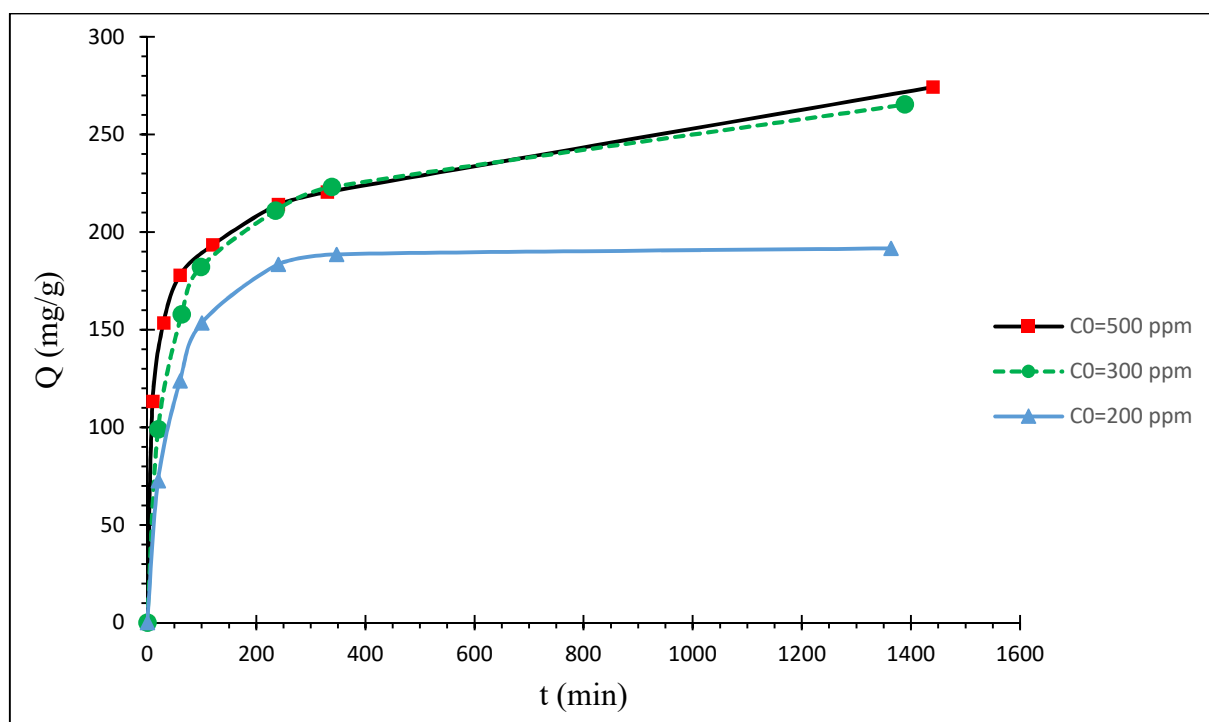


Figure IV.4 Effect of contact time and initial concentration on adsorption of OG onto PANI

IV.4. Adsorption kinetics modeling

To investigate the adsorption processes of OG on OFI-A, four kinetic models such as pseudo-first order, pseudo-second order, intra-particle diffusion and Elovich were selected to fit the experimental kinetic data.

IV.4.1 Pseudo-first order

Lagergren (1898) proposed a pseudo first order kinetic model expressed by the equation III.1 quoted in chapter III.

In order to obtain the rate constants, the straight line plots of $\ln(q_e - q_t)$ against t for different initial dye concentrations of OG have been analyzed (Figure IV.5). The rate constant k_1 , the equilibrium capacity and correlation coefficients R^2 for adsorption of OG onto PANI adsorbent that calculated from these plots are listed in Tables IV.1.

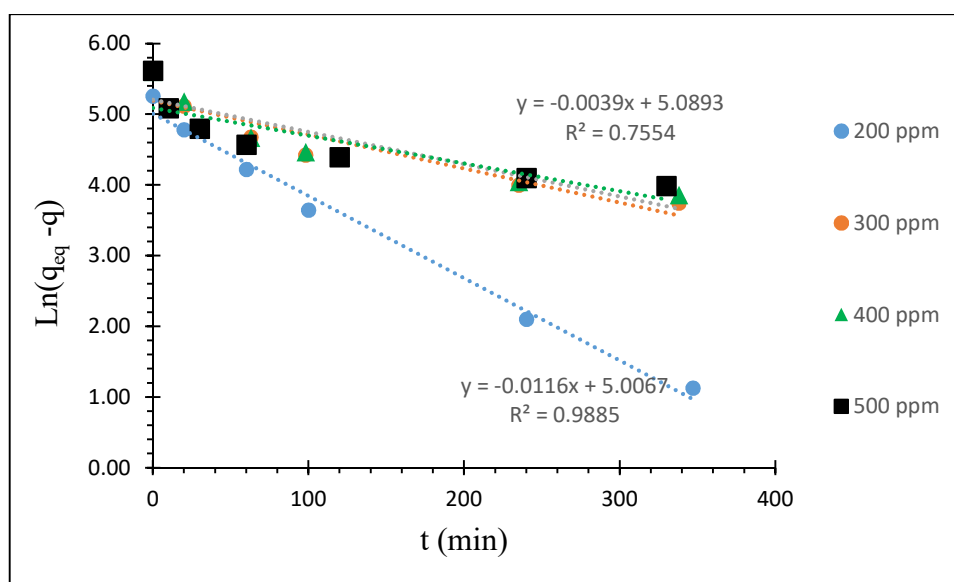


Figure IV.5 The pseudo-first order kinetic model for the adsorption of OG onto PANI

IV.4.2 Pseudo-second order

An expression also very often used is that of the pseudo-second order, which is given by the formula III.3 described in chapter III.

Figures IV.6 shows the application of the pseudo-second order kinetic model to the results obtained for the adsorption of OG onto doped PANI. The values of the equilibrium quantity adsorbed Q_e , the pseudo-second order constants k_2 and the regression coefficients R^2 are given in Table IV.1.

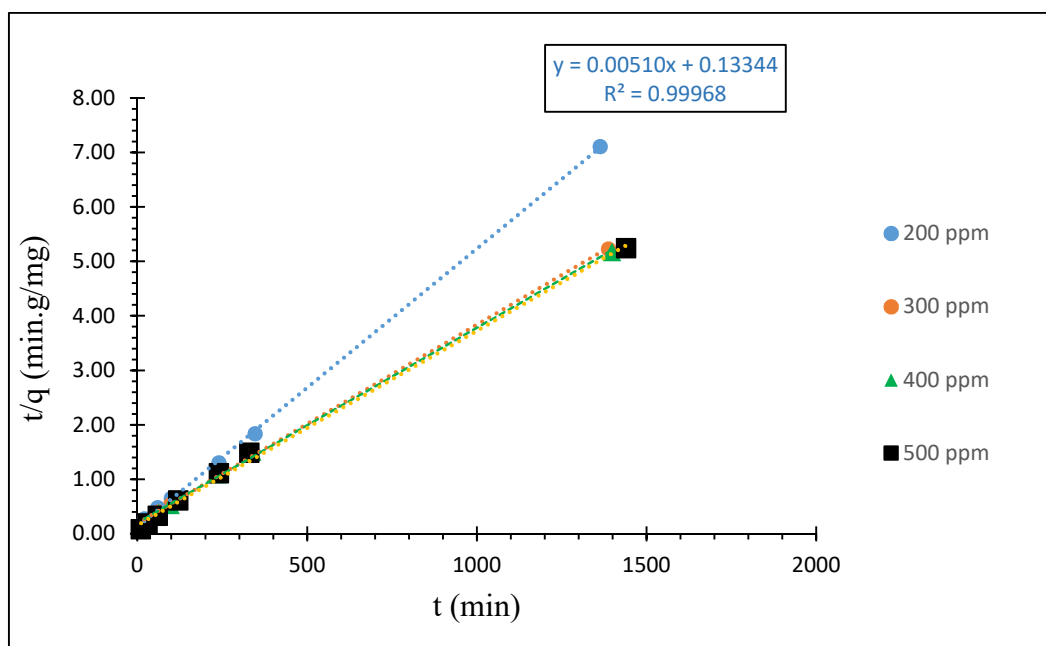


Figure IV.6 The pseudo-second order kinetic model for the adsorption of OG onto PANI

IV.4.3. Elovich model

Figures IV.7 shows the application of the Elovich model to the results obtained for the adsorption of OG onto doped PANI. The values of the equilibrium quantity adsorbed Q_e , the Elovich constants α , β and the regression coefficients R^2 are given in Table IV.1.

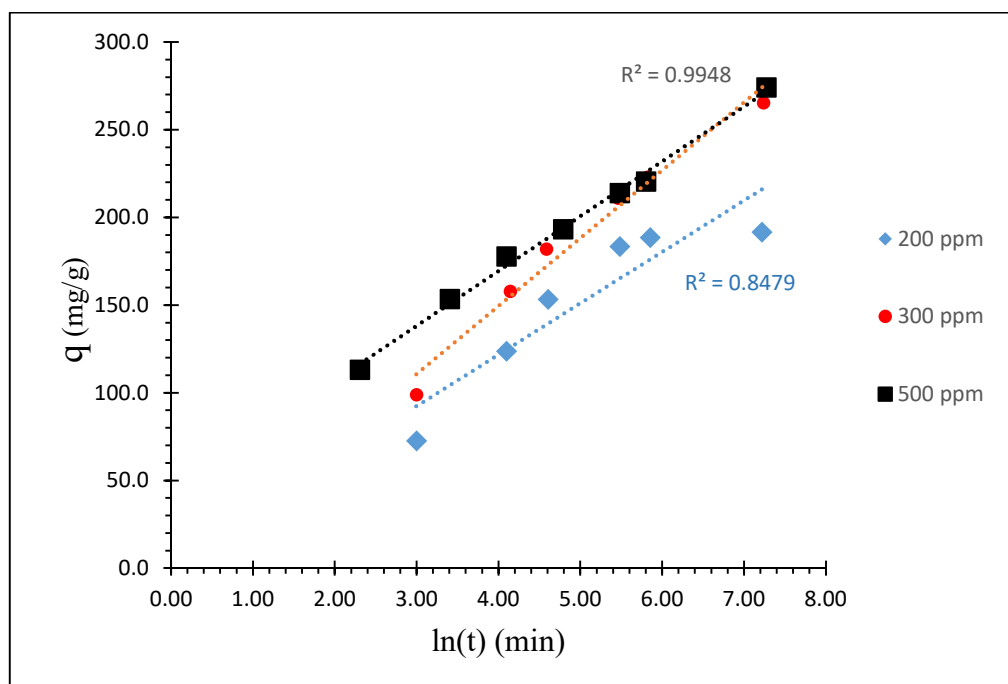


Figure IV.7 Elovich model for the adsorption of OG onto PANI

IV.4.4. Intra-particle model

Different articles referring to this kinetic approach of intra-particles diffusion are generally based on the work of Weber and Morris (1963) on the adsorption of simple aromatic compounds on activated carbon. Where they showed that the quantity adsorbed (Q_t) is a linear function of the square root of the contact time ($t^{1/2}$), which the slope is assimilated to the speed constant (k_{int}). The kinetic expression of intra particles diffusion often presented simply by equation III.6. Figures IV.8 shows the graphical presentation of this model, the value of the external diffusion constant k_{int} , as well as those of I and R^2 are listed in Tables IV.1.

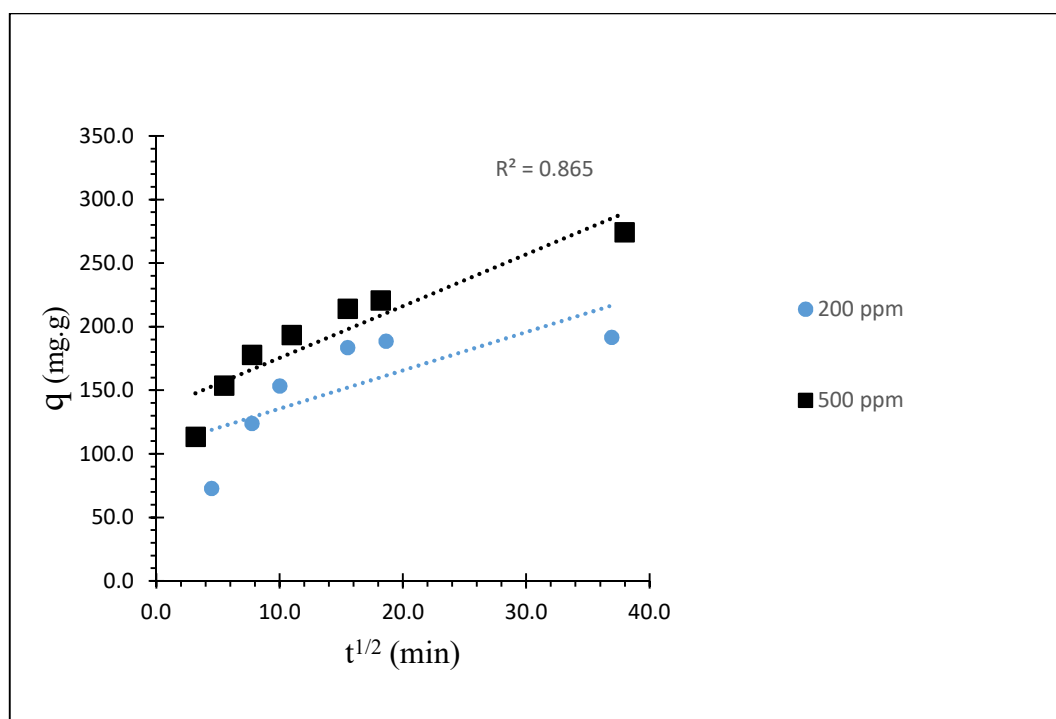


Figure IV.8. Intra-particle diffusion model for the adsorption of OG onto PANI

Table IV.1 Kinetic parameters for the adsorption of OG onto PANI

| C ₀ (ppm) | Q _{Exp} (mg/g) | Pseudo-first order | | | Pseudo-second order | | | Elovich | | | Intra-particle diffusion | | |
|-------------------------|----------------------------|------------------------------|--|----------------|------------------------------|--|----------------|---------|-------|----------------|---|-------|----------------|
| | | Q _{eqcal} (mg/g) | K ₁ (min ⁻¹) | R ² | Q _{eqcal} (mg/g) | K ₂ (g.mg ⁻¹ .min ⁻¹) | R ² | α | β | R ² | k _{int} (g.mg ⁻¹ .min ^{1/2}) | I | R ² |
| 200 | 191.7 | 149.4 | 1.16E-02 | 0.9885 | 198.1 | 1.95E-04 | 0.9997 | 34.24 | 0.034 | 0.848 | 3.01 | 105.5 | 0.561 |
| 300 | 265.4 | 179.9 | 4.80E-03 | 0.8640 | 274.7 | 6.68E-05 | 0.9990 | 33.55 | 0.026 | 0.978 | 4.369 | 121.9 | 0.796 |
| 400 | 269.9 | 182.8 | 4.58E-03 | 0.8389 | 279.3 | 6.23E-05 | 0.9988 | 29.47 | 0.025 | 0.968 | 4.517 | 120.5 | 0.780 |
| 500 | 274.2 | 160.3 | 3.87E-03 | 0.769 | 268.8 | 7.5E-05 | 0.9968 | 88.44 | 0.032 | 0.9948 | 4.072 | 134.9 | 0.865 |

Based on the correlation coefficients (R^2) value, the pseudo-second order describe in a good way the adsorption kinetic of OG dye onto PANI. The comparative results using various kinetic models for the adsorption of OG with an initial dye concentration of 200 mg/L are presented in Figure III.9.

It is clear that the pseudo-second order kinetic fitted well for the adsorption of OG onto PANI compare to other models. The Elovich model can be considered as a fitted model for the first 120 min and thereafter the data deviated. Thus, the model represents the initial stages adsorption, but it can not be applied to entire adsorption process. Therefore, the pseudo-first order and intra-particles models were inapplicable to this system. The correlation coefficients and the calculated values of 'q_e' for pseudo-second order kinetic model are in good agreement with the experimental results. From the results obtained, the adsorption systems studied belong to the pseudo-second order kinetic model.

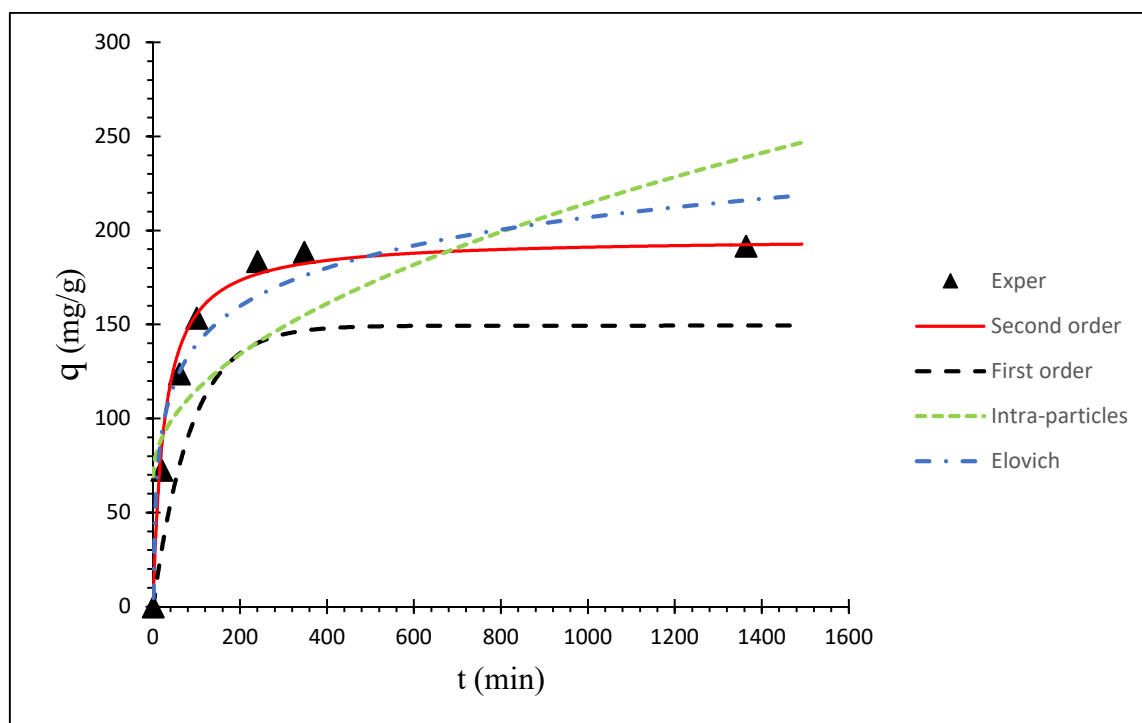


Figure IV.9 Comparison between the measured and modelled time profiles for the adsorption of OG onto PANI

IV.5. Adsorption isotherms modeling

The adsorption isotherm, which characterise the thermodynamic equilibrium between an adsorbent and an adsorbate, is obtained from batch experiments where the concentration of the adsorbate remaining in the fluid phase after adsorption.

50 mg of doped PANI was successively introduced in series of 100 ml beakers, each beaker contains 50 mL of OG solution with pH = 2 and initial concentrations ranging from 100 to 700mg/L. The beakers were carried in an isothermal shaker at a temperature of 25°C and shaking speed 125 rpm. And keep the mixture for 24 hours until the equilibrium is reached we trace the adsorbed quantity of OG q_e (mg/g) as a function of the equilibrium concentration of adsorbate remaining in the solution C_e (mg/L) [17]. The obtained results are shown in Figures IV.10. The three used isotherms to explain the equilibrium uptake of solute are Freundlich, Langmuir and Temkin isotherms, which are introduced in chapter.III.

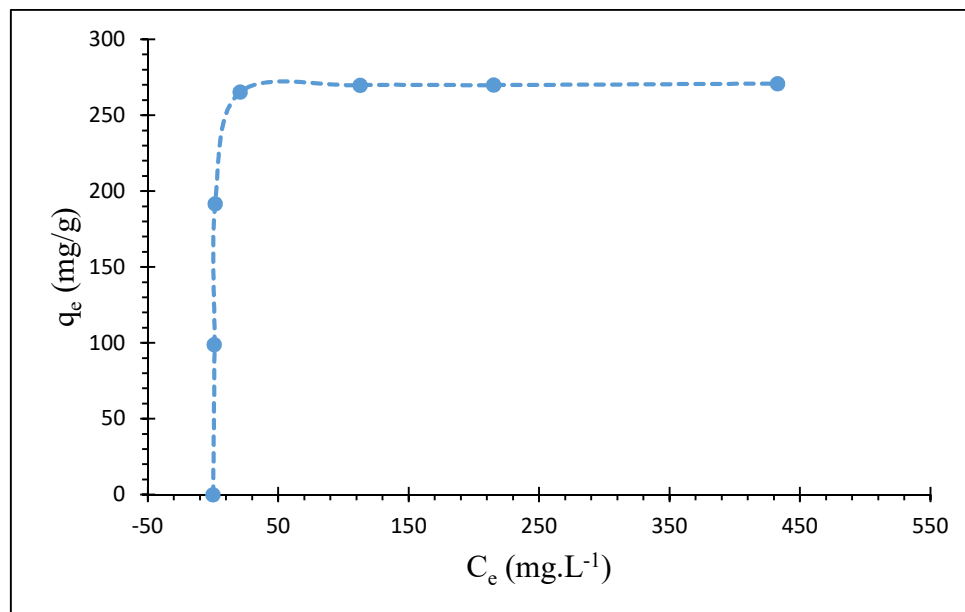


Figure IV.10 Adsorption isotherm of OG adsorption onto PANI

IV.5.1. Freundlich isotherm

The first model that can represent our isotherm is the Freundlich equation, which is expressed according to relation III.7. The plot of $\ln(q_e)$ as a function of $\ln(C_e)$ figure (IV.12) allows us to determine n and k_F . The calculated parameters of this model are listed in Table IV.2.

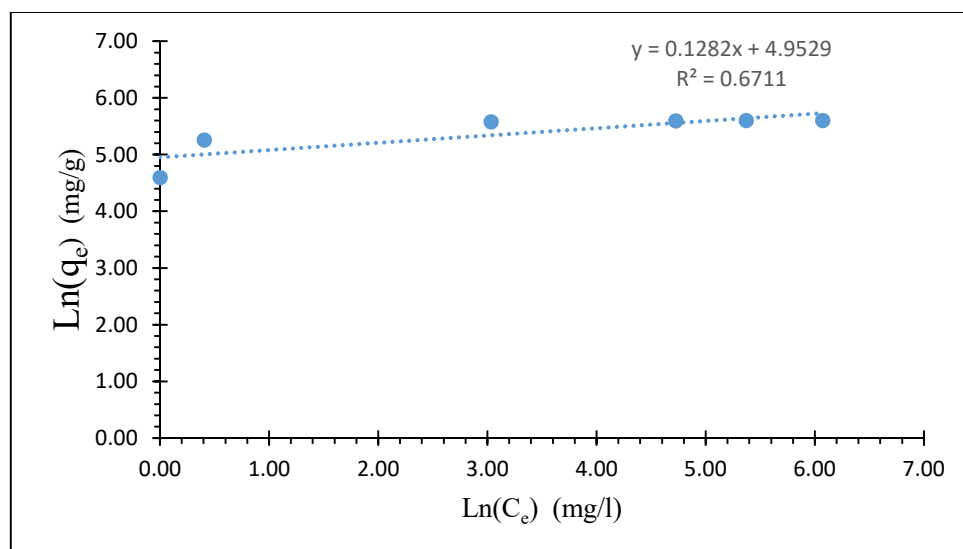


Figure III.11 Freundlich isotherm for the adsorption of OG onto PANI

III.5.2 Langmuir isotherm

Langmuir isotherm is expressed by the equation III.9 given in chapter.III. The plot of C_e/q_e as a function of C_e makes it possible to determine Q_{\max} and k_L . The results of this model are cited in Table IV.2 and represented graphically in Figures IV.12

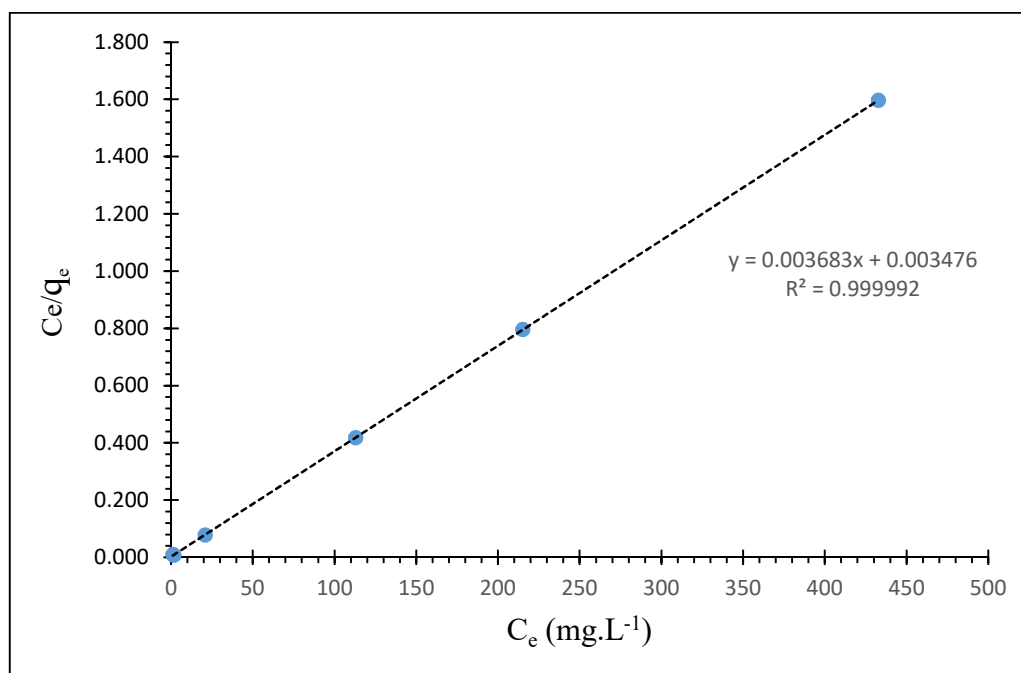


Figure III.12 Langmuir isotherm for the adsorption of OG onto PANI

IV.5.3 Temkin isotherm

Temkin isotherm is expressed by equation III.12. The plot of q_e versus $\ln(C_e)$ is presented in figure IV.13, the calculated constants of Temkin equation are given in table.IV.2

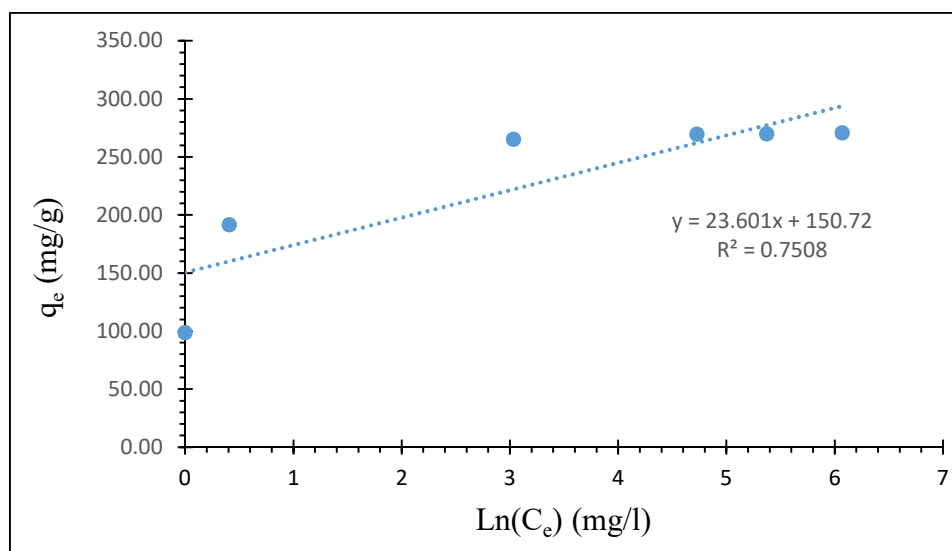


Figure VI.13 Temkin isotherm for the adsorption of OG onto PANI

Table .IV.2 different isotherms parameters and correlation coefficients of OG adsorption onto PANI (at 25 °C and pH = 2)

| Adsorbent | Langmuir | | | | Freundlich | | | Temkin | | |
|-----------|----------------------------|--------------------------|----------------|----------------|----------------|------|----------------|--------------------------|--------|----------------|
| | Q _{max} (mg/g) | K _L (L/mg) | R _L | R ² | K _F | n | R ² | K _T (L/mg) | b | R ² |
| PANI | 271.52 | 1.06 | 0.002 | 0.999 | 141.6 | 7.80 | 0.671 | 593.6 | 105.03 | 0.751 |

Based on the correlation coefficient (R^2) value, the adsorption isotherm for OG adsorption onto PANI can better be described by Langmuir equation. Moreover, the dimensionless constant R_L lies within the favorable limit (0 - 1). The comparative fit of Langmuir, Freundlich and Temkin isotherms by plotting experimental values of q_e versus C_e and obtained models are given in Figure IV.14. From this Figure and correlation coefficients, it is clearly observe that the Langmuir model is the best-fit model for the adsorption of OG onto PANI.

Figure IV.14 shows that the adsorption of OG onto PANI follows the **H2** curve type, which characterized by a sharply vertical part of the initial slope, indicating highly strong interactions between the OG and the PANI. All the OG molecules in solution are adsorbed onto the PANI. Which indicate a high affinity of OG ions to the PANI.

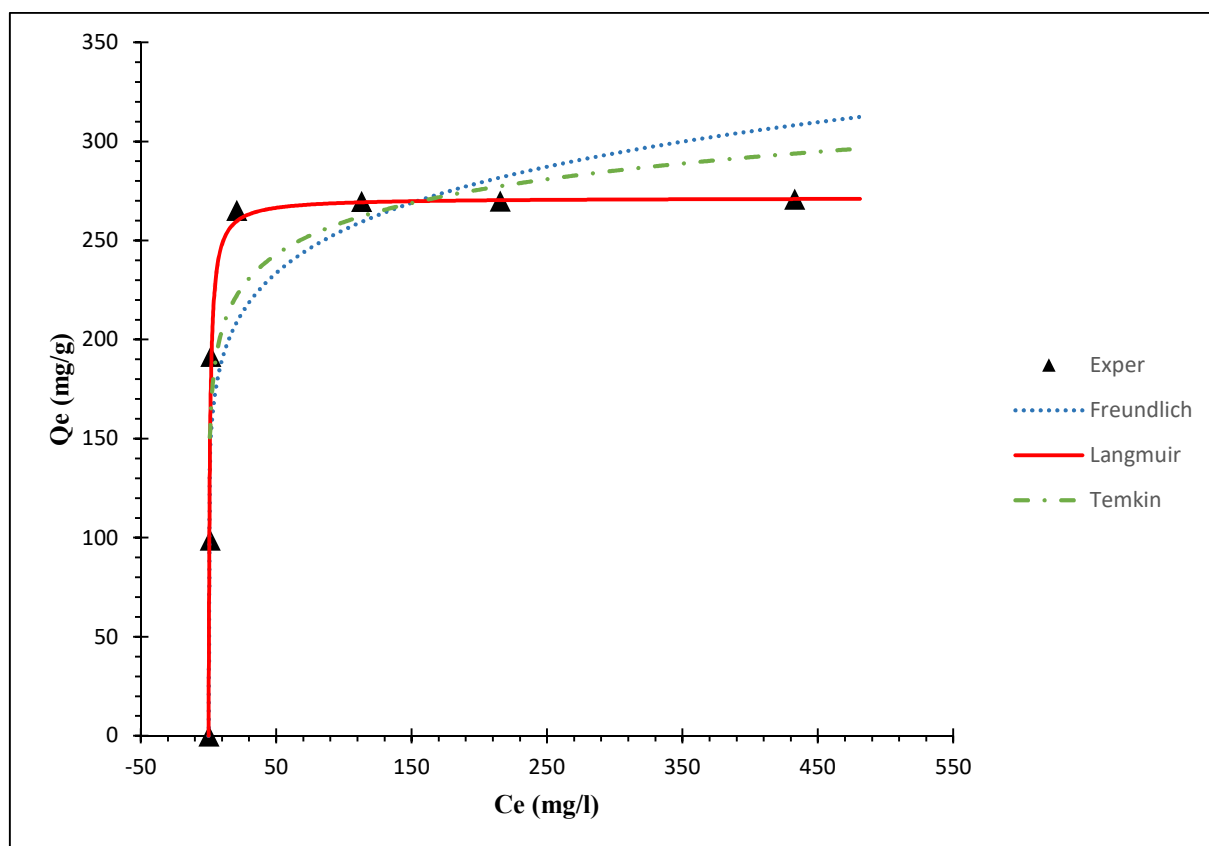


Figure IV.14 Comparison of equilibrium isotherms for the adsorption of OG onto PANI

IV.6 Thermodynamic studies

We studied the influence of temperature on the adsorption of OG. However, a mass of 50 mg of each adsorbent is suspended in a solution of 50 ml with OG concentrations ranging from 100 to 700 mg/l. The temperatures of the mixtures have been fixed at 25, 35, 45 and 55°C using a thermostatic shaker. Figure.IV.15 shows the effect of temperature on the adsorption of OG onto PANI.

The distribution constant K_d was calculated according to equation III.14, the results of the distribution constant K_d are represented graphically in Figures IV.16 Thermodynamic parameters such as standard free energy (ΔG°), standard enthalpy (ΔH°) and standard entropy (ΔS°) were determined using equations III.15 and III.16. The results of these measurements are listed in Table IV.3.

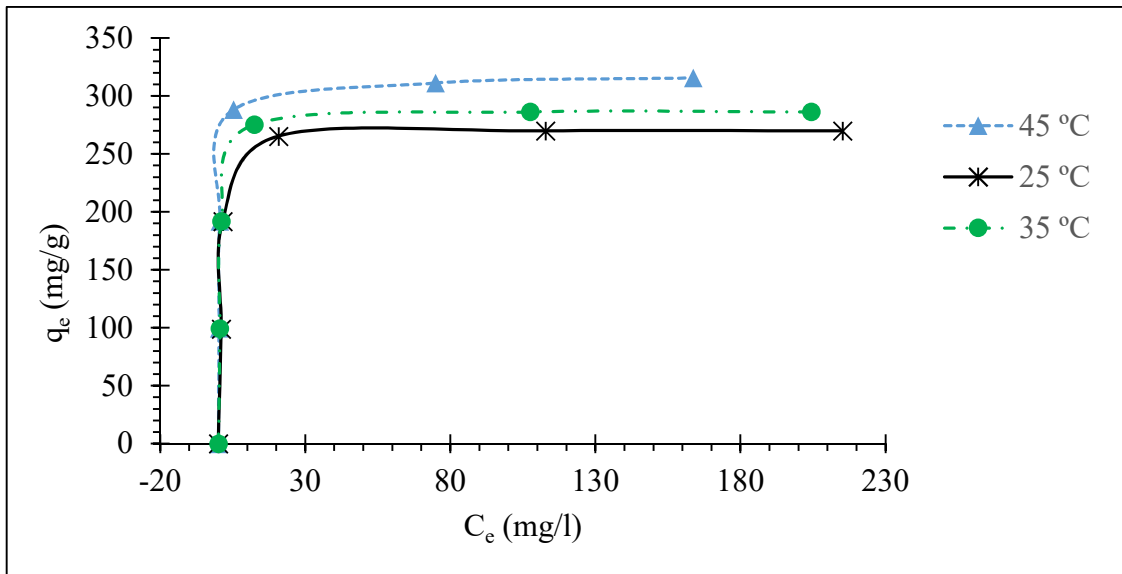


Figure III.15 Effect of temperature on the adsorption of OG onto PANI

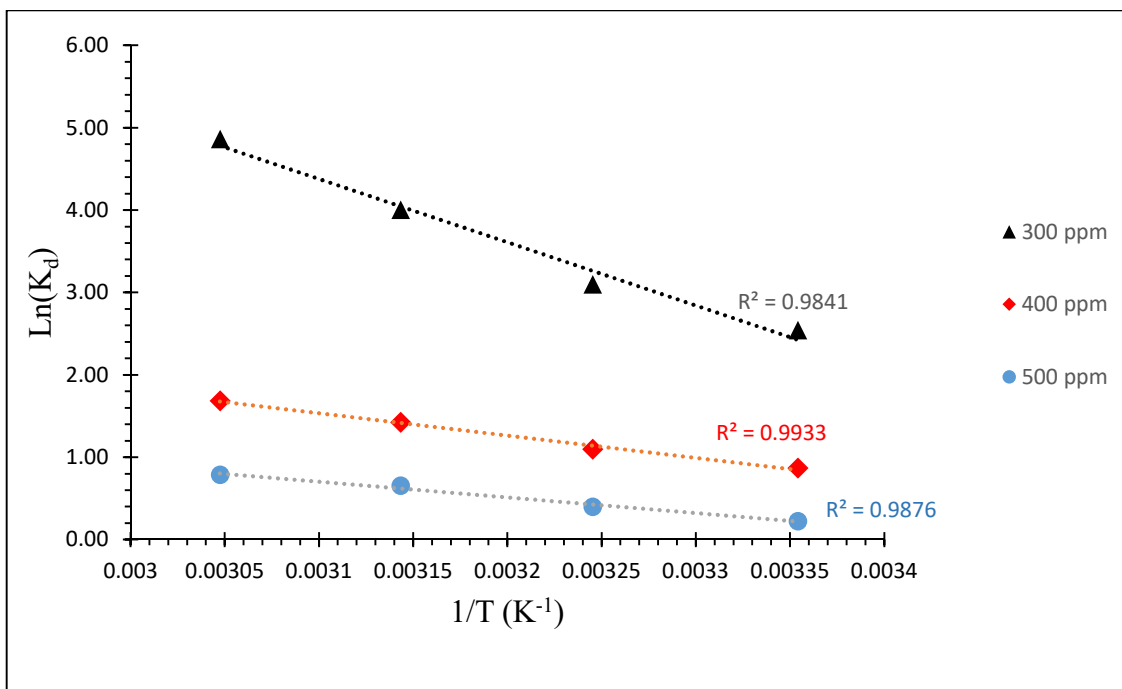


Figure IV.16 Plot of $\ln(K_d)$ versus $1/T$ for the adsorption of OG onto PANI

Table IV.3 Thermodynamic parameters for the adsorption of OG onto PANI

| Adsorbent | C ₀ (ppm) | ΔH° (KJ / mol) | ΔS° (KJ / mol.K) | ΔG° (KJ / mol) | | | R ² |
|-----------|----------------------|-----------------------------|-------------------------------|-----------------------------|--------|--------|----------------|
| | | | | 298 K | 308K | 318K | |
| PANI | 300 | 63.8 | 0.234 | -6.02 | -8.36 | -10.71 | 0.9841 |
| PANI | 400 | 22.6 | 0.083 | -2.10 | -2.93 | -3.75 | 0.9933 |
| PANI | 500 | 15.8 | 0.055 | -0.547 | -1.096 | -1.644 | 0.9876 |

The positive enthalpy values indicate that the OG adsorption reaction onto PANI is endothermic and from the obtained enthalpy values, we can conclude that the adsorption has a physical nature ($\Delta H < 50$ KJ/mol) [17]. The negative values of the Gibbs free energy demonstrate the spontaneity of the adsorption process of OG onto PANI, where the adsorption of OG onto PANI is favorable at high temperature. The positive value of the entropy change confirms that the molecules gain degrees of freedom during the adsorption process, that means OG molecules in the aqueous phase are rather ordered than at the interface solid/liquid [18].

IV.7. REFERENCES

- [1]. Goswami M., Sahoo S., Meikap A.K., Gosh R., Characterization, optical and DC electrical properties of polyaniline and zinc sulphide nanocomposites, International Conference on Nanoscience Engineering and Technology , Chennai, 2011, 314-318.
- [2]. Abdelaziz Rahy, Mohamed Sakrout, Sanjeev Manohar, Sung June Cho, John Ferraris, D. J. Yang, Polyaniline nanofiber synthesis by co-use of ammonium peroxydisulphate and sodium hypochlorite, Chemical Matter 20(15), 2008, 4808-4814
- [3]. Chandrasekhar P., Conducting polymers, fundamentals and applications: A practical approach (Kluwer Academic publishers, Boston, 1999)
- [4]. MacDiarmid A.G., Yang L.S., Huang W.S., Humphrey B.D., Polyaniline: Electrochemistry and application to rechargeable batteries, Synthetic metals, 18, 1987, 393-398
- [5]. Shabnam Virji, Jesse D. Fowler, Christina O. Baker, Jiaying Huang, Richard B. Kaner, Bruce H. Weiller Polyani line nanofiber composites with metal salts: Chemical sensors for hydrogen sulfide, Small 1(6), 2005, 624-627
- [6]. David W. DeBerry, Modification of the electrochemical and corrosion behavior of stainless steels with an electroactive coating, Journal of Electrochemical Society, 135(5), 1988, 1022-1026.
- [7]. Mark R. Anderson, Benjamin R. Mattes, Howard Reiss, Richard B. Kaner, Conjugated polymer films for gas separations, Science 252, 1991, 1412-1415.
- [8]. Charles R. Martin, Template Synthesis of Electronically Conductive Polymer Nanostructures, Accounts of chemical research, 28(2), 1995, 61-68
- [9]. Hongjin Qiu, Meixiang Wan, Barry Matthews, Liming Dai, Conducting polyaniline nanotubes by template-free polymerization, Macromolecules 34(4), 2001, 675-677.
- [10]. Xinyu Zhang , Warren J. Goux , and Sanjeev K. Manohar, Synthesis of polyaniline nanofibers by “nanofiber seeding”, Journal of American Chemical Society, 126(4), 2004, 4502-4503
- [11]. K. Gopalakrishnan, M.Elango, M. Thamilselvan, Optical studies on nano -structured conducting Polyaniline prepared by chemical oxidation method, Archives of Physics Research, 3(4), 2012, 315-319.
- [12]. Ali Olad, Sepideh Behboudi, Ali Akbar Entezami, Preparation, characterization and photocatalytic activity of TiO₂/polyaniline core-shell nanocomposite, Bulletin of Materials Science 35(5), 2012, 801-809
- [13]. O.Hamdaoui, E. Naffrechoux, Modeling of adsorption isotherms of phenol and chlorophenols onto granular activated carbon. Part II. Models with more than two parameters, J. Hazard. Mater. 147 401– 411. (2007).

- [14] Q.H. Fan, D.D. Shao, J. Hu, W.S. Wu, X.K. Wang. Comparison of Ni²⁺ sorption to bare and ACT-graftattapulites: effect of pH, temperature and foreign ions, *Sur. Sci.* 602 778 – 785. (2008).
- [15] S. Preethi, A. Sivasamy. Removal of safranin basic dye from aqueous solutions by adsorption onto corncob activated carbon, *Ind. Eng. Chem. Res.* 45 7627–7632. (2006).
- [16] M. Choudhary, M.B. Ray, S. Neogi, Evaluation of the potential application of cactus (*Opuntia ficus-indica*) as a bio-coagulant for pre-treatment of oil sands process-affected water. *Sep. Purif. Technol.* 209, 714–724 (2019)
- [17] A.A.P. Cid, I.V. Ugalde, A.M.H. González, J.G. Serrano, Textile dyes removal from aqueous solution using *Opuntia ficus-indica* fruit waste as adsorbent and its characterization. *J. Environ. Manag.* 130, 90–97 (2013)
- [18] H. Soltani, A. Belmokhtar, F.Z. Zeggai, A. Benyoucef, S. Bousalem, K. Bachari, Copper(II) removal from aqueous solutions by PANI-clay hybrid material: fabrication, characterization, adsorption and kinetics study. *J. Inorg. Organomet. Polym. Mater.* 29, 841–850 (2019)

CHAPTER V

ADSORPTION OF ORANG G ONTO PANI@OFI-A

V.1 Introduction

Adsorption has advantages over the other methods for water treatment because of inexpensive, more proficient, simple design and the simplicity of the application process [1–3]. excellent adsorption competence of various adsorbents to remove Orange-G (OG) has been proved by many researchers. Conductive polymers as polyaniline (PANI) are more important in wide regions. Now PANI is applied as a hybrid material with other composite to test its potency. Among these nanomaterials we find:

PANI@SiO₂ [4], PANI@Al₂O₃ [5], PANI@TiO₂ [6], PANI@ZnO[7], PANI@SiC[8], PANI@V₂O₅ [9], PANI@MoS₂ [10], Fe₃O₄@Polyaniline/Itaconic Acid [11] and PANI@Graphene Oxide [12]. In this chapter we will investigate the adsorption of OG dye on to a new developed hybrid material PANI@OFI-A, which synthesis from OFI-A powder and polyaniline by a chemical reaction in presence of APS as oxidant.

V. 2 Adsorption Study

To study the effect of different parameters such as adsorbent dosage, pH and initial concentration batch experiments were carried out for the adsorption of anionic dyes (OG) onto PANI@OFI-A in a thermostatic orbital shaker at a constant speed of 125 cycles per minute at 25°C. The adsorption experiments were carried-out by agitating 50 mL of dye solutions with various concentrations. After agitation, the dye solutions were separated from the adsorbent by centrifugation for 5 minutes at a speed of 4200 rpm. Dye concentrations in the supernatant solutions were measured using a UV-Vis spectrophotometer. The effect of pH on dye removal was studied over a pH range of 2-11. The Initial pH of the dye solution was adjusted by the addition of 1 M solution of HCl or NaOH. To find the optimum amount of adsorbent per unit mass of the adsorbate, 50 mL of dye solution was contacted with different amounts of adsorbent till equilibrium was reached. The kinetic experiments were carried out by incubating 50 mg of adsorbent in 100 mL beaker contains 50 mL of OG solutions with concentration range 100-1000 mg/L using a mechanical shaker. The samples were withdrawn at predetermined time intervals and centrifuged. The effect of temperature on the adsorption characteristics was studied by carrying out a series of experiments a temperatures of 25, 35, 45 and 55°C using thermostatic shaker.

V.3. Effect of different parameters on the adsorption of OG onto PANI@OFI-A

V.3.1. Effect of adsorbent dosage

The effect of adsorbent dose on the adsorption of OG was investigated by incubating different quantities of PANI@ OFI-A in 50 mL of 400 ppm OG solution for 24 h. The experimental result for the adsorbents is given in Figure V.2. It is observed that the dye removal for the PANI@OFI-A increase as the adsorbent mass increases from 0.2 to 2.5 g/L all other parameters were fixed. This is due to the availability of more surface functional groups at higher concentration. [13], the adsorbent dose of 1.5g/L has the ability to remove the total OG dye from the solution.

$$\text{Dye Removal \%} = \frac{C_0 - C_f}{C_0} * 100\%$$

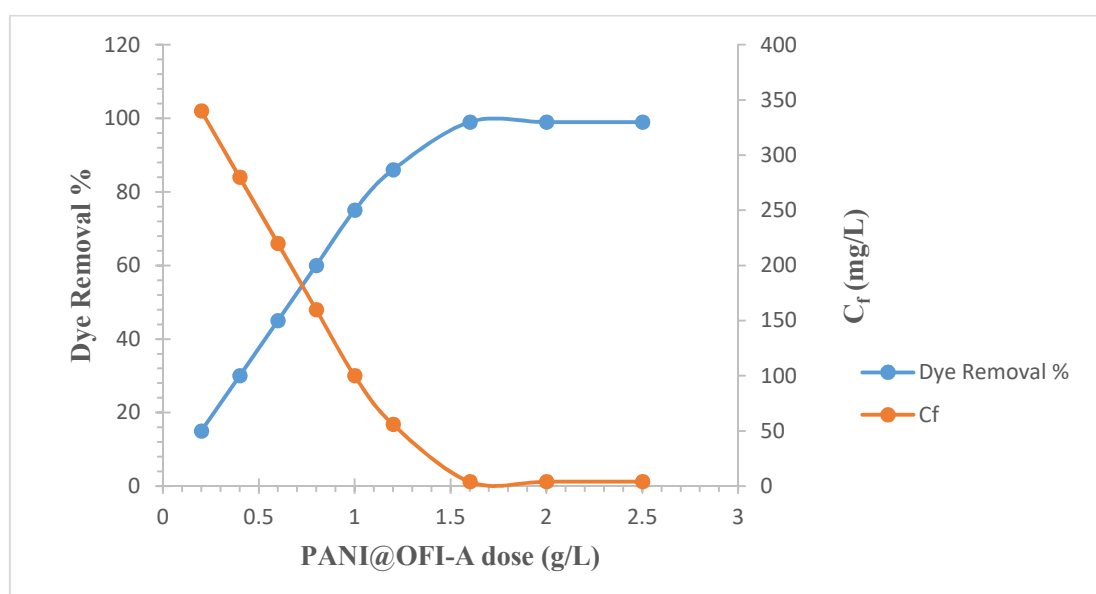


Figure V.1 Effect of adsorbent dosage on the adsorption of OG onto PANI@OFI-A

V.3.2. Effect of pH

The pH value of the dyes solution plays an important role in controlling the adsorption of OG onto the adsorbent material [14]. For pH experiments, 400 mg.L⁻¹ OG solutions were introduced with appropriate amounts of hydrochloric acid (HCl) and sodium hydroxide (NaOH) to adjust the pH within the range of 1 to 12 as shown in Fig.V.3.

0.05 g of PANI@OFI-A nanocomposite was incubated in 50 mL of the prepared solutions for 2 hours at room temperature. As the pH value increased from 1 to 12, the OG removal percentage decreases.

The maximum removal percentage occurred at pH=2, which was calculated as 305 mg.g^{-1} . It was higher for the hybrid material compared to the OFI-A and PANI adsorbents, owing to the enhanced surface area when polymer matrix are added. In addition, the ($-\text{OH}$) group from activation procedure was expected to link hydrogen ions at a weak pH value while amine groups ($-\text{NH}_2$) were readily protonated under acidic conditions, which contributes to the increase of adsorption due to electrostatic attraction with sulfonate ion ($-\text{SO}_3^-$) of OG [15]. Moreover, at low pH values, the ($-\text{NH}_2$) groups of PANI@OFI-A are principally busy by $[\text{H}^+]$ in solution, which results in a high OG adsorption. With increasing pH values, protons would be liberated from ($-\text{NH}_2$) of PANI@OFI-A and this reduce the adsorption [16].

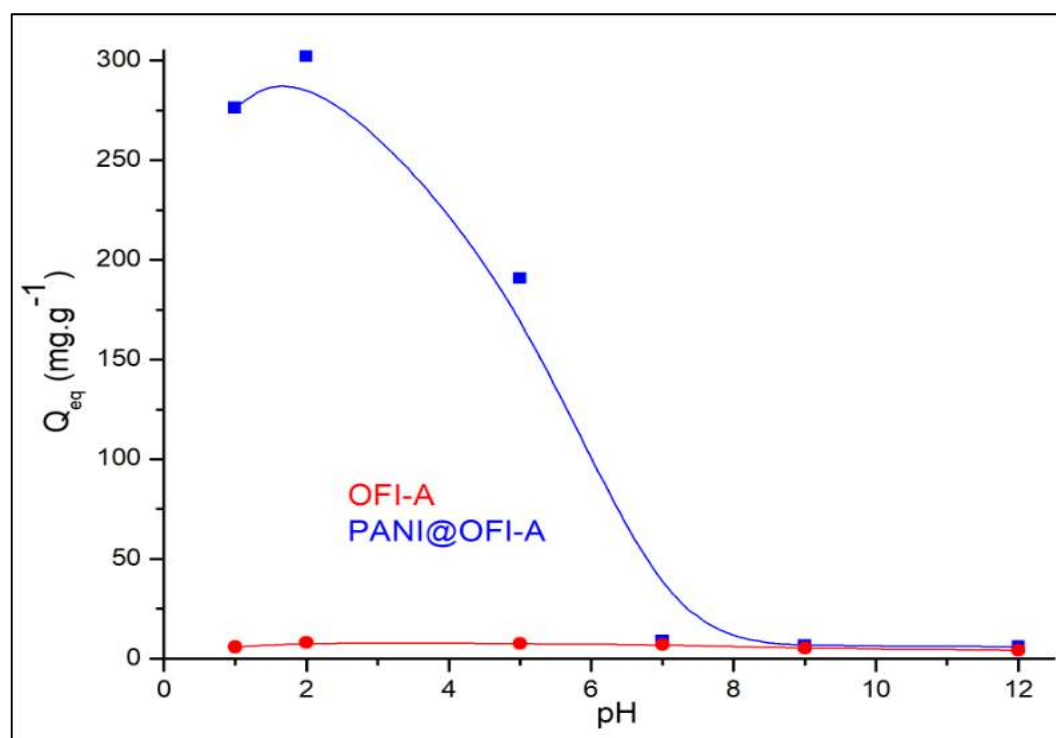


Figure.V.2. Effect of pH values on the adsorption of OG onto PANI@OFI-A

V.3.3. Effect of Initial OG Concentration and Contact Time

The effect of contact time on the adsorption of OG was investigated by incubating 0.05 g of PANI@OFI-A in 50 mL of OG solution for 10, 30, 60, 120, 240, 360 and 1440 min. As illustrated in Fig.V.4, the adsorption capacity increases with increasing the incubation time, and almost reached equilibrium at around 360 min for the initial concentration of 100 ppm, 200 ppm and 300 ppm, but for initial concentration of 400 ppm, 500 ppm more time is required to reach the equilibrium, therefore a duration of 24 h is chosen to confirm the equilibrium.

The hybrid adsorbent PANI@OFI-A needs more time to reach equilibrium compared to (OFI-A) adsorbent which needs 30 min.

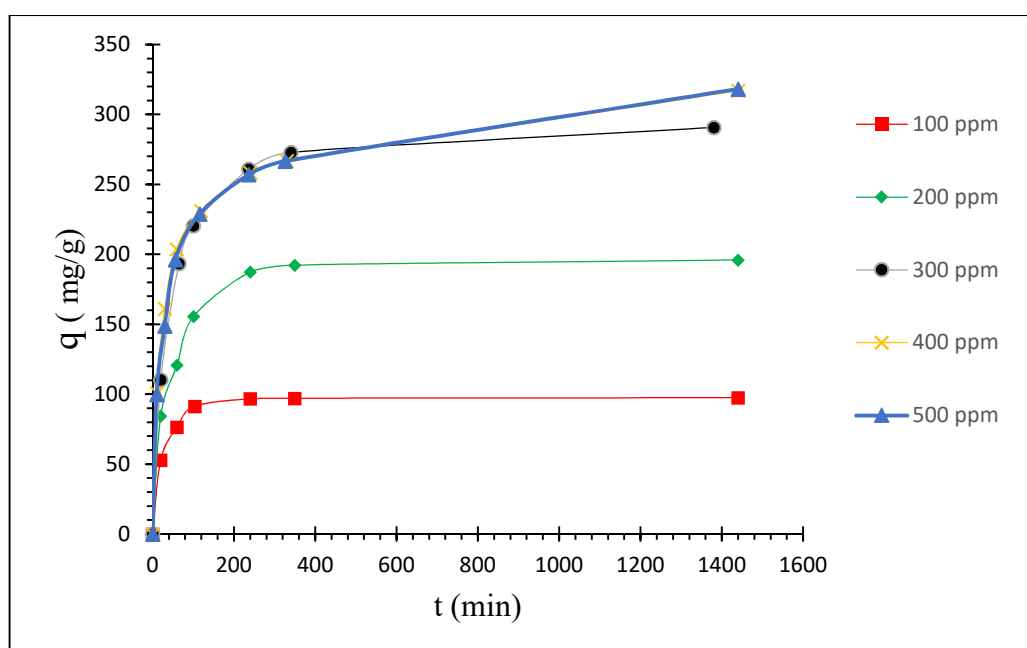


Figure.V.3. Effect of contact time on adsorption of OG onto PANI@OFI-A

V.4. Adsorption kinetics modeling

Four kinetic models such as pseudo-first order, pseudo-second order, intra-particle diffusion and Elovich were selected to investigate the adsorption processes of OG on OFI-A

V.4.1. The pseudo-first order model

The pseudo-first order kinetic model, which is expressed by the equation III.1 quoted in chapter.III, has been applied for the adsorption of OG onto our hybrid adsorbent.

The plot of $\ln(q_{eq}-q)$ versus incubation time (t) of different OG initial concentration are presented in figure.V.4, the rate constant k_1 , adsorbed quantity and correlation coefficients R^2 for

adsorption of OG onto PANI@OFI-A adsorbents were calculated from these plots are given in (Tables V.1).

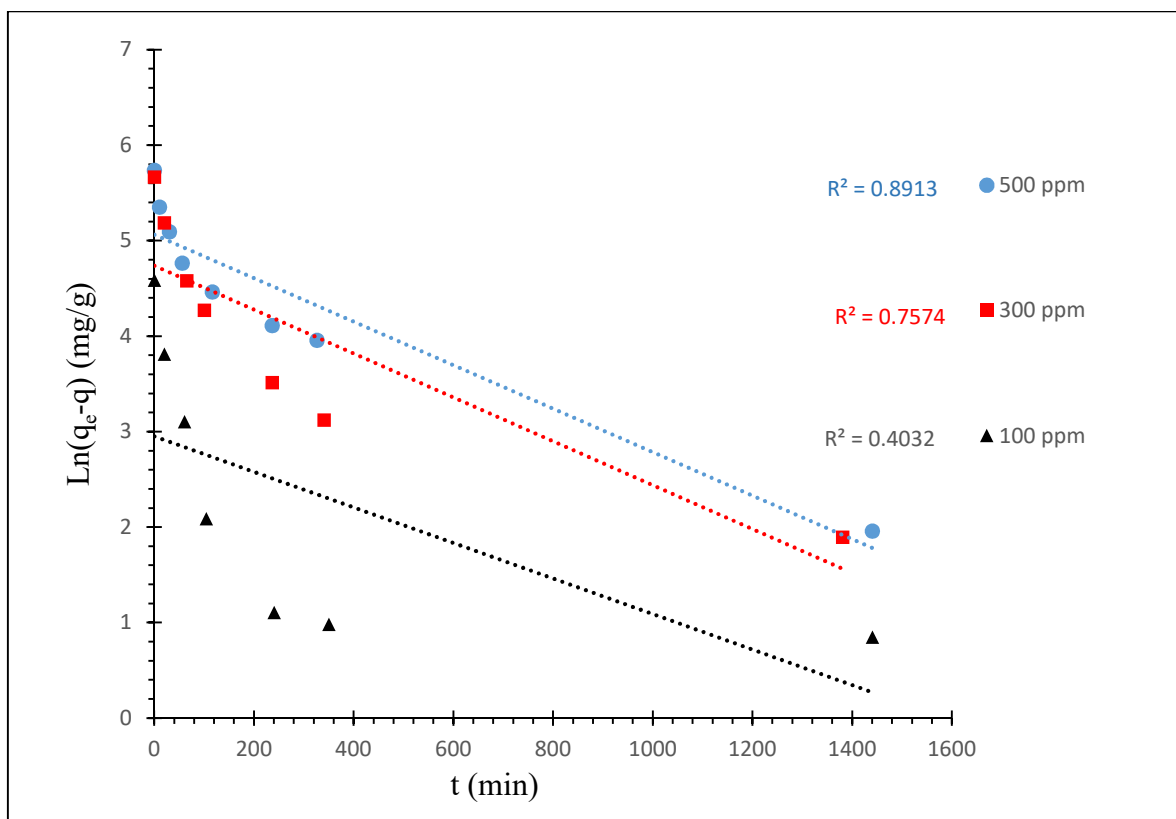


Figure V.4 The pseudo-first order kinetic model for the adsorption of OG onto PANI@OFI-A

V.4.2. The pseudo-second order kinetic model

The second model that can represent our kinetic model is the pseudo-second order equation, which is expressed according to equation III.3.

Figure V.5 shows the plot of t/q as a function of incubating time (t), the second-pseudo order constants as K_2 , equilibrium capacity and correlation coefficients R^2 are calculated and presented in (Tables V.1)

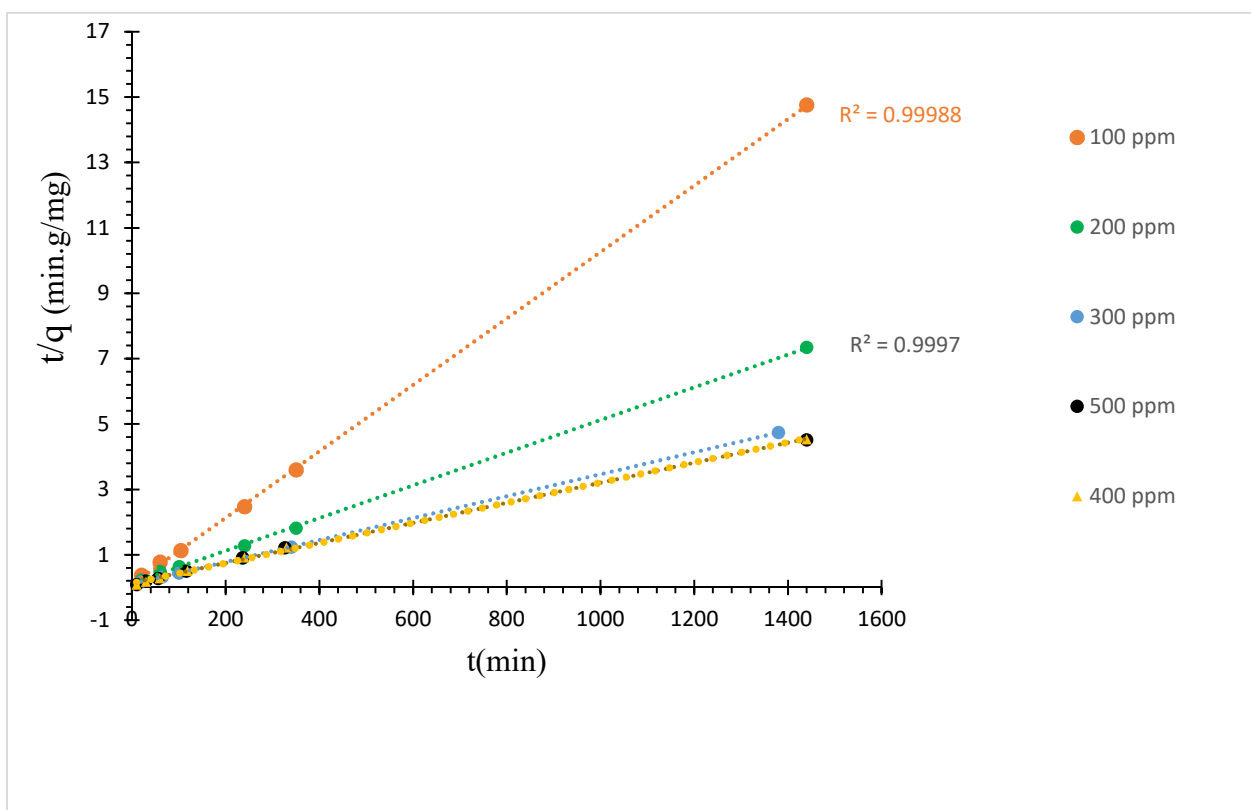


Figure V.5 The pseudo-second order kinetic model for the adsorption of OG onto PANI@OFI-A

V.4.3. Elovich model kinetics model

In reactions involving chemisorption of adsorbate on a solid surface without desorption of products, adsorption rate decreases with time due to an increased surface coverage.

Elovich equation is one of the most useful models for the describing such activated chemisorption. The linear form of the Elovich model is described by equation.III.5.The Elovich constants can be calculated from plot of q_t versus $\ln(t)$ (Figure V.6). [9]

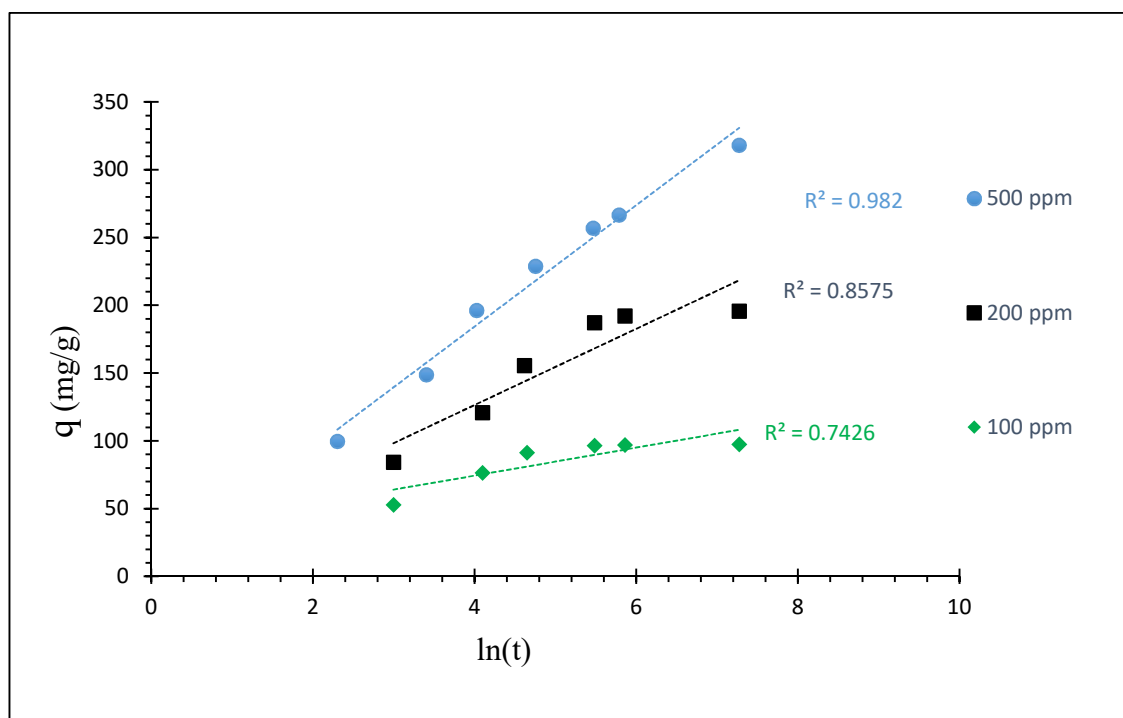


Figure V.6 Elovich model for the adsorption of OG onto PANI@OFI-A

V.4.4. The intra-particle model

The equation.III.6 describes the intra-particles model.

Figure.V.8 present the plot of the adsorbed quantity of dye in function of the square root of incubating time, values of k_{int} and 'I' are obtained from the slope and intercept of the plot respectively these values are given in Tables V.1.

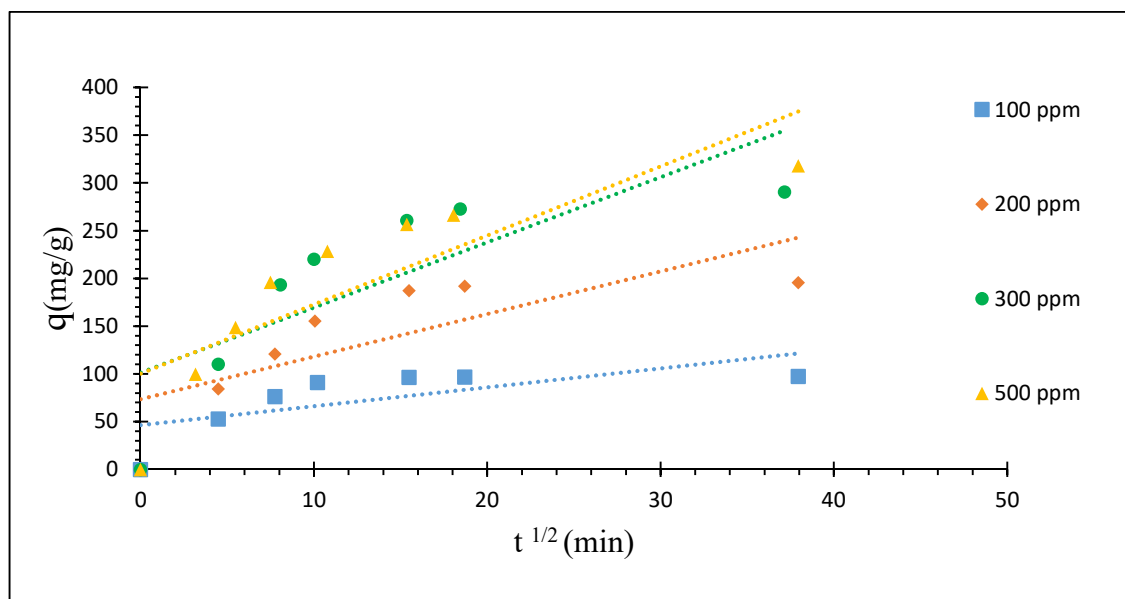


Figure V.7. Intra-particle diffusion model for the adsorption of OG onto PANI@OFI-A

Based on the correlation coefficient (R^2) value, the adsorption kinetic for PANI@OFI-A can better be described by pseudo-second order.

Figure V.8. shows the comparative results using various kinetic models for the adsorption of OG with an initial dye concentration of 400 mg/L. The pseudo-second order kinetics fitted well for The adsorption of OG onto PANI@OFI-A compare to other models. For Elovich model fitted for the first 120 min and thereafter the data deviated from linearity. Thus, the model represents the initial stages adsorption, but it can not be applied to entire adsorption process [11]. But the two other models do not fit the adsorption specially for the first pseudo model.

Table V.1 Kinetic parameters for the adsorption of OG onto PANI@OFI-A

| C ₀ (ppm) | Q _{Exp} (mg/g) | Pseudo-first order | | | Pseudo-second order | | | Elovich | | | Intra-particle diffusion | | |
|-------------------------|----------------------------|----------------------------|--|----------------|------------------------------|--|----------------|----------|---------|----------------|---|-------|----------------|
| | | Q _{cal} (mg/g) | K ₁ (min ⁻¹) | R ² | Q _{eqcal} (mg/g) | K ₂ (g.mg ⁻¹ .min ⁻¹) | R ² | α | β | R ² | k _{int} (g.mg ⁻¹ .min ^{1/2}) | I | R ² |
| 100 | 96.04 | 16.25 | 0.0024 | 0.4032 | 97.1 | 9.79 E -04 | 0.9998 | 312.1 | 0.101 | 0.7426 | 1.9411 | 46.12 | 0.7097 |
| 200 | 191.17 | 64.88 | 0.0023 | 0.6132 | 194.9 | 2.1 E -04 | 0.9997 | 52.08 | 0.03725 | 0.8575 | 4.3138 | 73.32 | 0.6345 |
| 300 | 282.81 | 114.32 | 0.0023 | 0.7574 | 289.5 | 1.08 E -04 | 0.9999 | 57.47 | 0.02439 | 0.8975 | 6.581 | 101.4 | 0.599 |
| 400 | 303.37 | 152.5 | 0.0023 | 0.8891 | 309.98 | 8.18 E -05 | 0.9990 | 70.99 | 0.02464 | 0.9729 | 6.7215 | 104.8 | 0.6706 |
| 500 | 303.94 | 157.9 | 0.0023 | 0.8913 | 311.05 | 7.74 E -05 | 0.9990 | 57.91 | 0.02387 | 0.982 | 6.831 | 100.8 | 0.4707 |

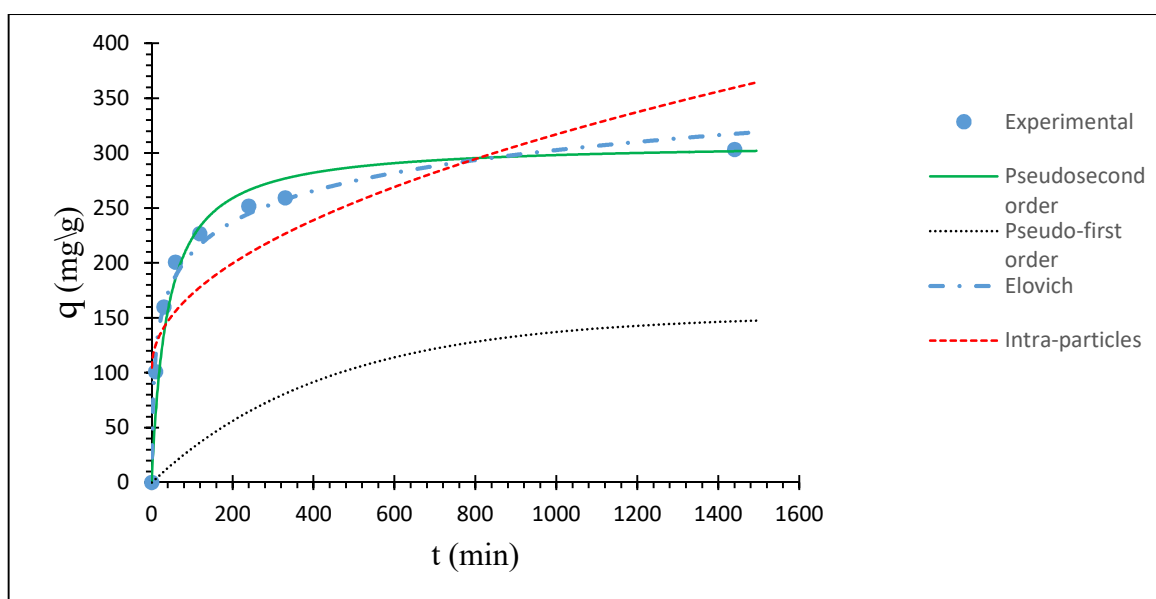


Figure V.8 Comparison between the measured and modelled time profiles for the adsorption of OG onto PANI@OFI-A

V.5 Adsorption Isotherms

The adsorption isotherm is an equation relating the amount of solute adsorbed onto the solid and equilibrium concentration of the solute in solution at constant temperature.

Freundlich, Langmuir and Temkin isotherms were used to explain the equilibrium uptake of OG onto PANI@OFI-A.

V.5.1 Freundlich isotherm

The first model, which can presents our isotherm, is Freundlich equation The Freundlich equation that is given in chapter.III by the equation (III.7).

The Freundlich equation constant which are k_f and n can be calculated from the plot of $\ln(q_e)$ virus $\ln(C_e)$ figure .V.9.

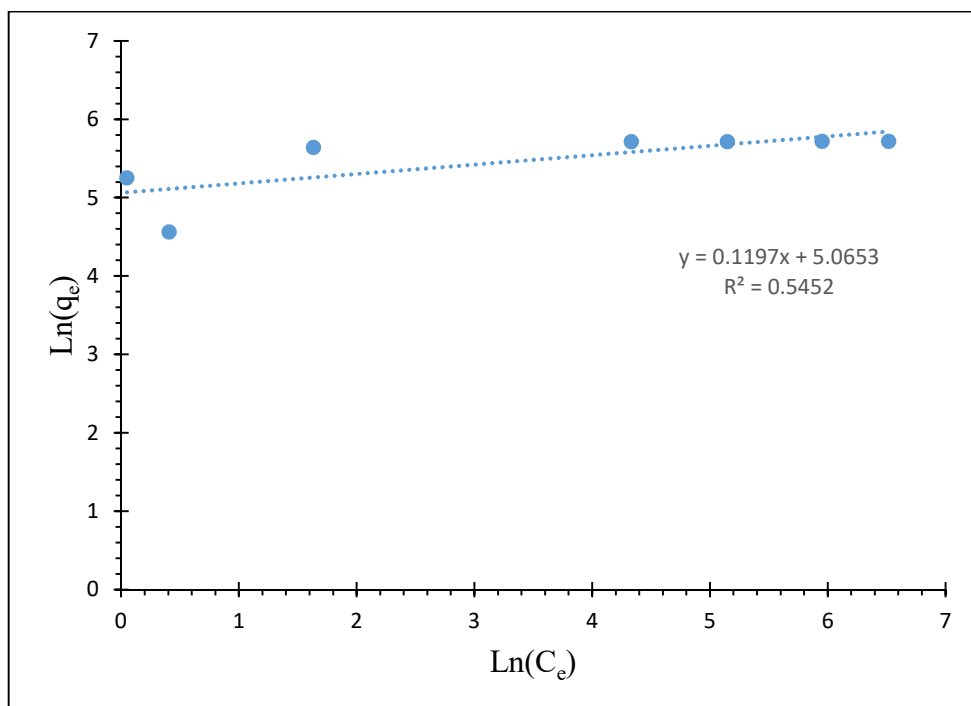


Figure V.9 Freundlich isotherm for the adsorption of OG onto PANI@OFI-A

V.5.2 Langmuir isotherm

The Langmuir adsorption isotherm fit to the adsorption of OG dye by our nanocomposite adsorbent has been verified.

FigureV.1 represents the plot of linear form of Langmuir model, which described by equation (III.10).the bellow plot able the determination of Langmuir isotherm constants K_L , R_L and the maximum adsorption capacity Q_{max} .

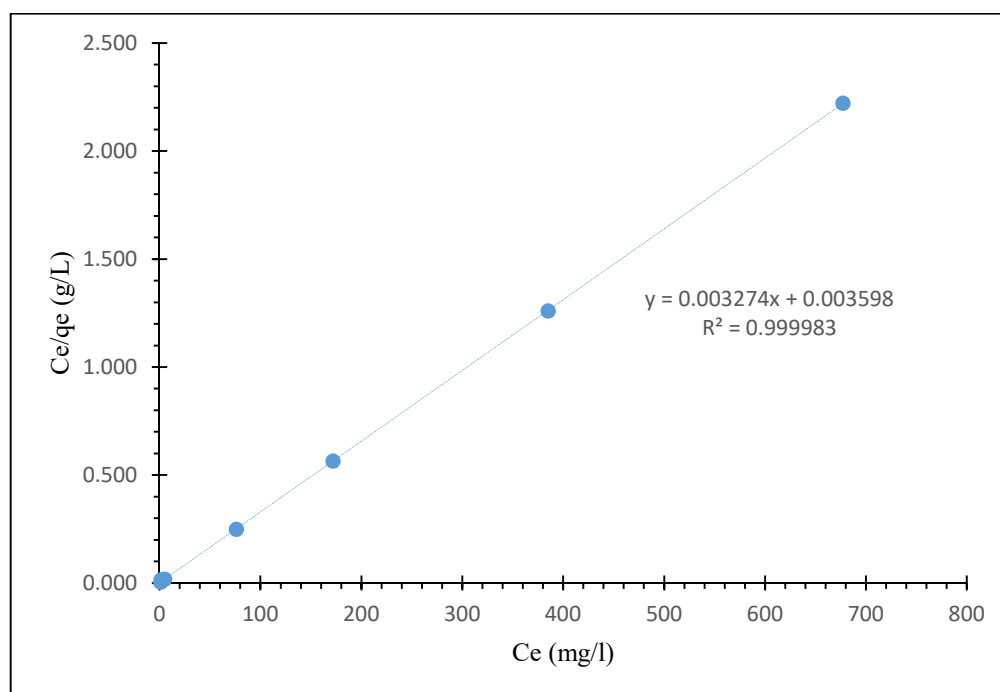


Figure V.10 Langmuir isotherm for the adsorption of OG onto PANI@OFI-A

V.5.3 Temkin isotherm

Tikmen is one of the models has been selected to fit the OG adsorption onto PANI@OFI-A hybrid material adsorbent.

Figure.V.11 shows the application of linear form of Temkin isotherm on the experimental results of adsorption, from this plot we can determine the Temkin equation constants, K_T and b

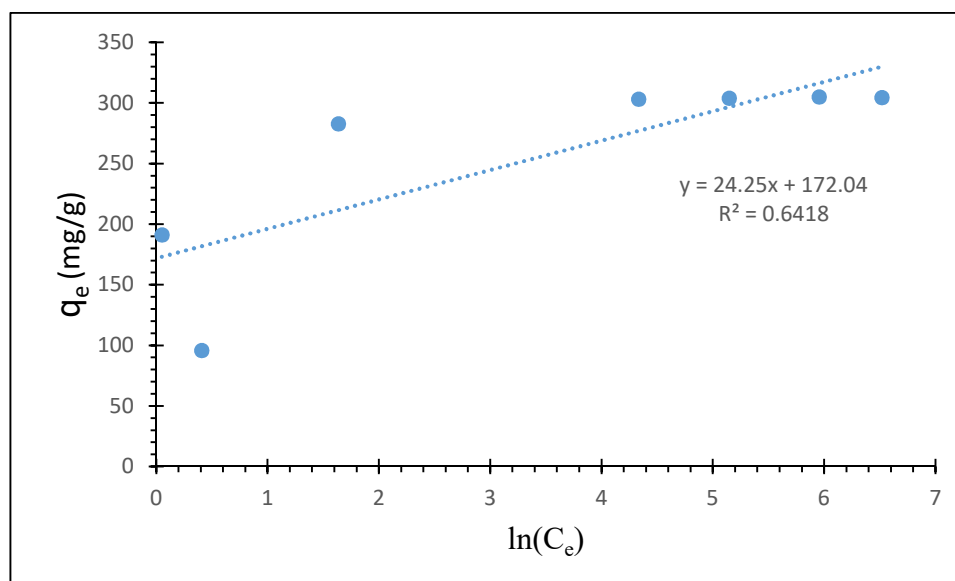


Figure V.11 Temkin isotherm for the adsorption of OG onto PANI@OFI-A

Freundlich, Langmuir and Temkin isotherm constants and their correlation coefficients for the PANI@OFI-A adsorbent are given in Tables V.2

Based on the correlation coefficient (R^2) value, which is very closed to 1, among the three selected isotherms Langmuir isotherm is the best fitted model to the experimental results of OG adsorption by PANI@OFI-A. Moreover, the dimensionless constant R_L lies within the favorable limit ($0 < R_L < 1$), Freundlich and Temkin are not fitting the experimental results.

Figure V.12 shows that the adsorption of OG onto PANI@OFI-A follows the **H2** curve type, which characterized by a sharply vertical part of the initial slope, indicating highly strong interactions between the OG and the PANI@OFI-A. All the OG molecules in solution are adsorbed onto the adsorbent. Which indicate a high affinity of OG ions to the PANI@OFI-A.

Table .V.2 different isotherms parameters and correlation coefficient of OG onto PANI@OFI-A (at 25 °C and pH =2):

| Adsorbent | Langmuir | | | | Freundlich | | | Temkin | | |
|------------|---------------------|-----------------|-------|-------|------------|------|-------|-----------------|------|-------|
| | Q_{max} (mg/g) | K_L (L/mg) | R_L | R^2 | K_F | n | R^2 | K_T (L/mg) | b | R^2 |
| PANI@OFI-A | 303.94 | 0.91 | 0.001 | 0.999 | 158.4 | 8.35 | 0.55 | 1205 | 98.4 | 0.64 |

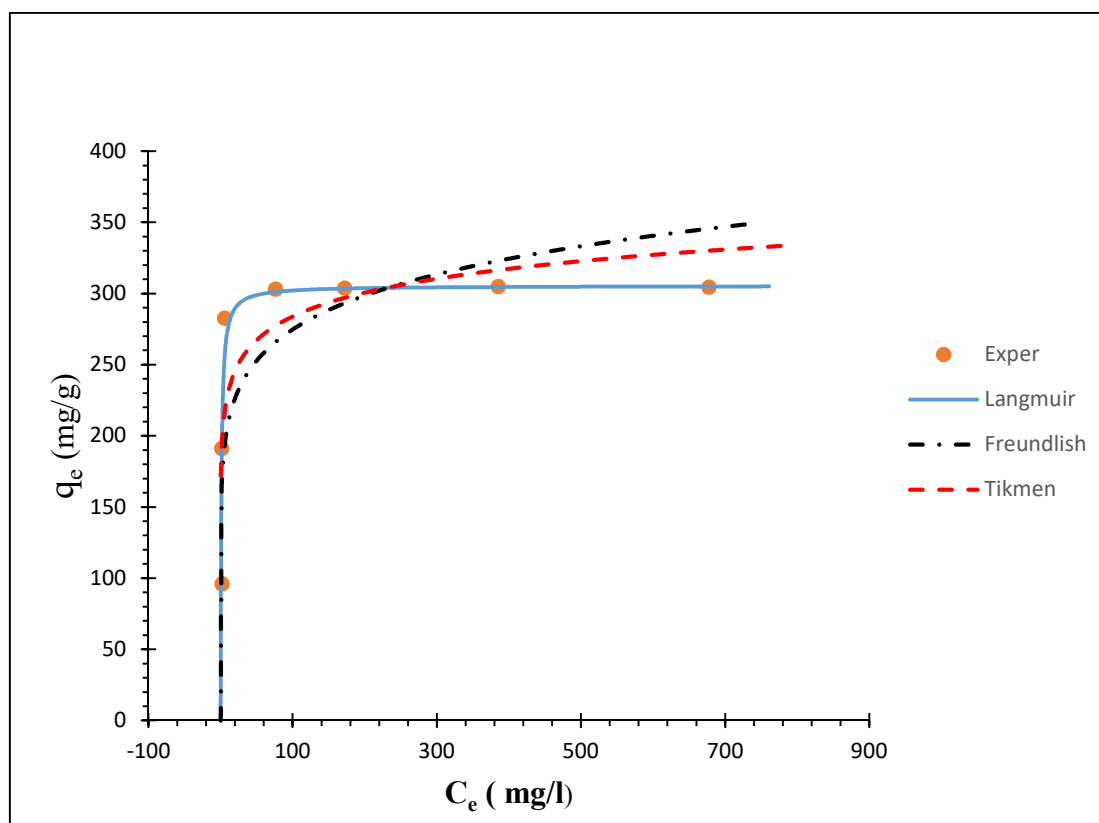


Figure V.12 Comparison of equilibrium isotherms for the adsorption of OG onto PANI@OFI-A

V.6 Thermodynamic studies

To investigate the effect of temperature on the adsorption of OG, experiments were conducted at 25, 35, and 45 °C, the results are represented in Figure V.13.

The free energy change (ΔG°), enthalpy change (ΔH°) and entropy change (ΔS°) can be calculated using equilibrium constants K_d variation with temperature. The values of thermodynamic parameters were calculated using the following relationships:

The calculated thermodynamic parameters are listed in Table V.3.

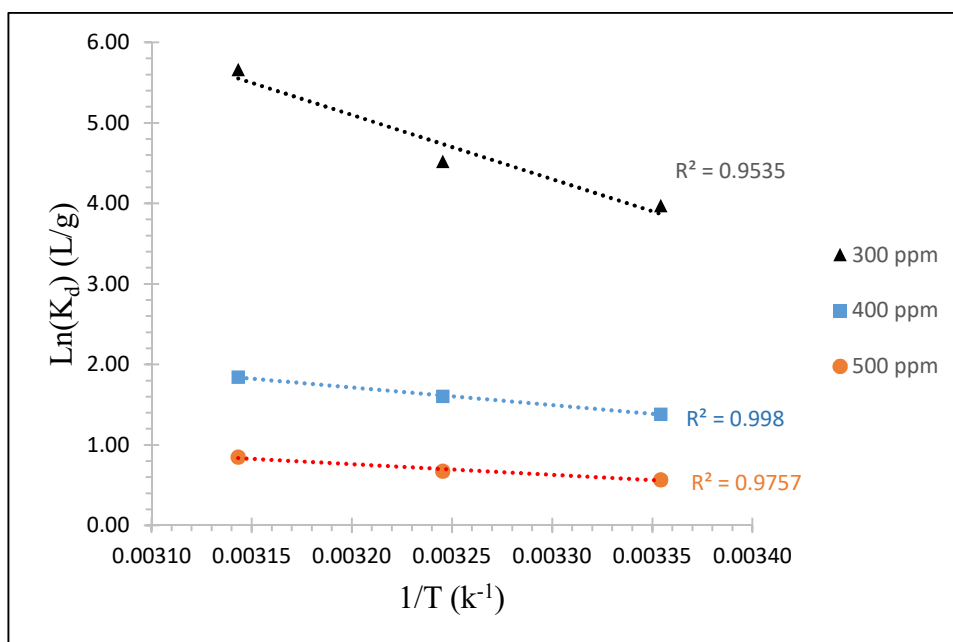


Figure V.13 Plot of $\ln(K_a)$ versus $1/T$ for the adsorption of OG onto PANI@OFI-A

Table V.3 Thermodynamic parameters for the adsorption of OG onto PANI@OFI-A

| Adsorbent | C ₀ (ppm) | ΔH° (KJ / mol) | ΔS° (KJ / mol.K) | ΔG° (KJ / mol) | | | R ² |
|------------|----------------------|-----------------------------|-------------------------------|-----------------------------|--------|--------|----------------|
| | | | | 298 K | 308K | 318K | |
| PANI@OFI-A | 300 | 66.3 | 0.2546 | -9.59 | -12.13 | -14.68 | 0.954 |
| PANI@OFI-A | 400 | 18.3 | 0.0727 | -3.42 | -4.15 | -4.87 | 0.976 |
| PANI@OFI-A | 500 | 11.0 | 0.0415 | -1,38 | -1.79 | -2.21 | 0.998 |

The enhancement of adsorption at higher temperature may be due to increase in the diffusion rate of the adsorbate molecules across the external boundary layer and in the internal pores of the adsorbent particle, owing to the decrease in the viscosity of the solution [17].

The negative values of ΔG° indicated the feasibility and spontaneity of the adsorption process the positive values of ΔH° described the endothermic nature of the overall adsorption process. [16]. The positive values of ΔS° may be interrelated to the extent of hydration of anionic dye molecules. The reorientation or restructuring of water around dye molecules is very unfavorable in terms of entropy, since the reorientation disturbs the existing water structure and imposes a new and more ordered structure on the surrounding water molecules. Therefore, the positive entropy change may be attributed to the increasing disorder because the number of water molecules surrounding dye molecules decreases and thus the degree of freedom of the water molecules increases.

V.7. REFERENCES

- [1] A.M. Donia, A.A. Atia, W.A. Al-amrani, A.M. El-nahas, Effect of structural properties of acid dyes on their adsorption behaviour from aqueous solutions by amine modified silica. *J. Hazard. Mater.* 161, 1544–1550 (2009)
- [2] N. Ouasfi, S. Bouzekri, M. Zbair, H. Ait Ahsaine, S. Bakkas, M. Bensitel, L. Khamliche, C. Doukkali, E. Jadida, Carbonaceous material prepared by ultrasonic assisted pyrolysis from algae (*Bifurcaria bifurcata*): response surface modeling of aspirin removal. *Surf. Interfaces* 14, 61–71 (2019)
- [3] A. Elouahli, M. Zbair, Z. Anfar, H.A. Ahsaine, H. Khallok, R. Chourak, Z. Hatim, Apatitic tricalcium phosphate powder: high sorption capacity of hexavalent chromium removal. *Surf. Inter-faces* 13, 139–147 (2018)
- [4] A. Belalia, A. Zehhaf, A. Benyoucef, Preparation of hybrid material based of PANI with SiO₂ and its adsorption of phenol from aqueous solution. *Polym. Sci. Ser. B* 60, 816–824 (2018)
- [5]. S. Benykhlef, A. Bekhoukh, R. Berenguer, A. Benyoucef, E. Morallon, PANI-derived polymer/Al₂O₃ nanocomposites: synthesis, characterization and electrochemical studies. *Colloid Polym. Sci.* 294, 1877–1885 (2016)
- [6]. F. Chouli, I. Radja, E. Morallon, A. Benyoucef, A novel conducting nanocomposite obtained by p-anisidine and aniline with titanium(IV) oxide nanoparticles: synthesis, characterization, and electrochemical properties. *Polym. Compos.* 38, 254–260 (2017)
- [7]. S. Daikh, F.Z. Zeggai, A. Bellil, A. Benyoucef, Chemical polymerization, characterization and electrochemical studies of PANI/ZnO doped with hydrochloric acid and/or zinc chloride: differences between the synthesized nanocomposites. *J. Phys. Chem. Solids* 121, 78–84 (2018)
- [8]. F.Z. Kouidri, R. Berenguer, A. Benyoucef, E. Morallon, Tailoring the properties of polyanilines/SiC nanocomposites by engineering monomer and chain substituents. *J. Mol. Struct.* 1188, 121–128 (2019)
- [9]. D. Ouis, F.Z. Zeggai, A. Belmokhtar, A. Benyoucef, B. Meddah, K. Bachari, Role of p-benzoquinone on chemically synthesized nanocomposites by polyaniline with V₂O₅ nanoparticle. *J. Inorg. Organometal. Polym. Mater.* (2020). <https://doi.org/10.1007/s10904-020-01508-7>
- [10]. E.S. Lyle, C. McAllister, D.C. Dahn, R. Bissessur, Exfoliated MoS₂-polyaniline nanocomposites: synthesis and characterization. *J. Inorg. Organomet. Polym. Mater.* 30, 206–213 (2020)
- [11]. E. Parthiban, N. Kalaivasan, S. Sudarsan, Dual responsive (pH and magnetic) nanocomposites based on Fe₃O₄@polyaniline/itaconic acid: synthesis, characterization and

- removal of toxic hexavalent chromium from tannery wastewater. *J. Inorg. Organomet. Polym. Mater.* 30, 4677–4690 (2020)
- [12]. M.K.M. Nodeh, S. Soltani, S. Shahabuddin, H.R. Nodeh, H. Sereshti, Equilibrium, kinetic and thermodynamic study of magnetic polyaniline/graphene oxide based nanocomposites for cipro-floxacin removal from water. *J. Inorg. Organomet. Polym. Mater.* 28, 1226–1234 (2018)
- [13] Z. Yang, T.A. Asoh, H. Uyama, Removal of cationic or anionic dyes from water using ion exchange cellulose monoliths as adsorbents. *Bull. Chem. Soc. Jpn.* 92, 1453–1461 (2019)
- [14] E. Ghiasi, A. Malekzadeh, Removal of various textile dyes using LaMn(Fe)O₃ and LaFeMn_{0.5}O₃ nanoperovskites; RSM optimization, isotherms and kinetics studies. *J. Inorg. Organometal. Polym. Mater.* 30, 2789–2804 (2020)
- [15] Y. Tang, X. Yin, M. Mu, Y. Jiang, X. Li, H. Zhang, T. Ouyang, Anatase TiO₂@MIL-101(Cr) nanocomposite for photocatalytic degradation of bisphenol A. *Colloids Surf. A* 596, 124745 (2020)
- [16] Montes de Oca, J. Casas López, I. Oller, S. Malato Rodríguez, Degradation of alachlor and pyrimethanil by combined photo-Fenton and biological oxidation. *J. Hazard. Mater.* 155, 342–349 (2008)

GENERAL

CONCLUSION

General Conclusion

In the present work, a low cost adsorbent was prepared through an in-situ oxidative polymerization method, which could enhance the removal of Orange-G dye. Various characterization techniques, including FTIR, DRX, TGA and SEM showed the successful formation of hybrid adsorbent. The capacity of PANI@OFI-A, PANI and OFI-A to remove OG was studied using equilibrium and kinetic models. The adsorption processes required 30 minutes for OFI-A and 24 hours for PANI and PANI@OFI-A to reach the perfect equilibrium. The pH of contact solutions played a substantial role in the adsorption capacity of the adsorbent for OG dye. It was found that the optimum pH for OG removal was (pH=2). The maximum adsorption capacity of PANI@OFI-A, PANI and OFI-A was determined to be 303.94 mg.g⁻¹, 271.52 mg.g⁻¹ and 8.04 mg.g⁻¹ respectively, at an equilibrium concentration of 400 mg. L⁻¹ and the temperature of 25 °C. Adsorption kinetic model was determined as a pseudo-second-order with a correlation coefficient $R^2 > 0.996$ for all adsorbent, the adsorption data was best adapted by the Langmuir isotherm model with $R^2 > 0.999$ for each adsorbent.

The thermodynamic studies of OG adsorption by the three different adsorbent show that the process is physisorption, the adsorption OG dye by OFI-A is a spontaneous and exothermic process, which is favorable at low temperature. Regarding the PANI and the synthesis nanocomposite PANI@OFI-A adsorbents, the process is spontaneous and endothermic; the adsorption of OG dye onto the last two adsorbents is favorable at high temperature.

The novelty of this study is that NaOH-activation and PANI-reinforcement of the structure of Opuntia Ficus Indica can importantly enhance adsorption effectiveness. This investigation is to offer a suggestion cleaner production method for a promising hybrid adsorbent with adsorption process, perfect sustainability and wide application in the water treatment by innovative material design.

Perspectives:

As the new developed hybrid material PANI@OFI-A showed good results as an adsorbent for the removal of sulfonate dye Orange G we can check its capacity for the elimination of other anionic dyes and check its properties as an electrical conductive material.

ABSTRACT

This study investigated the removal of Orange-G dye (OG) using a hybrid adsorbent developed from *Opuntia Ficus Indica* (OFI) activated with NaOH (OFI-A) were reinforced by polyaniline (PANI) by a fast chemical method. PANI@OFI-A and OFI-A adsorbents having different physicochemical characteristics as FTIR, XRD, TGA, SEM and nitrogen adsorption isotherms are used to analyze the structure of the resulting materials. Besides, the effect of several parameters including contact time (0–24 h), pH (1–12) and initial OG concentration (300–1000 mg.L⁻¹) were evaluated on the adsorption efficiency. The modified OFI-A by PANI was employed as an excellent adsorbent for the removing of OG from aqueous solutions. The results indicated that OG adsorption basically relies on adsorbing time, solution pH and initial OG concentration. Furthermore, the PANI@OFI-A also shows a high adsorption capacity of 303.94 mg.g⁻¹ for OG, quite higher than that of OFI-A (8.04 mg.g⁻¹) and PANI (271.52 mg.g⁻¹). The kinetic results were adapted well to the pseudo second order kinetic model for three samples prepared. Based on the obtained results, the PANI@OFI-A has potential to be used in sensitive environment that need to completely remove OG.

Keywords: PANI · *Opuntia Ficus Indica* · Orange-G dye · Adsorption · Isotherms · Kinetics

RESUME

Cette étude a examiné l'élimination du colorant Orange-G (OG) à l'aide d'un adsorbant hybride développé à partir d'Opuntia Ficus Indica (OFI) activé avec du NaOH (OFI-A) renforcé par de la polyaniline (PANI) par une méthode chimique rapide. Les adsorbants PANI@OFI-A, PANI and OFI-A ayant des caractéristiques physico-chimiques différentes telles que FTIR, XRD, TGA, SEM et isothermes d'adsorption d'azote sont utilisés pour analyser la structure des matériaux obtenus. Par ailleurs, l'effet de plusieurs paramètres dont le temps de contact (0–24 h), le pH (1–12) et la concentration initiale d'OG (300–1000 mg.L⁻¹) ont été évalués sur l'efficacité d'adsorption. L'OFI-A modifié par PANI a été utilisé comme excellent adsorbant pour l'élimination de l'OG des solutions aqueuses. Les résultats ont indiqué que l'adsorption d'OG dépend essentiellement du temps d'adsorption, du pH de la solution et de la concentration initiale d'OG. De plus, le PANI@OFI-A montre également une capacité d'adsorption élevée de 303,94 mg.g⁻¹ pour OG, bien supérieure à celle d'OFI-A (8,04 mg.g⁻¹) et de PANI (271,52 mg.g⁻¹). Les résultats cinétiques ont été bien adaptés au modèle cinétique du pseudo second ordre pour les trois échantillons préparés. Sur la base des résultats obtenus, le PANI@OFI-A a le potentiel d'être utilisé dans un environnement sensible nécessitant une élimination complète du colorant Orange G.

Mots clés : Nanocomposite, PANI, Orange-G colorant, adsorption, cinétique, isotherm

ملخص

بحثت هذه الدراسة في إزالة صبغة Orange-G (OG) باستخدام مادة ماصة هجينة تم تطويرها من اوراق التين الشوكي (OFI) و تم تنشيطها باستخدام NaOH (OFI-A) وتم تقويتها بواسطة بوليانيولين (PANI) بطريقة كيميائية سريعة. يتم استخدام الممتازات، PANI @ OFI-A و PANI و OFI-A التي لها خصائص فيزيائية و كيميائية مختلفة مثل FTIR و XRD و SEM و TGA ومتساويات امتصاص النيتروجين لتحليل بنية المواد الناتجة. بالإضافة إلى ذلك، تم تقييم تأثير العديد من المعلمات بما في ذلك وقت التلامس (0-24 ساعة)، ودرجة الحموضة (1-12) وتركيز OG الأولي (300-1000 مغ/ لتر) على كفاءة الامتصاص. تم استخدام OFI-A المعدل بواسطة PANI كمتناز لإزالة صبغة OG من المحاليل المائية. أشارت النتائج إلى أن امتصاص OG يعتمد أساساً على وقت الامتصاص ودرجة الحموضة في المحلول وتركيز OG الأولي علاوة على ذلك ، يُظهر PANI @ OFI-A أيضاً قدرة امتصاص عالية تبلغ 303.94 مغ / جرام أعلى بكثير من قدرة امتصاص OFI-A (8.04 مغ/ جرام) قدرة امتصاص PANI (271.52 مغ/ جرام) تم تكيف النتائج الحركية بشكل جيد مع النموذج الحركي من الدرجة الثانية للعينات الثلاث التي تم تحضيرها. بناءً على النتائج التي تم الحصول عليها، يمكن استخدام PANI @ OFI-A في بيئة حساسة تحتاج للإزالة التامة لصبغة OG

الكلمات المفتاحية: البوليانيولين، التين الشوكي، الممتازات، الامتصاص، الممتازات الهجينة